Exploiting a novel organotypic model of SOX2-driven early squamous lung cancer to identify potential routes to chemoprevention

Philip Simon Barry

This dissertation is submitted for the degree of
Doctor of Philosophy
at the University of Cambridge

Darwin College
July 2019

Preface

Declaration

This dissertation is the result of my own work and includes nothing which is the outcome of work done in collaboration except as declared in the Preface and specified in the text. It is not substantially the same as any that I have submitted, or, is being concurrently submitted for a degree or diploma or other qualification at the University of Cambridge or any other University or similar institution except as declared in the Preface and specified in the text. I further state that no substantial part of my dissertation has already been submitted, or, is being concurrently submitted for any such degree, diploma or other qualification at the University of Cambridge or any other University or similar institution except as declared in the Preface and specified in the text. It does not exceed the prescribed word limit for the relevant Degree Committee.

Philip S. Barry
July 2019

Exploiting a novel organotypic model of SOX2-driven early squamous lung cancer to identify potential routes to chemoprevention

Philip S. Barry

Lung cancer is a devastating disease and is the leading cause of cancer related death globally. Squamous cell lung cancer (SQC) accounts for around 25% of all lung cancer diagnoses. Better strategies for the early detection, prevention and treatment of lung cancer are urgently needed. Using a novel *in vitro* model of SOX2-driven early SQC I performed a screen using tool compounds and compounds in late phase clinical development for potential efficacy in chemoprevention. I combined this approach with targeted genetic ablation studies to identify/characterise targets that may be key to the progression of SOX2-driven squamous cell carcinomas. In particular I highlight an AKT isoform dependence in SQC that could be exploited in future clinical chemoprevention studies.

Lay Summary

Philip S. Barry

For my friends & family who have been wondering what I have been doing the last 3 years:

Cancer occurs when your own cells behave abnormally, growing and multiplying uncontrollably. Changes in your DNA, known as mutations, are responsible for normal cells becoming cancerous. These mutations can occur in your DNA by errors made during normal cell replication or as a result of external environmental factors, such as cigarette smoke. Mutations can cause genes to be permanently switched on or off, no longer under the control of your cell's normal regulatory mechanisms.

Cancers have certain mutations that are regarded as “driver mutations”. Driver mutations provide cancer cells with growth advantages that allow them to grow, multiply and avoid death. Understanding what these mutations are and how they confer growth advantages to cancers is important for understanding how to treat cancers more effectively.

Lung cancer is a devastating disease and is the leading cause of cancer related death globally. My project focussed on squamous cell lung cancer (SQC), a sub-type of lung cancer that accounts for a quarter of all lung cancer diagnoses. In order to reduce deaths from lung cancers, better strategies for detection, prevention and treatment of the disease are needed.

I studied a common driver mutation that causes the SOX2 gene to be uncontrollably switched on in early SQC. When SOX2 is switched on it causes many other genes to switch on and off. My aim in this project was to look at the impact of switching certain genes off that SOX2 switched on. To study this, I used cancer cell lines derived from human cancer samples, and a novel 3D cell culture model developed by my lab. The 3D cell culture model was created using normal human cells from the lung, genetically modified to copy the SOX2 driver mutation. When grown in a 3D environment replicating where these cells grow in the human lung, they show increased growth and create tumours that closely replicate SQC disease in a dish.

I used a number of methods to switch genes off and investigated how necessary these genes were for promoting growth in SOX2-driven cancer. I identified a dependency for a gene, AKT3, that had previously not been implicated in this disease setting. When AKT3 was switched off SOX2-driven cancer cells were prevented from growing, but importantly, did not impact cells that did not have this mutation in the 3D culture model or cancer cell lines. My project provides new evidence that using drugs to switch off AKT3 in SOX2-driven cancer could be used as a treatment strategy in the future.

“Hofstadter’s Law: It always takes longer than you expect, even when you take into account Hofstadter’s Law.“

Douglas Hofstadter, (1979)

Acknowledgements

I would like to start by thanking my PhD supervisor, Frank, for the support, guidance and encouragement that you provided throughout my PhD. Not only were you a huge source of intellectual guidance but also emotional support for when times got tough, and without whom, I am certain I would not have finished this PhD.

I'd like to give an enormous amount of thanks and gratitude to Lucia. You patiently taught me all I needed to know in the lab in my first two years. Without you I would still be trying to learn how to do a PCR reaction, or an immunohistochemistry stain... And of course, thank you for all of your hard work in developing the OTC model, used throughout my project, as well as assistance with experiments and providing samples.

My thanks goes to the Evan lab, in particular the bosses, Gerard & Trevor, for allowing me to work in your lab and present at lab meetings. To the members of the Evan lab, past and present, who have helped or advised me in any way during my time in the lab - it was much appreciated, thank you!

I hope you have enjoyed the extra desk space Ben...

To Linsey, thanks so much for all of the experimental assistance and support that you provided for me in my final year, it was really appreciated.

To Steph, I'm sorry for giving you lots of fiddly samples to embed for histology, you never complained and always did a much better job than I could ever do!

To those of you in the Biochemistry Department that kept me sane (mostly), thanks for putting up with me, you know who you are.

A huge thanks goes to Joel and George. You both gave me some brilliant feedback on chapter drafts, I really did appreciate it guys. You'll both be glad to know that I am now enrolled on a basic grammar course now too...

Thanks to Will and Paddy, you introduced me to the wonderful world of LaTeX, so that I could write and assemble this thesis (thesis.tex). MS Word would probably still be loading to this day...

A huge thanks to the friends that I made away from the lab in Cambridge, you kept me going when everything seemed too much. Cheers to the sweaty sanctuary, that is, Dar Bar on a Friday night.

To The Galapagogos (all 13 members, past and present, that I had the pleasure to have played with), I had some of the best times playing guitar with you guys over the 3 years, I dont think I will ever get chance to play gigs as frequently, on excessively large stages, through ridiculously huge Marshall stacks, or in as many listed buildings ever again!

As an aside, below are my most played songs in each of my first 3 years of my PhD (data courtesy of Spotify). Music was there to get me through the long hours in the windowless cell culture room and the late nights in the lab. It turns out that these song titles inadvertently told quite an amusing narrative for the timeline of a PhD student... The naive wonderment of one's first year self, the realisation in second year of what one will actually achieve with one's project and the desperation to simply “make it to the end“ in one's final year. I’d also like to acknowledge the part that Deftones played during my times alone in the lab on those late nights (that is, full volume at all times).

Most played songs during my PhD project: The Story of a PhD Student
2016: *Shaolin Monk Motherfunk - Hiatus Kaiyote*
2017: *Off Peak Dreams - Ghostpoet*
2018: *Keep Doing What You're Doing - Tangled Hair*

Thanks to mum and dad for believing in me, your continual support throughout my further education and, no doubt, my future is really appreciated - even if I don't say it as much as I should. Of course, it goes without saying too, thanks for putting me up *and* putting up with me through the painful write-up process!

Finally, to Fay, without you this whole thing would not have been possible. You have been my rock from the beginning, and have continually given me support, reassurance and confidence in what I am capable of. I look forward to the next chapters ahead for us together. Lots of love.

Abbreviations

ABC: Avidin-biotin complex
ADC: Adenocarcinoma
AKT: Protein kinase B
ALI: Air-liquid interface
AML: Acute myeloid leukemia
AMPK: Adenosine monophosphate-activated protein kinase
ARE: Antioxidant response elements
AT2: Alveolar type 2 cell
AZ: AstraZeneca
BCA: Bicinchoninic acid
BET: Bromodomain and extraterminal domain protein
BPE: Bovine pituitary extract
BSA: Bovine serum albumin
CAF: Cancer-associated fibroblast
Cas9: CRISPR-associated protein 9
CDK4: Cyclin-dependent kinase 4
CIS: Carcinoma *in situ*
CNA: Copy number alteration
COPD: Chronic obstructive pulmonary disease
CRISPR: Clustered regularly interspaced short palindromic repeats
CT: Computerized tomography
Ct: Cycle threshold
CTC: Circulating tumour cell
CTLA4: Cytotoxic T-lymphocyte-associated protein 4
DAB: 3,3'-diaminobenzidane
DMSO: Dimethyl sulfoxide
Dox: Doxycycline
ECL: Enhanced chemiluminescence
ECM: Extracellular matrix
EGF: Epidermal growth factor
EGFR: Epidermal growth factor receptor
EMT: Epithelial-mesenchymal transition
ERK: Extracellular-signal-regulated kinase
ESC: Embryonic stem cell
ESCC: Esophageal squamous cell carcinoma
FDA: U.S. Food and Drug Administration

FDR: False discovery rate
FGFR: Fibroblast growth factor receptor
FISH: Fluorescence *in situ* hybridisation
FoxO: Forkhead box O transcription factor
GEMM: Genetically engineered mouse models
GSK3: Glycogen synthase kinase 3
H&E: Hematoxylin and eosin
H3K27Ac: Histone H3 lysine 27 acetylation
hBEC: Human bronchial epithelial cell
HGD: High grade dysplasia
HM: Hydrophobic motif
HMG: High mobility group
HNSCC: Head and neck squamous cell carcinoma
IGF1: Insulin-like growth factor
IHC: Immunohistochemistry
InDel: Insertion or deletion
JNK: c-Jun N-terminal kinase
KRAS: Kirsten rat sarcoma viral oncogene homolog
KSFM: Keratinocyte serum-free medium
KT: Non-virally immortilised human bronchial epithelial cell line
LGD: Low grade dysplasia
LogFC: Logarithmic fold change
LOH: Loss of heterozygosity
LUAD: Lung adenocarcinoma
LUSC: Lung squamous cell carcinoma
MAPK: Mitogen-activated protein kinases
MSC: MicroRNA signature classifier
mTORC: Mechanistic target of rapamycin complex
NBF:Neutral buffered formalin
NHS: UK National Health Service
NHTBE: Normal human tracheobronchial epithelial cells
NICE: UK National Institute for Health and Care Excellence
NLST: The National Lung Screening Trial
NSCLC: Non-small cell lung cancer
NSG: Non-obese diabetic severe combined immunodeficiency mouse
NTC: Non-targeting control
OoC: Organ-on-a-chip
OTC: Organotypic culture
PAM: Protospacer adjacent motif
PD1: Programmed cell death protein 1
PD-L1: Programmed death ligand 1
PDMS: Polydimethylsiloxane

PDX: Patient derived xenograft
PFA: Paraformaldehyde
PH: Pleckstrin homology domain
PI3K: Phosphoinositide 3-kinase
PRAS40: Proline-rich AKT substrate of 40 kDa
PTEN: Phosphatase and tensin homolog
PVDF: Polyvinylidene fluoride
RAR: Retinoic acid receptor
Rb: Retinoblastoma protein
RECIST: Response evaluation criteria in solid tumors
RIPA: Radioimmunoprecipitation
S6: Ribosomal protein S6
S6K1: Ribosomal protein S6 kinase 1
SCC: Single cell clone
SCLC: Small cell lung cancer
SD: Standard deviation
sgRNA: Single guide ribonucleic acid
shRNA: Short hairpin ribonucleic acid
SIK2: Salt inducible kinase 2
siRNA: Small interfering ribonucleic acid
SNP: Single-nucleotide polymorphism
SOX2: Sex determining region Y-box 2
SQC: Squamous cell carcinoma
TBP: TATA-box binding protein
TCGA: The Cancer Genome Atlas
TEER: Transepithelial resistance
TEP: Tumour-educated platelets
TERT: Telomerase reverse transcriptase
TIDE: Tracking of InDels by decomposition
TMA: Tissue microarray
TNBC: Triple negative breast cancer
TNF: Tumour necrosis factor
TSC2: Tuberous sclerosis complex 2
TSS: Transcriptional start site
TTF1: Thyroid transcription factor 1
TUNEL: Terminal deoxynucleotidyl transferase dUTP nick end labeling
UCSC: University of California Santa Cruz genome browser
USPSTF: United States Preventive Services Task Force
VC: Vehicle control
VEGF: Vascular endothelial growth factor
VOC: Volatile organic compound
WT: Wild type

Contents

List of Figures

List of Tables

Chapter 1

Introduction

1.1 Squamous cell lung cancer

1.1.1 Lung cancer epidemiology

Lung cancer is the leading cause of cancer related death in the world. In the United States, lung cancer kills more people than prostate, breast and colon cancers combined (Cruz et al., 2011). In the UK, lung cancer kills 21% of all cancer patients, with deaths being highest in patients in the 70-80 years old age bracket (CRUK, 2018). Lung cancer is not only a problem in developed countries, but rates are increasing in underdeveloped regions in the world. Worldwide, lung cancer was responsible for 1.4 million deaths in 2008 (Cruz et al., 2011).

In the UK, the percentage of patients that are alive 5 years after their initial lung cancer diagnosis is only 10%. The disease has a dismal outlook from diagnosis, this is in part due to early stage lung cancers being largely asymptomatic. At the time of diagnosis tumours are often advanced with limited treatment options (Cheng et al., 2016).

There is clearly a need to lower lung cancer incidence and mortality worldwide and a number of ways to address this will be discussed throughout this thesis including, smoking cessation, earlier detection, better targeted therapies and chemoprevention strategies.

1.1.2 Clinical and pathological features

Lung cancers are categorised based on their histologic subtypes, small cell lung cancer (SCLC) and non-small cell lung cancer (NSCLC). NSCLC is further divided into adenocarcinoma (ADC), squamous cell carcinoma (SQC) and large cell carcinoma. The histologic subtypes tend to occur in distinct anatomical locations, SQC in the central major bronchi and ADC in small bronchi, bronchioles or alveolar epithelia (Lemjabbar-Alaoui et al., 2015; Davidson et al., 2013).

SQC accounts for around 25% of all lung cancer diagnoses, and is almost entirely associated with cigarette smoking status (Pesch et al., 2012). Compared to ADC that generally

occurs in the distal airways, SQC arises in the larger proximal airways from the bronchial epithelium (Davidson et al., 2013).

SQCs are histologically characterised by keratinization of individual cells, intercellular bridges between cells and squamous pearl formation (Kumar et al., 2013). Histological markers are often used in the clinic to distinguish ADC from SQCs. SQCs can be identified by thyroid transcription factor 1 (TTF1) negativity plus cytokeratin 5/6 and p63 or p40 (ΔNp63, a p63 isoform) positivity (Pelosi et al., 2011; Bishop et al., 2012).

1.2 Molecular pathogenesis of advanced SQC

Genomic and genetic alterations of advanced invasive SQCs have been well characterised. Data from the cancer genome atlas (TCGA) demonstrates that SQC has a higher genomic complexity and a high overall mutation burden (Hammerman et al., 2012). The mutation burden in SQC is the second highest compared to 20 other tumour types in the TCGA (Figure 1.1). The high mutational burden in SQC is likely due to a number of reasons; exposure to mutagens present in cigarette smoke, loss of DNA repair pathways and/or chromosomal instability.

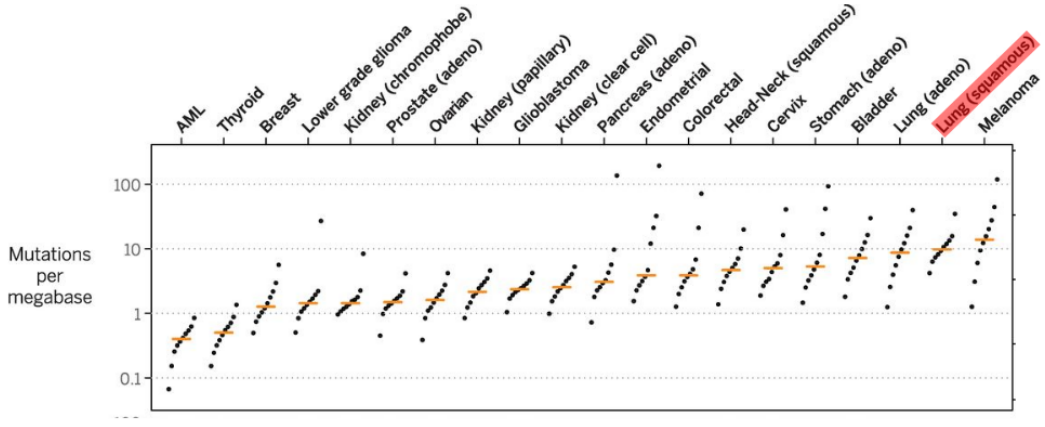

Figure 1.1: Squamous cell lung cancer has a high mutation burden compared to other cancer types.
Squamous cell lung cancer, of the tumours analysed in the TCGA, has the second highest mutation burden at 8.1 mutations per megabase. Adapted from (Martincorena and Campbell, 2015).

1.2.1 3q amplification targets SOX2 in invasive SQC

At the level of whole chromosome somatic copy number alterations, a significant difference between lung ADC and SQC is selective amplification of chromosome 3q (Hammerman et al., 2012). Gene amplification is defined as an increase in the copy number of a particular chromosomal region. Amplification events on chromosome 3q target 60% of SQCs (Hussenet et al., 2010). Mapping of 3q amplifications have revealed a number of candidate oncogenes involved in tumorigenesis at 3q26.33 locus, *PRKCI* (Justilien et al., 2014), *TP63* (Massion et al., 2003b), *PIK3CA* (Yamamoto et al., 2008), *DCUN1D1* (Sarkaria et al., 2006) and *SOX2* (Bass et al., 2009).

More detailed analysis of 3q amplification and functional studies have found that SOX2 is amplified to higher levels than other genes around this locus such as *TP63*, *PIK3CA*, *DCUN1D1* (Bass et al., 2009; McCaughan et al., 2010). Functional studies using RNA interference to knock down genes in the 3q26.33 locus, found that SOX2 knockdown had the most anti-proliferative impact on 3q26.33 amplified cell lines (esophagus and lung derived squamous cell carcinoma cell lines) compared to knockdown of 13 other coamplified genes on 3q including, PI3KCA, P63 and DCUN1D1 (Bass et al., 2009).

Over-expressing SOX2 in lung epithelial cell lines significantly increases migratory activity *in vitro*, as well as increasing anchorage independent growth in soft-agar colony formation assays (Hussenet et al., 2010). The migration assays used Calu-1, BEAS-2B and H226 cells, and the soft-agar colony formation assays only used BES-2B cells. BEAS-2B are a virally immortilised bronchial epithelial cell line, integration of viral genes can cause genomic instability and malignant transformation. Calu-1 cells are derived from a lung ADC, where SOX2 amplification is extremely rare. Together this makes these cell models inappropriate to study SOX2 amplification in SQC, and therefore supports the need for more representative models.

SOX2 is consistently amplified in 20-60% of lung SQC, percentages vary depending on methods used to decipher this. Methodologies of detection, thresholding discrepancies, as well as patient cohort differences and tumour heterogeneity all contribute to variation in the percentages reported. Data from cbioportal (www.cbioportal.org) reporting on lung

squamous cell carcinoma data from the TCGA provisional dataset containing 511 samples gives *SOX2* amplification status in 48% of patients.

Fluorescence *in situ* hybridization (FISH) methods of detecting *SOX2* amplification have also been used; however, this is a less sensitive method, and has been applied to much smaller patient cohorts than the SNP 6.0 array platform used in the TCGA data on cbioportal (Brcic et al., 2012).

1.2.2 SOX2 overexpression is a common event in invasive SQC

Copy number increases, or amplification events of a chromosomal region, are generally associated with overexpression at both the mRNA and protein level (Albertson 2006). TCGA data (511 samples) shows a SOX2 mRNA upregulation in 47% of samples. SOX2 amplification shows a consistent increase of SOX2 transcription when compared to diploid samples (Figure 1.2). Using IHC to look at SOX2 protein overexpression 79% of 66 squamous cell lung cancer biopsies showed overexpression of SOX2 protein (Brcic et al., 2012). Another study examined tumour samples from 33 squamous cell lung cancer patients and significantly correlated SOX2 protein overexpression with gene amplification (Yoon et al., 2016).

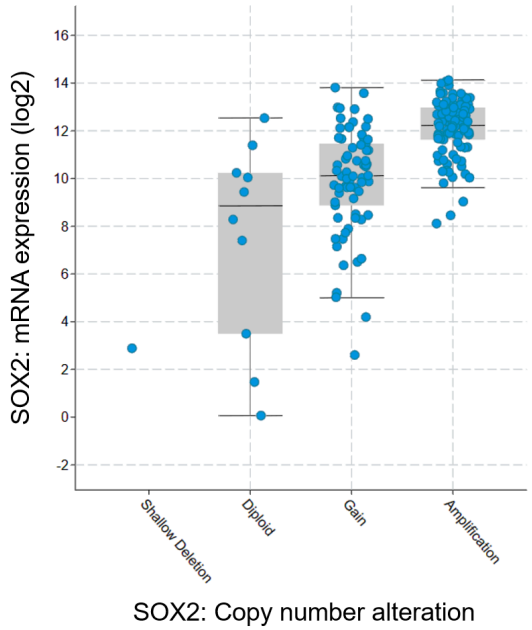

Figure 1.2: *SOX2* amplification events are associated with increased mRNA expression in SQC.
SOX2 mRNA expression data and associated copy number variations in human squamous cell lung tumours. TCGA data was accessed via www.cbioportal.org (511 samples), copy number alterations were analysed and plotted against mRNA expression profiles using RNA Seq V2 RSEM values. Box and whisker plots show the lower and upper quartile values as the ends of the grey box and the median marked inside the box. The whiskers show the variability outside the upper and lower quartiles, calculated using $\pm$ (1.5 x Interquartile Range). Outliers are shown outside of the whiskers.

1.2.3 Genetic alteration of *TP53*, *CDKN2A* and other genes in advanced SQC

There are a number of frequent genetic alterations reported in advanced SQCs. One of the most commonly mutated genes is *TP53*, 90% of 178 samples were found to have mutations in this key tumour suppressor gene (Hammerman et al., 2012). Under normal conditions p53 is tightly controlled, MDM2 binding to p53 signals proteasomal degradation of p53. Some of the major functions of p53, in response to cellular stresses, include growth arrest, apoptosis and DNA repair, mediated through key target genes such as *p21*, *BAX* and *GADD45*, and many other target genes (Tanaka et al., 2018). However, mutated *TP53* can acquire oncogenic function. Frequent single mutations, R175 and R273H, have shown to accelerate metastasis in mouse models (Liu et al., 2000; Olive et al., 2004).

Another common genetic alteration is in the *CDKN2A* locus, inactivated in 72% of SQC cases via methylation, mutation or homozygous deletion (Hammerman et al., 2012). This locus codes for 2 tumour suppressors, p16 and p14. p16 inhibits cyclin-dependant kinases 4 and 6 (CDK4 and 6), activating retinoblastoma (Rb) proteins. Rb is a tumour suppressor protein that is involved in G1 to S phase transition of the cell cycle. Rb binds to and represses E2F family transcription factors, inhibiting progression to S-phase. p14 inhibits MDM2, an inhibitor of p53, thereby activating p53 and initiating cell cycle arrest or apoptosis (Zhao et al., 2016). Other common mutations found in samples from 178 squamous cell lung tumours were in *PTEN* (13%), *PIK3CA* (17%), *KEAP1* (15%) and *NFE2L2* (16%) (Hammerman et al., 2012).

Phosphatase and tensin homolog (PTEN) dephosphorylates PIP_3, and results in inhibition of the AKT signalling pathway. This is inactivated via mutation or deletion. *PIK3CA* encodes the p110α catalytic subunit of phosphatidylinositol 3-kinase (PI3K), and mRNA is upregulated in 58% of SQCs. PI3K signalling activates many downstream signal transducers including AKT. PIK3CA is upregulated in squamous cell lung cancers via amplification and overexpression, however, knockdown in squamous cell line studies has shown limited impact on proliferation (Bass et al., 2009).

Kelch-like ECH-associated protein 1 (KEAP1) is a repressor of nuclear factor erythroid-2-related factor 2 (NRF2). NRF2 is a transcription factor that regulates pathways via binding to antioxidant response elements (ARE) driving transcription of genes that maintain cellular redox homeostasis and genes involved in xenobiotic detoxification. Inactivation of KEAP1 leads to upregulation of NRF2 which has been implicated in chemoresistance of lung cancers (Singh et al., 2006). NRF2 has also been shown to protect against chemical carcinogen-induced tumorigenesis, NRF2-null mice were more likely to develop tumours following exposure to benzo(a)pyrene compared to WT mice (Ramos-Gomez et al., 2001). In a Japanese study comparing lung cancer patients with a control cohort, low NRF2 transcription levels, as a result of a SNP in the NRF2 promoter, was linked with increased risks of developing NSCLC (Suzuki et al., 2013). Depending on the context NRF2 has been shown to have both oncogenic and tumour suppressor roles, and further research is required to elucidate disease-specific molecular mechanisms for the role of NRF2 in SQC.

1.3 Molecular pathogenesis of preinvasive squamous cell lung cancer

As opposed to advanced disease, the molecular drivers of preinvasive early SQC are less well understood, although Teixeira et al. (2019) recently reported a unique data set of preinvasive SQC lung lesions. Greater understanding of the pathogenesis of early preinvasive SQC is important for the identification of novel therapeutic targets for chemoprevention strategies (Section 1.6.4) and potentially the treatment of advanced disease (Section 1.6).

1.3.1 Histological progression

Similar to ideas proposed in carcinomas of other organs such as colon, SQC is thought to develop from normal epithelium through a series of histological changes, accumulating genetic aberrations and increasing disorder of the epithelium as it develops into invasive SQC (Vogelstein and Kinzler, 1993). The process begins with a normal bronchial epithelium, developing basal cell hyperplasia through squamous metaplasia, low (LGD) and high (HGD) grade dysplasia, and carcinoma *in situ* (CIS) before the development of invasive carcinoma (Figure 1.3) (Wistuba et al., 1999; Wistuba, 2012). That said, the sequence of molecular events involved in the initiation and driving of this progression remains unclear. This has been a difficult field to study due to the difficulty in diagnosing bronchial metaplasia and dysplasia, and technical challenges posed by limited numbers of small heterogeneous bronchial biopsies.

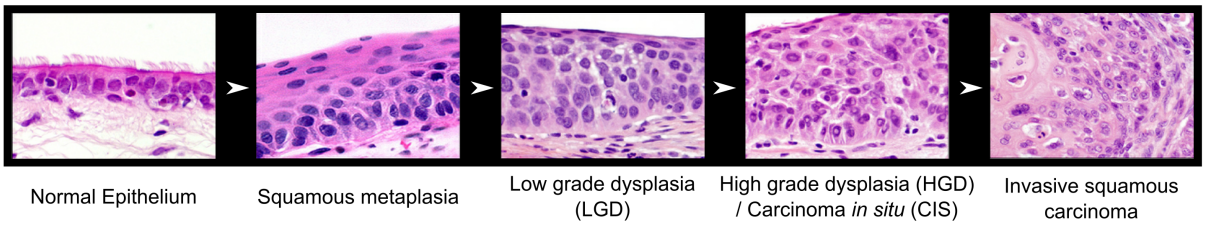

Figure 1.3: Histological progression involved in the pathogenesis of SQC. Progression of histological changes from normal bronchial epithelium through squamous metaplasia, dysplasias, carcinoma *in situ* and invasive SQC. Adapted from (Wistuba, 2012).

1.3.2 Field cancerisation

The term "field cancerisation" refers to areas of epithelial surface adjacent to neoplastic lesions that appear histologically normal and share molecular abnormalities found in tumours. These molecular changes precede the onset of histological changes (Franklin et al., 1997; Wistuba et al., 1999). A study using whole-transcriptome expression profiling in NSCLC tumours and cytologically normal control samples of the airway at varying distances from the tumours showed differentially expressed gene patterns that could distinguish smokers with and without lung cancers, as well as gradient airway expression patterns where marker expression in the airways increased as the distance to the tumour decreased (Kadara et al., 2014). The field cancerisation principle was used to develop a gene expression classifier in cells taken from bronchial brushings in the main stem bronchus that could assess the probability of lung cancer (Elashoff et al., 2015). This classifier, based on the expression of 26 genes and patient age, increased the diagnostic performance of bronchoscopy and had high sensitivity across different lesion sizes, location and cell type. It has the potential to lower the number of more invasive procedures following a bronchoscopy that may show benign lesions.

McCaughan et al. (2011) demonstrated in a small, longitudinal cohort that "field cancerisation" can arise from pre-invasive clonal expansion and subsequent dispersal of cells around the epithelial airways. An earlier, single clinical case example of this was demonstrated showing an identical point mutation in *TP53* at multiple sites across the entire tracheobronchial tree, with no tumour present, suggesting a single progenitor epithelial

clone may migrate and populate other areas of the bronchial mucosa (Franklin et al., 1997).

These studies show that pre-invasive lesions may provide clinical opportunities for early detection or chemoprevention in individuals at high risk of SQC, such as long-term smokers.

1.3.3 Loss of heterozygosity (LOH) and deletions characterise the earliest stages of SQC

Analysis of preneoplastic lesions, CIS, and invasive carcinoma from surgically resected tumours show increases in locus specific LOH associated with histological progression. LOH refers to a genetic event that results in a loss of an allele, leading to haploinsufficiency or loss of gene expression. Early and frequent alterations include allelic losses on 3p (3p21, 3p22-24, 3p25) and 9p21 (*CDKN2A*) (Mao et al., 1997; Wistuba et al., 1999).

Wistuba et al. (1999) note that in 30% of histologically normal foci there was allelic loss at one or more chromosomal regions. Losses at other 3p regions occurred only in more advanced lesions (dysplasias and CIS), as well as in the *TP53* gene. Deletions of parts of 13q (*RB* gene coding Rb protein) were almost entirely associated with invasive carcinoma.

1.3.4 Consistent *TP53* mutation

Disrupted *TP53* has been identified as a key, early molecular event (Franklin et al., 1997; McCaughan et al., 2011; Teixeira et al., 2019). This has been found in both pre-invasive lesions and dysplasias, and consistently suggest that *TP53* mutations are acquired at an early stage, indicating that it offers a key advantage and clonal survival benefit (Sundaresan et al., 1992; Zheng et al., 1994). Taken together with *TP53* disruption seen in all CIS and tumours with metastasis in a 1994 study, and in 90% of tumours in the TCGA, it implies persistence and requirement for *TP53* mutation in the progression of SQC (Zheng et al., 1994; Hammerman et al., 2012).

1.3.5 Amplification events in the progression of preinvasive SQC

In bronchoscopic studies, low grade dysplasias are found much more frequently than high grade dysplasias, suggesting that small numbers of low grade lesions acquire advantageous genetic alterations in order for progression to high grade dysplasia (George et al., 2007). Upon follow up of lesions, half of the patients with high grade lesions progressed to develop lung cancer 2 years after the initial consultation, while none of the low grade lesions progressed to invasive carcinoma during the follow up period.

Another longitudinal study that followed patients with low and high grade dysplasia looked at chromosome 3 profiles. They found that all low grade lesions carried normal copy numbers of chromosome 3, but all high grade lesions had 3q amplifications, suggesting that there was a critical point between these histological stages where 3q amplification was required for progression (McCaughan et al., 2010). Amplification and copy number variations proved to be an accurate biomarker for assessing the progression risk of dysplastic lesions in the bronchial epithelium (Van Boerdonk et al., 2014; Teixeira et al., 2019) (Figure 1.4).

Further investigations found that in a number of individuals clinical progression of high grade dysplasia was associated with incremental amplification of *SOX2*, offering evidence for the role of *SOX2* amplification in promoting disease progression (McCaughan et al., 2010). *SOX2* amplification was also associated with overexpression, analysed by IHC staining.

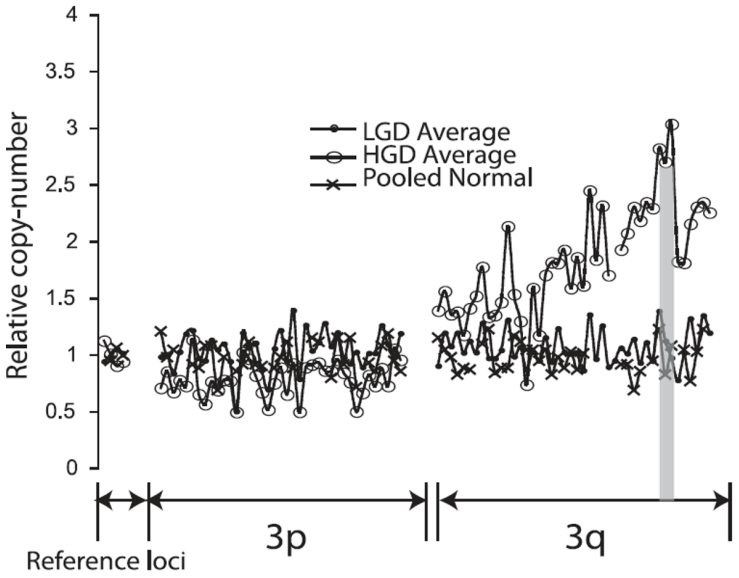

Figure 1.4: High grade bronchial dysplasias show amplification of 3q, low grade dysplasias show normal copy number of 3q.
Pooled averages of relative copy numbers across chromosome 3 in low grade and high grade bronchial dysplasia biopsies. Adapted from (McCaughan et al., 2010).

SOX2 expression has been analysed in a range of NSCLC biopsies (Yuan et al., 2010). SOX2 was significantly elevated in 31/32 squamous dysplasia and CIS compared to normal bronchial epithelia. SOX2 is implicated as a driver oncogene in the histological progression of bronchial dysplasia in preinvasive early SQC. In an *in vitro* organotypic model using human bronchial epithelial cells developed in my lab, SOX2 overexpression combined with loss of p53 in the correct microenvironmental setting drives a dysplastic phenotype that phenocopies the human disease (Correia et al., 2017). This organotypic model will be used throughout this thesis to address my aims.

p63 is a transcription factor and is a homologue of p53, but in contrast to p53, loss of function mutations in p63 are extremely rare in cancer (Hagiwara et al., 1999). p63 copy number increases are found in almost all SQC tumour samples and very rarely in adenocarcinoma samples (Massion et al., 2003a). Copy number increases were greater in lesions graded severe dysplasia or high, and was accompanied by higher expression. p63, overexpressed in many head and neck squamous cell carcinomas (HNSCC), was found to promote survival in HNSCC lines by suppressing p73-dependent apoptotic signals (Rocco et al., 2006). Another study by Ye et al. (2014) show that p63 promoted proliferation via the AKT pathway in esophageal squamous cell lines, knockdown of p63

reduced proliferation together with pAKT. These studies suggest that p63 amplification or overexpression in squamous cell carcinomas may play an early role in the pathogenesis of SQC.

Similar genomic and genetic alterations associated with progression of preinvasive SQC have been identified in esophageal squamous cell carcinomas (ESCC). 3q amplification has been demonstrated in ESCC (Chang et al., 2010) (Weiss et al., 2003), as well as common deletion or mutation of *CDKN2A* and *TP53* early in the progression of ESCC tumours (Yang et al., 2017a). Gen et al. (2010b) identified *SOX2* as the target gene in 3q amplification in ESCC, and showed that 62/89 ESCC tumours overexpressed SOX2. The similarity between the progression of SQC and ESCC is important, it enables the study of SOX2 amplified squamous cell carcinomas to be applied to both the lung and the esophagus.

1.4 SOX2

1.4.1 SOX2 structure and DNA binding

SOX genes encode a family of pleiotropic transcriptional regulator proteins, of which there are 20 members. They are characterised by a highly conserved high mobility group (HMG) DNA binding domain made up of around 80 amino acids (Bowles et al., 2000) (Figure 1.5A). The HMG domain was first identified in *Sry*, a gene responsible for the initiation of male sex determination (Gubbay et al., 1990). SOX proteins bind to DNA specific sequence motifs through their HMG domain, consisting of three α helices (Kamachi and Kondoh, 2013) (Figure 1.5B). Binding of SOX proteins alone is not sufficient to activate transcription, and requires formation of a protein complex with other factors (Kamachi et al., 2000).

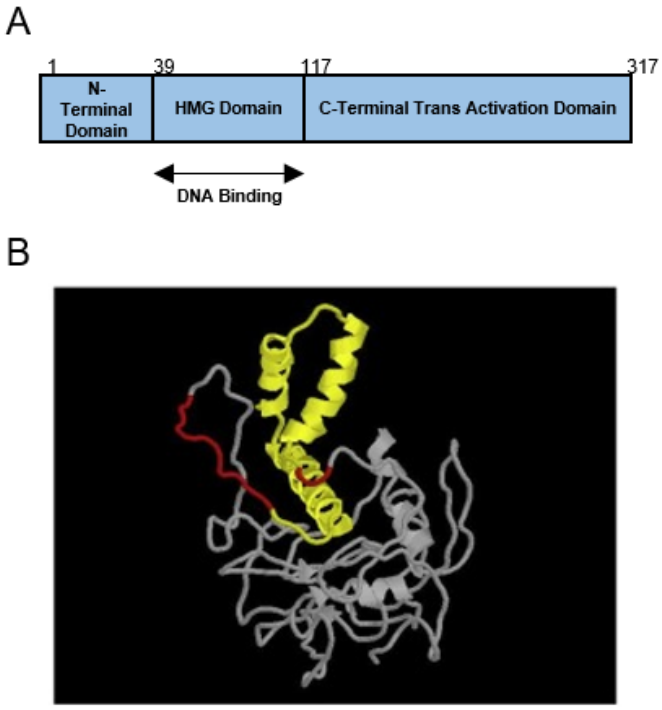

Figure 1.5: SOX2 protein domains and 3D structure.
A. Schematic of human SOX2 protein domains adapted from (Schaefer and Lengerke, 2019). **B.** 3D crystal structure of human SOX2 protein modulated with RasMol, yellow indicates the HMG domain, adapted from (Novak et al., 2019).

SOX2 is a single exon, intronless gene and is one of the 4 "Yamanaka Factors" (SOX2, OCT4, c-MYC and KLF4). Together, these reprogram somatic cells to embryonic-like state induced pluripotent stem cells (iPSCs) (Takahashi and Yamanaka, 2006). SOX2 functions in a number of different cellular and tissue specific roles. This is mediated by tissue or cell-type specific co-factors (Kamachi et al., 2000). Distinct SOX2 binding partners have been found in a range of cellular contexts; SOX2-OCT4 in embryonic stem cells (Boyer et al., 2005), SOX2-BRN2 in neural progenitor cells (Tanaka et al., 2004) and SOX2-p63 in squamous carcinoma cells of the lung and esophagus (Watanabe et al., 2014).

1.4.2 SOX2 in development

SOX2$^{-/-}$ mice are embryonically lethal, and show essential roles for SOX2 in embryonic development (Avilion et al., 2003). SOX2 is essential in maintaining pluripotency in human

ES cells (hESCs), reduction of SOX2 in hESCs results in differentiation into primarily cells of the trophectoderm and loss of stem cell antigen expression (Fong et al., 2008). SOX2 stabilises the pluripotent state of ES cells by maintaining sufficient OCT4 levels (Masui et al., 2007).

Controlling SOX2 levels is very important, small increases in SOX2 protein trigger ESCs to begin differentiation into cells with neuroectoderm, mesoderm and trophectoderm associated markers, highlighting a critical role for SOX2 regulation within defined limits in development (Kopp et al., 2008).

SOX2 is important in the maintenance of adult stem cells of different tissues such as; brain, trachea, retina, cervix, bronchial epithelium and esophagus (Arnold et al., 2011). SOX2 has a critical role in squamous differentiation of the airways (Gontan et al., 2008; Que et al., 2009).

1.4.3 SOX2 in lung development

SOX2 is very important in the development of the lung, studied using mouse models. Deletion of SOX2 in the ventral epithelial domain of the anterior foregut (precursor to lungs and esophagus) leads to death at birth from respiratory failure as a result of abnormal differentiation of the tracheal cartilage (Que et al., 2009). The tracheal epithelia are also abnormally differentiated, with increased mucus producing cells and reduced numbers of basal, ciliated and club cells compared to wild-type. When SOX2 was deleted in adult mice, the basal cells of the airway epithelium showed a reduced capacity to proliferate, and *in vivo* responses to airway injuries show a reduced rate of repair following injury and reduction in differentiated cell populations.

In addition to this, when SOX2 is overexpressed during embryonic lung development branching and formation of bronchial-alveolar structures is inhibited (Gontan et al., 2008). There is a requirement for SOX2 levels to drop and respond to branch inducing signals, initiating branching morphogenesis of the lung. Tight regulation of SOX2 is maintained in the adult lung too, proximal airways are defined by SOX2 expression, while distal airways are defined by SOX9 expression (Mccauley et al., 2017).

1.4.4 SOX2 is a lineage survival oncogene

I have already discussed the essential role for SOX2 in stem cell maintenance and squamous differentiation (Section 1.4.2). The deregulation of SOX2 has been associated with the development of squamous cell carcinomas of the esophagus, lung (Bass et al., 2009), oral cavity (Ren et al., 2016), head & neck (Lee et al., 2014) and skin (Siegle et al., 2014). These observations are consistent with a role as a lineage survival oncogene. These are genes that are critical during development and promote proliferation of cells destined to a particular cell lineage, that gain oncogenic properties through deregulation of the lineage-survival mechanisms promoting tumour progression (Garraway and Sellers, 2006).

Bass et al. (2009) demonstrated that SOX2 is a lineage-survival oncogene in lung and esophageal squamous cell carcinomas, promoted squamous identity via induction of *TP63* and *KRT6A* when ectopically expressed in ADC cell lines, and showed the largest anti-proliferative effect of all genes tested from around the 3q26.33 amplification peak when suppressed in sqaumous lung or esophagus cell lines harbouring 3q amplification. They also showed that tumours expressing *SOX2* at high levels showed expression of both squamous differentiation (*TP63* and *KRT6A* correlated with *SOX2* expression in lung SQC tumours) and ESC-signatures. Although no significant association was found with SOX2 amplification or expression with clinical grade of tumours.

1.5 Impacts of SOX2 deregulation in cancer

Cancer is characterised by a number of hallmarks that comprise biological capabilities acquired during development of tumours (Hanahan and Weinberg, 2011). These include; sustaining proliferative signalling, evading growth suppressors, activating invasion, genome instability, resisting cell death, deregulating cellular energetics. Due to the pleiotropic nature of SOX2, its deregulation has been implicated in the mediation of multiple hallmarks of cancer. The following sections discuss the impacts of SOX2 deregulation in cancers, in particular, proliferation, apoptosis and migration, summarised (Figure 1.6).

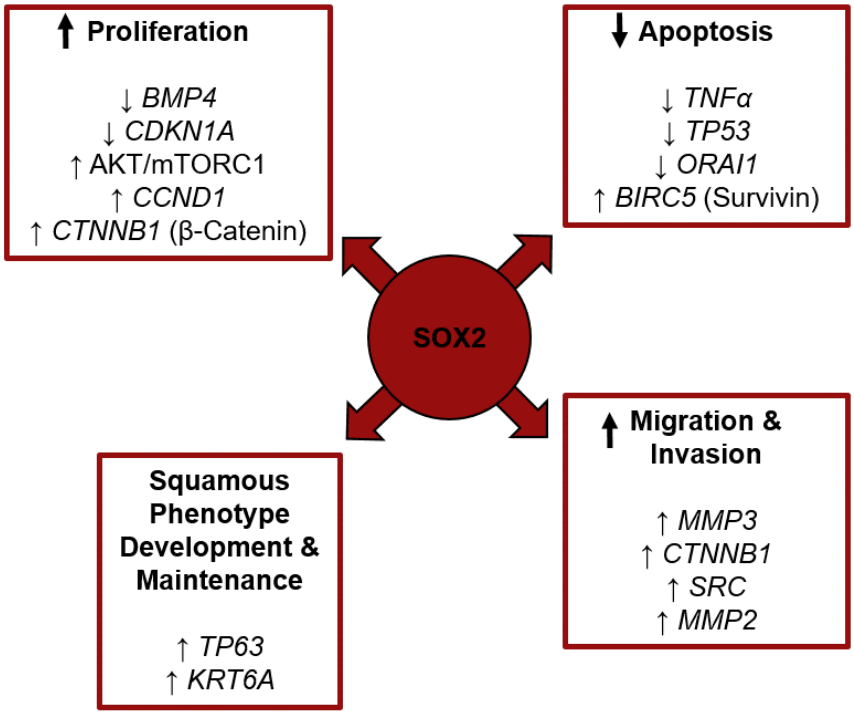

Figure 1.6: Cellular processes impacted by deregulated SOX2 in various types of cancer.
A summary of some of the downstream impacts of SOX2 deregulation in cancers, discussed in Section 1.5.

1.5.1 Proliferation

SOX2 has been associated with proliferation in a number of cancer types, with a range of mechanisms. In both *in vitro* and *in vivo* xenograft studies, SOX2 promoted proliferation and survival in NSCLC derived cells (Chou et al., 2013). SOX2 has been found to promote the growth of lung SQC via downstream suppression of bone morphogenetic protein 4 (BMP4) (Fang et al., 2014). Cell line studies, xenograft models and clinical specimens showed BMP4 downregulation when SOX2 was expressed, and that reactivation of BMP4 could account for growth inhibition.

Growth was sustained in lung SQC via specific downregulation of CDKN1A, a cyclin dependent kinase inhibitor, by SOX2 showing the tumorigenic effect of SOX2 in SQC (Fukazawa et al., 2016). A study in esophageal cancer shows that high SOX2 expression promoted proliferation and invasion in clinical specimens and cell line studies (Wang et al., 2014b).

SOX2 has been shown to promote proliferation *in vitro* and *in vivo* of esophageal squamous cell carcinomas through activation of the AKT/mTORC1 pathway (Gen et al., 2013). Further studies in breast cancers show SOX2 promoting cellular proliferation and tumorigenesis, facilitating the G1/S transition by upregulating cyclin D1 (Chen et al., 2008).

1.5.2 Apoptosis

SOX2 has been shown to exert many anti-apoptotic effects in cancer and enables evasion of apoptosis. Silencing SOX2 in NSCLC cells leads to upregulation of key apoptotic inducers, tumour necrosis factor-α (TNF-α) and p53 (Chen et al., 2013). This was combined with a decrease of survivin expression, rescue experiments demonstrated that ectopic survivin blocked SOX2-silencing-mediated cell death. SOX2 is necessary for the evasion of apoptosis in prostate cancer cells (Lin et al., 2012). SOX2 knockdown induced apoptosis via upregulation of p27, down regulating cyclin E and inhibiting survivin.

Apoptosis-resistant properties of prostate cancer cells have also been shown to be mediated by SOX2 (Jia et al., 2011). This was through deregulation of store-operated Ca^{2+} entry by downregulation of ORAI1 by SOX2, a process that has been shown to confer resistance to apoptosis (Abeele et al., 2003).

1.5.3 Migration and invasion

SOX2 has been implicated to increase the migratory and invasiveness of cancer cells. Mouse lung carcinoma cell lines with down regulated SOX2 significantly suppressed the metastatic potential when injected into syngeneic mice (Xiang et al., 2011). A panel of serous ovarian carcinoma tissues showed that overexpression of SOX2 related to increased migration and invasion phenotypes, and suggested that SOX2 targets Src kinase that is involved in cell migration, invasion and adhesion in serous ovarian carcinoma cells (Wang et al., 2014a).

Exogenous expression of SOX2 in laryngeal squamous cell carcinoma cells promoted a β-catenin dependent increase in migratory and invasive capabilities (Yang et al., 2014).

Tumour cell invasiveness has been shown to decrease 4.5-fold in melanoma cells that constitutively express high levels of SOX2 when SOX2 was knocked down (Girouard et al., 2012). Conversely, in the same study a melanoma cell line that normally expresses low levels of SOX2 was transduced to overexpress SOX2, promoting cell invasiveness nearly 4-fold. The reduction in invasiveness in the first cell line as a result of SOX2 reduction was suggested to be mediated by matrix metalloproteinase 3 (MMP3), and investigations using clinical samples showed correlations between SOX2 and MMP3 expressing cells in tumour edges infiltrating into the surrounding stroma.

1.5.4 Squamous tumour phenotype

SOX2 plays an essential role in developing the squamous identity of tumours and cancer cells. The squamous markers of differentiation, p63 and cytokeratin 6A, show correlation with SOX2 expression in SQCs (Bass et al., 2009). Furthermore, ectopic expression of SOX2 in ADC cell lines induces the expression of p63 and cytokeratin 6A, demonstrating the role that SOX2 promotes squamous identity.

Ferone et al. (2016) provide further evidence for SOX2 defining squamous differentiation using a *Pten;Cdkn2ab*-deficient mouse model. Overexpression of SOX2 in club cells or AT2 cells, the peripheral alveolar stem cells and cells of orgin for ADC, induced peripheral SQC rather than ADC. This demonstrates that SOX2 is able to determine squamous tumours regardless of the targeted lung stem cell population.

In a study using a KRAS-driven mouse model of ADC, SOX2 overexpression led to an increased tumour-associated neutrophil infiltrate, together with an adeno-squamous transdifferentiation (Mollaoglu et al., 2018). ADC and SQC tumours have distinct tumour immune microenvironments and this study suggests that SOX2 orchestrates this process, which in turn, impacts the identity of the tumour.

1.6 Preventative and therapeutic strategies for SQC

1.6.1 Smoking Cessation

Across the globe it was suggested that 4.83 million premature deaths were attributable to smoking in the year 2000 (Ezzati and Lopez, 2003). Lung cancer was responsible for 17.5% of the premature deaths worldwide and was in the top three leading causes of death, along with cardiovascular disease and chronic obstructive pulmonary disease (COPD).

In a study focussing on the US, hazard ratios were calculated by comparing deaths among current smokers and those that have never smoked. Lung cancer was associated with the highest hazard ratio for death among smokers as well as former smokers (Jha et al., 2013). However, there is significant data to show that smoking cessation drastically improves overall survival. The earlier in adulthood that smokers quit, the more that overall lifespan is increased (Jha et al., 2013). Adults that quit smoking between the ages of 25-34 had almost identical survival curves to non-smokers, this concurs with figures from the UK since 1950 (Figure 1.7). The airways of current smokers have been shown to have an increased proliferative index, an effect that lasts many years in former smokers but overall gradually decreases following smoking cessation (Lee et al., 2001).

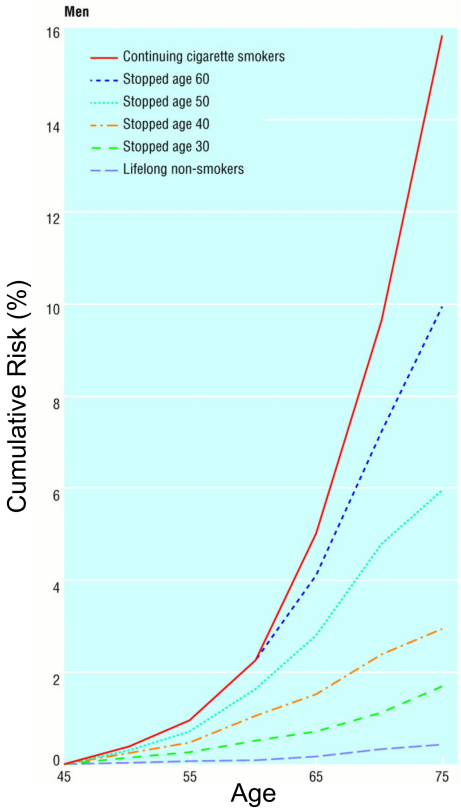

Figure 1.7: Smoking cessation reduces the risk of death from lung cancer later in life.
The reduction in risk of death from lung cancer is enhanced the earlier in life that individuals quit smoking. Adapted from (Peto et al., 2000), representing data from the UK.

1.6.2 Current therapeutic options

Patients with SQC have few treatment options. When detected at an early stage, the most successful treatment option for patients with SQC is surgical resection, and is the primary mode of treatment in early stage NSCLC (Lackey and Donington, 2013). However, there are limited options with later stage disease and often palliative care involving general cytotoxic chemotherapy and radiotherapy are the only options. Here, both targeted and non-targeted therapies will be discussed.

Non-targeted therapies

There have been advancements in NSCLC chemotherapy regimens in the last 2 decades with the introduction of platinum doublets, a combination of a platinum-based compound

such as cisplatin or carboplatin with a third generation agent such as gemcitabine. These regimens have contributed to a significant increase in efficacy compared to single agent therapies, but SQC-specific chemotherapy headway has stalled. Overall progress in this area has been in response rates and increased tolerability, with no significant increases in survival rates (Baxevanos and Mountzios, 2018).

It is important to note that squamous and non-squamous NSCLC disease should not be regarded as the same. There are distinct differences in both histopathological features and mutational profiles, and this should be reflected in targeted treatments (Cheng et al., 2016). This has been demonstrated in recent years by advances in FDA approved first-line treatment option for patients with non-squamous NSCLC, such as Pemetrexed (chemotherapy), Bevacizumab (VEGF inhibitor) and Pembrolizumab (PD1 inhibitor), but just one FDA approved first line treatment option for SQC, Necitumab (EGFR inhibitor), discussed in the next section (Thatcher et al., 2015). This presents a clear unmet need to improve the first line treatment of patients with squamous subtype NSCLC.

Targeted therapies

EGFR inhibition

Epidermal growth factor receptor (EGFR) is mutated in only 4% of SQC, and is more commonly mutated in ADC (Hammerman et al., 2012). However, overexpression of EGFR is more frequent in SQCs than ADC (Prabhakar, 2015). A number of EGFR inhibitors have been taken into clinical trials for NSCLC.

Erlotinib, a first generation EGFR small molecule inhibitor, was compared against standard second line treatment option docetaxel in patients with advanced squamous cell lung cancers (Peters et al., 2017). Erlotinib showed no benefits in progression free survival. Subsequently, next generation EGFR inhibitors were developed.

Yang et al. (2017b) systematically review existing studies using Erlotinib and Gefitinib (both first generation EGFR inhibitors) and Afatinib (second generation inhibitor) in the treatment of NSCLC. The efficacies of Erlotinib and Gefitinib were comparible, however,

the safety profile of Gefitinib was more favourable than Erlotinib. Afatinib did not show greater efficacy than the first generation inhibitors, it showed marginal increases in effectiveness as a second line treatment against NSCLC patients with advanced squamous cell cancers. In the UK, NICE (National Institute for Health and Care Excellence) guidance recommends Afatinib for the treatment of EGFR mutation-positive locally advanced or metastatic NSCLC (NICE, 2019). As this mutation is uncommon in squamous NSCLC it does not make for a broad treatment option for SQC.

Necitumumab, a second generation EGFR targeting monoclonal antibody, was found to significantly increase overall survival in patients with advanced SQC when combined with a platinum doublet, compared to platinum doublet alone. A significant 1.6 months increase in median overall survival was observed (Thatcher et al., 2015). Necitumumab used in combination with Gemcitabine and Cisplatin received FDA approval to be used as first line treatment in advanced squamous cell lung cancer in 2015. This treatment combination is not approved for use in the UK on the NHS, as EGFR expression testing for SQC tumours is not widely used, no improvement in quality of life despite survival benefit and lacking cost effectiveness for NHS resources (NICE, 2019).

Cetuximab, a monoclonal antibody targeting EGFR, showed promising data in SQC subpopulations in a recent phase III trial. Patients with SQC subtype and EGFR-FISH positivity showed a doubling of median overall survival when treated with Cetuximab when compared to control groups (Herbst et al., 2018). Overall survival was defined as the duration from registration to the trial to death due to any cause. With the study's co-primary objectives regarding progression free survival in EGFR positive patients and overall survival in the entire study population not being met, Cetuximab was deemed not suitable for treatment of NSCLC, however it did offer some support for future late stage SQC targeted therapies to continue to be pursued.

FGFR inhibition

Fibroblast growth factor receptor (FGFR) is a tyrosine kinase involved in cell proliferation, differentiation, angiogenesis and migration. Alterations in the FGFR family, amplification

or mutation, occurs in 20% of squamous cell lung cancers, making it an attractive target for the disease (Hashemi-Sadraei and Hanna, 2017).

A number of FGFR inhibitors have made it to the clinic. Notably a phase II study using AZD4547, an FGFR1/2/3 selective inhibitor, took a cohort of advanced squamous NSCLC patients with FGFR positive tumours. Although there was an acceptable safety profile for AZD4547, the cohort showed minimal activity with FGFR inhibition and was therapeutically inadequate (Aggarwal et al., 2017).

PI3K inhibition

Buparlisib, a pan-PI3K inhibitor was tested in the Phase II study BASALT-1. NSCLC patients were selected based on PI3K pathway activation then split into squamous and non-squamous groups for treatment. However no improvement in clinical outcome was met when compared with existing chemotherapeutic strategies (Vansteenkiste et al., 2015).

Taselisib, a class I PI3K α inhibitor, was tested as part of a phase II sub-study of the Lung-MAP umbrella trial (Clinical Trials ID NCT02785913). Advanced SQC patients with *PIK3CA* mutations were selected for treatment with Taselisib and compared to docetaxel treatment. This study failed to meet its primary endpoint of response rate using the response evaluation criteria in solid tumours (RECIST) rules in a subset of *PIK3CA* mutation positive patients, and was subsequently closed (Langer et al., 2019).

PD-1 inhibition

In recent years checkpoint inhibitor therapies targeting programmed cell death protein 1 (PD1) and cytotoxic T-lymphocyte-associated protein 4 (CTLA-4) has been an area of focus. PD1 and CTLA-4 are expressed on the surface of activated T cells, they act as “immune checkpoints” that regulate immune response (Figure 1.8). Cancer cells can evade this immune response by expressing extracellular ligands, inhibiting the anti-tumour T cell response (Peters et al., 2018).

The FDA approved Nivolumab, a human anti-PD1 monoclonal antibody, for use as a second line treatment for SQC in 2015. Patients receiving Nivolumab showed a 3.2 month increase in overall survival compared to standard of care second line treatment with docetaxel (Gandara et al., 2015). Subsequently, in 2017, NICE Guidance recommended Nivolumab use in locally advanced or metastatic SQC after chemotherapy.

Another FDA approved human anti-PD1 monoclonal antibody, Pembrolizumab, has shown promising efficacy in both first and second line treatments for patients with advanced NSCLCs (Peters et al., 2018). However, survival benefits were only shown in patients with non-squamous tumour type, the squamous tumour type patients showed no statistical increase in survival.

PD-L1 inhibition

Atezolizumab is the first PD-L1 inhibitor to be approved by the FDA for metastatic NSCLC patients. This monoclonal antibody therapy showed benefits in overall survival and progression free survival when compared to standard of care second line treatment with docetaxel (Seetharamu et al., 2017). Atezolizumab shows efficacy in both squamous and non-squamous tumour types, as well as efficacy in patients regardless of their PD-L1 expression status.

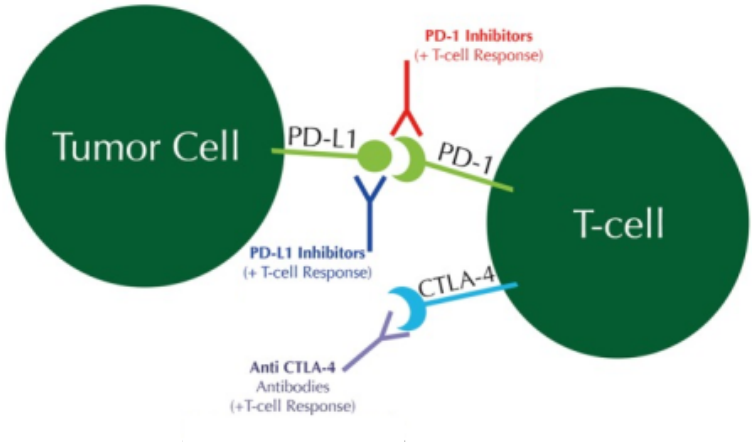

Figure 1.8: Immune checkpoints PD1 and CTLA-4 in activated T cells
Activated T cells express PD-1 and CTLA-4. Tumour cells can express PD-L1, which interacts with PD1 on active T cells leading to suppression of the anti-tumor T cell response. CTLA-4 is expressed in activated T cells and is a negative regulatory molecule against T cell response. Blocking CTLA-4 activates the anti-tumour T cell response by increasing the ratio of effector T cells to negative regulatory T cells. Adapted from (Derman et al., 2015).

National Lung Matrix Trial

A “basket trial” is a type of multi-arm trial, where patients are not randomized, but instead stratified into different arms based on some kind of genetic marker. Patient groups are tested with treatments targeted to the particular genetic marker, rather than the tumour type. The National Lung Matrix Trial is a “basket trial” seeking to increase the numbers of actionable genetic abnormalities in NSCLCs (ClinicalTrials.gov Identifier: NCT02664935). Patients are divided into treatment arms based on their tumour genetics, and treatments targeted accordingly. This trial started in 2015 and is due to complete in 2021 and currently has no published results. 10 treatment regimens are being trialled including; FGFR, mTORC1/2, MEK and AKT inhibitors.

1.6.3 Early Detection

One suggested way to lower SQC mortality rates is via early detection of cancer, as early stage disease is commonly asymptomatic and therefore often presents at an advanced stage when many treatments are ineffective (Blandin Knight et al., 2017).

The national lung screening trial (NLST), a United States-based trial, compared low dose CT and X-ray screening approaches. 53,454 asymptomatic participants considered to be at high risk for lung cancer were randomized to CT or X-ray screening annually for 3 years. Study follow up after 7 years showed participants in the CT screening group had 15-20% lower risk of dying from lung cancer than those in the X-ray group (Aberle et al., 2011).

The NELSON CT screening trial was a large programme that recruited 15,792 asymptomatic participants in The Netherlands and Belgium considered to be at high risk for lung cancer. Participants were randomized to CT scans at baseline, 1, 3 and 5.5 years after randomization. Study follow up after ten years show that lung cancer deaths were reduced by a highly significant 26% compared to control group (De Koning et al., 2018).

Although CT scans have shown to be more effective than X-rays in lung screening approaches, and lung cancer related deaths can be reduced with regular screening, there are a number of reasons opposing the implementation of lung cancer screening programmes. A key issue for healthcare systems is that in order for screening to be effective, high numbers of patients must be screened. This is at great expense to health care systems, not only financially but in resources and labour. Low dose CT scans still carry radiation risks, and more scans increases patients exposure to radiation that may cause lung damage. However if high risk groups are targeted, the benefits would far outweigh the low risk involved. CT scanning, particularly in the National Lung Matrix Trial, produced a high rate of false positives. This brings unnecessary distress to the patients involved and requires further procedures. However, the large majority were correctly identified as benign nodules, using non-invasive techniques.

One method explored to lower false positive rates used a plasma microRNA signature classifier (MSC). The MSC was retrospectively evaluated on samples collected from a screening trial using low dose CT scanning, and when both the MSC and CT scanning was combined a five-fold reduction in false positive rates from CT scanning alone was observed (Sozzi et al., 2014).

1.6.4 Chemoprevention

Chemoprevention is the use of agents to reverse or inhibit the progression of a disease, in this case, lung cancer. Chemoprevention agents have been very successful in cardiovascular disease, significantly reducing deaths from myocardial infarction and strokes (Sporn and Liby, 2005). Drugs that suppress cholesterol synthesis, inhibit platelet aggregation and lower blood pressure have all contributed to a significant reduction in cardiovascular mortality. The first statin, lovastatin, was FDA approved for use in chemoprevention of cardiovascular disease in 1987. However, chemoprevention of cancer is far behind that of cardiovascular disease. This is in part due to a lack of surrogate biomarkers that can provide readouts of efficacy for preventing cancer. In the case of cardiovascular disease, blood pressure and low-density cholesterol are considered very reliable surrogate biomarkers for cardiovascular disease, showing a clear relationship between disease and biomarker status, both of which can be quantified and monitored with ease (Albert, 2011).

One of the most successful cancer chemoprevention strategies to date has been tamoxifen for the prevention of breast cancer (Fisher et al., 1998). Women at increased risk of developing breast cancer administered daily tamoxifen for 5 years showed significant decreases in invasive and non-invasive breast cancer compared to placebo control groups, and showed no increased risk to other disease such as ischemic heart disease, and colon, rectal or ovarian cancers. Another example of successful chemoprevention of cancer lies with long term use of aspirin and the reduction in the risk of developing colorectal cancer (Drew et al., 2016). In 2015 the United States Preventive Services Task Force (USPSTF) included recommendation for routine low dose aspirin for the primary chemoprevention of colorectal cancer.

As discussed in section 1.1.1, lung cancer is the leading cause of cancer mortality in the world, and efforts to improve overall survival rates have not been as successful as those seen in other common cancers such as breast, prostate and colon. This is in part due to lung cancer patients often presenting symptoms at an advanced stage where surgical cure is no longer an option. However, 80-90% of lung cancers are associated with smoking and exposure to tobacco smoke, and generally occur in patients over the

age of 50. Therefore potential chemoprevention therapies could be targeted to patients at a high risk of developing cancer.

The concept of chemoprevention can be split into three subgroups, primary, secondary and tertiary chemoprevention. Primary chemoprevention aims to treat patients that are at high risk of cancer, but have no history of the disease and show no signs of premalignancy. In the case of lung cancer, patients that could be suitable for primary chemoprevention strategies would be current or former heavy smokers. Secondary chemoprevention aims to treat patients who have documented preinvasive disease. In the case of lung cancer, patients with evidence of bronchial dysplasia may be suitable for secondary chemoprevention agents. Tertiary chemoprevention aims to prevent recurrence or second primary tumours in patients that have had successful treatment for early cancer (Keith and Miller, 2013).

Although many chemoprevention agents have shown promise in pre-clinical models and *in vivo* models, the majority of phase III clinical trials in cancer chemoprevention completed to date have been negative. Challenges in progressing the field of cancer chemoprevention has been attributed to a number of factors; latency of cancer being much longer than clinical trial length, numbers of clinical trial participants having to be extremely large in order to generate a positive result due to low incidence of cancer (even in high-risk populations), and long term safety and side effect follow up data (Benetou et al., 2015). It is important to consider that preventative therapies should have favourable risk-benefit ratios. In other words, patients who are otherwise healthy and taking a primary chemoprevention agent would require an extremely low risk of side effects and toxicities, whereas secondary or tertiary chemoprevention agents in people with greater risks of developing cancer may warrant slightly higher risks of side effects. This makes considerations for new therapeutic compounds in this field difficult, as the long term safety data is not available, and the long-term, large scale clinical trials required to collect this data would be too expensive.

A study using myo-inositol, a compound with a similar structure to the head group of PI3K substrate phosphatidylinositol, showed regression of bronchial dysplasia in 6 out of 9 smokers treated, and an increase in expression of genes that are repressed upon PI3K

activation (Gustafson et al., 2010). Following this small scale trial, myo-inositol was taken into phase IIb clinical trials, but the responses in the myo-inositol group compared to the placebo control group were not statistically significant. A more targeted chemoprevention approach was proposed (Lam et al., 2016).

A number of other chemoprevention agents have been used in phase III clinical trials for lung cancer including, aspirin, beta carotene, retinol, vitamin E, 13-cis-retinoic acid and selenium, but all gave negative results, and in trials using beta carotene, incidence of lung cancer actually increased in cohorts of smokers (Keith and Miller, 2013). Although, to date, there has been no successful phase III trials for the chemoprevention of lung cancer, it remains an attractive goal. The chemoprevention trials discussed by Keith and Miller (2013) included many fundamental flaws and therefore do not faithfully represent the potential for chemoprevention of lung cancer. Chemoprevention trials cost a lot of money due to the large cohorts required to pick up cancers on a population level and require long periods of time for participant follow up to monitor effects on cancer incidence, that may take decades to present. There is still a lack of suitable, robust pharmacodynamic biomarkers to better monitor the efficacy of interventions in chemoprevention trials. Many of the trials reviewed did not include appropriate dosing of compounds, only including one dose with no evidence of efficacy at that dose, and with short-term treatment windows. Trials also used un-targeted patient cohorts, not those with increased risk of developing lung cancer. Participant follow up periods were often far too short to pick up any reduction in disease. The ideal chemopreventative agent would be well tolerated, the lung has a key advantage to reduce toxicity and minimise adverse effects whilst maintaining efficacy. The administration of therapeutics via inhalation and localised delivery as opposed to systemic administration would reduce systemic side effects and increase tolerability (Marko et al., 2000).

1.7 Modelling SQC *in vitro* and *in vivo*

Modelling SQC is required to further understand the pathogenesis of the disease and to identify new targets that could be targeted therapeutically for chemoprevention strategies

of pre-invasive disease and therapeutic strategies for advanced disease. *In vitro* and *in vivo* models provide advantages and disadvantages for studying disease.

In vitro models have advanced considerably from the conventional 2D submerged cultures on plastic that were almost exclusively used in the last century. Advances in tissue culture techniques involving genetic manipulation/control, 3D culturing, co-cultured additional cell types and matrices, have all enabled human disease to be recapitulated in a more physiologically relevant manner. *In vitro* models have advantages over *in vivo* models that include, lower costs, increased throughput, ease of genetic manipulation and use of human cells.

One of the main advantages of *in vivo* modelling is that it can enable the user to study tumour initiation very closely, in the correct microenvironmental context with added complexities of stromal and immune system interactions.

1.7.1 Organotypic culture models of bronchial epithelium

Rodent models have been crucial in advancing our understanding of lung development and disease, however, there are a number of differences between animal and human physiologies that necessitate human based models to complement mouse models. Human lungs have anatomical differences in the localization of stem and progenitor cells compared to rodents. Basal cells are the resident stem cells that regenerate epithelial lineages in the lung. In humans basal cells are present in the whole airway, however in rodents these cells are only present in the trachea (Boers et al., 1998). Humans also have more goblet cells and markedly fewer Clara cells than rodents (Rock et al., 2010).

Advancements in tissue engineering have enabled more complex models of the human bronchial epithelium to be developed. A key development was the introduction of the "Whitcutt Chamber" in 1988 that enabled cells to be cultured at the air-liquid interface (ALI), monolayers were exposed to air on the apical side and provided with nutrients from media on the basal side (Whitcutt et al., 1988). This enabled differentiation of airway cells taken from bronchial brushings or isolation from donated cadaver airways. The basic

model system has enabled researchers to use the system for a diverse set of applications ranging from drug screening, inhalation toxicology and basic research (Yamaya et al., 1992; Neuberger et al., 2011; Kastner et al., 2013).

A monolayer culture exposed to air on a flat membrane has many advantages including low cost and ease of handling compared to *in vivo* models, disadvantages include its limitation for high-throughput applications and suitability for only culturing cell types from the proximal not distal airway.

Further development of ALI models to recapitulate *in vivo* physiology involves increasing the complexity with added extracellular matrix and utilising more cell types native to the lung. An ALI model was developed that uses a collagen matrix embedded with fibroblasts as a medium for the epithelial layer to attach, maintained at the ALI (Choe et al., 2006).

1.7.2 Organotypic culture models of SQC

A model for squamous metaplasia of the bronchial epithelia was developed by culturing normal human tracheobronchial epithelial (NHTBE) cells at the ALI, and inducing squamous metaplasia via retinoic acid deficient media (Kim et al., 2007). Retinoic acid is involved in the differentiation of mucociliary pseudostratified bronchial epithelium. Lung tumours have reduced retinoic acid receptor (RAR) expression and retinoid deficiency is among early event contributing to lung tumorigenesis (Martinet et al., 2000).

Another model was developed that used NHTBE cells grown at ALI, when epidermal growth factor (EGF) was added to the medium on the basal side a hyperplastic phenotype was induced, characterised by increased proliferation and formation of a multi-layered epithelium (Lee et al., 2011). Again, this is a simplified method to attempt to model oncogenic signaling seen in NSCLCs. As discussed in Section 1.6.2, EGFR is mutated in many ADCs and overexpressed in many SQCs. Adding more ligand, EGF, is a crude attempt to recapitulate increased EGFR expression, an inducible overexpression of EGFR or mutated EGFR would be a more robust model that could provide a more physiologically relevant human SQC or ADC disease model.

Chen et al. (2018b) describe a lung SQC spheroid co-culture system that use primary patient-derived cell cultures embedded in a matrigel ECM with cancer-associated fibroblasts (CAFs). Overexpression of SOX2 in this system transitioned spheroids from a hyperplastic to dysplastic phenotype. When CAFs were co-cultured in the system the invasiveness of spheroids increased, but when SOX2 levels were very high, the presence of CAFs restored the hyperplastic state, suggesting a dynamic interaction between oncogenic signalling and the surrounding microenvironment. A limitation to this model is the lack of the ALI, that is a key physiological condition to recapitulate.

Kim et al. (2016) describe an ALI model using NHTBE and lentiviral SOX2 overexpression to drive a squamous metaplastic phenotype. They suggest that SOX2 cooperates with PIK3CA to induce hyperproliferative squamous metaplasia and inhibits mucociliary differentiation. This model lacks control of the SOX2 expression and ALI cultures were grown for 5-6 weeks when conducting experiments.

An ALI organoid methodology using patient derived tumour tissue was recently developed (Neal et al., 2018). These organoids, including a lung ADC model, preserved their primary tumour-immune microenvironment and enable accurate *in vitro* immunotherapy modelling and allow fast assessment of PD-1/PD-L1 checkpoint blockade (Section 1.6.2). This model will progress understanding of the complex tumour-immune microenvironment, but as it uses patient samples it involves large amounts of heterogeneity and variation between samples, and also requires further development for SQC samples.

Genetic aberrations in immortalised human bronchial epithelial cells were used to create a model of human bronchial dysplasia, this required stable knockdown of p53 and expression of oncogenic KRAS^{V12} (Sato et al., 2006). These cells were grown on a collagen-fibroblast matrix at the ALI, and a squamous metaplastic invasive phenotype developed however oncogenic KRAS mutation is very rarely seen in human SQC and this is therefore a model of limited relevance to the human disease.

These models do not recapitulate the human disease faithfully by combining both the microenvironmental context and appropriate molecular context present in the human disease. In this thesis, I use a novel model of bronchial dysplasia and early squamous cell lung cancer developed in my lab (Correia et al., 2017). Prior to this model, there were no

in vitro organotypic models that faithfully recapitulated bronchial dysplasia or early SQC using appropriate human cells in the correct microenvironmental context with relevant controllable genetic switches.

1.7.3 Patient derived xenograft (PDX) models of SQC

An alternative model to study SQC is to use patient derived xenografts (PDX), this involves the direct implantation of human tumour samples into immunocompromised mice. These models can be serially passaged and propagated as tissue explants. A key goal for PDX models is for tumour samples to preserve their native genotype and enable preclinical experiments to determine the most effective clinical regimen and personalise the treatment to the patient tumour.

A study from 2011 showed that it was possible to use PDX models of patients with refractory advanced cancers, screen a number of treatment regimens in propagated tumours in mice, and inform effective treatment regimens for the patients (Hidalgo et al., 2011). 63 drugs in 232 treatment regimens were screened in PDX models from 14 different patients. The response rate was 88%, drug treatment regimens were novel, and were not obvious second or third line treatment options. 11 out of 14 patients achieved a partial response, that is, tumour growth inhibition of over 50% following the novel treatment regimen. For 2 patients no effective treatment was found, and one patient died before receiving treatment. In this cohort, a NSCLC patient recieved a novel treatment regimen of Sorafenib (multiple tyrosine kinase inhibitor), Irinotecan (topoisomerase inhibitor) and Bevacizumab (vascular endothelial growth factor inhibitor).

More PDX models have been established for NSCLC patients, however only 40% of samples engrafted in mice successfully, indicating a severe disadvantage in these models for studying these types of tumours (Moro et al., 2012), particulary with regard to the 3Rs principles of reduction and refinement of animals in research. However, one positive to take from this was that those that did not engraft correlated with longer disease-free survival in patients. Of those that did engraft, genetic characteristics of the primary sample were maintained and stable for up to 20 passages.

Overall PDX models of lung cancers, and especially SQC, require further development, but may offer advantages to patients whose tumours engraft, as demonstrated in the pilot study by Hidalgo et al. (2011). Established models may provide the scope to sample tumour heterogeneity and enable basic science questions to be addressed. However, there are a number of limitations, large amounts of primary material are required, engraftment efficiencies are low and experimental costs are very high with low throughput. If the model is to be used to infer patient specific treatment regimen, several months may be needed to propagate and run the experiments on the PDX model deeming it not clinically useful for cancers with rapid disease progression.

1.7.4 Microfluidic and airflow devices

Microfluidic and airflow devices are discussed in Section 5.4.

1.8 PI3K-AKT signalling

A number of pathways have been implicated in the initiation or progression of SQC, with somatic alterations observed commonly in the TP53, RB1, PI3K and KEAP1 pathways (Hammerman et al., 2012). The focus of this thesis will be on the PI3K-AKT axis, and its role in driving bronchial dysplasia and early SQC.

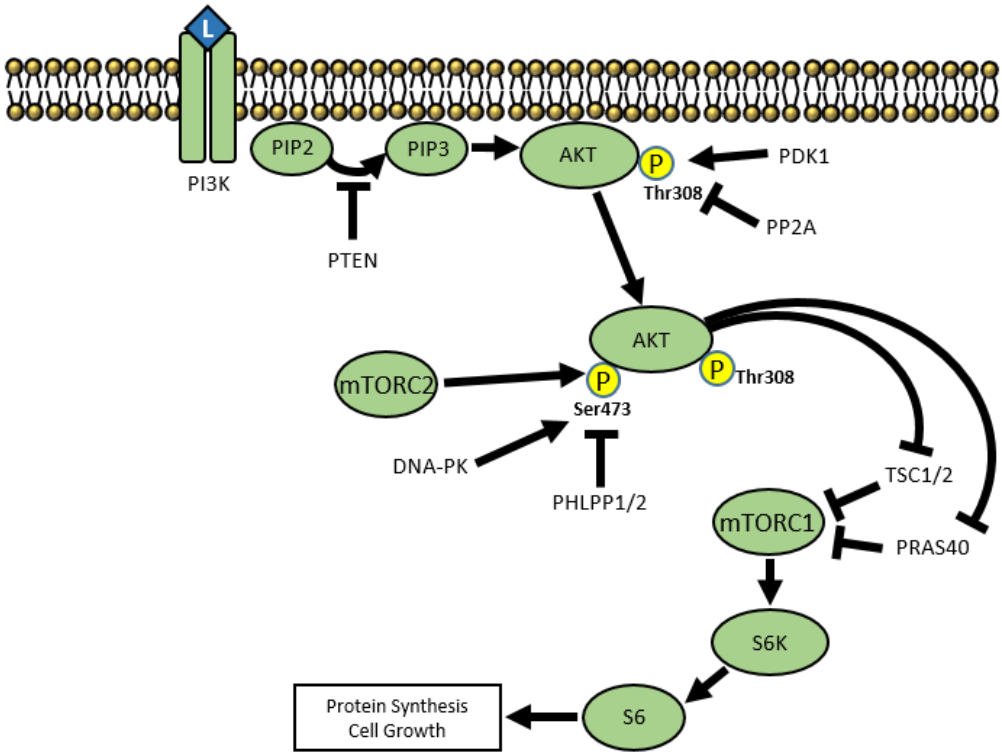

Figure 1.9: PI3K-AKT signalling pathway overview

Upon binding of an extracellular ligand (L) PI3K receptors dimerise and activate intracellular kinase domains. This starts a signalling cascade via the effector protein, AKT. Downstream signalling of AKT drives protein synthesis, growth and cell cycle progression.

1.8.1 PI3K-AKT signalling

Phosphoinositide 3-kinases (PI3K) are a family of intracellular signal transducer enzymes, divided into four classes based on structure, regulation and lipid substrate specificity. Class I PI3Ks are the most widely implicated in cancers and phosphorylate the inositol head group of phosphoinositides, producing lipid messengers PI3,4P_2 and PIP$_3$ (Manning and Toker, 2017). One of the primary direct downstream effectors of PI3K is AKT, a serine/threonine-specific protein kinase. AKT has 3 main domains, pleckstrin homology (PH) domain, a kinase domain, and a hydrophobic motif (HM) regulatory domain at the carboxyterminal end (Figure 1.10A). AKT has 3 highly homologous isoforms, each share the main domains. The PH domain mediates lipid-protein and protein-protein interactions, the kinase domain contains the conserved catalytic subunit and the HM domain,

a hydrophobic and proline-rich domain. PI3,4P_2 and PIP_3 induce activation of AKT by directly binding to the PH domain (James et al., 1996; Franke et al., 1997). Cytosolic inactive AKT is recruited to the membrane where it engages a lipid messenger, leading to AKT phosphorylation by phosphoinositide-dependent protein kinase 1 (PDK1) or mechanistic target of rapamycin complex 2 (mTORC2) (Alessi et al., 1997; Sarbassov et al., 2005).

1.8.2 **AKT phosphorylation**

AKT1 has 2 key residues that are phosphorylated during activation, Thr308 and Ser473 (AKT2 at Thr309 and Ser474, AKT3 at Thr305 and Ser472) (Alessi et al., 1996) (Figure 1.10A), although many other activation and regulation phosphorylation sites have been implicated in order to fine tune AKT signalling (Di Maira et al., 2005; Gulen et al., 2012; Guo et al., 2014). PDK phosphorylates AKT at Thr308, however for maximal activation of AKT Ser473 phosphorylation is required. mTORC2 phosphorylates AKT at Ser473, or DNA-PK can phosphorylate this residue when mTORC2 is inhibited in response to DNA damage (Bozulic et al., 2008) (Figure 1.9).

Phosphatase and tensin homolog (PTEN) is responsible for terminating signal activation by dephosphorylating PIP_3, and the AKT phosphatases, protein phosphatase 2A (PP2A) and PH domain leucine-rich repeat protein phosphatases 1/2 (PHLPP1/2), act on the Thr308 and Ser473 residues respectively (Andjelković et al., 1996; Maehama and Dixon, 1998; Gao et al., 2005).

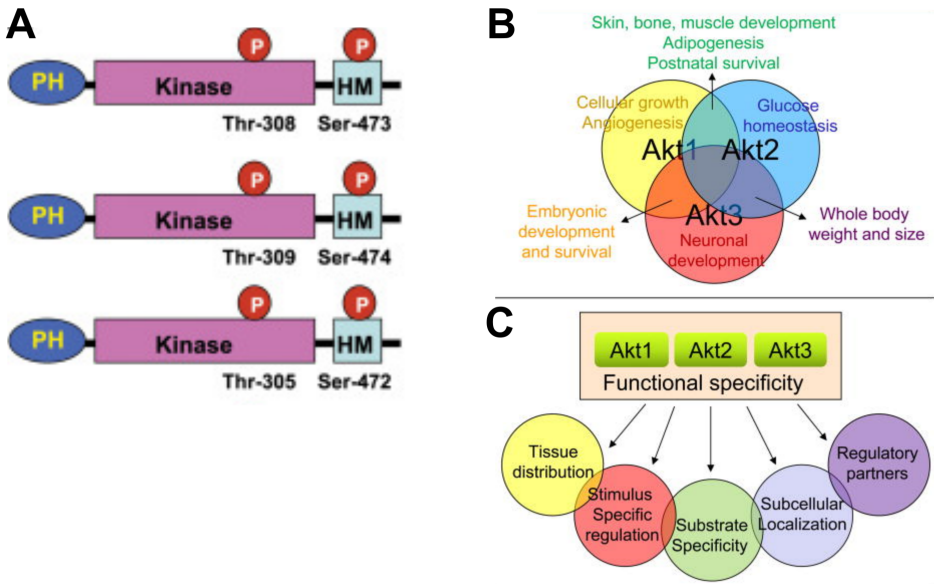

Figure 1.10: Despite the 3 AKT isoforms sharing 80% sequence homology distinct physiological functions exist.
A Domain structure of AKT isoforms all have pleckstrin homology domain (PH) at the amino terminal followed by a kinase domain and hydrophobic motif domain at the carboxy-terminal. Significant phosphorylation sites are shown (P). **B** Overlapping and specific functions for AKT isoforms, elucidated from phenotypic analysis of single and double AKT isoform knockout mice. **C** Mechanisms postulated for AKT isoform functional specificity. Adapted from (Hanada et al., 2004; Gonzalez and McGraw, 2009).

1.8.3 AKT downstream signalling

AKT is a major node in cell signalling, involved in many cellular functions such as survival, growth, metabolism and proliferation. There are reports of over 100 direct substrates of AKT, a number of which will be described here.

Glycogen Synthase Kinase 3 (GSK3) was the first AKT substrate to be reported (Cross et al., 1995). AKT phosphorylates GSK3 on an amino-terminal motif and inhibits GSK3 signalling, that is notably part of the Wnt-β-catenin pathway.

The forkhead box O (FoxO) transcription factors control a diverse set of gene targets involved in adaptation to fasting, insulin-like growth factor 1 (IGF1) signalling and apoptosis. AKT activation leads to FoxO proteins being translocated out of the nucleus, and subsequent blocking of their transcriptional programs. AKT suppresses the FoxO signalling associated with apoptosis induction (BIM and PUMA) and cell-cycle arrest (p21,

p27) (Manning and Cantley, 2007; van der Vos and Coffer, 2011).

AKT phosphoylates and inhibits tuberous sclerosis complex 2 (TSC2), an inhibitor of mTORC1. The AKT-mediated phosphorylation of TSC2 relieves inhibition and activates mTORC1 (Manning and Toker, 2017). Another AKT substrate involved in mTORC1 regulation is proline-rich AKT substrate of 40 kDa (PRAS40) (Sancak et al., 2007). PRAS40 is phosphorylated by AKT, preventing its inhibition of mTORC1 activating downstream signaling, such as key effector, ribosomal protein S6 Kinase 1 (S6K1) (Figure 1.9). S6K1 phosphorylates the S6 ribosomal protein (S6) and induces protein synthesis at the ribosome, and has been implicated in promoting cell cycle progression and proliferation (Volarević et al., 2000; Riemenschneider et al., 2006).

1.8.4 **PI3K-AKT signalling in SQC**

A number of studies have implicated PI3K-AKT signalling as an early event in the pathogenesis of SQC and crucial in tumorigenesis. 206 bronchial biopsies from 21 patients showed AKT activation in 27% hyperplasia/metaplasia and 58% dysplastic lesions suggesting a requirement for AKT signalling in the progression of premalignant bronchial lesions (Han et al., 2009). Another study examining cytologically normal bronchial epithelial cells from smokers with dysplasia or lung cancer showed that PI3K signalling was increased, suggesting that PI3K activation in the proximal airways occurred prior to tumorigenesis at an early point in the pathogenesis of SQC (Gustafson et al., 2010). This was further corroborated by reductions in proximal PI3K signalling when PI3K inhibition was used, and regression of dysplastic lesions were observed. Further human disease data from the TCGA shows that around half of all SQC tumours showed alterations in the PI3K/AKT pathway (Hammerman et al., 2012).

There are very few GEMMs that faithfully recapitulate genotypes commonly seen in the human SQC disease, however, 2 different GEMMs have shown evidence of PI3K/AKT upregulation, as opposed to ERK signalling that is often seen in lung adenocarcinomas. *Lkb1;Pten* null mice developed SQC that recapitulates histology, gene expression and microenvironment of the human disease (Xu et al., 2014). When compared to a *Kras*^{G12D}

driven mouse model of lung adenocarcinoma the *Lkb1;Pten* null SQC tumours showed high pAKT and low pERK expression. A SOX2 driven *Lenti-SOX2;Lkb1*$^{fl/fl}$ mouse model showed low pERK expression and high mTOR signalling (Mukhopadhyay et al., 2014). It is also worth mentioning that Ferone et al. (2016) report a lung SQC mouse model that closely recapitulates the human disease phenotype, using overexpressed SOX2 in combination with *Pten;Cdkn2ab*, however to date, there is no data on relative PI3K/AKT signalling in this model.

1.8.5 Cross talk between PI3K-AKT and RAS-MAPK pathways

The PI3K-AKT pathway can cross-talk with other major signalling pathways, such as the RAS-MAPK pathway. The RAS-MAPK pathway is another major signalling pathway that is involved in many cellular processes, transducing signals from extracellular stimuli to the cell nucleus to activate specific genes. The two pathways are intimately linked, with inhibition of one pathway showing activation in the other pathway (Mendoza et al., 2011). A kinome-wide siRNA screen has shown that when ERK is inhibited in the RAS-MAPK pathway general enhancement of AKT activation is observed (Lu et al., 2011). They can also work in a cooperative manner, and share downstream effectors such as S6 ribosomal protein (S6) that is involved in transcription of genes related to cell cycle progression and translation (Mendoza et al., 2011).

1.8.6 AKT isoforms

The three AKT isoforms are highly homologous and share many of the downstream effectors, however, distribution and phenotypic analysis suggest that there are distinct isoform-specific functions. AKT1 is the most widely expressed isoform across all human tissues, AKT2 is particularly enriched in insulin-responsive metabolic tissues and AKT3 is highly expressed in the brain (Uhlén et al., 2015). Consistent with tissue distributions *AKT1*$^{-/-}$ mice show high numbers of embryonic lethality (Cho et al., 2001b). *AKT2*$^{-/-}$ mice develop diabetes-like syndrome (Cho et al., 2001a) and *AKT3*$^{-/-}$ mice display a reduced

brain size (Easton et al., 2005). Here individual and compound AKT isoform knockout phenotypes are summarised (Fortier et al., 2011) (Figure 1.10B).

Beard Jr et al. (2018) identify an isoform specific function for AKT2 in the maintenance of claudin-5 dependent barrier integrity in brain microvascular endothelial cells as part of the blood-brain barrier. Rajala and Rajala (2018) describe the substrate, plenty of SH3s (POSH), as a specific downstream substrate of AKT2 in the retina. AKT2, but not AKT1 or AKT3 showed stable interactions with POSH, with AKT2 null mice show increased susceptibility to light-induced retinal degeneration, postulated to be via the lack of regulation of POSH in a protein complex (in the c-Jun N-terminal kinase (JNK) signaling pathway) that induces cell death. Levenga et al. (2017) describe unique expression patterns for all 3 AKT isoforms in the hippocampus in the brain. As well as this, they describe an isoform-specific function for AKT1. AKT1, not AKT2 or AKT3 is required for late phase long term potentiation (L-LTP), a pattern of synaptic activity that increases signal transmission between two neurons, by regulating activity-induced protein synthesis.

To date, only a small number of AKT isoform specific downstream effectors have been identified, and do not account for the range of isoform specific phenotypes observed in genetic studies. Studies to decipher the mechanisms for isoform specific functions are ongoing, suggested mechanisms that are likely to contribute are, molecular features of the isoforms currently unknown, subcellular localisation, relative expression levels, regulatory partners and somatic mutations in the isoform gene (Figure 1.10C).

1.8.7 **AKT isoforms in cancer**

AKT isoforms have been increasingly shown to have important roles in numerous cancer types in recent years. The first described activating mutation for an AKT isoform was the AKT1 E17K mutation in breast cancer (Carpten et al., 2007). This mutation results in constitutive kinase activation, the PH domain changes to allow constitutive membrane localisation, but is only present at low frequencies of 2-9% of breast cancers. Another study highlights a set of 20 recurrent mutations in AKT isoforms, and analysed AKT signalling and effects on growth in preclinical models, they concluded that mutants did not

activate signalling or growth when compared to WT AKT (Kyung and Lauring, 2016). They propose that the majority of AKT isoform mutations are passenger events.

Significant research has been conducted on AKT isoform roles in breast cancer that show non-redundant functions of AKT1 and AKT2 in cancer progression. AKT2 downregulation in breast cancer cells inhibited proliferation and antiapoptotic activity, whereas AKT1 downregulation promoted cell migration and epithelial-mesenchymal transition (EMT) properties, postulated to be via ERK activation (Irie et al., 2005). This highlights distinct roles for AKT isoforms as well as cross-talk between AKT and ERK signalling.

In a viral oncogene-induced mouse model of lung adenocarcinoma, using jaagsiekte sheep retrovirus, a distinct role for AKT1 in tumour inhibition, rather than AKT2 or AKT3, was demonstrated (Linnerth-Petrik et al., 2014). AKT1 knockout mice showed significant delays in lung tumour initiation and growth, whereas AKT2 knockout accelerated the initiation and growth of lung tumours drastically, as did AKT3 knockout albeit not in a statistically significant manner. This highlights further distinct isoform-specific, tissue-specific, and context-dependant roles for AKT.

Upregulation of AKT3 has been implicated in conferring resistance to AKT inhibitors in breast cancers (Stottrup et al., 2016). In AKT inhibitor resistant cells AKT3 was upregulated via epigenetic mechanisms, these cells showed enhanced invasive properties as well as resistance to AKT inhibition. AKT inhibitor sensitivity was restored when AKT3, not AKT1 or AKT2, was knocked down, as well as a reduction in invasive phenotypes. Further roles for AKT isoforms in cancer, and specifically lung SQC, are discussed in Chapter 4.

1.9 Thesis aims & overview

The aims of this thesis are to:

1. Adapt a novel organotypic model of early squamous cell lung cancer to screen small molecule tool compounds to identify druggable targets for the chemoprevention of SOX2-driven SQC.

2. Interrogate hits from the small molecule compound screens using genetic approaches in the OTC model to identify plausible therapeutic targets for the chemoprevention of SQC.

The results of my research are presented in Chapters 3, 4 and 5. Each results chapter contains an introduction and discussion with future plans incorporated.

Chapter 3 describes how the OTC model was adapted to screen tool compounds for both the primary and secondary chemoprevention of SQC. Compounds identified in the chemoprevention screens were validated in a panel of human squamous cell lines, and further tool compounds were used in the OTC model to corroborate screen “hits”.

Chapter 4 describes genetic knockout and knockdown approaches in the OTC model and *SOX2*/non *SOX2*-amplified squamous cell lines to further explore the necessity of the targets identified in Chapter 3 for the progression and maintenance of SOX2-driven SQC.

Chapter 5 describes other potential novel targets for the chemoprevention of SQC as well as an innovative way to leverage the OTC model for early detection or testing alternative types of therapeutics for lung cancer.

Chapter 2

Materials & Methods

2.1 Cell culture protocols

2.1.1 Cells lines

Table 2.1: Summary of cell lines.

Cell Line	Growth Media	Derivation	Comments
KT	cKSFM	Non-virally immortalised hBEC cell line	Starting cell line for deriving cells for use in OTC model.
KTshP53 iSOX2	cKSFM	Sequential lentiviral transduction of KT cell line	Cells used in the OTC model to model the bronchial epithelium. Constitutive p53 knockdown & doxycycline-inducible SOX2 overexpression drives dysplastic/early SQC phenotype.
MRC-5	DMEM + 10% FBS	Human foetal lung fibroblast cell line	Fibroblasts used in the OTC model embedded within the collagen matrix layer.
TE-6	RPMI1640 + 10% FBS	Human squamous cell esophageal carcinoma cell line	Used in drug screen proliferation studies.
KYSE-140	RPMI1640 + 10% FBS	Human squamous cell esophageal carcinoma cell line	Used in drug screen proliferation studies.Used for inducible shRNA studies.
KYSE-30	RPMI:Hams F12 (1:1) + 5% FBS + 2mM Glutamine	Human squamous cell esophageal carcinoma cell line	Used in drug screen proliferation studies. Used for inducible shRNA studies.
H520	RPMI1640 + 10% FBS	Human squamous cell lung carcinoma cell line	Used in drug screen proliferation studies.
LK-2	RPMI1640 + 10% FBS	Human squamous cell lung carcinoma cell line	Used in drug screen proliferation studies.
KYSE-410	RPMI1640 + 10% FBS + 2mM Glutamine	Human squamous cell esophageal carcinoma cell line	Used in drug screen proliferation studies.
TE-10	RPMI1640 + 10% FBS	Human squamous cell esophageal carcinoma cell line	Used in drug screen proliferation studies.
TE-7	RPMI1640 + 10% FBS	Human squamous cell esophageal carcinoma cell line	Used in drug screen proliferation studies.
A549	DMEM + 10% FBS	Human lung adenocarcinoma cell line	Used in drug screen proliferation studies.
NBT-II	EMEM + 10% FBS	Rat bladder carcinoma cell line	Used to produced conditioned medium for primary hBEC culture.

Cell lines used throughout this thesis are summarised in Table 2.1, briefly; human bronchial epithelial cells immortalised using the introduction of human telomerase reverse transcrip-

tase (hTERT) and overexpression of cyclin dependent kinase 4 (CDK4) (hereafter referred to as KT cells, or KT background) were kindly provided by Dr John D. Minna (The University of Texas Southwestern Medical Centre, Dallas, Texas). These cells, along with cell lines derived from them were cultured in keratinocyte serum-free medium (KFSM) supplemented with 5 ng/mL human recombinant epidermal growth factor (EGF) and 50 μg/mL bovine pituitary extract (BPE) (Thermo Fisher Scientific), hereafter referred to as cKSFM.

MRC-5, HEK293T and A549 cell lines were cultured in complete Dulbecco's modified eagle medium (DMEM) + 10% foetal bovine serum (FBS). TE-6, TE-10, LK-2, KYSE-140 and H520 cells lines were cultured in complete Roswell Park Memorial Institute 1640 (RPMI 1640) + 10% FBS. KYSE-410 and TE-7 cell lines were cultured in complete RPMI 1640 + 10% FBS + 2 mM L-Glutamine. KYSE-30 cell line was cultured in complete RPMI 1640:Ham's F12 (1:1) + 2mM L-Glutamine + 5% FBS. NBT-II cell line was cultured in complete Eagle's minimum essential medium (EMEM) + 10% FBS.

NBT-II conditioned medium was produced by growing NBT-II cells to 100% confluence, changing medium, then harvesting medium every day, for up to 4 days. Harvested medium was filtered through a 0.22 μm filter and stored at -20°C.

Primary normal human bronchial epithelial cells (hBECs)(Lonza) were cultured on plates pre-coated with NBT-II conditioned medium, NBT-II conditioned medium was incubated over night in plates at 37°C, then medium was removed. hBECs were cultured in PneumaCult Plus Expansion medium + supplied 50X supplements (Stem Cell Technologies), with 0.96 μg/mL hydrocortisone (Stem Cell Technologies). As detailed in Mou et al. (2016) dual SMAD signalling pathway inhibition enables expansion of primary basal cells with addition of 1 μM DMH-1 (BMP4 inhibitor), 1 μM A83-01 (TGFβ inhibitor), 10 μM Y27682 (ROCK inhibitor) and 1 μM CHIR99021 (GSK3 inhibitor) to medium.

All cells were cultured in a humidified incubator maintained at 37°C and 5% CO_2.

2.1.2 The organotypic culture (OTC) model

The organotypic culture models of bronchial dysplasia/early squamous cell lung cancer, hereby referred to as the OTC model, were setup as outlined in (Correia et al., 2017).

Briefly, on day 1, 12 or 24 well transwell plates with 0.4 μm porous membrane inserts (Corning) were seeded with a collagen-fibroblast mix. A collagen solution was prepared on ice; 2.6 mL Collagen I rat tail (Corning) diluted to 3 mg/mL, 375 μL 10X DMEM+3.7% $NaHCO_3$, 375 μL Tet-System Approved FBS (Takara Bio), and 81 μL 7.5% sodium bicarbonate. The solution was carefully mixed avoiding generation of bubbles. The collagen solution pH was adjusted to 7.25-7.4 with 1M NaOH, and 375 μL MRC-5 fibroblasts resuspended in DMEM+10% Tet-System Approved FBS at 5 x 10^5 cells/mL was added to the collagen and mixed again. 200 μL (12 well plates) or 70 μL (24 well plates) of collagen-fibroblast mix was seeded onto the top of each transwell membrane, incubated at 37°C for 30 min, then cKSFM was added to top and bottom chambers of transwells and incubated at 37°C.

On day 5, following contraction of the collagen-fibroblast mixtures into discs on top of the transwell membranes, medium was removed from the top chamber of the transwell and collagen disc. 50 μL (12 well plate) or 15 μL (24 well plate) KTshP53iSOX2 derived cells at 8 x 10^6 cells/mL in cKSFM was added to each collagen disc and allowed to attach for 4 hr at 37°C, before cKSFM was then added on top to cover the cells.

On day 8, once epithelial cells were 100% confluent, they were brought to the air-liquid interface (ALI) by removing all medium from the upper chamber of the transwell, and replacing the bottom chamber with 600 μL (12 well plate) or 300 μL (24 well plate) cKSFM $\pm$ 1 μg/mL doxycycline in the bottom chamber such that only the collagen disc was in contact with medium. Medium was changed every 2-3 days.

2.1.3 Compound screens

Primary chemoprevention studies using the OTC model

The OTC model was setup, as described in section 2.1.2, until day 8. At the same time as the ALI was created, test compounds at the concentrations indicated in figures and results chapters were added diluted in cKSFM ±doxycycline. Medium and compounds were changed every 48 hr.

Secondary chemoprevention studies using the OTC model

The OTC model was setup, as described in section 2.1.2, until a clear SOX2 driven phenotype was present in doxycycline treated wells when observed at low magnification, this was usually after 4 days at the ALI. Once a clear phenotype was present, test compounds were added diluted in cKSFM ±doxycycline. Medium and compounds were changed every 48 hr.

Compounds

Compounds were purchased from Selleckchem, Tocris Bioscience, and Sigma. They were dissolved and stored in concentrated dimethyl sulfoxide (DMSO) stocks at -20°C, unless stated otherwise. When compounds were used *in vitro* final DMSO concentrations never exceeded 0.1%. Vehicle controls, complete medium plus DMSO, were used in all compound studies. Compounds used in OTC chemoprevention screens are listed in Table 2.2, along with their intended molecular target and clinical trial status.

Table 2.2: Compounds used in primary and secondary chemoprevention screens.

Compound	Target	Clinicaltrials.gov listing
AZD2014	mTORC1/2	Currently in multiple Phase I/II trials.
AZD5363	AKT1/2/3	Currently in multiple Phase I/II trials.
AZD8835	PI3K α/δ	Phase I breast cancer trial completed.
LY294002	PI3K $\alpha/\beta/\delta$	Phase I trials terminated.
Selumetinib	MEK1/2	Currently in multiple Phase I/II/III trials.
AKTi1/2	AKT1/2	Not used in any clinical trials.
Afuresertib	AKT1/2/3	Currently in multiple Phase I/II trials.
MK-2206	AKT1/2/3	Currently in multiple Phase I/II trials.
HG-9-91-01	SIK1/2/3	Not used in any clinical trials.
JQ1	BRD2/3/4/T	Not used in any clinical trials.

2.1.4 Differentiation ALI cultures

Normal human bronchial epithelial cells were plated on NBT-II conditioned medium coated 24 well transwells (see section 2.1.1) with 0.4 μm porous membrane inserts (Corning) at 1 x 10^5 cells per well in PneumaCult Plus Expansion medium (Stem Cell Technologies). Cells were grown until 100% confluent, then brought to the ALI by removing the medium from the upper and lower chambers of the transwell and replacing with 500 μL ALI maintenance medium in the lower chamber; 43.4 mL PneumaCult ALI medium (Stem Cell Technologies), 5 mL 10X ALI Supplements (provided with ALI medium), 500 μL ALI maintenance supplements (provided with ALI medium), 50 μL hydrocortisone stock (Stem Cell Technologies), 100 μL 0.2% Heparin solution (Stem Cell Technologies) and 500 μL 100X penicillin/streptomycin solution. Medium was changed twice a week and cells were maintained at the ALI for at least 18 days to differentiate, before being fixed with 10% neutral buffered formalin (NBF) (Sigma) for 1 hr, and stored at 4°C in phosphate-buffered saline (PBS).

2.1.5 Resazurin assay

Numbers of viable cells were quantified using the resazurin assay. Cells were seeded in 96 well plates, cell numbers were optimised for each cell line and assay length such that cells were still in logarithmic growth phase at the time of analysis. Resazurin sodium salt (Sigma) was dissolved in PBS at 1mg/mL, protected from light and stored at 4°C. 20

μL of resazurin solution was added to 100 μL of complete medium in 96 well plates and incubated for 90 min at 37°C. Supernatant was transferred to a white opaque 96 well plate and fluorescence measured at 560ex/590em on a Tecan Infinite M200 (Lifesciences).

2.2 Molecular biology protocols

2.2.1 DNA plasmids

pSpCas9(BB)-2A-GFP (Px458) was a gift from Feng Zhang (Addgene # 48138). psPAX2 was a gift from Didier Trono (Addgene # 12260). pMD2.G was a gift from Didier Trono (Addgene # 12259). EZ-tet-pLKO-Blast was a gift from Cindy Miranti (Addgene # 85973). Tet-pLKO-Puro was a gift from Dmitri Wiederschain (Addgene # 21915). Tet-pLKO-Puro-shSCR was a gift from Kyren Lazarus. Tet-pLKO-Puro-shAKT1, Tet-pLKO-Puro-shAKT2, Tet-pLKO-Puro-shAKT3 were gifts from Rebecca Chin.

2.2.2 Plasmid modification by annealed oligonucleotide cloning

Plasmids were digested using restriction enzymes (NEB) in appropriate NEBuffer for 1-2 hr at 37°C. Reactions were set up in 50 μL with 5 μg of plasmid DNA. Digested plasmids were separated by agarose gel electrophoresis. Digestion products were visualised using a Dark Reader transilluminator (Clare Chemical Research) and cut out from the gel. DNA was extracted and purified using the Zymoclean Gel DNA recovery kit (Zymo Research) as per manufacturer's instructions.

Forward and reverse oligonucleotides (Sigma) were annealed using a thermocycler T3000 (Biometra) at 95°C for 10 min, then gradual cooling in 5°C steps for 5 min at a time down to 60°C. Annealed oligonucleotides were ligated into 20 ng digested plasmid using T4 DNA Ligase in a total reaction volume of 20 μL, and incubated at room temperature (r.t.) for 30 min.

Competent DH5α (Thermo Fisher Scientific), XL-10 (Thermo Fisher Scientific) or NEB Stable *E.Coli* (NEB) were transformed with 5 μL of ligation mixture and incubated on ice for 5 min, followed by heat shock at 42°C for 30 sec and 2 min on ice. 10 fold volume of LB was added to transformed bacteria and incubated in a shaker at 37°C for 1 hr at 200 rpm. Bacterial out-growth cultures were then plated on LB-agar plates + 50 μg/mL ampicillin and incubated at 37°C overnight. Single colonies were picked and grown in LB + 50 μg/mL ampicillin overnight in a shaker at 37°C and 200 rpm. Bacterial cultures were centrifuged at 2500 g for 20 min. Plasmid DNA was isolated using GenElute plasmid miniprep kit (Sigma) as per manufacturer's instructions. Plasmid modifications were validated by sequencing using relevant primers by Department of Biochemistry Sequencing Facility, University of Cambridge.

2.3 *In vitro* genetic manipulation protocols

2.3.1 Lentiviral production and transduction

Lentiviral particles were generated in HEK293T cells. 5x10^6 HEK293T cells were plated in 10 cm plates. The next day the cells were transfected using Lipofectamine LTX and Plus reagent (Thermo Fisher Scientific) with 4.5 μg experimental vectors plus 3 μg psPAX2 and 1 μg MD2.G. 6 h after transfection, transfection media was changed to DMEM + 20% FBS. Viral media was harvested from the cells after a further 48 h, filtered through a 0.45 μm filter and stored in aliquots at -80°C.

For lentiviral transduction, target cells were seeded into 6 well plates such that they were 70% confluent the next day, then transduced with lentiviral particles using 8 μg/mL polybrene diluted in complete medium. Cells were transduced for 48 h, and allowed to recover in complete medium for 24 h. Cells were selected with appropriate antibiotic for 3 days after non-transduced control cells had died. Selection media was replenished every 2 days.

2.3.2 CRISPR-Cas9-mediated gene knockouts

Gene knockout cell lines were produced by using Cas9 nuclease to make double stranded breaks in targeted DNA. Error prone non-homologous end joining repair pathways produce InDels and frame-shifts resulting in premature stop codons, and loss of gene function. sgRNAs were designed using the online tool (crispr.mit.edu) targeting early exons in the gene. KTshP53iSOX2 were plated at 5 x 10^5 cells per well in a 6 well plate. Next day, 1250 ng plasmid was diluted with Opti-MEM (Thermo Fisher Scientific) and Lipofectamine LTX with Plus reagent (Thermo Fisher Scientific) was used to make up transfection mixes as per manufacturer's instructions. Mixes were added dropwise to cells and medium changed after 6 h transfection.

3-4 days after transfection cells were detached using 3X trypsin-EDTA, followed by pelleting and washing with PBS. Cells were pelleted and resuspended in PBS + DNAase + 2% BSA. Cell were selected for GFP expression using fluorescent activated cell sorting (FACS) using the MoFlo MLS DakoCytomation Sorter. Non-transfected cells were used to determine the gating necessary to capture double GFP positive cells (GFP++), as parental cells were already GFP positive due to constitutively expressed GFP-shP53 construct.

2.3.3 Screening for CRISPR-Cas9-induced genetic disruption

Expanded populations from single cells sorted based on GFP++ were screened for target gene disruption. Briefly, short regions around the targeted Cas9 double strand break sites were amplified and sequenced to determine genetic disruption before functional protein analysis via western blotting.

Forward and reverse primers were designed to regions 150-300 bp up and downstream of respective sgRNA binding sites. PCR reactions were carried out on a G-Storm Thermocycler, each primer set PCR programme was determined experimentally. Amplified products were separated on an agarose gel, bands were visualised and cut out of the gel using a dark reader transilluminator (Clare Chemical Research). PCR products were extracted and purified using the Zymoclean Gel DNA recovery kit (Zymo Research) as per man-

ufacturer's instructions. Purified DNA was sequenced and compared to non-transfected (WT) KT cell lines. Sequencing was carried out by members of the Department of Biochemistry Sequencing Facility, University of Cambridge.

2.3.4 siRNA mediated gene knock down

ON-TARGET plus siRNA reagents (Dharmacon Horizon Discovery) were used, according to manufacturer's instructions. Briefly, KYSE-140 and KYSE-30 cells were reverse transfected using the SMART Pool: ON-TARGET Plus SIK2 siRNA and appropriate non-targeting control (NTC) siRNA was used at a final concentration of 25 nM in a mix together with DharmaFECT 1 reagent and serum-free media. Medium was changed 24 h after transfection. RNA was extracted 48 h and protein 96 h post siRNA transfection for analysis of transient knockdown.

2.4 RNA manipulation protocols

2.4.1 RNA extraction

RNA was extracted from cultured cells using the RNeasy Plus Mini kit (Qiagen) according to manufacturer's instructions.

2.4.2 cDNA synthesis

cDNA was synthesised using the Multiscribe High Capactiy Reverse Transcription kit with RNase inhibitor (Thermo Fisher Scientific). A total of 1 μg of RNA was used in 20 μL reaction volumes and thermocycler T3000 (Biometra) conditions used according to manufacturer's instructions.

2.4.3 Reverse transcription quantitative polymerase chain reaction (RT-qPCR)

RT-qPCRs were performed using SYBR green reagents (Applied Biosystems). A master mix of 5 μL SYBR green and 0.5 μL reverse (R) and forward (F) primer stock (2:2:25, R:F:H_2O of 100 μM primer stocks) was prepared on ice and 1 μL cDNA and 3.5 μL H_2O mixes were added per well. A QuantStudio 5 Real-Time PCR machine (Thermo Fisher Scientific) was used with the following thermal cycling conditions: 95°C for 10 min, followed by 40 cycles of 95°C for 15 sec then 60°C for 1 min. Melt curve analysis was carried out to confirm specific, single amplicon generation. Default thresholds for the cycle threshold (Ct) values was determined by the QuantStudio 5 software. Relative gene expression was calculated using the $\Delta\Delta$Ct method, normalising to internal housekeeping gene, TATA-box binding protein (*TBP*).

2.5 Protein manipulation Protocols

2.5.1 Protein extraction and quantification

For 2D cell cultures, cells were harvested from plates on ice. Cells were washed with cold PBS, then incubated with radioimmunoprecipitation assay (RIPA) buffer for 5 min. Lysates were scraped off the plates using a cell scraper, transferred to a microcentrifuge tube, vortexed and centrifuged at 4°C, 20000 x g for 30 min in a benchtop centrifuge. Supernatants were transferred to fresh microcentrifuge tubes and stored at -80°C.

For harvesting from the OTC model, medium was removed from the top and bottom transwell chambers then sealed from the bottom with parafilm. Cells were washed with PBS then incubated with 3X Trypsin-EDTA for 10 min at 37°C. The Trypsin-EDTA was pipetted up and down over the collagen disc to dislodge cells, and incubated for a further 5 minutes at 37°C. Trypsinised cells were then collected into a microcentrifuge tube containing DMEM +10% FBS on ice and pelleted at 4°C, 3000 x g for 5 min in a benchtop centrifuge.

The cell pellet was resuspended in RIPA buffer, incubated on ice for 5 min, vortexed and incubated on ice for a further 5 min. The lysate was centrifuged at 4°C, 20000 x g for 30 min and supernatants were transferred to fresh microcentrifuge tubes and stored at -80°C.

Protein concentration was quantified from cell lysates using the Pierce bicinchoninic acid assay (BCA) protein kit (Thermo Fisher Scientific). A standard curve of bovine serum albumin (BSA) standards was used to estimate the concentration of test samples. Standards and samples were incubated with BCA reagent at 37°C for 30 min, then absorbance at 562 nm was determined using a SpectraMax Plus 384 spectrophotometer (Molecular Devices).

2.5.2 **Western blotting**

Polyacrylamide resolving gels were hand cast and prepared at varying acrylamide percentages (8-12%) depending on the size of target proteins for optimal resolution. Briefly, H_2O, acrylamide bis-acrylamide (Severn Biotech), 1.5 M Tris-HCl (pH 8.8), 0.1% SDS, ammonium persulfate and tetramethylethylenediamine was used to make resolving gels, and a 4% acrylamide stacking gel was used. 10-30 μg of protein was loaded onto 4-12% Tris-Acrylamide gels and separated by SDS-polyacrylamide gel electrophoresis (SDS-PAGE). Proteins were transferred to a polyvinylidene fluoride (PVDF) membrane (Millipore) by electroblotting, 40 V for 1 h at 4°C. Protein transfer and loading efficiency was assessed with Ponceau S (Sigma) staining. The PVDF membranes were blocked with the appropriate blocking buffer for 1 h r.t., then with primary antibody diluted in blocking buffer was incubated overnight at 4°C. Then membranes were incubated with appropriate secondary antibodies conjugated to horseradish peroxidase (HRP) in blocking buffer for 1 h r.t. Membranes were visualised by chemiluminescence using Pierce enhanced chemiluminescence (ECL) western blotting substrate kit (Thermo Fisher Scientific) and exposing to X-ray films (Fujifilm).

2.5.3 Chromatin immunoprecipitation (ChIP)

The Magna ChIP G Kit (Millipore) was used, according to manufacturer's instructions. Briefly, cells were cultured in 20 cm plates until 70-80% confluence, and protein-DNA complexes cross-linked with 1% formaldehyde in complete medium for 10 min at r.t. Reaction was quenched with addition of 10X glycine, and cells washed twice with ice cold PBS. Cells were harvested in PBS containing protease inhibitor using a cell scraper, pelleted at 4°C, 800 x g for 5 min and resuspended in cell lysis buffer. After 15 min incubation on ice, the suspension was centrifuged at 4°C, 800 x g for 5 min. The pellet was then resuspended in nuclear lysis buffer and sonicated to produce chromatin fragments of ~500 bp using a Covaris E220 sonicator. Sheared chromatin was incubated with protein G magnetic beads and appropriate antibody, see table 2.6, overnight, rotating at 4°C. Next day, the bead complexes were washed with a series of wash buffers, followed by protein removal and reverse cross linking with proteinase K in elution buffer, rotating at 62°C for 2 h. DNA was purified using spin columns before analysis using PCR.

2.6 Histology & immunostaining protocols

2.6.1 OTC processing for histology

Collagen-fibroblast discs and attached epithelial cells were fixed using 10% NBF (Sigma) overnight, then transferred to 70% ethanol before being processed and embedded vertically into paraffin blocks ready for sectioning by Histology Department of the MRC Cambridge Stem Cell Institute, Cambridge or Steph Mackie, Department of Biochemistry, Cambridge.

2.6.2 Hematoxylin & eosin (H&E) staining

4.5 mm sections were cut and sent for H&E staining in the Histology Department of the MRC Cambridge Stem Cell Institute, Cambridge. Sections were deparaffinised in xylene,

rehydrated in decreasing concentrations of ethanol, and stained with hematoxylin and eosin. Sections were then mounted using DPX mountant (Sigma).

2.6.3 Immunohistochemistry (IHC) staining

4.5 mm sections were deparaffinised in xylene and rehydrated in decreasing concentrations of ethanol. Antigen retrieval was performed by simmering in sodium citrate buffer in a microwave for 10 min. Endogenous hydrogen peroxidase was blocked with 3% hydrogen peroxide for 30 min at r.t. Sections were blocked using blocking serum from the Vectastain ABC kit (Vector Laboratories) for 20 min r.t. Primary antibodies were diluted in blocking solution and incubated overnight at 4°C. Secondary antibodies from the ABC kit (Vector Laboratories) were incubated for 30 min r.t. Avidin-biotin complex was incubated for 30 min r.t., before developing sections using the DAB peroxidase substrate kit (Vector Laboratories). Slides were counterstained with haematoxylin then dehydrated through increasing concentrations of ethanol, before clearing in xylene and mounted using DPX mountant (Sigma). Images were acquired using AxioImager M2 microscope (Zeiss).

2.6.4 Immunofluoresence (IF) staining ALI cultures

Cells were washed with PBS then fixed on transwell membranes with 4% PFA for 15 min at r.t. Fixed cells were then washed 3 times with PBS and stored at 4°C until required. Transwells were sealed with parafilm and staining procedure carried out in the sealed well. Cells were permeabilised with PBS + 0.3% Triton X-100 for 15 min r.t., then blocked with blocking buffer (PBS + 5% normal goat serum (NGS), 1% BSA, 0.1% Triton X-100) for 45 min r.t. Primary antibodies were diluted in blocking buffer and incubated overnight at 4°C. Alexa Fluor conjugated secondary antibodies (Thermo Fisher Scientific) diluted in blocking buffer (1:2000) were incubated for 2 h at r.t. Nuclei were counterstained with Hoechst 33258 (1:5000) (Sigma). Transwell membranes were cut out and mounted using ProLong Gold Antifade mountant (Thermo Fisher Scientific). Images were acquired using AxioImager M2 microscope (Zeiss).

2.6.5 Terminal deoxynucleotidyl transferase dUTP nick end labeling (TUNEL) IF staining

The ApopTag Fluorescein *In Situ* Apoptosis Detection Kit (Millipore) was used according to manufacturer's instructions.

2.6.6 Human Tissue Microarray (TMA)

TMA sections were kindly provided by Dr Doris M Rassl and Dr Robert Rintoul. Surgical and endobronchial patient biopsy specimens from Papworth Hospital NHS Trust, Cambridge, UK were embedded for use in the TMA.

2.7 Antibodies

Table 2.3: Antibodies used for western blotting.

Antibody	Company	Catalogue No.	Source	Dilution	Buffer
SOX2	R & D Systems	MAB2018	Mouse	1:1000	3% BSA
β-Actin	Santa Cruz	SC69879	Mouse	1:5000	3% BSA
β-Tubulin	CST	2128	Rabbit	1:1000	3% BSA
pAKT (Ser473)	CST	9271	Rabbit	1:500	3% BSA
pAKT (Thr308)	CST	13038	Rabbit	1:500	5% Milk
Total AKT	CST	9272	Rabbit	1:1000	3% BSA
pS6 (Ser240/244)	CST	5364	Rabbit	1:4000	3% BSA
Total S6	CST	2217	Rabbit	1:2000	3% BSA
SIK2	Millipore	07-1378	Rabbit	1:1000	3% BSA
pERK1/2 (Thr202/Tyr204)	CST	9101	Rabbit	1:1000	3% BSA
Total ERK1/2	CST	9107	Mouse	1:1000	3% BSA
α-Tubulin	Santa Cruz	SC32293	Mouse	1:1000	3% BSA
Cytokeratin 5	Abcam	ab53121	Rabbit	1:1000	3% BSA
P63	Invitrogen	PA5-36069	Rabbit	1:1000	3% BSA
AKT1	Santa Cruz	SC5298	Mouse	1:500	3% BSA
AKT2	Santa Cruz	SC5270	Mouse	1:500	3% BSA
AKT3	Atlas Antibodies	HPA026441	Rabbit	1:1000	5% Milk
Secondary anti-mouse IgG HRP	Sigma	A9044	Rabbit	1:15000	Same as primary antibody
Secondary anti-rabbit IgG HRP	Sigma	A6154	Goat	1:15000	Same as primary antibody

Table 2.4: Antibodies used for immunohistochemistry.

Antibody	Company	Catalogue No.	Source	Dilution
SOX2	R & D Systems	MAB2018	Mouse	1:2000
Ki67	Thermo Fisher Scientific	RM-9106-S1	Rabbit	1:200
SIK2	Milliopore	07-1378	Rabbit	1:100
AKT1	St Johns Laboratory Ltd	STJ9 1546	Rabbit	1:1000
AKT2	St Johns Laboratory Ltd	STJ9 1552	Rabbit	1:1000
AKT3	Atlas Antibodies	HPA026441	Rabbit	1:1000
Secondary Antibody, Universal Kit	Vectastain	PK-6200		1:200

Table 2.5: Antibodies used for immunofluorescence.

Antibody	Company	Catalogue No.	Source	Dilution
Cytokeratin 5	Abcam	ab53121	Rabbit	1: 500
Acetylated Tubulin	Sigma Aldrich	T7451	Mouse	1:1000
Mucin 5AC	Thermo Fisher Scientific	MA5-12178	Mouse	1:100
Secondary anti-Rabbit IgG Alexa Fluor 488	Thermo Fisher Scientific	A11008	Goat	1:500
Secondary anti-Mouse IgG Alexa Fluor 555	Thermo Fisher Scientific	A21424	Goat	1:500

Table 2.6: Antibodies used for chromatin immunoprecipitation.

Antibody	Company	Catalogue No.	Source	Dilution
SOX2	R & D Systems	AF2018	Goat	5 μg per IP
IgG control	R & D Systems	AB108	Goat	5 μg per IP

2.8 Oligonucleotides

Table 2.7: Oligonucleotides used for SYBR Green RT-qPCR. 5'→ 3'.

Gene	Forward	Reverse
AKT1	CAAGCCCAAGCACCGC	GGATCACCTTGCCGAAAGTG
AKT2	GCAAGGCACGGGCTAAAG	CCCGCACCAGGATGACTT
AKT3	GAAGAGGAGAGAATGAATTGTAGTCCA	AGTAGTTTCAAATAGTCAAAATCATTCATTG
SIK2	CAGCAGCTGCAGGAACATAG	GACTTGGCTGTGGGTAGGAG
TBP	AGTGAAGAACAGTCCAGACTG	CCAGGAAATAACTCTGGCTCAT

Table 2.8: Oligonucleotides used for PCR amplification and sequencing of CRISPR-Cas9 edited cells. 5'→ 3'.

Gene	Forward	Reverse
AKT1 exon 3	ATGCCATGGGAAGACATGGG	AGATGGGGGTCAGAGAGCTT
AKT2 exon 3	CAGGTCAGCAAGGAAGGAAG	GCTTGTGGGACTTGGTCATT
AKT3 exon 5	ACATCTTTCTGCAAATGGTAGC	GACAGAAGCTATCCAGGCTGT

Table 2.9: Oligonucleotides used for PCR amplification of ChIP products. 5'→ 3'.

Gene	Forward	Reverse
AKT3	GGGGCTTGTTGTTGACTTTG	GGGAAGCCTGAGGACGAG
SIK2	CGCGCTGTACTTGTAGGTGA	GGAGGGGTGCAGAGACCT

Table 2.10: sgRNA and shRNA sequences. shRNA loop sequences in italics. 5'→ 3'.

Gene	sgRNA sequence
AKT1 exon 3	GAGCGACGTGGCTATTGTGA
AKT2 exon 3	CTCTTCAGCAGGAAGTACCG
AKT3 exon 5	TCTTTTATGATGGGTTGTAG
	shRNA sequence
AKT1	GCTACTTCCTCCTCAAGAATG *CTCGAG* CATTCTTGAGGAGGAAGTAGC
AKT2	CTTCGACTATCTCAAACTCCT *CTCGAG* AGGAGTTTGAGATAGTCGAAG
AKT3	CTGCCTTGGACTATCTACATT *CTCGAG* AATGTAGATAGTCCAAGGCAG
Scramble	CCTAAGGTTAAGTCGCCCTCG *CTCGAG* CGAGGGCGACTTAACCTTAGG

Chapter 3

Rational compound screening for chemoprevention of SOX2-driven squamous cell lung cancer using an organotypic cell culture model

3.1 Introduction

Chemoprevention has been discussed as a strategy to lower SQC incidence and mortality worldwide in chapter 1. In theory, chemoprevention is divided into primary and secondary chemoprevention. Primary chemoprevention refers to the treatment of individuals at high risk of developing lung cancer, but with no evidence of precancer, such as long-term heavy smokers. Secondary chemoprevention refers to the treatment of individuals with evidence of precancer, such as bronchial dysplasia.

The PI3K-AKT signalling pathway has been shown to be activated in bronchial dysplasia and squamous cell lung cancers both in *in vivo* models and in human disease (Han et al., 2009; Memmott and Philip, 2010; Xu et al., 2014). PI3K-AKT activation is also recapitulated in the SOX2-driven OTC model of bronchial dysplasia, the precursor lesion to squamous cell lung cancer (Correia et al., 2017), and increased pAKT signalling upon exogenous SOX2 expression has been shown in embryonic stem cells (ESCs) (Golden et al., 2013).

Current *in vitro* models of SQC and early precancer disease are limited (Section 1.7) and therefore the OTC model was adapted to screen drugs to identify targets that could be targeted by preventative therapies.

With this in mind, a small-scale screen with a selection of compounds was performed in order to identify potential targets for chemoprevention of SQC (Table 2.2). Hits from the screen would be validated using genetic ablation studies (Chapter 4) and used to inform druggable targets for prevention of SQC. Initial compound selection was based on immediate access within the laboratory at the time as well as cost effectiveness and availability from chemical suppliers. Compounds that exhibited reversion of the dysplastic phenotype or prevented the dysplastic phenotype from developing would guide further genetic ablation studies based on the compound's molecular targets, as well as cell line studies.

Further target exploration is shown in Chapter 5, using RNA-sequencing data generated from the OTC model for novel target identification (unpublished, Dr L. Correia, University of Cambridge) (Appendices, Table 7.1).

3.2 Chemoprevention compound screens using the OTC model

A schematic setup for the standard OTC model developed previously by Correia et al. (2017) is shown (Figure 3.1A). This SOX2-driven model recapitulates the key genetic lesions reported in the human disease in appropriate cells in the relevant microenvironment. Western blot analysis confirms upregulation of the AKT signalling pathway upon SOX2 induction (Figure 3.1B), which was reported previously using immunohistochemical (IHC) staining on sections from the OTC model (Correia et al., 2017). Activation of AKT signalling recapitulates clinical specimens (Correia et al., 2017); an example is shown that captures a border between a high grade dysplasia and normal epithelium (Figure 3.1C). Here, SOX2 is highly expressed in the high grade dysplasia with consecutive sections showing increased proliferation together with an upregulation of pAKT signalling. This provided the rationale for selection of a panel of compounds targeting the PI3K-AKT signalling pathway to begin small molecule compound screens using the OTC model.

The OTC model developed and presented by Correia et al. (2017) required further optimisation for medium throughput screening purposes. The original model was developed in a 12 well plate format. Here, throughput was increased to a 24 well plate format that enabled more replicates and drugs per plate to be screened. Further improvements to the imaging quality of the model for phase contrast microscopy were made. Experimental refinements on collagen concentration, volume, and fibroblast seeding density within the collagen were made in order to make phase contrast microscopy images clearer, without compromising the SOX2-driven phenotype. The data for the optimisation process of the OTC model for drug screening is not shown.

The first screen was a primary chemoprevention assay where compounds were added at the same time as doxycycline (experimental schematic shown in Figure 3.2A). The impact of inhibitors on the development of lesions was monitored via phase-contrast microscopy and compared to vehicle controls (VC). Lesions can be observed in phase-contrast microscopy images as clusters of cells growing out of the monolayer, which can be visualised more easily from cross sectional H&E images, where epithelial thickening and

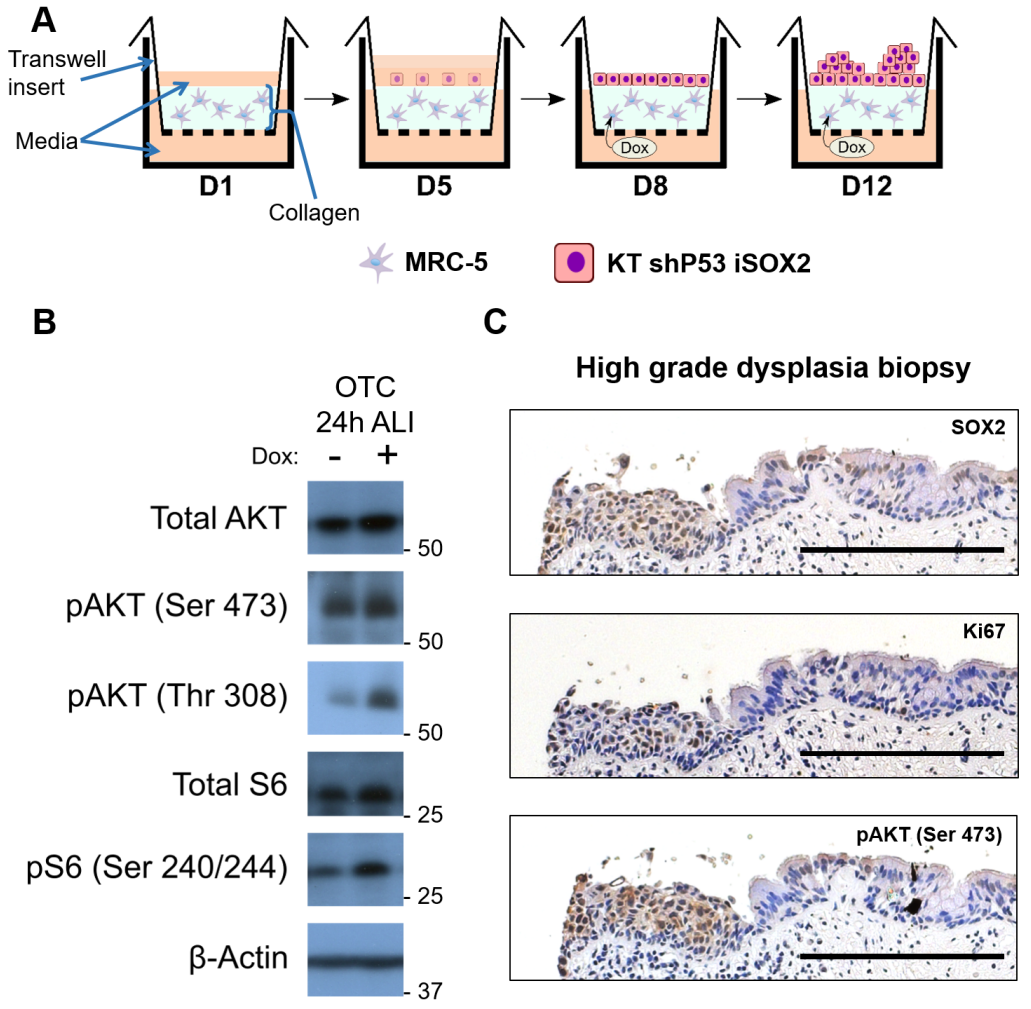

Figure 3.1: AKT signalling is upregulated in SOX2 positive high grade bronchial dysplasias.
A. Schematic outlining the setup of the OTC model. On day 1, transwell inserts were seeded with collagen embedded with human lung-derived MRC-5 fibroblasts. On day 5, immortalised human bronchial epithelial cells with constitutive p53 shRNA-mediated knockdown and Tet-On inducible SOX2 transgene (hereafter referred to as KT-shP53iSOX2) were seeded on top of the collagen disc submerged in media. On day 8, once the epithelial monolayer was confluent, cells were brought to the air-liquid interface (ALI) via removal of media from the apical side and doxycycline added to the basal medium to induce SOX2 expression. After 4 days at ALI plus doxycycline dysplastic lesions developed in the epithelial layer (Correia et al., 2017). **B.** Western blot showing AKT activation and downstream signalling in the OTC model after 24 h of SOX2 activation via doxycycline at ALI. **C.** Adapted from Correia et al. (2017), IHC staining for SOX2, Ki67 and pAKT (Ser473) on a human biopsy showing a junction between normal epithelium (RHS of the section) and a high grade dysplastic lesion (LHS of the section). IHC scale bars = 200 μm.

uncontrolled growth out from the epithelial layer can be seen (Figure 3.2B). AZD5363, a pan-AKT inhibitor prevented dysplastic lesions forming upon SOX2 induction (Figure 3.2B). MEK1/2 inhibition using Selumetinib appeared to accentuate the phenotype when compared to vehicle controls (Figure 3.2B). Of the other compounds, PI3K $\alpha/\delta/\beta$ inhibition using LY294002, and allosteric pan-AKT inhibition using MK-2206 had little effect; mTORC1/2 inhibition using AZD2014 had a moderate impact on the phenotype (Figure 3.2B).

The same group of compounds used in the primary chemoprevention model were applied to a secondary chemoprevention model. In this assay, compounds were added to the OTC model once a distinct phenotype was present 4 days after bringing cells to the ALI and doxycycline addition (experimental schematic shown in Figure 3.3A). The impact of inhibitors on established lesions was monitored and compared to vehicle controls. AZD5363, reverted dysplastic lesions back to a monolayer phenotype (Figure 3.3B). Similarly to the primary chemoprevention screen, certain compounds accentuated the SOX2-driven phenotype, Selumetinib and LY294002 resulted in large focal outgrowths (Figure 3.3B). Pan-AKT inhibition using MK-2206 showed little impact on established lesions, and AZD2014 showed moderate reduction of lesions (Figure 3.3B).

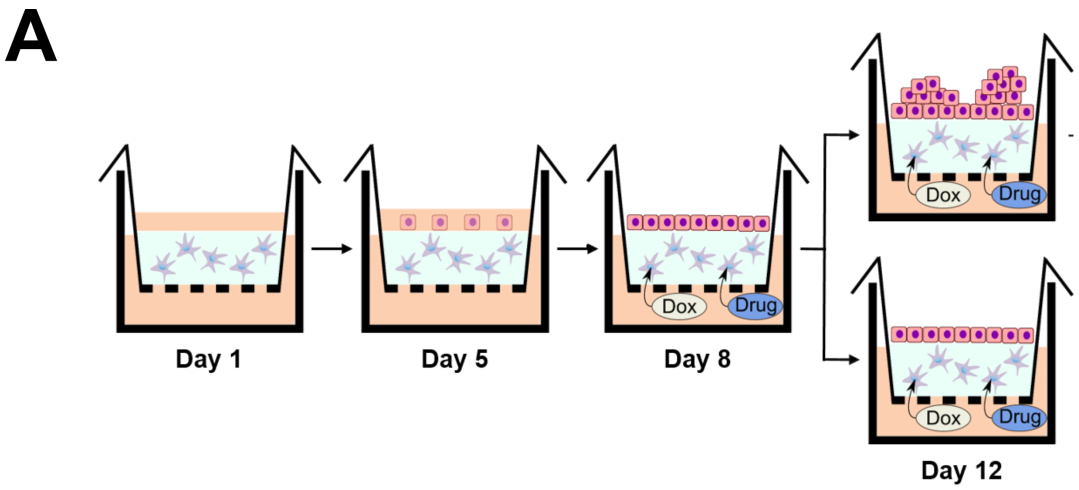
A
Day 1
Day 5
Day 8
Dox
Drug
Dox
Drug
Dox
Drug
Day 12

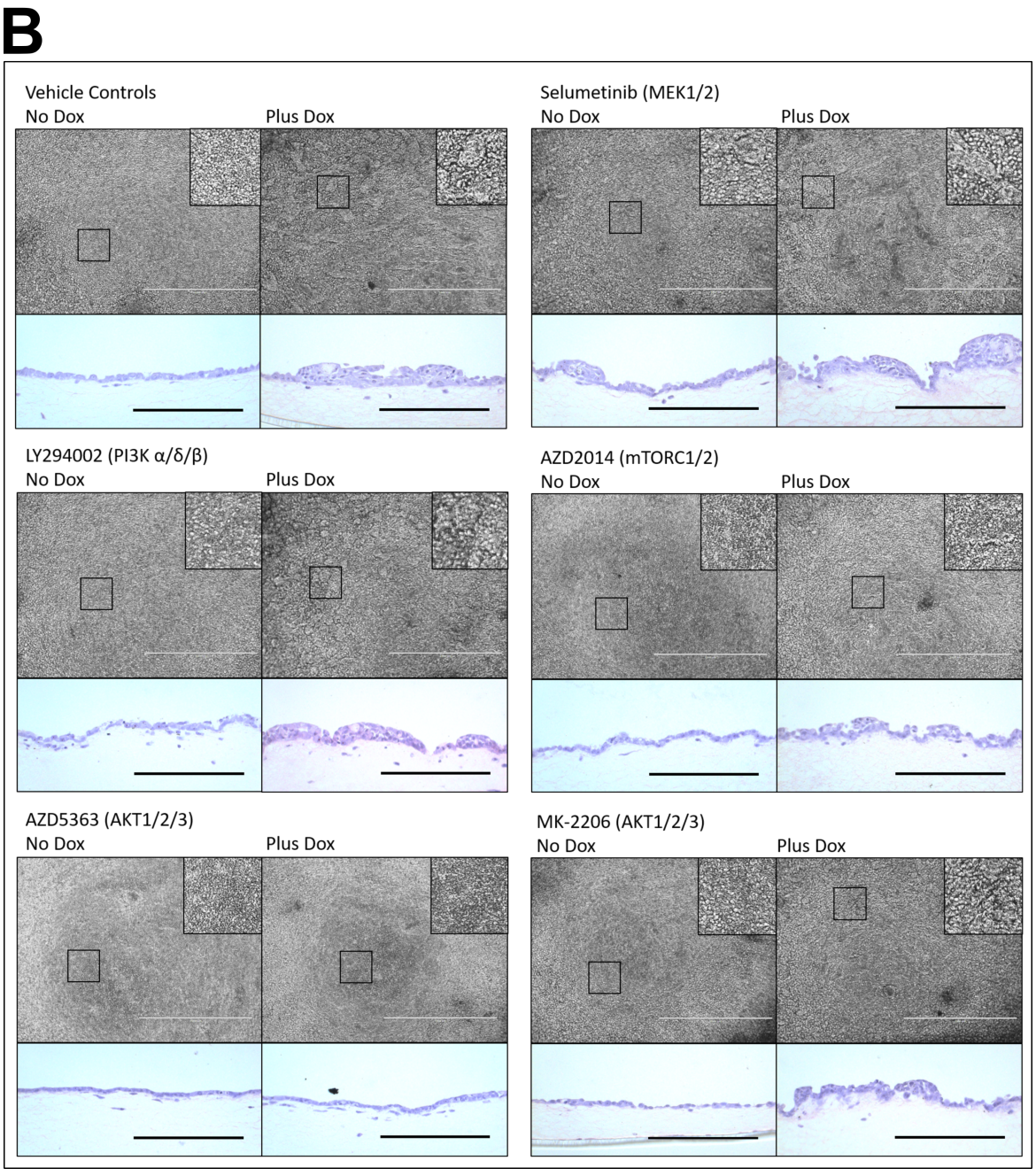
B
Vehicle Controls
No Dox
Plus Dox
Selumetinib (MEK1/2)
No Dox
Plus Dox
LY294002 (PI3K α/δ/β)
No Dox
Plus Dox
AZD2014 (mTORC1/2)
No Dox
Plus Dox
AZD5363 (AKT1/2/3)
No Dox
Plus Dox
MK-2206 (AKT1/2/3)
No Dox
Plus Dox

Figure 3.2: Pan-AKT inhibition using AZD5363 prevents dysplastic lesions developing in primary chemoprevention screens using the OTC model.
A. Schematic showing primary chemoprevention screening experimental setup. Test compounds were added at the same time that epithelial cells were brought to ALI and doxycycline added. Cells were treated every 48 h with test compounds ±doxycycline for a total of 96 h at ALI. Phenotypic responses were monitored via phase-contrast microscopy, prior to fixation & processing for histology. Compounds were used at following concentrations; Selumetinib - 0.3μM, LY294002 - 50 μM, AZD2014 - 1 μM, AZD5363 - 5 μM, MK-2206 - 5 μM. **B.** Phase-contrast images (top) and H&E sections (bottom) after 96 h treatment. Low magnification phase-contrast images capture overall phenotype and the insets show areas at higher magnification. H&E images show cross sections of the epithelial cells on the collagen-fibroblast matrix. The compound name and cognate protein target in parentheses are shown above each image set. Images and histology are representative across 3 experimental repeats. Phase-contrast scale bars = 1000 μm. H&E scale bars = 200 μm.

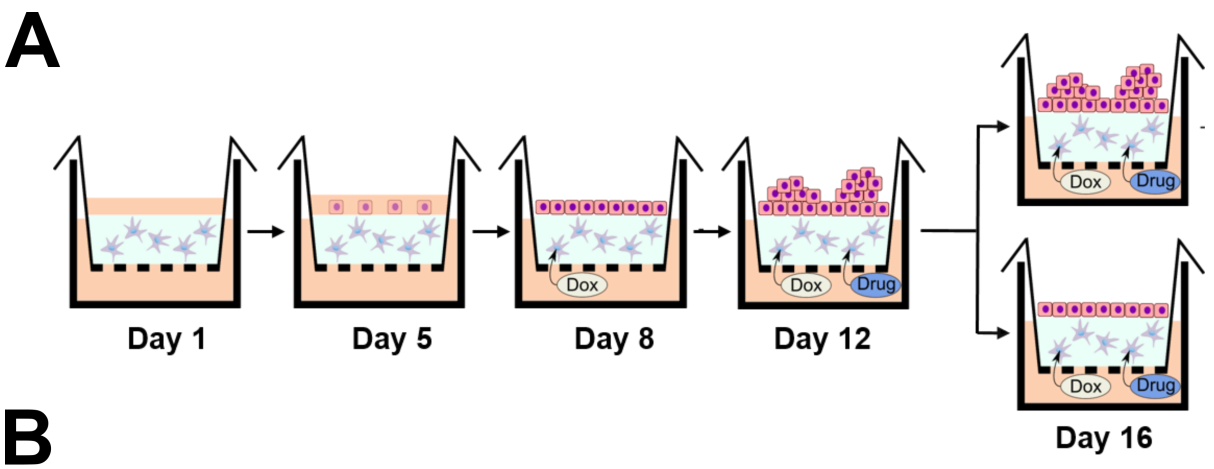
A
Dox
Drug
Day 1
Day 5
Day 8
Day 12
Day 16

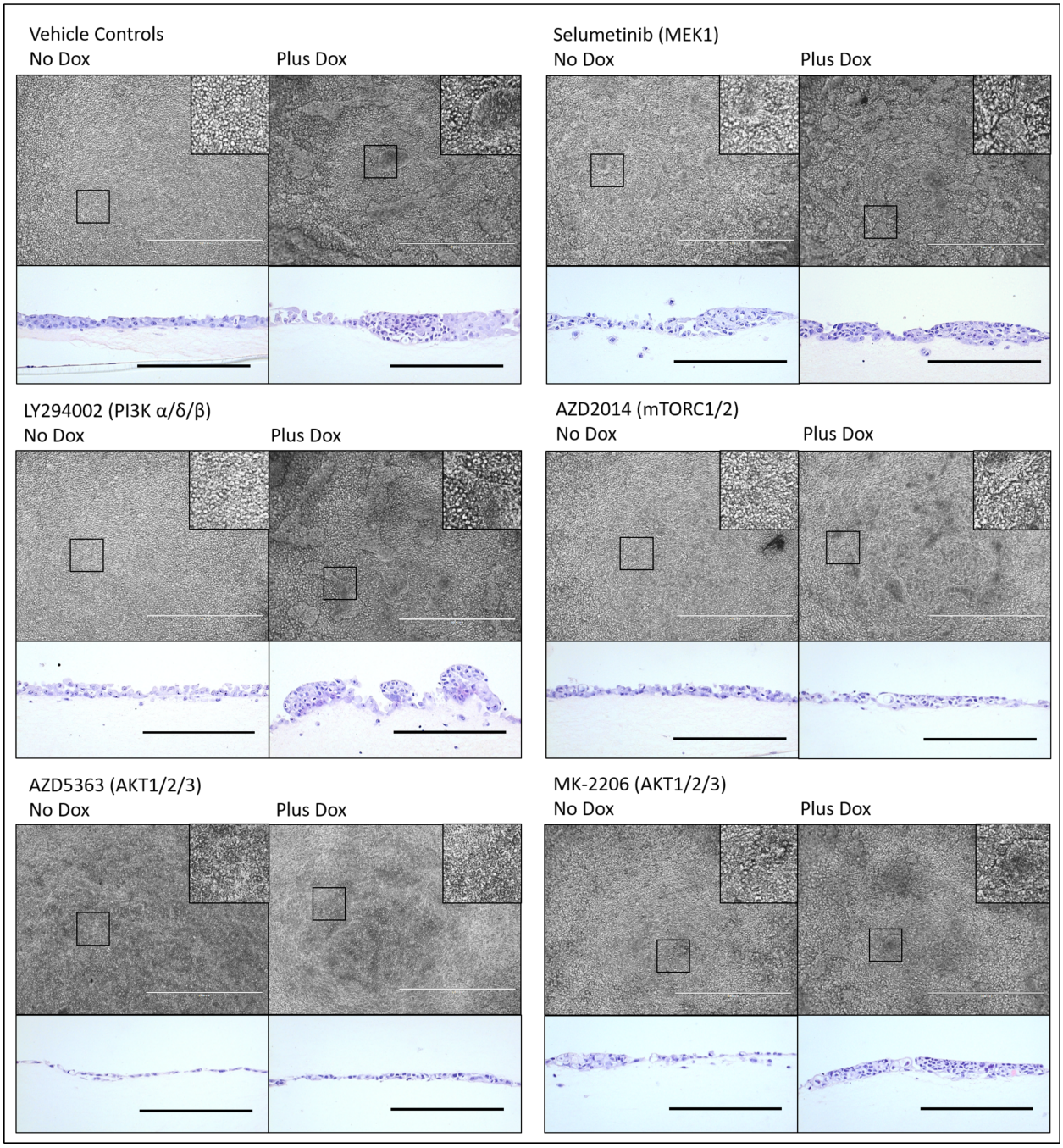
B
Vehicle Controls
No Dox
Plus Dox
Selumetinib (MEK1)
No Dox
Plus Dox
LY294002 (PI3K α/δ/β)
No Dox
Plus Dox
AZD2014 (mTORC1/2)
No Dox
Plus Dox
AZD5363 (AKT1/2/3)
No Dox
Plus Dox
MK-2206 (AKT1/2/3)
No Dox
Plus Dox

Figure 3.3: Pan-AKT inhibition using AZD5363 reverts dysplastic lesions to a monolayer epithelium in secondary chemoprevention screens using the OTC model. **A.** Schematic showing secondary chemoprevention screening experimental setup. Epithelial cells were brought to ALI and doxycycline added. Test compounds were added once a clear dysplastic phenotype was present at day 12. Cells were then treated every 48 h with test compounds and $\pm$doxycycline for a total of 96 h treatment. Phenotypic responses were monitored via phase-contrast microscopy, prior to fixation & processing for histology. Compounds were used at following concentrations; Selumetinib - 0.3μM, LY294002 - 50 μM, AZD2014 - 1 μM, AZD5363 - 5 μM, MK-2206 - 5 μM. **B.** Phase-contrast images (top) and H&E sections (bottom) after 96 h compound treatment. Low magnification phase-contrast images capture overall phenotype and the insets show areas at higher magnification. H&E images show cross sections of the epithelial cells on the collagen-fibroblast matrix. The compound name and cognate protein target in parentheses are shown above each image set. Images and histology are representative across 3 experimental repeats. Phase-contrast scale bars = 1000 μm. H&E scale bars = 200 μm.

The OTC model had not previously been used extensively for testing efficacy of small molecule inhibitors. It was therefore necessary to determine whether administering compounds on the basal side of the transwell would impact the epithelial cells on the apical side, atop of the collagen-fibroblast matrix, and show that intended targets were engaged and downstream signalling was altered in an expected fashion. In order to identify the appropriate dose for each compound, experiments were performed using the OTC model with concentration ranges based around previously reported data (Martelli et al., 2003; Huynh et al., 2007; Yan, 2009; Davies et al., 2012; Pike et al., 2013): Selumetinib 5-0.3 μM, LY294002 50-12.5 μM, AZD2014 1-0.06 μM, AZD5363 10-1 μM, MK-2206 10-1 μM. The highest dose that showed no signs of cytotoxic denudation of the epithelial layer was used in the compound screens.

Downstream effectors of the RAS-MAPK and PI3K-AKT signalling pathways in epithelial cells after treatment in the OTC are shown (Figure 3.4). All compounds used in the primary and secondary chemoprevention screens had impacts on their relevant downstream effector proteins that was consistent with previous studies using these compounds (Martelli et al., 2003; Huynh et al., 2007; Yan, 2009; Davies et al., 2012; Pike et al., 2013). Selumetinib showed moderate reduction on total ERK, pERK and pS6. LY294002 treatment showed reduction in pS6. MK-2206 and AZD2014 treatment both showed a reduction in pAKT and total S6/pS6 signalling. AZD5363 treatment showed an increase

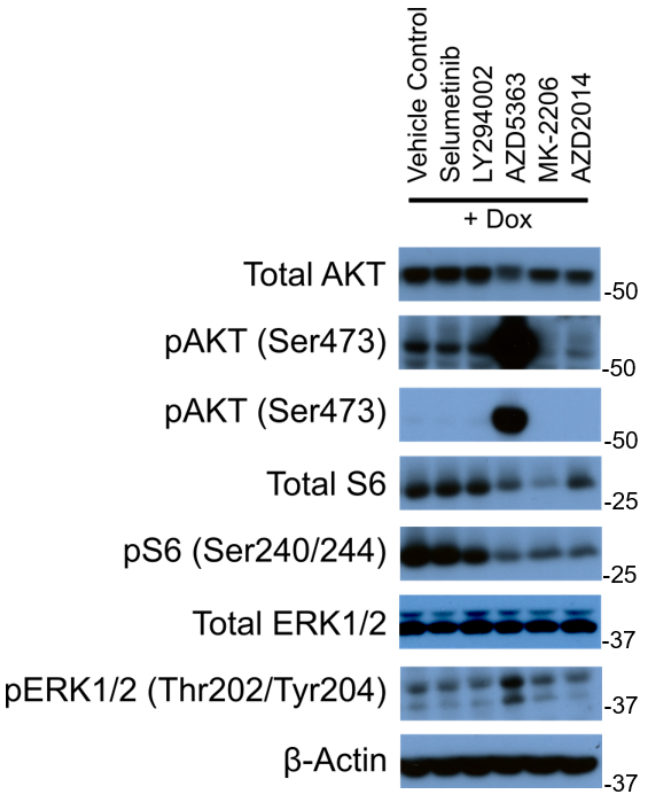

Figure 3.4: Compounds show engagement with intended targets and alteration of relevant downstream signalling pathways when used in the OTC model.
Western blot showing signalling proteins of the PI3K-AKT and RAS-MAPK pathways in the OTC model following treatment with compounds. Lysates of epithelial cells were generated from 48 h treated secondary chemoprevention assays in the OTC model using PI3K, AKT, mTOR and MEK inhibitors, as shown in Figure 3.3. Western blot representative of 3 experimental repeats.

of pAKT, and reduction of total S6/pS6 signalling. An increase of pAKT seems counter-intuitive for an AKT inhibitor however, AZD5363 inhibits AKT in an ATP competitive manner, PIP_3 binds AKT and causes AKT to be localised at the cell membrane in a hyper-phosphorylated but inactive state.

The pan-AKT inhibitor, AZD5363, emerged from both the primary and secondary chemoprevention screens as a candidate compound to investigate further, due to the desirable phenotypic impacts in primary and secondary chemoprevention preventing and reversing SOX2-driven dysplastic phenotypes in the OTC model.

3.3 AKT inhibition using AZD5363 reduces cell numbers by increasing cell death in the OTC model

Dose response studies using AZD5363 showed a dose-dependent impact on cell numbers and AKT signalling (Figure 3.5). In the OTC model, cell numbers significantly increase when SOX2 is overexpressed (Figure 3.5B), and treatment with 5 μM and 10 μM AZD5363 $\pm$doxycycline resulted in a significant reduction in cell number (Figure 3.5B). The resultant impact on overall histological phenotype associated with increasing doses of AZD5363 are shown (Figure 3.5A). Dose-dependent effects on downstream signalling were also observed by western blot; increased levels of pAKT and reduction of total S6/pS6 with increasing concentrations of AZD5363 (Figure 3.5C).

It has been shown that treating the OTC model with the pan-AKT inhibitor, AZD5363, reverted dysplastic lesions to a monolayer, which correlated with a reduction in cell numbers. SOX2 positive cells remained after treatment with AZD5363 (Figure 3.6). Using TUNEL IF (Section 2.6.5) to assess apoptosis there was a significant increase in apoptotic cells after 6 h treatment in the secondary chemoprevention OTC model (Figure 3.7B). Figure 3.7A shows that intended targets engaged (as seen in Figure 3.4) and impacted downstream effectors in the OTC model following a 6 h treatment with AZD5363.

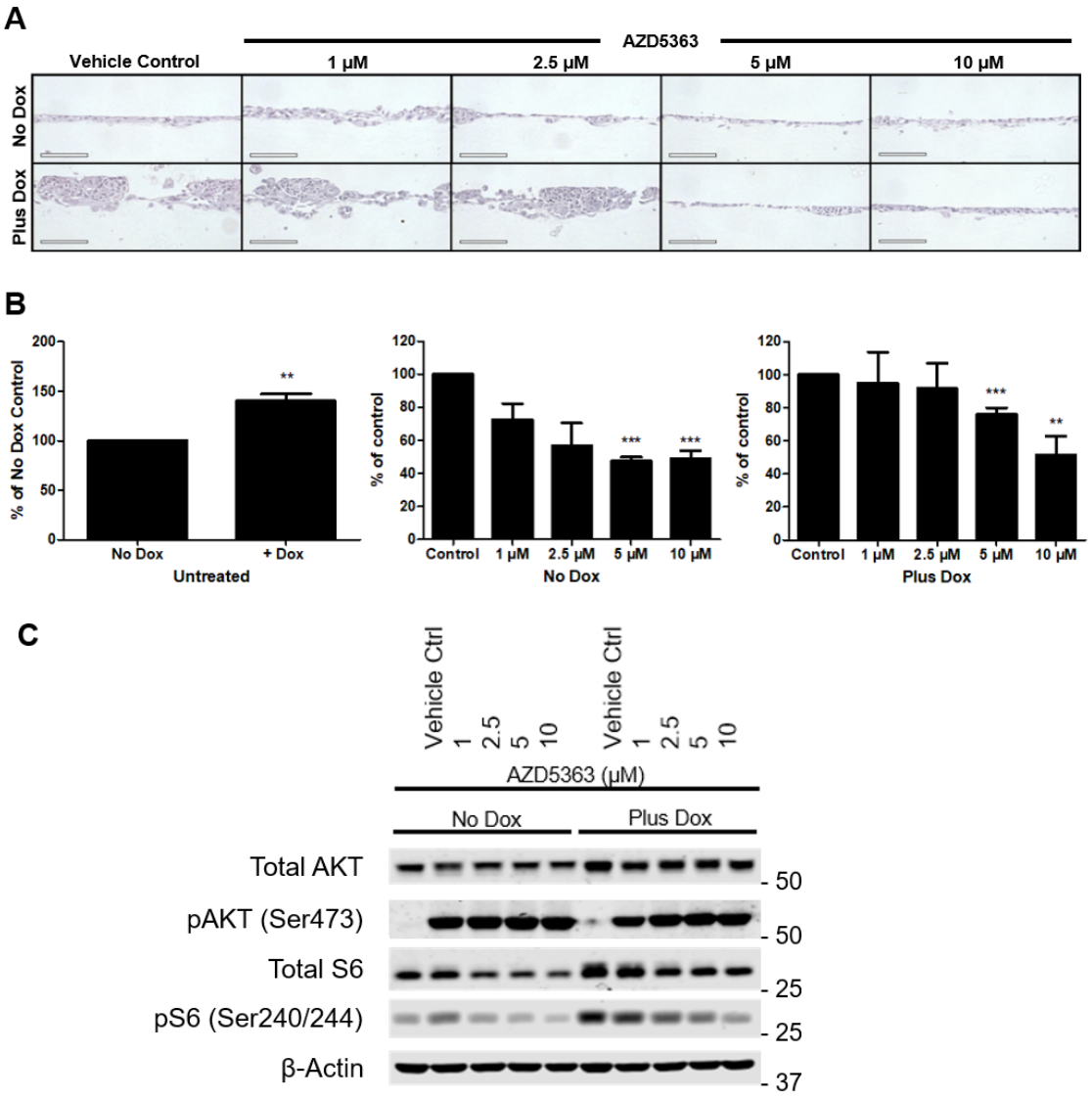

Figure 3.5: AZD5363 reduces cell numbers and impacts downstream AKT signalling in the OTC model in a dose-dependent manner.
A. H&E sections following a 96 h AZD5363 treatment in secondary chemoprevention assays. **B.** Cell counting following AZD5363 treatment. Cells were dissociated from the collagen-fibroblast matrix using trypsin and counted after 96 h secondary chemoprevention in the OTC model. SOX2 induction in the untreated OTC model caused a significant increase in cell numbers. 5 μM and 10 μM AZD5363 treatment caused a significant reduction in cell numbers compared to relative controls. **C.** Western blot showing AKT signalling proteins in the OTC model following treatment with AZD5363. There is a dose-dependent reduction in S6 and pS6 signalling when AZD5363 was used in the OTC model in a secondary chemoprevention assay. Histology images are representative of 3 experimental repeats. Cell counting results represent the mean $\pm$SEM from 3 experimental repeats. Scale bars in H&E images = 100 μm. Significant differences compared to relevant vehicle controls were determined using an unpaired t-test, two tailed P values: * $p \leq 0.05$, ** $p \leq 0.01$, *** $p \leq 0.001$.

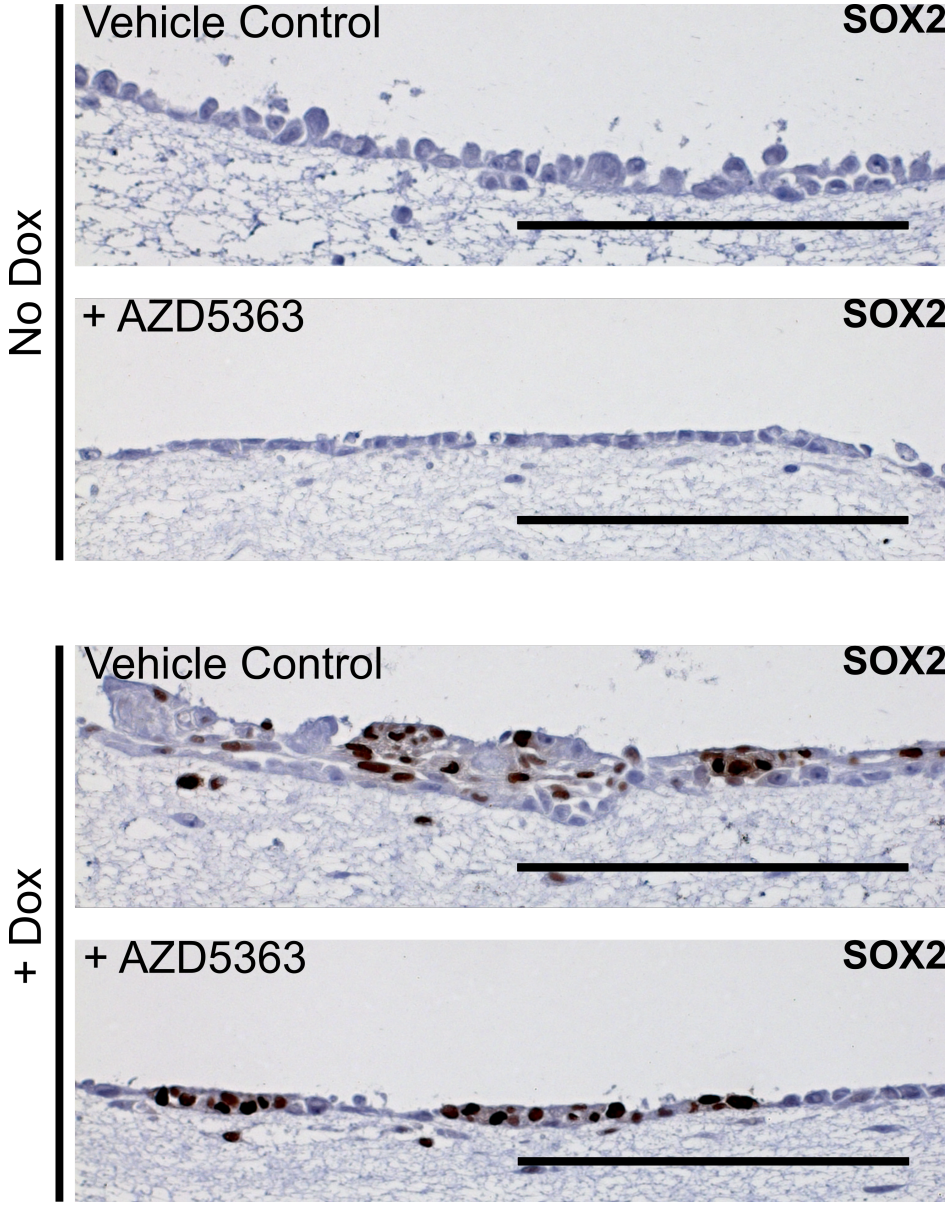

Figure 3.6: SOX2 positive cells remain following treatment of the OTC model with AZD5363.
IHC for SOX2 after 48 h AZD5363 treatment in secondary chemoprevention assays. Scale bars = 200 μm. Images and histology are representative of 3 experimental repeats.

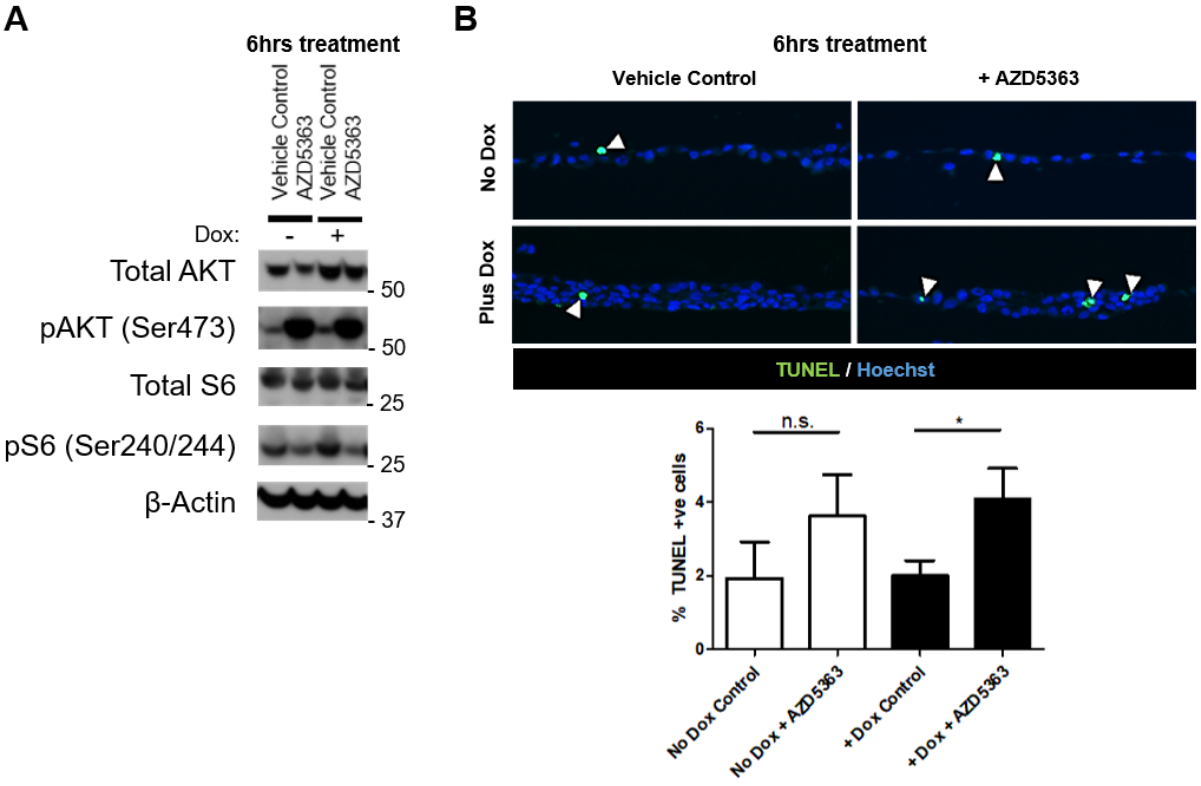

Figure 3.7: AZD5363 treatment significantly increases apoptosis in the SOX2-driven OTC model.
A. Western blot showing compound efficacy at a short time point of 6 h treatment in the OTC model using 5 μM AZD5363. **B.** TUNEL IF images of 6 h 5 μM AZD5363 treated secondary chemoprevention assays. Quantification of TUNEL positive cells is shown in the bar graph. White triangles indicate TUNEL positive cells. Images were taken across whole sample sections and percentage of TUNEL positive cells was quantified, quantifications represent the mean $\pm$SD from 3 experimental repeats. Significant differences were determined using an unpaired t-test, two tailed P values: * $p \leq 0.05$, ** $p \leq 0.01$, *** $p \leq 0.001$. Western blot was a pilot experiment. Images are representative of 3 experimental repeats.

3.4 AKT inhibition using AZD5363 in squamous cell line panel

Having established AZD5363 as a compound that shows impact in chemoprevention assays using the OTC model, validating the compound in other *in vitro* models was pursued. A panel of commercially available cell lines derived from lung squamous cell carcinoma, esophageal squamous cell carcinoma and lung adenocarcinoma was screened using resazurin-based approach in 2D tissue culture proliferation assays with AZD5363 (Czekanska, 2011) (Section 2.1.5). There were varying degrees of sensitivity to the AKT inhibitor; compared to the vehicle controls, H520, KYSE-140 and TE-6 cell lines showed significant inhibition of proliferation with p-values $\leq$0.001, while A549 and KYSE-410 proliferation was inhibited with p-values $\leq$0.05 (Figure 3.8A).

The panel of cell lines, with the exception of A549, were considered to be of squamous cell phenotype and origin. This was validated by western blot probing for squamous cell markers p63 and cytokeratin 5, as well as SOX2 (Figure 3.8B). Not all cell lines that were considered to be of squamous origin were found to be positive for these squamous cell markers. KYSE-140, TE-7, TE-6, TE-10 all showed strong dual p63 and cytokeratin 5 positivity. KYSE-30 and KYSE-410 showed a strong p63 and modest cytokeratin 5 phenotype. H520 and LK-2 cell lines had no detectable p63, and minimal cytokeratin 5 (Figure 3.8B).

Taken together, the KYSE-140 and TE-6 cells were the only squamous cell carcinoma cell lines that showed inhibition of proliferation after treatment with 5 μM AZD5363 giving p-values $\leq$0.001 (Figure 3.8A). These cell lines also express high SOX2 levels, consistent with increased SOX2 copy number (Figure 3.8C).

Downstream effectors of the PI3K-AKT and RAS-MAPK signalling pathways in the panel of cell lines in traditional 2D tissue culture growth conditions are shown (Figure 3.9). Across the panel of cell lines used, there was varying expression levels and activation via phosphorylation of the PI3K-AKT and RAS-MAPK signalling pathways. KYSE-140, TE-6 and TE-10 cells showed high pAKT levels. A549, KYSE-140, TE-7 and TE-10 cells

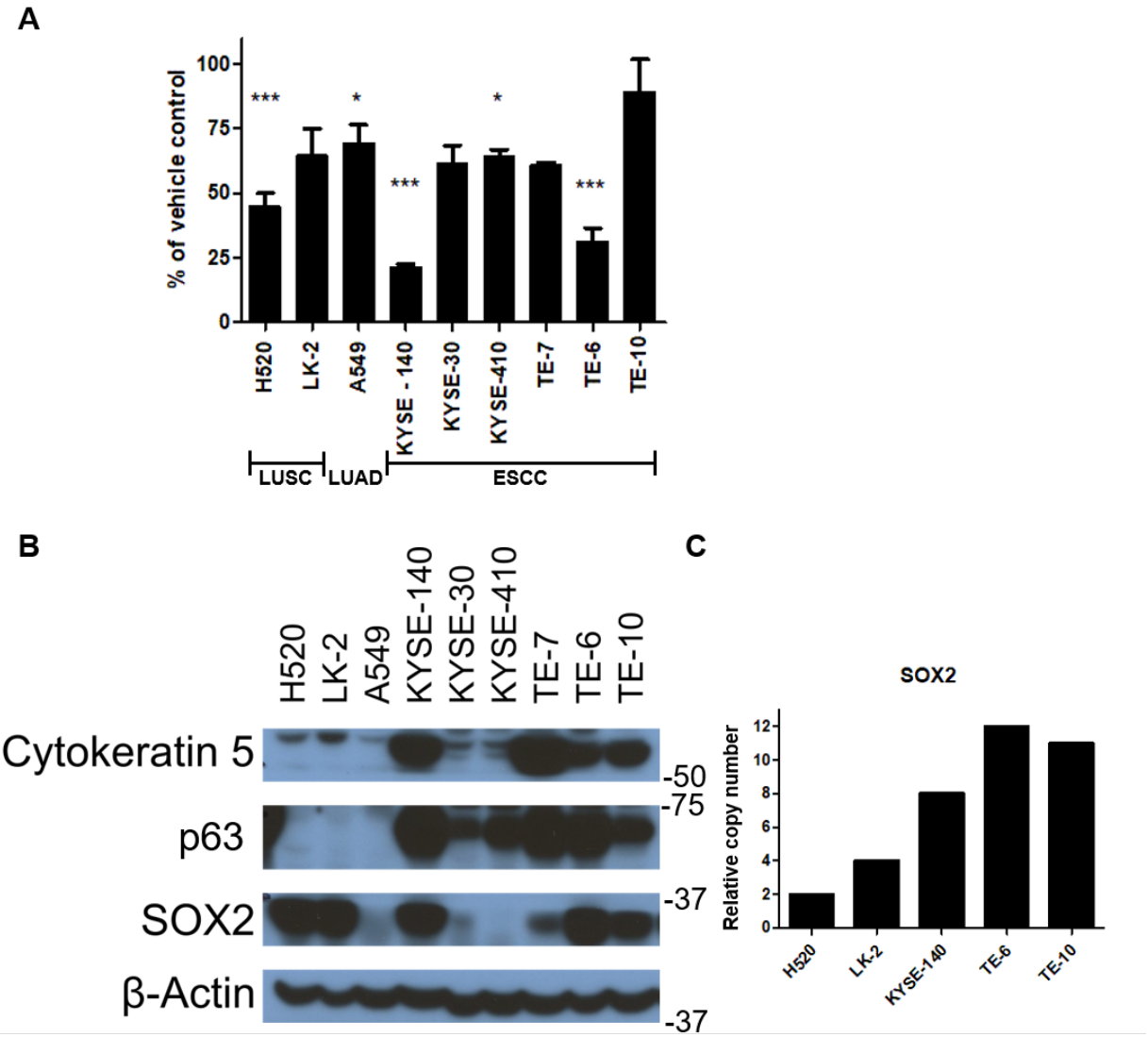

Figure 3.8: AZD5363 inhibits proliferation in a subset of squamous cell carcinoma cell lines

A. Proliferation assay ± 5 μM AZD5363 for 96 h on a panel of cell lines. The resazurin assay was used to measure viable cells after treatment compared to vehicle controls. Adjusted percentage of vehicle controls are shown for each cell line. **B.** Western blot on cell line panel samples for phenotypic markers of squamous cells, p63 and cytokeratin 5, and SOX2 expression status. **C.** SOX2 relative copy number status of SOX2 positive cell lines, adapted from the COSMIC database and Gen et al. (2010a). SOX2 relative copy number data was not available for TE-7 cell line. LUSC = lung squamous cell carcinoma, LUAD = lung adenocarcinoma, ESCC = esophageal squamous cell carcinoma. Significant differences between VC and drug treated cells were determined using an unpaired t-test, two tailed P values: * $p \leq 0.05$, ** $p \leq 0.01$, *** $p \leq 0.001$ for proliferation assays. Western blot is representative of 2 experimental repeats. Proliferation data represents the mean ± SD from 3 experimental repeats.

showed high pERK levels.

AZD5363 efficacy in squamous carcinoma cell lines with SOX2 amplification ± AZD5363 is shown (Figure 3.10). Increased levels of pAKT are indicative of the compound reaching its intended molecular target, as an ATP-competitive inhibitor. Reduction of pS6 was observed in KYSE-140 and TE-6 cell lines with AZD5363. TE-10 cells showed a very modest reduction in pS6 with treatment and an increase in pERK when treated with AZD5363 (Figure 3.10).

Of the SOX2-amplified, p63/cytokeratin 5 positive cells, TE-10 was insensitive to pan-AKT inhibition (Figure 3.8A). Data from the Cancer Cell Line Encyclopedia show that TE-10 cells carry a mutation in RASA1, a negative controller of MEK-ERK signalling, that activates MEK-ERK signalling and is present in NSCLCs sensitive to MEK inhibition (Hayashi et al., 2018; Barretina et al., 2012), (Cancer Cell Line Encyclopedia). This provides a functional explanation for the limited response to AKT inhibition.

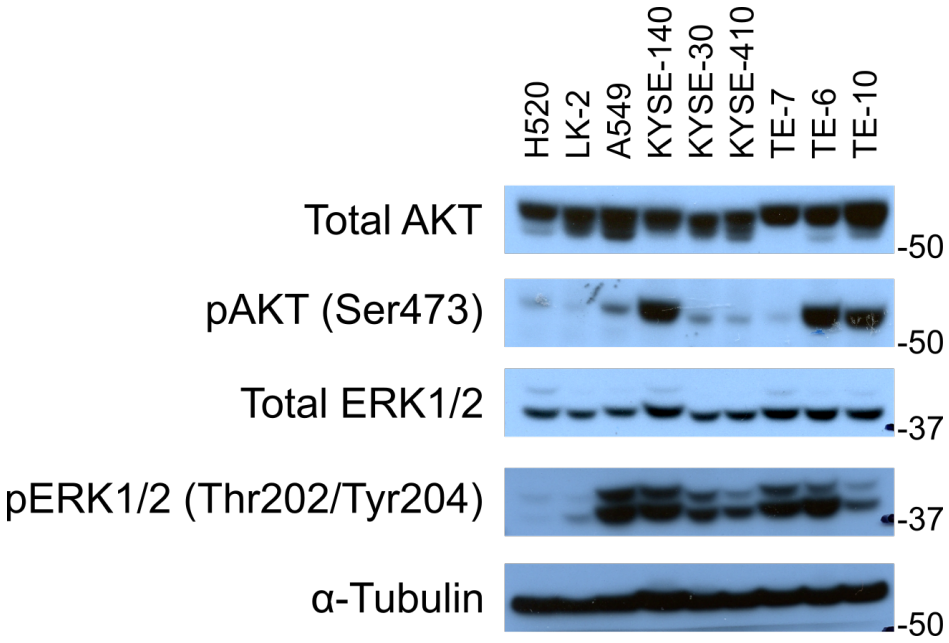

Figure 3.9: Cell line panel has differing levels of activation in AKT and MAPK signalling pathways.
Western blot on cell line panel samples for AKT and MAPK signalling pathways. KYSE-140, TE-6 and TE-10 cell line have high pAKT signalling. A549 and KYSE-140 have high pERK signalling. Western blot is representative of 2 experimental repeats.

Figure 3.10: Cell lines validated for squamous phenotype and SOX2 expression treated with AZD5363 engage intended targets and alter downstream signalling pathways.
Western blot AKT and ERK signalling on KYSE-140, TE-6 and TE-10 cell lines treated for 96 h with 5 μM AZD5363 in standard 2D tissue culture. Western blot is representative of 3 experimental repeats.

3.5 Pan-AKT inhibition rather than AKT1/2 inhibition prevents lesions developing and reverts established lesions to a monolayer in the OTC model.

Following the use of two pan-AKT inhibitors, AZD5363 and MK-2206 in primary and secondary chemoprevention screens, only AZD5363 showed phenotypic impact in the model, despite both inhibitors engaging the intended targets (Figures 3.2, 3.3, 3.4). In cell-free kinase assays the reported IC50 values for AKT isoforms 1/2/3 are 3 nM/8 nM/8 nM respectively for AZD5363, and 8 nM/12 nM/65 nM respectively for MK-2206, therefore it was hypothesised that the impact of AZD5363 in the OTC model was based on the increased efficacy to AKT3 compared to the lesser impact of MK-2206 in the OTC model (IC50 values as stated on *www.selleckchem.com* chemical website).

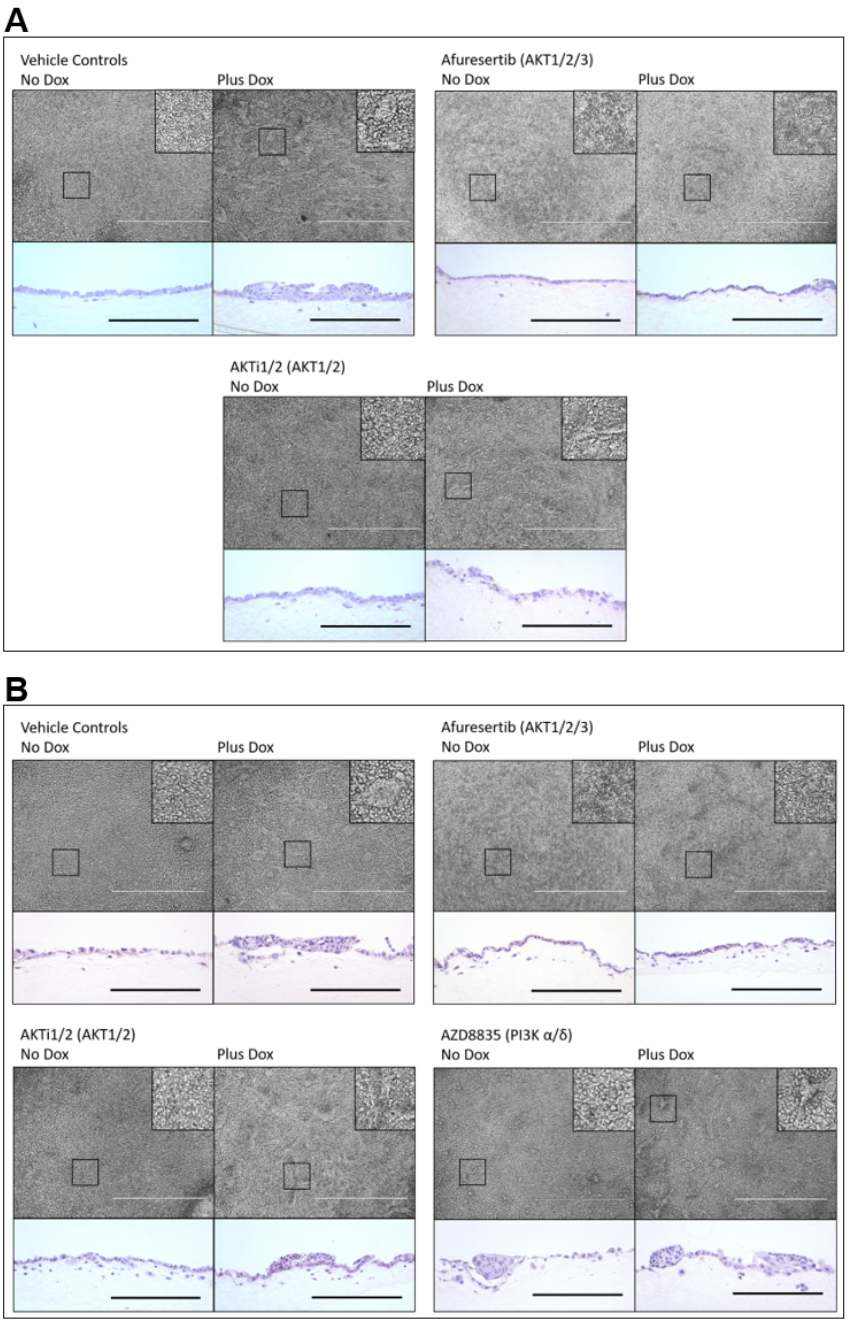
A
Vehicle Controls
No Dox
Plus Dox
Afuresertib (AKT1/2/3)
No Dox
Plus Dox
AKTi1/2 (AKT1/2)
No Dox
Plus Dox
B
Vehicle Controls
No Dox
Plus Dox
Afuresertib (AKT1/2/3)
No Dox
Plus Dox
AKTi1/2 (AKT1/2)
No Dox
Plus Dox
AZD8835 (PI3K α/δ)
No Dox
Plus Dox
C
Vehicle Control
Afuresertib
AKTi1/2
+ Dox
Total AKT
pAKT (Ser473)
Total S6
pS6 (Ser240/244)
β-Actin
-50
-50
-25
-25
-37
Vehicle Control
AZD8835
+ Dox
Total AKT
pAKT (Ser473)
Total S6
pS6 (Ser240/244)
β-Actin
-50
-50
-25
-25
-37

Figure 3.11: Pan AKT inhibitor, Afuresertib, prevents and reverts dysplastic phenotype in both primary and secondary chemoprevention assays in the OTC model. AKT1/2 inhibitor, AKTi1/2, does not.
A. Primary chemoprevention assay in the OTC model. Experimental setup was the same as outlined in the schematic in Figure 3.2. 5 μM Afuresertib and 5 μM AKTi1/2 treatments were used. Phase-contrast images and H&E sections after 96 h compound treatment. Low magnification images capture overall phenotype and the insets show areas at higher magnification. H&E images show cross sections of the epithelial cells on the collagen-fibroblast matrix. The compound name and cognate protein target in parentheses are shown above each image set. **B.** Secondary chemoprevention assay in the OTC model. Experimental setup was the same as outlined in the schematic in Figure 3.3. 5 μM Afuresertib, 5 μM AKTi1/2 and 2.4 μM AZD8835 treatments were used. **C.** Western blot showing AKT and PI3K inhibitor efficacy on downstream effectors. Protein lysates were from epithelial cells in 48 h treated secondary chemoprevention assays using the OTC model. Phase-contrast scale bars = 1000 μm. H&E scale bars = 200 μm. Western blots are representative of 2 experimental repeats. Histology and images are representative across 3 experimental repeats.

Since there was a suggestion that the compound with less activity against AKT3 had a lesser impact on the dysplastic phenotype a further two tool compounds were used to interrogate further the impact of compound AKT isoform specificity. Afuresertib has similar IC50 values in cell-free kinase assays (AKT1/2/3, 0.1 nM/2 nM/3 nM respectively) for the AKT isoforms as AZD5363, and AKTi1/2 is a highly selective AKT1 and AKT2 inhibitor (AKT1/2/3,58 nM/210 nM/2119 nM respectively). In both primary and secondary chemoprevention assays using the OTC model Afuresertib prevented and reversed SOX2-driven dysplasia (Figure 3.11A,B). The AKT1/2 specific inhibitor did not prevent dysplastic lesions or reverse lesions to a monolayer. Target engagement with compounds in the OTC model are shown, increasing pAKT and reducing pS6 with Afuresertib, and reducing pAKT and pS6 with AKTi1/2 when compared to the doxycycline treated vehicle controls (Figure 3.11C).

AZD8835, a more potent specific inhibitor of PI3K than LY294002 used earlier in the chapter (Figures 3.2 and 3.3), was more effective in reducing downstream S6/pS6 signalling (Figure 3.11C), but did not reverse developed lesions in the OTC model (Figure 3.11B).

The relative impact of SOX2 amplification on cell line sensitivity to a series of compounds using KYSE-140 as a SOX2-amplified and KYSE-30 as a non SOX2-amplified SQC line was investigated. Proliferation assays using PI3K, mTORC1/2, pan-AKT and MEK1/2 in-

hibitors showed that only AKT inhibition had a significant impact on proliferation in KYSE-140 cell line (Figure 3.12). This suggested a preferential vulnerability to AKT inhibition in SOX2-amplified squamous cell lines.

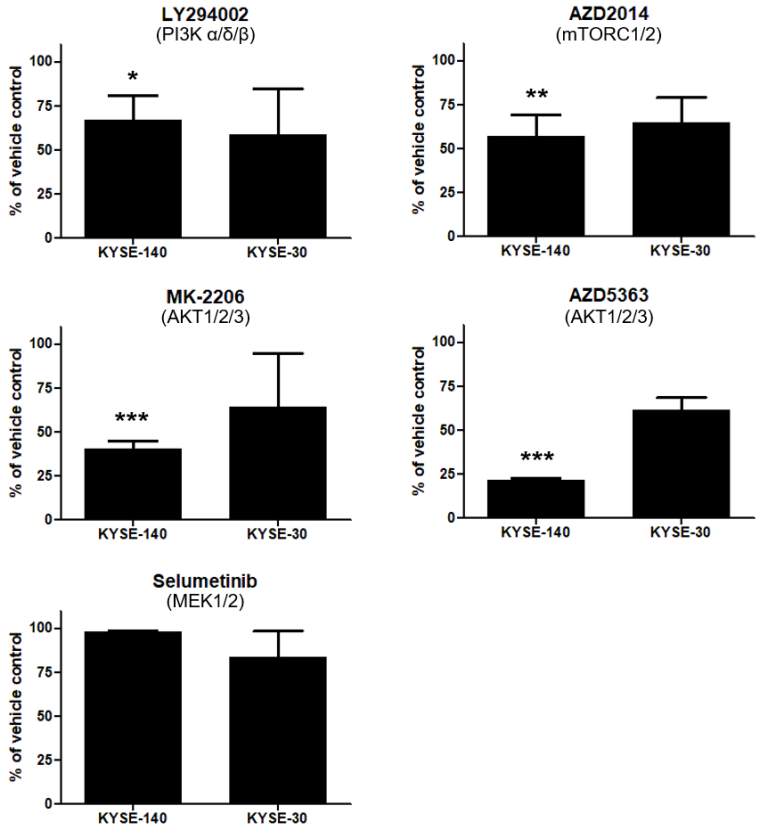

Figure 3.12: AKT inhibition reduces proliferation in SOX2-amplified squamous cell carcinoma cell lines. Inhibition of other nodes in the PI3K/AKT and RAS/MAPK pathways does not show as profound impact on proliferation.
Proliferation assays using KYSE-140 and KYSE-30 cell lines. Cells were treated with 25 μM LY294002, 0.1 μM AZD2014, 5 μM MK-2206, 5 μM AZD5363 and 1 μM Selumetinib for 96 h. The resazurin assay was used to measure viable cells after treatment compared to vehicle controls. Proliferation data represents the mean $\pm$SD from 3 experimental repeats. Significant differences between VC and drug treated cells were determined using an unpaired t-test, two tailed P values: * $p \leq 0.05$, ** $p \leq 0.01$, *** $p \leq 0.001$ for proliferation assays.

3.6 Discussion

3.6.1 Summary

It was demonstrated that the OTC model can be used for rational screening of compounds in the chemoprevention of SQC. Of the various nodes in the PI3K-AKT pathways, pan-AKT inhibition, rather than AKT1/2 inhibition, was effective at both prevention of dysplastic lesions and reversion of established lesions in primary and secondary chemoprevention assays. AKT inhibition was validated in SOX2-amplified and non SOX2-amplified squamous carcinoma cell lines, showing a preferential growth inhibition in SOX2-amplified cells. The results of this study provide a rationale for the continued investigation of AKT inhibition in SOX2-driven squamous cell carcinomas.

3.6.2 Using the OTC model for phenotypic screening of compounds in the chemoprevention of SQC

In this chapter it was demonstrated for the first time that the OTC model can be used to screen small sets of compounds for the chemoprevention of SQC, using a phenotypic screening approach adopted increasingly by industrial drug discovery programmes (Zheng et al., 2013). In a previous study, a basic organotypic culture model of bronchial hyperplasia used human bronchial epithelial cells, grown at the ALI and induced with EGF, to screen a small number of compounds for the chemoprevention of bronchial hyperplasia (Lee et al., 2011). The OTC model I used in this study constitutes a more clinically applicable model, with the added microenvironment complexity of the collagen-fibroblast matrix and relevant genetic abberations to the human disease. It should be noted that, although doxycycline has been implicated as an anticancer agent in some studies, the effects of doxycycline have no impact on the growth of non-transduced KT “wild-type” cells, and the OTC model uses much lower concentrations of doxycycline than those concentrations that have demonstrated significant growth inhibition (Lamb et al., 2015; Correia et al., 2017).

Due to the 3D nature of the model, presenting images of 3D lesions using 2D phase contrast images for this thesis proved challenging. Higher magnification inserts in figures were used to highlight areas of significance, without retracting from the advantage of capturing approximately 75% of each transwell in low magnification images, removing the potential of human bias in selection of areas of transwell to image (Figures 3.2 and 3.3). Like many advanced cell culture models, the OTC model requires a certain amount of training and familiarity to use consistently as a screening platform, due to its qualitative rather than quantitative readout. This is obtainable within a month of using the model, and has clear advantages over genetically engineered mouse models in this aspect.

3.6.3 Targeting AKT as opposed to other nodes in the PI3K-AKT/RAS-MAPK pathways has favourable phenotypic impacts

PI3K inhibition in the chemoprevention screens had no impact on the phenotype. This was surprising to observe as PI3K is a major upstream activator of AKT (Figures 3.2 and 3.3). It may be expected that inhibition of a major upstream activator of AKT such as PI3K would mimic the effects of pan-AKT inhibition. The PI3K inhibitors showed downstream reduction in pS6 signalling, but AKT activation was unchanged, suggesting a PI3K independent activation of AKT upon SOX2 induction (Mahajan and Mahajan, 2012). Mahajan and Mahajan (2012) discuss a large and diverse group of tyrosine and serine/threonine kinases that directly activate AKT, promoting proliferative signals. It has been shown that PI3K inhibition only reduces AKT activation on a short term transient basis, and re-activation of AKT occurs in a PI3K-independent manner (Dufour et al., 2013). mTORC1/2 inhibition had minimal impact on the phenotype. This was surprising too, as mTORC2 is involved in activation of AKT.

The MEK1/2 inhibitor, Selumetinib, was included in the panel of compounds. It has been shown that dysplasia and early SQC characteristically have upregulation of PI3K-AKT signalling as opposed to the RAS-MAPK pathway that is often upregulated in adenocarcinomas of the lung. So it was hypothesised that MEK inhibition would not have a marked impact in an OTC model of early SQC. Both pathways converge on the downstream ef-

fector protein S6, and Selumetinib showed very modest impact on downstream effectors pERK and pS6 when SOX2 was upregulated in the OTC, with the phenotype appearing to be accentuated with large outgrowths. However, Selumetinib showed strong reduction in pS6 signalling when SOX2 was not induced, suggesting that SOX2 upregulation activated S6 in a MEK-independent manner.

The impact of the pan-AKT inhibitor AZD5363 compared to pan-AKT inhibitor MK-2206 was profound in both chemoprevention assays (Figures 3.2 and 3.3). Both compounds inhibited AKT as expected, with relevant and comparable target engagement and downstream effectors altered (Figure 3.4). However, no alterations in biochemical signalling were consistently associated with a phenotypic response; for example, a reduction in pS6 and pAKT signalling did not relate to a particular phenotypic output. This is not to say that there may not be a biochemical signal associated with prevention/reversal of dysplasia, as only a limited number of signalling proteins in the PI3K-AKT and RAS-MAPK pathways were investigated. One signal alteration of note is the increased pERK signalling with AZD5363 treatment, which could be as a result of cross-inhibition between the two pathways. Mendoza et al. (2011) describe how activated AKT is involved in a negative feedback of ERK activation via RAF, so when AKT is inhibited the negative feedback is removed. This has also been described with MEK inhibition triggering a signal rebound activating PI3K-AKT signalling (Hayashi et al., 2008; Manchado et al., 2016).

A limitation of the drug screens in this study from a pharmacological point of view was that full IC50 dose response, for example a semi-log dose-response, data was not generated for each compound in the OTC. In this study, a small range of doses were used based on previous concentrations used in the literature, with the highest non-toxic dose used for further investigation. The transwell and collagen disc setup of the OTC model renders it unsuitable for standard biochemical assays such as formazan-based assay MTT, resazurin and Cell Titer-Glo to generate IC50 curves. Manual harvesting of cells from the OTC for counting is extremely time consuming. That said, the medium-throughput assessment of small molecule inhibitors using a qualitative phenotypic readout in a complex, clinically relevant OTC model is advantageous as clear phenotypic responses were observed in the small compound screen performed in this study. Although some compounds were

used at *in vitro* concentrations that may not be clinically relevant or achievable, doses were used that were known to engage the intended molecular target and used to guide target identification for future chemopreventative compounds.

3.6.4 **AZD5363 increased apoptotic cell numbers**

Reversion of established lesions to a monolayer when treated with AZD5363 correlated with significant reduction in cell numbers, as well as a significant increase of apoptotic cells when treated with the compound (Figures 3.5 and 3.7). AKT-dependent apoptosis is most likely responsible for the reduction in cell numbers and reversion of established lesions to a monolayer (Manning and Toker, 2017). This was consistent with preclinical data for this compound: AKT inhibition using AZD5363 induced apoptosis in *PTEN*/*PIK3CA* mutant, RAS-wild type cell lines (Davies et al., 2012). Induction of apoptosis and autophagy has also been shown in response to AKT suppression and ERK upregulation in neuroglioma (Lou et al., 2016).

A curious, but significant, observation throughout this study was the consequence of AZD5363 mediated AKT inhibition in the OTC model when SOX2 was not induced. Cell numbers significantly reduced and apoptotic cells were seen to increase (although non-significantly) with AZD5363 treatment in experimental controls with no doxycycline added. The epithelial cells in the OTC model have constitutive p53 knockdown and small focal outgrowths can occur as a consequence of p53 deregulation alone. The reductions in cell numbers and increased apoptotic rates in control experiments minus doxycycline most likely relate to these lesions being impacted. AKT inhibition reverts and prevents the growth of infrequent focal p53 deregulated lesions (no doxycycline OTC) as well as the larger diffuse lesions driven by cooperating p53 and SOX2 deregulation (plus doxycycline OTC). The SOX2-driven phenotype was focussed on in this study as 3q/SOX2 amplification is a crucial driving event in the progression of early SQC (Section 1.3.5), representing a clinically relevant genotype and phenotype. However, p53 disruption is found to be an early event in the progression of SQC (Section 1.3.4) (Sundaresan et al., 1992) and if a chemoprevention strategy targeted at SOX2-driven lesions was also effective on early

p53 deregulated lesions this would be clinically advantageous.

3.6.5 AKT inhibitors with less potency towards AKT3 did not recapitulate AZD5363 treatments

Disparities between phenotypic outcomes with the two AKT inhibitors, AZD5363 and MK-2206, led to investigations using alternative AKT inhibitors. These studies supported initial hypotheses regarding the isoform specificity of the AKT inhibitors. Pan-AKT inhibitors with increased activity to AKT3, as well as AKT1 and AKT2 (AZD5363, Afuresertib), showed similar prevention and reversal of dysplastic lesions (Figure 3.11). Conversely, AKT inhibitors with less potency for AKT3 (MK-2206 and AKTi1/2) did not have an impact. These results imply that AKT3 may be important in driving and maintaining the dysplastic phenotype.

3.6.6 SOX2-amplified squamous cell lines showed sensitivity to AKT inhibition

Although the OTC model is a unique and tractable model to study early SQC using a limited number of clinically relevant genetic aberrations, there are still limitations to its use. The model is simplified, in terms of numbers of genetic aberrations and numbers of cell types, and artificially created, so it was important to confirm that findings were not artefacts of the OTC model by using alternative *in vitro* models. Cell lines derived from human squamous carcinomas were used to validate key findings from the chemoprevention screens using the OTC model.

There are limited options when it comes to lung derived squamous cell carcinoma cell lines. I discovered that H520 and LK-2 cell lines, regarded as “gold standard” for SOX2 positive lung SQC lines, were not dual positive for markers of squamous origin (Figure 3.8). This is an important finding for the research community as many of the cell lines currently used may not possess suitable phenotypic markers that are required to conduct

clinically relevant research. As a consequence of this finding, esophageal squamous cell carcinoma cell lines were utilised throughout this study. Squamous cell carcinomas of the lung and esophagus share key genetic events in the progression of preinvasive disease (Section 1.3.5). AKT inhibition in squamous cell carcinoma cell lines was most effective in SOX2-amplified cell lines rather than non SOX2-amplified/expressing lines (Figure 3.8). Data comparing SOX2-amplified (KYSE-140) and non SOX2-amplified (KYSE-30) cell lines screened with compounds targeting multiple nodes in the PI3K-AKT pathway supported the OTC chemoprevention screen results (Figure 3.12). The SOX2-amplified cell line showed the greatest inhibition when AKT inhibitors were used, compared to the non SOX2-amplified cell line which did not display >50% reduction in proliferation following treatment with any of the PI3K-AKT pathway inhibitors.

3.6.7 **Conclusions**

Taken together, the OTC chemoprevention screens and cell line screens suggest that SOX2-driven squamous cell carcinomas are most vulnerable to AKT inhibition, when targeting the PI3K-AKT and RAS-MAPK pathways. Studies in the OTC model with a number of AKT inhibitors with varying potencies to the 3 AKT isoforms suggest that there may be particular dependence on AKT3 in formation of the dysplastic phenotype. Genetic studies investigating AKT isoform necessity in squamous cell carcinomas are carried out in Chapter 4.

Chapter 4

AKT isoform inhibition in SOX2-amplified squamous cell carcinomas

4.1 Introduction

In Chapter 3 pan-AKT inhibition using the small molecule compound, AZD5363, was effective in chemoprevention of dysplastic lesions using the OTC model as well as reducing proliferation in squamous carcinoma cell lines. In this chapter validation of these small molecule inhibitor studies was performed using genetic approaches to knockout genes using CRISPR-Cas9 and knockdown gene expression using RNA interference.

To date, the role of AKT isoforms in cancer has mainly been reported in melanomas and breast and ovarian carcinomas (Section 1.8.7). Therefore, the role in progression and maintenance of squamous carcinomas and SQC was investigated.

4.2 AKT isoform expression in the OTC model

In Chapter 3, AKT inhibitors with different potency for AKT isoforms had varying phenotypic impact in the OTC model and in a panel of squamous carcinoma cell lines. Therefore, the expression of the AKT isoforms in the model upon SOX2 deregulation was studied. RNA-sequencing data, generated by Dr L. Correia (unpublished, University of Cambridge, UK), (Appendices, Table 7.1), from the OTC model $\pm$doxycycline at 4 days ALI showed specific upregulation of AKT3, but not AKT1 or AKT2, after SOX2 overexpression (Figure 4.1A). The significant increase of AKT3 was validated by RT-qPCR (Section 2.4.3), as well as a significant increase in AKT2 (Figure 4.1B). To determine if AKT isoform protein levels reflected the transcriptional data, western blotting was performed. All three AKT isoform protein levels increased with deregulated SOX2 after 48 h (Figure 4.1C).

A

Gene	LogFC	P- Value	FDR
AKT1	0.0102	0.944	0.987
AKT2	0.0356	0.803	0.913
AKT3	0.6152	$9x10^{-5}$	0.0009

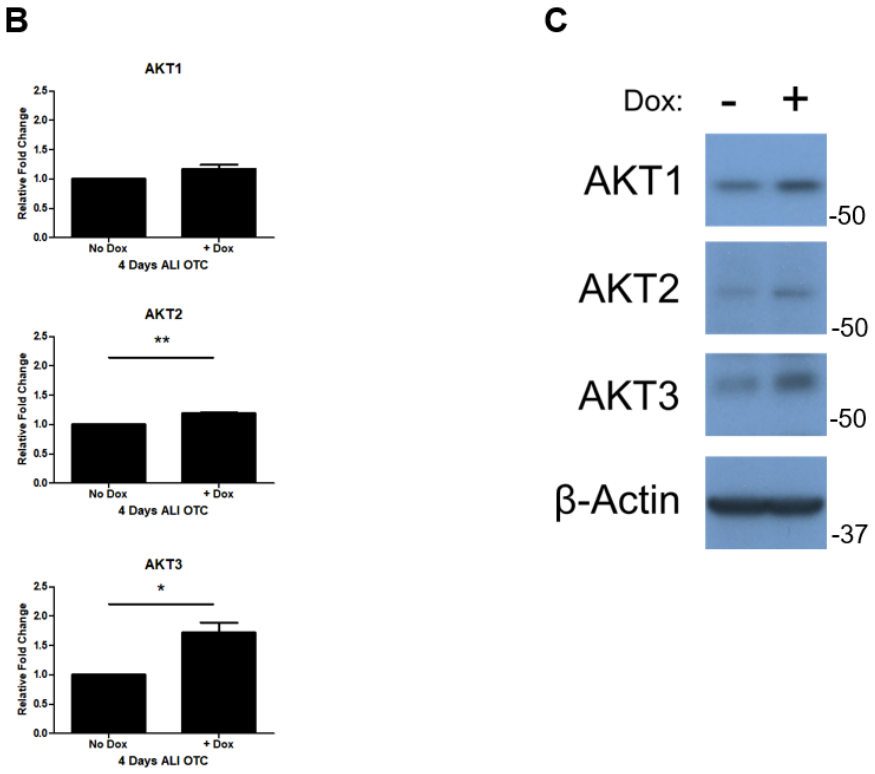

Figure 4.1: AKT2 and AKT3 mRNA are significantly upregulated upon SOX2 induction in the OTC model and all 3 AKT isoforms are upregulated at the protein level. **A.** RNA-sequencing results for AKT isoforms, comparing plus dox to no dox at 4 days ALI in the OTC model. LogFC = Log Fold Change. FDR = False Discovery Rate. **B.** RT-qPCR analysis validating RNA-sequencing results. RT-qPCR was performed using SYBR green chemistry, and expression of AKTs calculated using the $\Delta\Delta$Ct method relative to the comparative no dox control, normalising to the *TBP* housekeeping gene. **C.** Western blot showing AKT1, AKT2 and AKT3 protein levels increasing upon SOX2 activation in the OTC model. Samples from epithelial cells in 48 h $\pm$doxycyline OTC model. RNA-sequencing experiments performed by Dr L. Correia (University of Cambridge, UK) represent 3 experimental repeats. RT-qPCR results represent the mean $\pm$SD from 3 experimental repeats. Significant differences were determined using an unpaired t-test, two tailed P values: * $p \leq 0.05$, ** $p \leq 0.01$, *** $p \leq 0.001$. Western blot data representative of 2 experimental repeats.

4.3 AKT isoform expression in human SQC tumour samples

To confirm that SOX2 over expression and subsequent effects on AKT isoform expression were not artefacts of the OTC model, the TCGA data was interrogated for the expression of the three AKT isoforms in SOX2-amplified SQCs (Hammerman et al., 2012) and separately a locally constructed tissue microarray with clinical specimens of high-grade bronchial dysplasia was used.

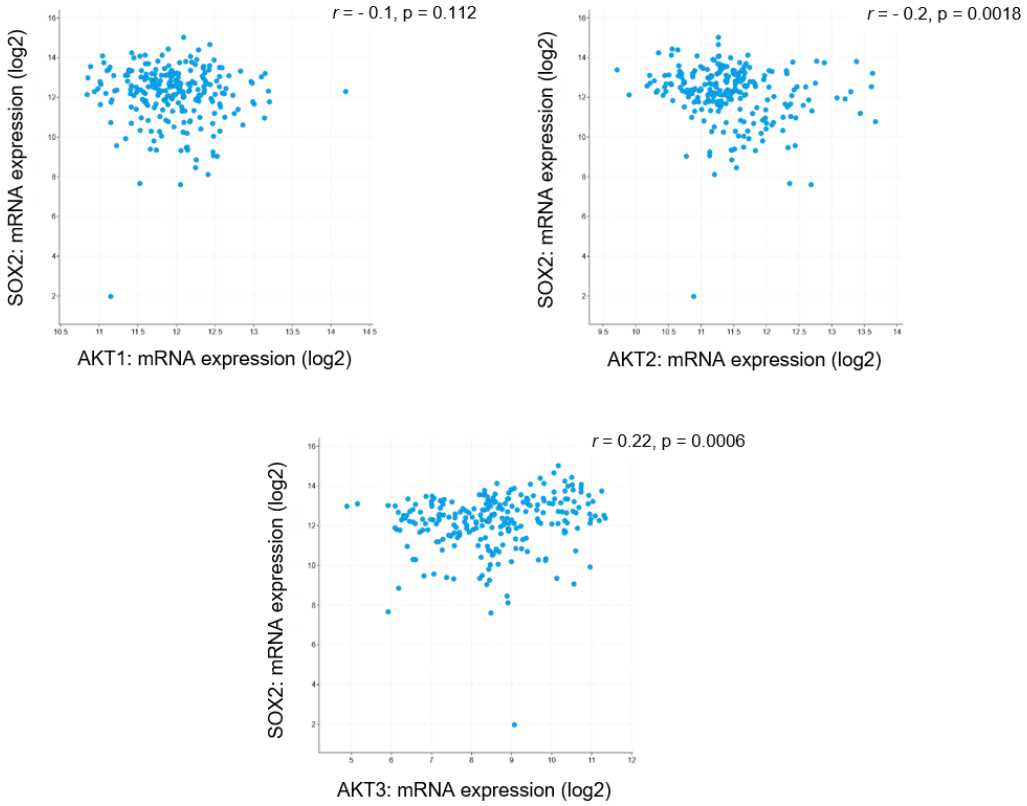

Figure 4.2: AKT3 mRNA expression shows a positive correlation in SOX2-amplified human squamous cell lung tumours.
mRNA expression data from SOX2-amplified squamous cell lung cancer patients. TCGA data was accessed via www.cbioportal.org, samples were selected for SOX2 amplification CNA events (242/511 patient samples). SOX2-amplified samples were analysed for SOX2 and AKT isoform expression correlation. *r* = Spearman rank correlations, and associated p-values. Non-log scales were used for statistical calculation and the log-scale axis for visualization as demonstrated by Tang et al. (2017).

Analysis of SOX2-amplified squamous cell lung tumour samples from the TCGA showed a significant positive correlation between SOX2 and AKT3 mRNA expression determined by Spearmans rank correlations $p \leq 0.001$. No significant correlation between SOX2 and AKT1 was observed, and a significant negative correlation between SOX2 and AKT2 expression determined by Spearmans rank correlation $p \leq 0.01$ (Figure 4.2).

AKT1, 2 and 3 expression in human biopsies of SOX2 positive high grade dysplasia show that all high grade dysplastic lesions analysed had varying degrees of AKT isoform expression (Figure 4.3). These data show that SOX2 and AKT3 isoform expression are not artifacts of the OTC model, and that AKT1 and AKT2 can also co-occur in SOX2 positive human disease.

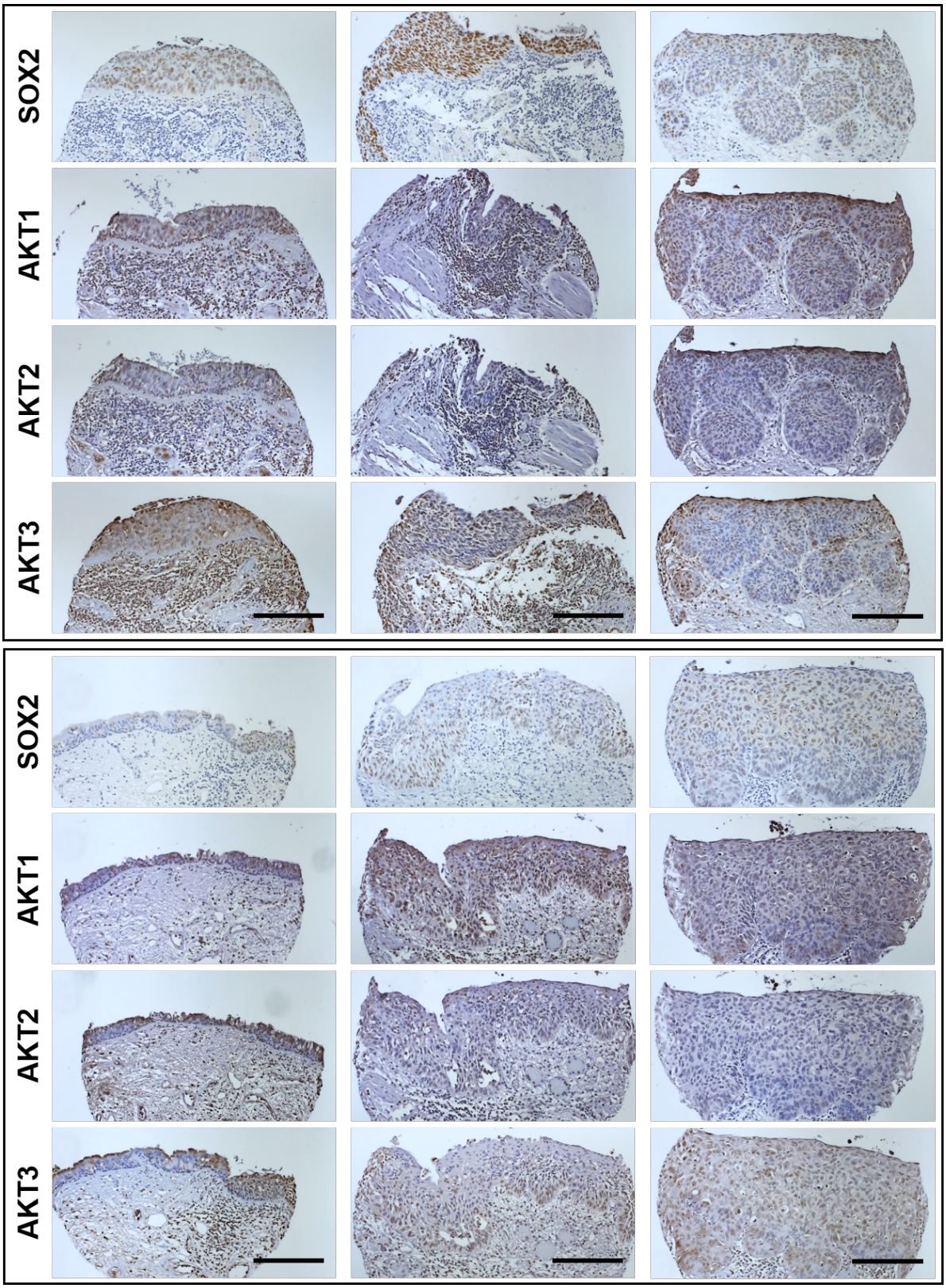
SOX2
AKT1
AKT2
AKT3
SOX2
AKT1
AKT2
AKT3

Figure 4.3: AKT1, AKT2 and AKT3 are all expressed in SOX2 positive human biopsies of high grade bronchial dysplasia.
Human Tissue Microarray was stained using IHC for SOX2, AKT1, AKT2 and AKT3. SOX2, AKT1, AKT2 and AKT3 stained sections are not consecutive cuts, but from the same biopsy. All 6 biopsies are from different patients. Lesions were assessed by a consultant thoracic histopathologist to be high grade bronchial dysplasia. Appendices in Chapter 7 show IHC secondary antibody only controls for TMA. Scale bars = 200 μm.

4.4 AKT isoform expression in human squamous carcinoma cell lines

Expression profiles for the AKT isoforms in cell lines from Chapter 3 confirmed as squamous phenotype were analysed (Figure 4.4). The H520 cell line was included as these are a commonly used model for SOX2-driven SQC, despite lacking detectable levels of p63. Transcript levels of the AKT isoforms did not necessarily correlate to protein levels detectable by western blot in this panel of cell lines. Observable band shifts in western blotting analysis allowed the phosphorylation status of the AKT isoforms to be inferred (Figure 4.4B). TE-6 and TE-10 have hyperphosphorylated AKT1. KYSE-140, TE-6, TE-10 and H520 have hyperphosphorylated AKT2. KYSE-140, TE-6, TE-10 and H520 have hyperphosphorylated AKT3. Despite KYSE-30 having the highest abundance of AKT3 mRNA and protein levels, it does not appear to be activated via phosphorylation.

As demonstrated earlier, pan-AKT inhibitors that have potency to AKT3 have been shown to be effective in chemoprevention screens using the OTC model (Chapter 3). From a panel of squamous carcinoma cell lines KYSE-140 and TE-6 cells were inhibited significantly in proliferation studies when treated with AKT inhibitor, AZD5363 (Figure 3.8). Both of these cell lines have amplification of the *SOX2* locus and express SOX2 at high levels. I have shown upregulated transcription of AKT isoforms, in particular AKT3, as a consequence of SOX2 deregulation in the OTC model (Figure 4.1). This correlated with TCGA mRNA data from human SQC disease (Figure 4.2). AKT isoforms are upregulated at the protein level in the OTC model as a consequence of SOX2 deregulation; SQC cell lines

and human data from high-grade bronchial dysplasia biopsy IHC staining showed that the protein expression of all three AKT isoforms was not an artefact of the OTC model (Figures 4.4 and 4.3).

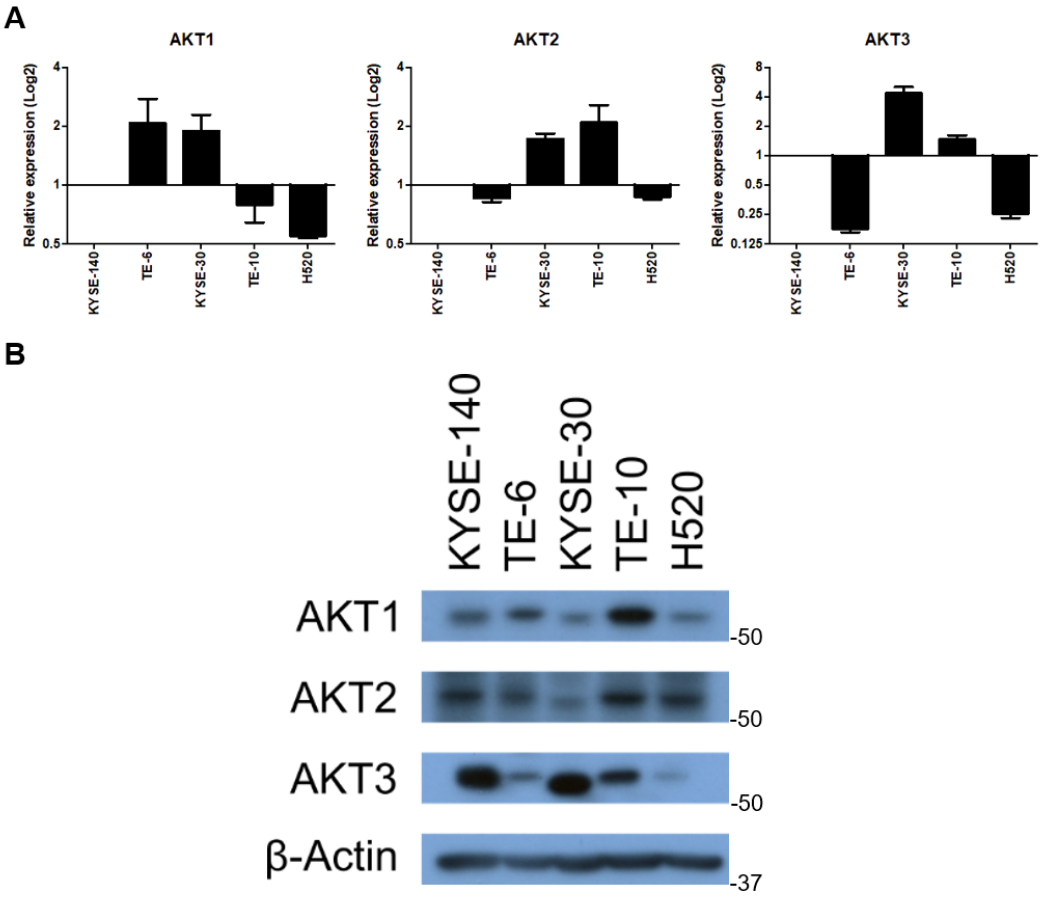

Figure 4.4: Squamous cell carcinoma cell lines have varying levels of expression of AKT isoforms at the mRNA and protein level.
A. RT-qPCR analysis of AKT isoform mRNA expression in squamous cell carcinoma cell lines. qPCR was performed using SYBR green chemistry, and expression levels of the AKT isoforms was calculated using the $\Delta\Delta$Ct method relative to KYSE-140 expression, normalising to the *TBP* housekeeping gene. **B.** Western blot on squamous cell carcinoma cell line samples for AKT isoform expression. Band shifts were used to infer phosphorylation status for each AKT isoform. RT-qPCR results represent the mean $\pm$SD from 3 experimental repeats, western blot data representative of 2 experimental repeats.

4.5 Generation of KTshP53iSOX2 cells with AKT isoform knockouts

To test the hypothesis that AKT3 is necessary for the initiation of SOX2-driven dysplastic lesions in the OTC model, genetic knockouts of the 3 AKT isoforms in KTshP53iSOX2 cell lines was performed using CRISPR-Cas9 to generate knockout cell lines. sgRNAs targetted to exon 2-5 of each AKT isoform were designed and cloned into the px458 plasmid (Section 2.3.2 for sgRNA design method). px458 contains an sgRNA scaffold, Cas9 endonuclease and a GFP reporter. Three sgRNAs per target were screened for efficiency in disrupting genomic DNA at the desired break point during sgRNA validation (data not shown).

Validated sgRNAs, cloned into px458, were transiently transfected into KTshP53iSOX2 cells. Due to the constitutively expressed shP53-GFP construct, parental cells were GFP positive to begin with, and thus, transfected cells were single cell sorted on the basis of super GFP positivity (GFP++) (Figure 4.5A). Single-cell clones were expanded and screened using PCR with subsequent sequencing conducted to identify genomic disruption around the sgRNA binding site (Figure 4.5B,C). 5 AKT1 CRISPR clones, 14 AKT2 CRISPR clones and 5 AKT3 CRISPR clones expanded from 96 wells of single cells. Examples of single cell clone sequencing chromatograms compared to parental cell WT controls with respective sgRNA binding and PAM sites labelled are shown (Figure 4.5C,D,E). TIDE web tool analysis confirms InDels in the sequencing chromatograms (Figure 4.5C,D,E).

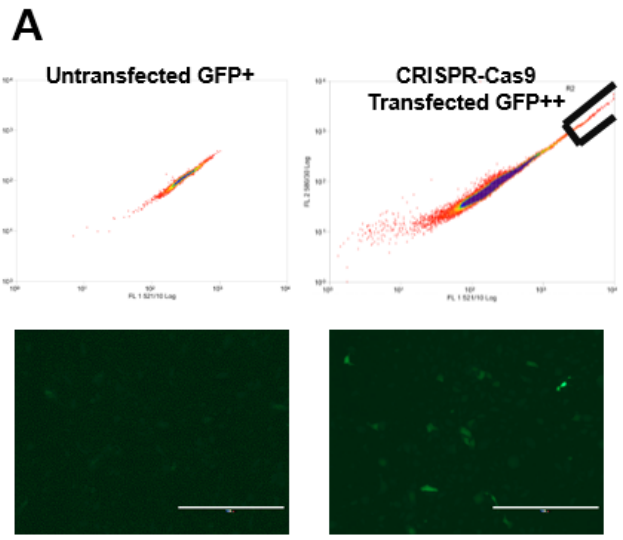
A
Untransfected GFP+
CRISPR-Cas9
Transfected GFP++

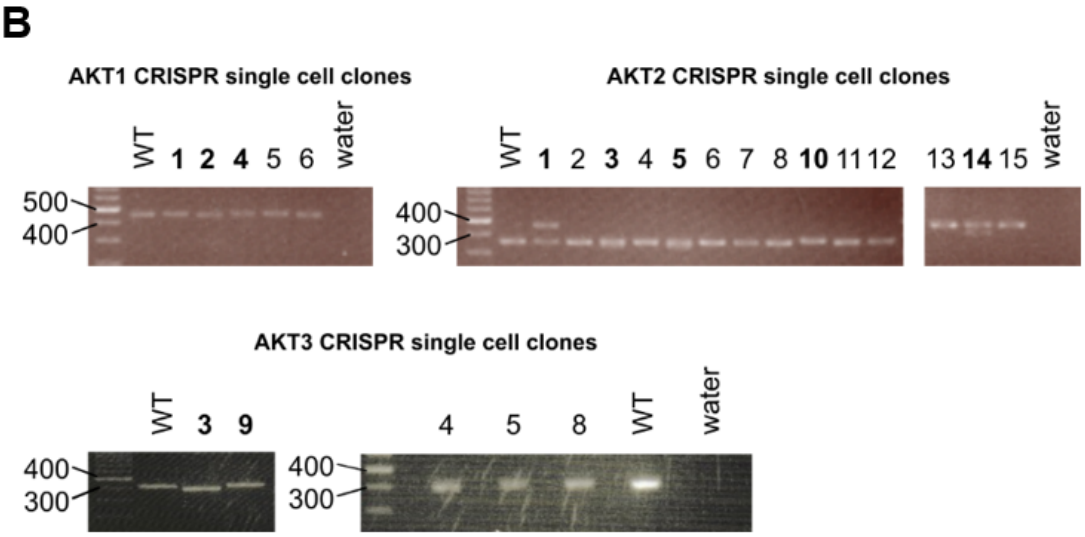
B
AKT1 CRISPR single cell clones
WT 1 2 4 5 6 water
500
400
AKT2 CRISPR single cell clones
WT 1 2 3 4 5 6 7 8 10 11 12 13 14 15 water
400
300
AKT3 CRISPR single cell clones
WT 3 9
400
300
4 5 8 WT water
400
300

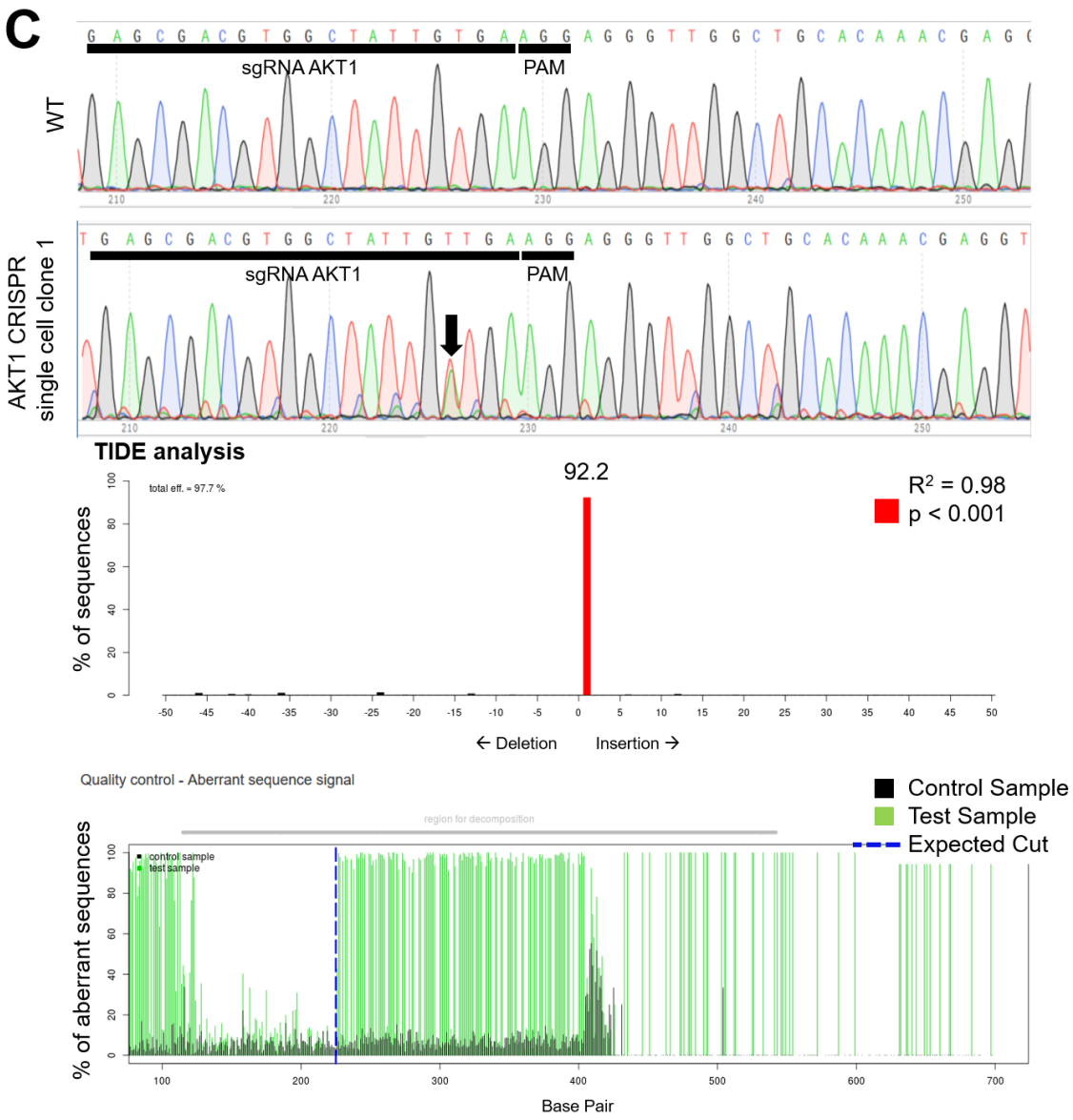
C
WT
sgRNA AKT1
PAM
AKT1 CRISPR
single cell clone 1
TIDE analysis
92.2
total eff. = 97.7 %
R2 = 0.98
p < 0.001
% of sequences
← Deletion
Insertion →
Quality control - Aberrant sequence signal
Control Sample
Test Sample
Expected Cut
% of aberrant sequences
Base Pair

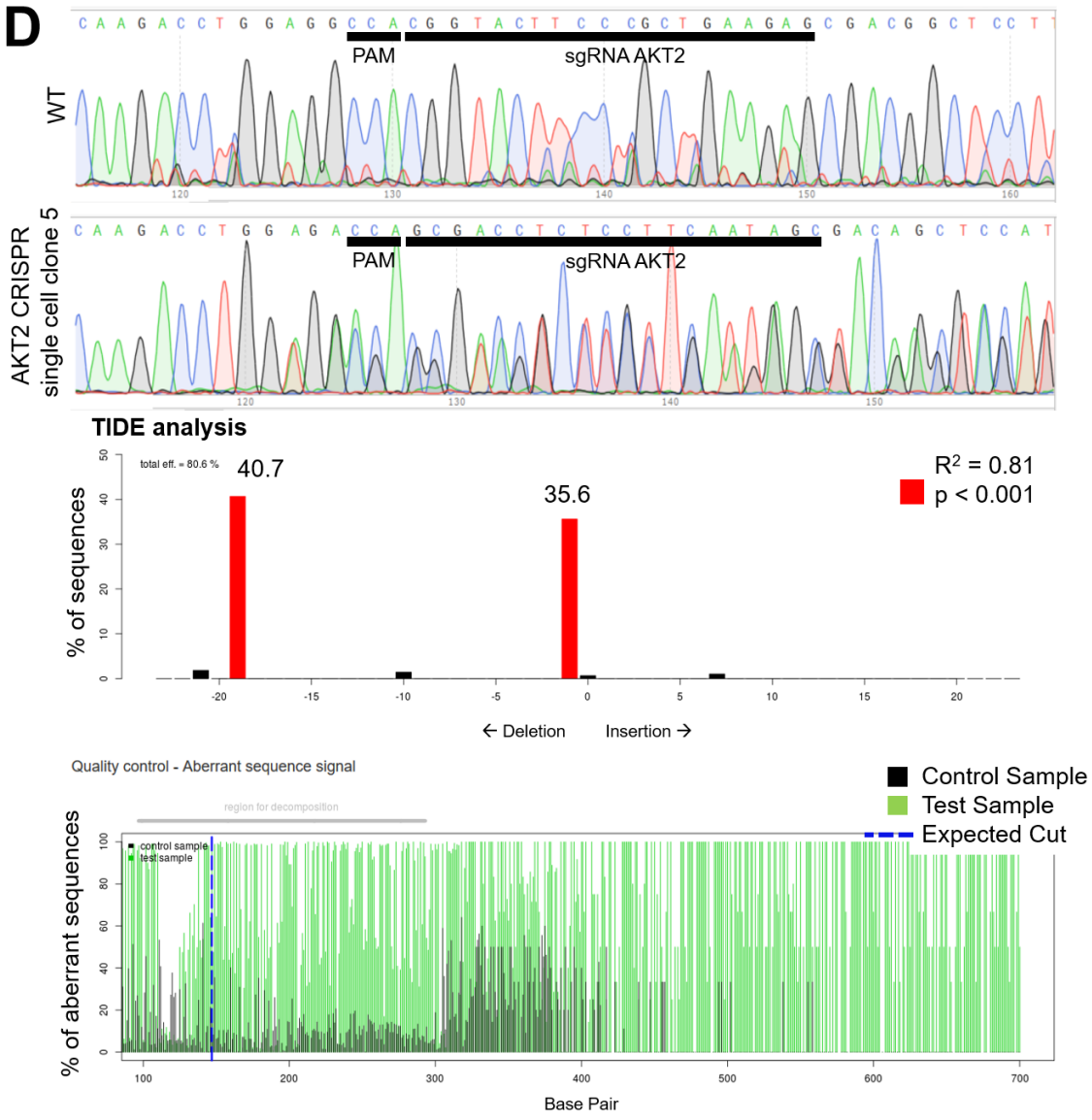
D
WT
PAM
sgRNA AKT2
AKT2 CRISPR single cell clone 5
PAM
sgRNA AKT2
TIDE analysis
total eff. = 80.6 %
40.7
35.6
R2 = 0.81
p < 0.001
% of sequences
← Deletion
Insertion →
Quality control - Aberrant sequence signal
region for decomposition
control sample
test sample
Control Sample
Test Sample
Expected Cut
% of aberrant sequences
Base Pair

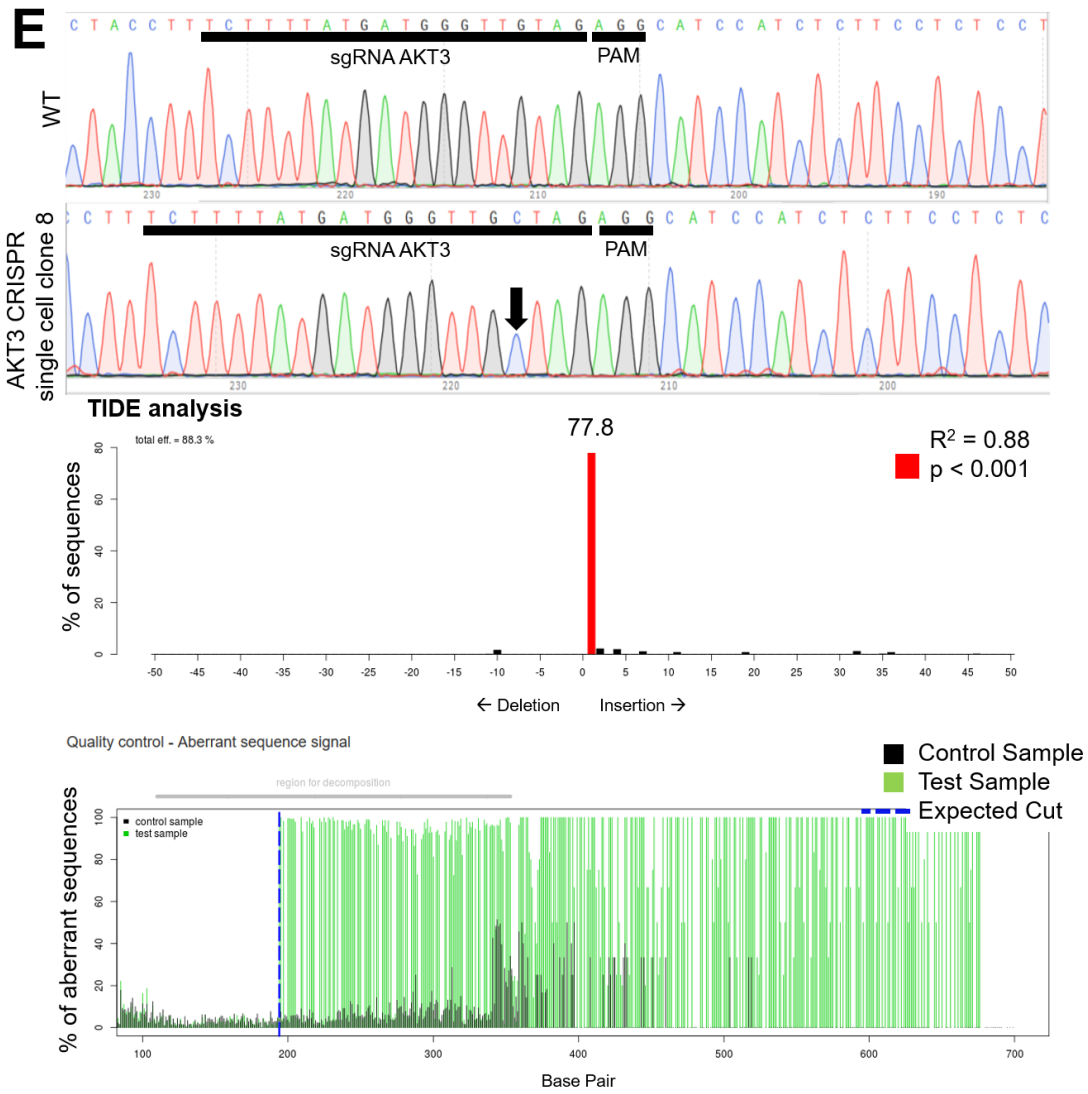

Figure 4.5: Generation of AKT1, AKT2 and AKT3 knockout single cell clone KTshP53iSOX2 cells using CRISPR-Cas9.
A. Single cell sorting for KTshP53iSOX2-GFP cells transiently transfected with px458. GFP flow cytometry dot plots and GFP images showed increased GFP expression relative to parental constitutive GFP-positive cells after transfection. A population of intense GFP-positive cells (GFP++) that were not present in the untransfected population was gated and sorted into single cells per well. **B.** PCRs on genomic DNA from expanded single-cell clones. Genomic regions targeted by sgRNAs were flanked by sequencing primers, amplicons were run on an agarose gel. Bands were extracted, sequenced and compared to KT cell controls (WT). **C., D., E.** CRISPR single cell clone sequencing. sgRNA and PAM sequences represented on sequencing chromatograms. TIDE web tool analysis (Brinkman et al., 2014) shows the spectrum and frequency of indels in the bar chart. Visualisation of the aberrant sequence of the WT control (black) and treated sample (green), with expected cut site (dotted blue line). **C.** AKT1 single cell clone 1 shows a 1bp insertion, indicated by the black arrow on the chromatogram. **D.** AKT2 single cell clone 5 shows a 1bp and 19bp deletion. **E.** AKT3 single cell clone 8 shows a 1bp insertion, indicated by the black arrow on the chromatogram.

Expanded CRISPR single cell clones were screened for the absence of AKT protein and SOX2 inducibility via administration of doxycycline. Western blots show CRISPR clones compared to parental cells and positive controls for the AKT isoforms (Figure 4.6). All

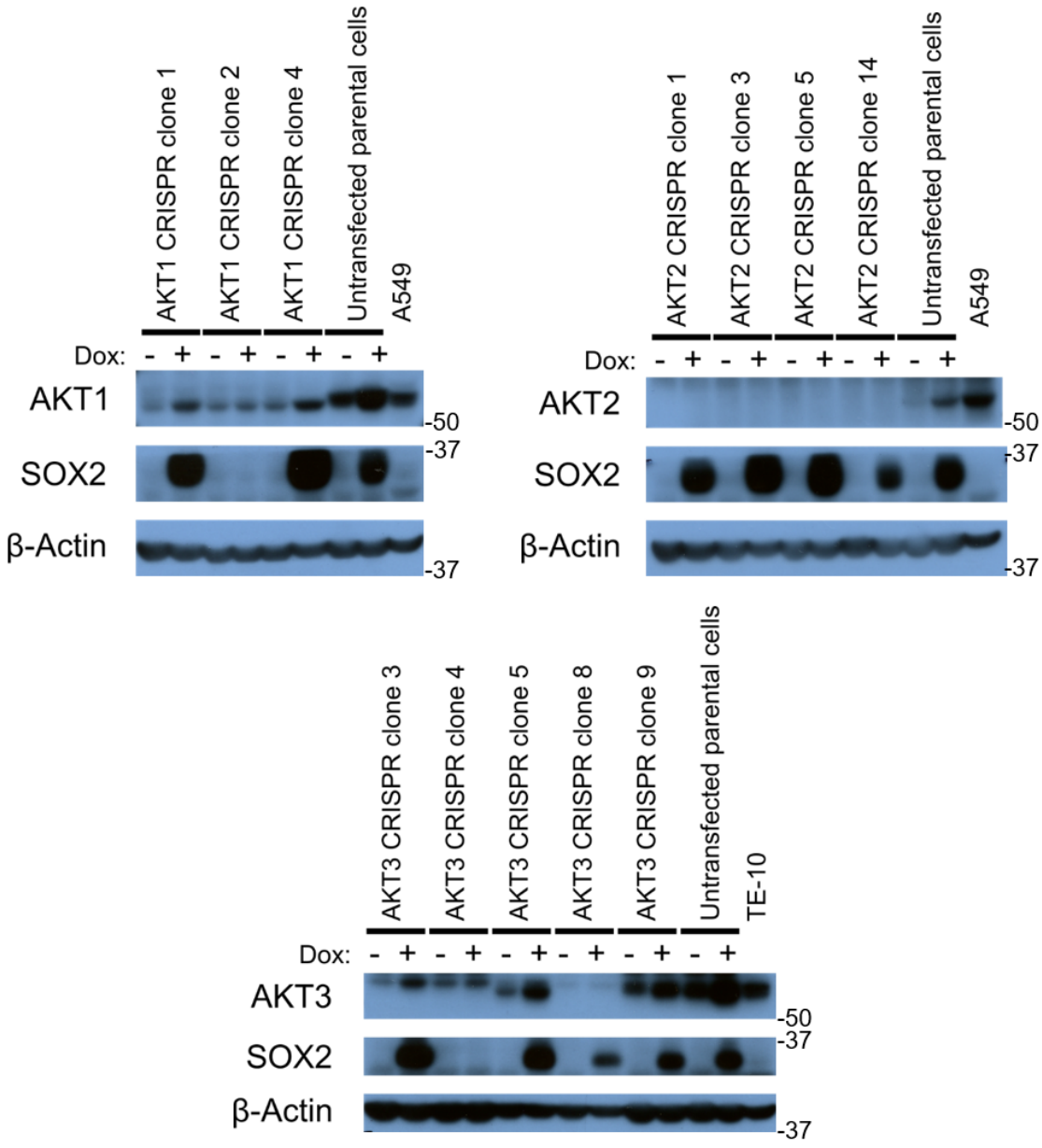

Figure 4.6: Validation of AKT1, AKT2 and AKT3 protein knockout using CRISPR-Cas9 in KTshP53iSOX2 single cell clones.
Western blots show single cell clone samples from Figure 4.5 grown in 2D culture ± 1 μg/mL doxycycline for 48 h. There were no AKT1$^{-/-}$ cell lines. All AKT2 CRISPR cell lines were AKT2$^{-/-}$ and SOX2 inducible. There was 1 AKT3$^{-/-}$ SOX2 inducible cell line.

AKT1 CRISPR clones showed truncated AKT1 when analysed using western blots which migrated at a lower molecular weight than the controls. All AKT2 CRIPSR clones were confirmed to be AKT2 knockout and SOX2 inducible. There was only one AKT3 knockout clone with inducible SOX2 (Figure 4.6).

It was unclear if truncated AKT1 bands from AKT1 CRISPR clones corresponded to functional proteins. Lysates generated from the AKT1 CRISPR clones were treated with phosphatase, to assess whether truncated AKT1 proteins retained their ability to be phosphorylated, and therefore infer functional activation of the protein. Figure 4.7 shows band shifts in all AKT1 CRISPR clones relating to truncated AKT1 de-phosphorylation. This result shows that none of the 96 single cell clones were likely to be functionally negative for AKT1. This is consistent with AKT1 but not AKT2 being required for expansion of immortalised bronchial epithelial cells from single cell clones. Further experimental analysis of the single AKT3$^{-/-}$ clone is outlined in the next section (Section 4.6). Results shown in Figure 4.1 are further confirmed by upregulation of all 3 isoforms of AKT in response to SOX2 deregulation in the parental KTshP53iSOX2 cells (Figure 4.6).

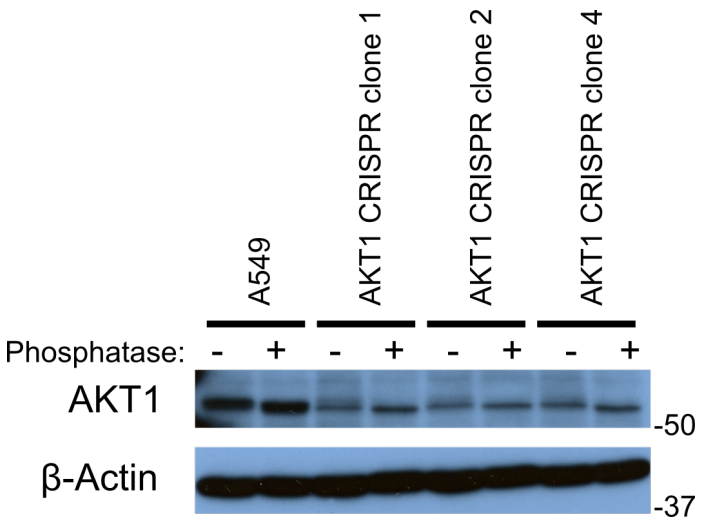

Figure 4.7: Truncated AKT1 in AKT1 CRISPRed KTshP53iSOX2 single cell clones retain ability to be activated via phosphorylation.
Western blot showing band shifts representing dephosphorylation with phosphatase treatment in all AKT1 truncated proteins. AKT1 CRISPR KT shP53 iSOX2 single cell clones were grown in 2D culture $\pm$ 1 μg/mL doxycycline for 48 h. Cells were lysed using RIPA buffer and a protease inhibitor, without phosphatase inhibitors. Lysates were then incubated at 37^{o}C $\pm$ calf intestinal alkaline phosphatase for 40 mins before following the western blotting protocol previously described (Section 2.5.2).

4.6 AKT2 is not required for the initiation and maintenance of SOX2-driven lesions in the OTC model

AKT2$^{-/-}$ or AKT3$^{-/-}$ KTshP53iSOX2 cells were seeded in the OTC model, as described (Section 2.1.2), to test the hypothesis that AKT3 was necessary for the initiation and maintenance of SOX2-driven dysplastic lesions. As noted in the previous section, no AKT1$^{-/-}$ cells were available. For KTshP53iSOX2 AKT2$^{-/-}$ cells, maintained at ALI in the OTC model, GFP imaging was used in conjunction with phase-contrast microscopy to visualise epithelial layers, made possible by the constitutive shP53-GFP construct in the KTshP53iSOX2 parental cells. KTshP53iSOX2 AKT2$^{-/-}$ cells generated dysplastic lesions that were phenotypically similar to the parental cells when SOX2 was activated (Figure 4.8). This showed that AKT2 is dispensable when combined with p53 knockdown and SOX2 overexpression in driving bronchial dysplasia.

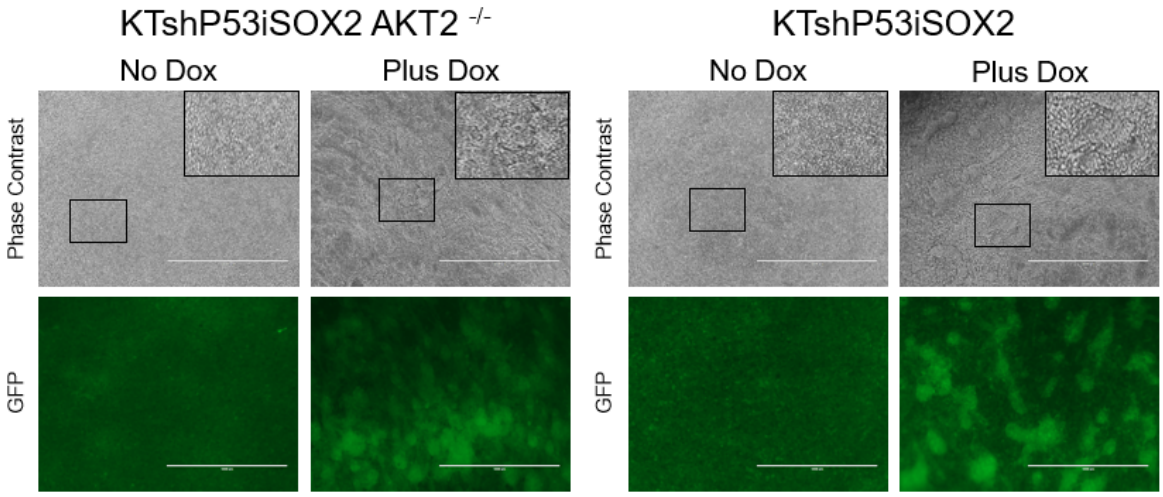

Figure 4.8: AKT2 is not required for the formation of dysplastic lesions in the OTC model.
KTshP53iSOX2 AKT2$^{-/-}$ cells were used in the OTC model. Cells were maintained at ALI $\pm$ 0.1 μg/mL doxycycline for 6 days. Phase-contrast and GFP images show KTshP53iSOX2 AKT2$^{-/-}$ cells formed dysplastic lesions similar to AKT2 wild-type control, KTshP53iSOX2 cells. Low magnification phase-contrast and GFP images capture overall phenotype, insets show areas at higher magnification. Images are representative of 3 experimental repeats. Scale bars = 1000 μm.

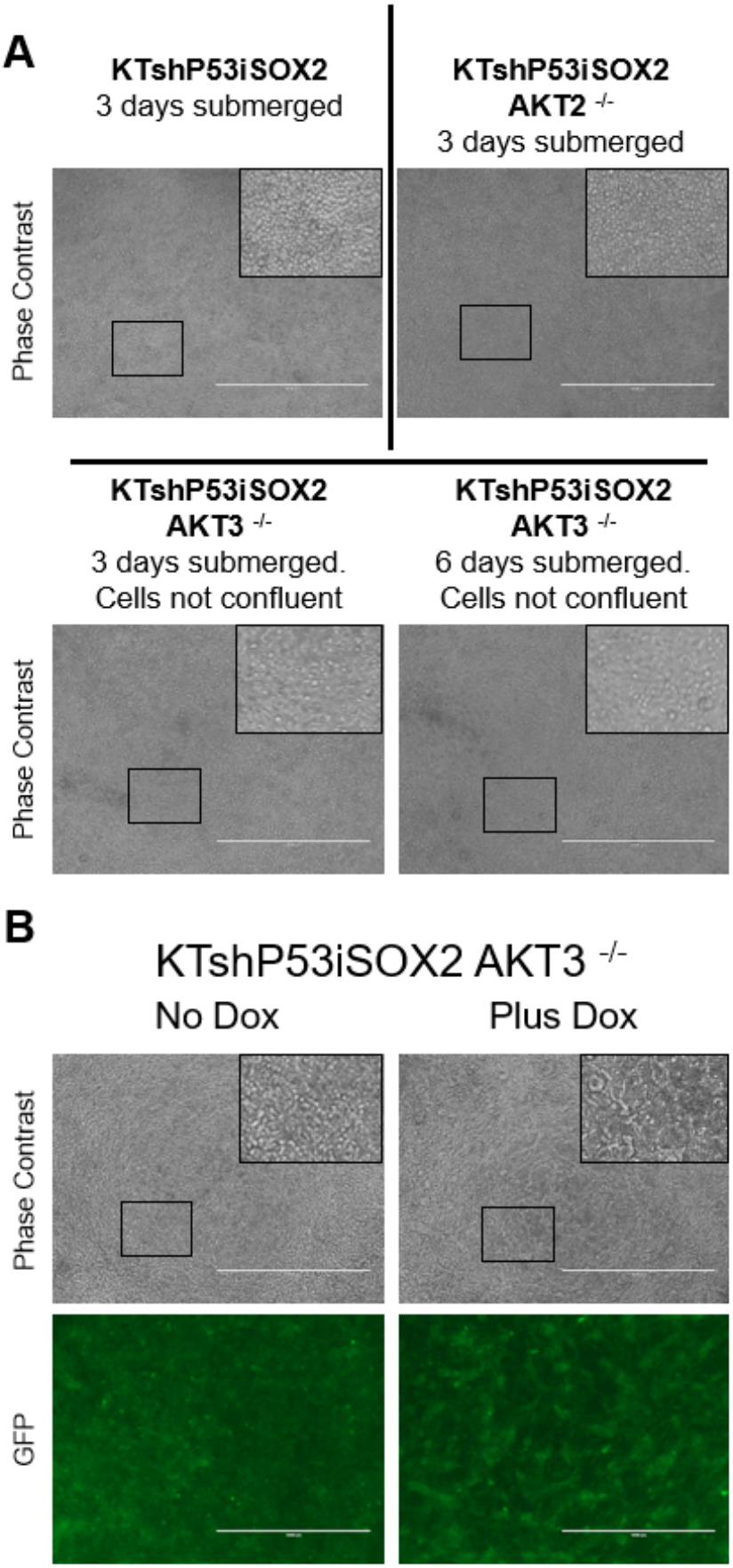
A
KTshP53iSOX2
3 days submerged
KTshP53iSOX2
AKT2 -/-
3 days submerged
Phase Contrast
KTshP53iSOX2
AKT3 -/-
3 days submerged.
Cells not confluent
KTshP53iSOX2
AKT3 -/-
6 days submerged.
Cells not confluent
Phase Contrast
B
KTshP53iSOX2 AKT3 -/-
No Dox
Plus Dox
Phase Contrast
GFP

Figure 4.9: AKT3 is required for the expansion of immortalised bronchial epithelial cells *in vitro*.
A. Phase-contrast images show AKT wild-type, AKT2$^{-/-}$ and AKT3$^{-/-}$ cells seeded at normal density for the OTC model setup. AKT3$^{-/-}$ cells did not reach confluence after 3 days submerged, unlike AKT2$^{-/-}$ and AKT wild-type cells which were then brought to ALI at day 3. **B.** AKT3$^{-/-}$ cells were brought to ALI after 6 days submerged. Phase-contrast and GFP images show epithelial layer reaches confluence after 6 days submerged followed by 6 days at ALI. Low magnification phase-contrast and GFP images capture overall phenotype, insets show areas at higher magnification. Images are representative of 3 experimental repeats. Scale bars = 1000 μm.

KTshP53iSOX2 AKT3$^{-/-}$ cells were slow to expand in normal tissue culture conditions and continued to expand slowly on the collagen-fibroblast matrix component of the OTC model (Figure 4.9A). Therefore, cells were left in submerged culture on the collagen-fibroblast matrix in the OTC model twice as long as AKT2$^{-/-}$ and control cells (Figure 4.9A). When brought to ALI, they continued to expand unusually slowly, taking a total of 12 days (6 days submerged then 6 days at ALI) from seeding the cells onto the collagen-fibroblast matrix to reach 100% confluence. However, when SOX2 was activated bare patches could be observed in the monolayer (Figure 4.9B). Taken together, this shows that AKT3 is necessary for the growth of these cells in culture and for continued propagation when SOX2 is deregulated.

4.7 Generation of KTshP53iSOX2 cells with inducible AKT isoform knockdown

As it was not possible to generate AKT1$^{-/-}$ KTshP53iSOX2 cells and interpretation of experiments on the sole AKT3$^{-/-}$ cell line was challenging due to the difficulty propogating cells, an alternative genetic approach was used. To generate doxycycline-inducible shRNA-mediated knockdown of AKT isoforms in KTshP53iSOX2 cells, oligonucleotides encoding AKT1, AKT2, AKT3 and scramble control target shRNA were synthesised. These shRNA constructs had been validated previously against the AKT isoforms (Zhou et al., 2014; Phung et al., 2015; Chin et al., 2015). Sense and antisense oligonucleotides

were annealed and cloned into the EZ-tet-pLKO-Blast construct. Lentiviral particles were produced and KTshP53iSOX2 cells were transduced with lentiviral supernatant (Section 2.3.1); cells were selected for stable integration using blasticidin. Lentiviral volumes were optimised to give maximal specific knockdown of the AKT isoforms (data not shown).

mRNA expression levels of the AKT isoforms in KTshP53iSOX2 ishSCR control cells after 48 h ±doxycycline showed expected upregulation of all AKT isoforms with SOX2 induction (Figure 4.10A). Sufficient knockdown of the relevant isoforms via inducible shRNAs was not evident at 48 h ±doxycycline. mRNA expression levels of the AKT isoforms in KTshP53iSOX2 with inducible shRNAs cells after 5 days ± doxycycline showed specific, significant knockdown of AKT isoforms (Figure 4.10B). Transduced cells had specific and significant knockdown of target proteins, as well as comparable SOX2 induction levels across cell lines (Figure 4.10C).

AKT1 protein levels in shAKT1 +dox were reduced to below the no dox control, shAKT3 +dox showed modest reduction in AKT1 when compared to shSCR+dox control cells (Figure 4.10C). Knockdown of AKT2 was specific to shAKT2 cells + dox. AKT3 knockdown in shAKT3 + dox was specific at the RNA level (Figure 4.10B), but had moderate impact on AKT1 and AKT2 at the protein level, as well as more qualitative reduction to AKT3 protein (Figure 4.10C). In summary, the shRNAs showed isoform specific knockdown at the RNA and protein level, with the exception of the shAKT3 construct having moderate impact on AKT1 protein as well as AKT3. The cells were used to investigate AKT isoform necessity in the formation of the dysplastic phenotype, discussed in the next section.

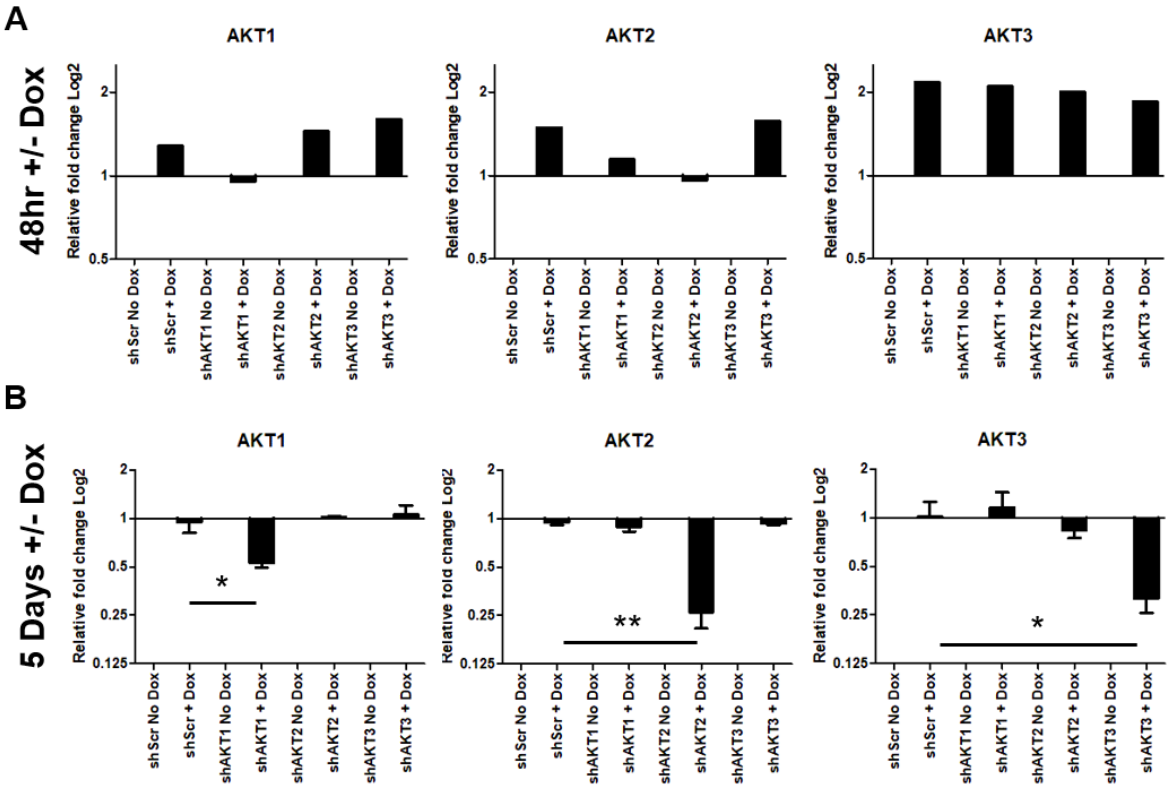
A
48hr +/- Dox
AKT1
AKT2
AKT3
Relative fold change Log2
shScr No Dox
shScr + Dox
shAKT1 No Dox
shAKT1 + Dox
shAKT2 No Dox
shAKT2 + Dox
shAKT3 No Dox
shAKT3 + Dox
B
5 Days +/- Dox
AKT1
AKT2
AKT3
Relative fold change Log2
*
**
*

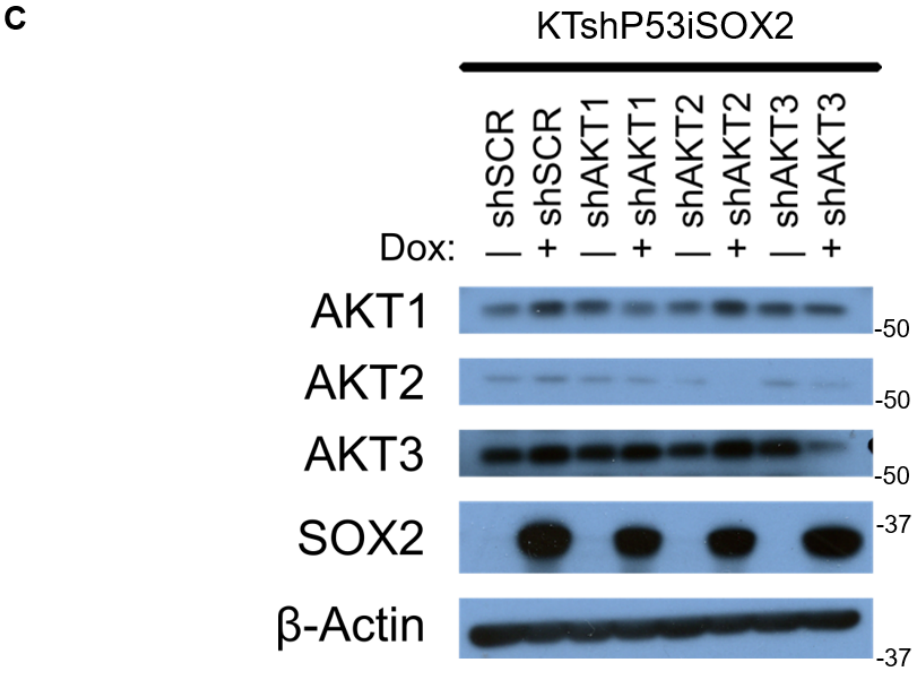
C
KTshP53iSOX2
Dox:
– shSCR
+ shSCR
– shAKT1
+ shAKT1
– shAKT2
+ shAKT2
– shAKT3
+ shAKT3
AKT1
AKT2
AKT3
SOX2
β-Actin
-50
-50
-50
-37
-37

Figure 4.10: Inducible knockdown of AKT1, AKT2 and AKT3 in the KTshP53iSOX2 cell line using doxycycline-inducible shRNA.
A. RT-qPCR analysis of AKT isoform mRNA expression in KT shP53 iSOX2 cells transduced with 600 μL of lentiviral constructs carrying shRNAs specific to the 3 AKT isoforms $\pm$ 0.5 μg/mL doxycycline for 48 h. RT-qPCR was then performed using SYBR green chemistry, and expression levels of the AKT isoforms was calculated using the $\Delta\Delta$Ct method relative to the comparative no dox control, normalising to the *TBP* housekeeping gene. **B.** RT-qPCR analysis of AKT isoform mRNA expression as in A. but treated for 5 days $\pm$ 0.5 μg/mL doxycycline. Significant differences compared to shSCR + doxycycline controls were determined using an unpaired t-test, two tailed P values: * p$\leq$0.05, ** p$\leq$0.01. **C.** Western blot on 5 day $\pm$ 0.5 μg/mL doxycycline treated cells for AKT isoforms and SOX2 expression. RT-qPCRs in A. were a pilot experiment. RT-qPCR results in B. represent the mean $\pm$SD from 3 experimental repeats. Western blot data is representative of 3 experimental repeats.

4.8 AKT3 knockdown significantly reduces SOX2-driven lesions in the OTC model

KTshP53iSOX2 cells with inducible shRNAs to the AKT isoforms were used in the OTC model to investigate the necessity of AKT isoforms in the SOX2-driven dysplastic phenotype. Cells were seeded in the OTC model previously described (Section 2.1.2), and brought to ALI with doxycycline added when confluent. I have already showed that cells required 5 days of doxycycline for knockdown of targets, and thus, cells were monitored and treated for a period of 7 days $\pm$doxycycline at ALI in the OTC. The phenotype was monitored via phase-contrast microscopy and GFP imaging (Figure 4.11A); GFP images were used to quantify lesions in ImageJ. Compared to scramble shRNA controls, cells with AKT3 knockdown had a significant reduction in the area covered by dysplastic lesions (Figure 4.11B). AKT1 and AKT2 knockdown showed no significant impact on phenotype when compared to controls (Figure 4.11B).

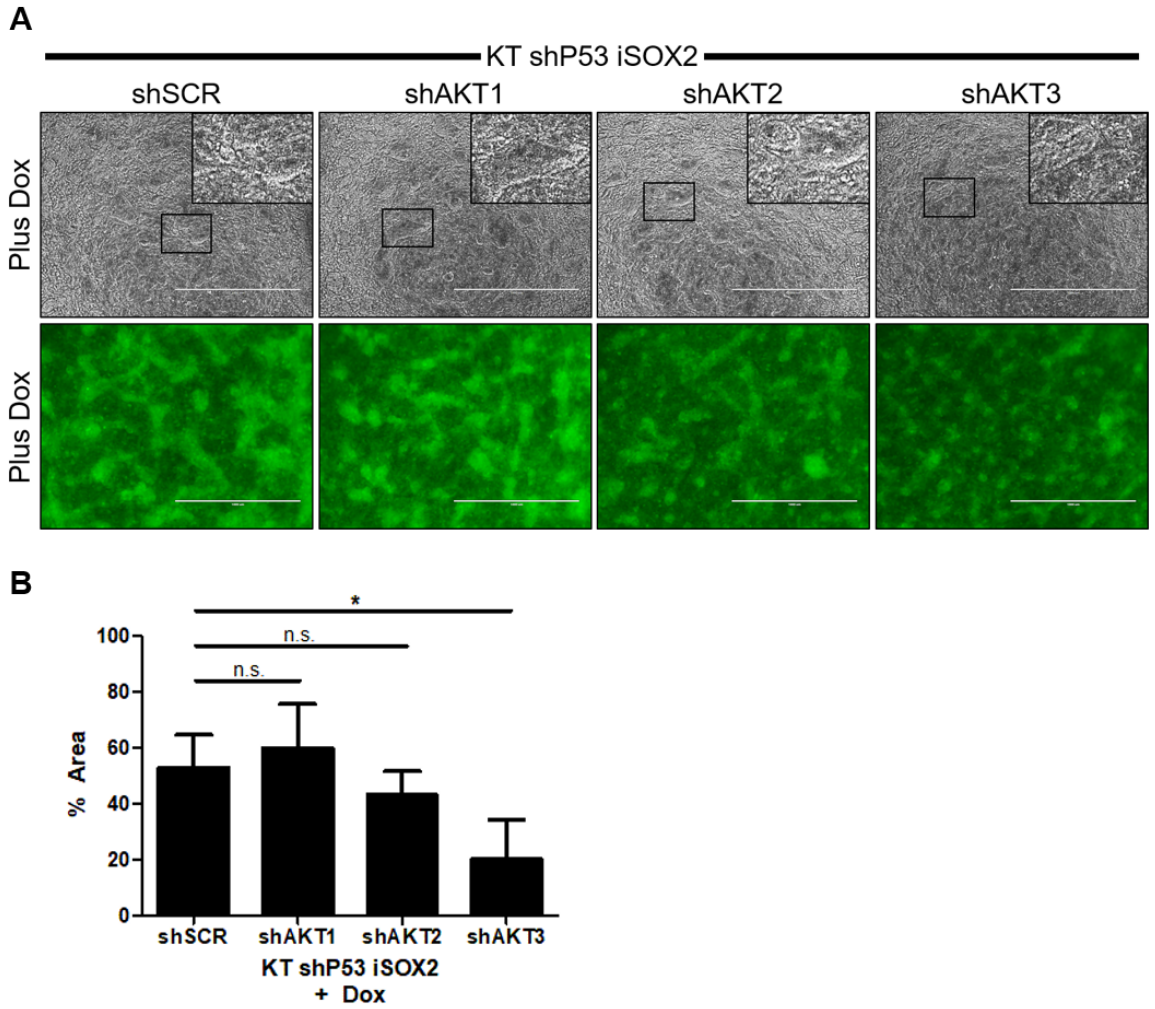

Figure 4.11: Knockdown of AKT3, but not AKT1 or AKT2, in the OTC model significantly reduces dysplastic phenotype.
A. KTshP53iSOX2 cells with inducible shRNAs to AKT1, AKT2 and AKT3 (generated in figure 4.10) used in the OTC model. Cells were maintained at ALI $\pm$ 0.5 μg /mL doxycycline for 7 days. Phenotype was monitored by phase-contrast and GFP microscopy. Cell lines in OTC model with no doxycycline maintained a confluent monolayer epithelium, data not shown. **B.** ImageJ quantification of lesions in experiments represented in A. GFP images were taken of OTCs using the same microscope settings and intensities for all images. Images were processed in ImageJ as follows: images were split into green colour channel, thresholds adjusted to detect lesions from monolayer, then "analyze particle" was used with the size threshold set to 1000-infinity pixel units to discriminate lesions from single or small patches of cells. Quantifications represent the mean $\pm$SD from experimental repeats. Significant differences compared to shSCR controls were determined using an unpaired t-test, two tailed P values: * $p \leq 0.05$, ** $p \leq 0.01$, *** $p \leq 0.001$.

4.9 Generation of squamous cell carcinoma cell lines with inducible AKT isoform knockdowns

Following results from Sections 4.8 and 4.6 I used inducible shRNA to the AKT isoforms in cell line studies to validate the findings from the OTC model that suggested an isoform specific dependence on AKT3 for formation of the dysplastic phenotype (Figures 4.11,4.9). Tet-pLKO-Puro constructs containing previously validated shRNAs to AKT1, AKT2 and AKT3 (Chen et al., 2015; Daulat et al., 2016; Chin et al., 2015) were used to produce lentiviral particles and used to create stable KYSE-30 and KYSE-140 cell lines. These cell lines were used as models of non *SOX2*-amplified and *SOX2*-amplified squamous cell carcinomas.

Both inducible shRNA cell lines after 7 days $\pm$ doxycycline showed specific knockdown of the corresponding AKT isoform mRNA, with scramble control not showing any significant impact on expression levels (Figure 4.12A). Corresponding protein levels at 7 days $\pm$ doxycycline are shown (Figure 4.12B). All shRNAs confirm protein knockdown of isoform specific targets; however, KYSE-140 shAKT1 shows a reduction in AKT3 expression, which was not observed in KYSE-30 shAKT1 cells. KYSE-140 shAKT3 showed a marginal impact on AKT1 protein, not reflected in the mRNA data (Figure 4.12B).

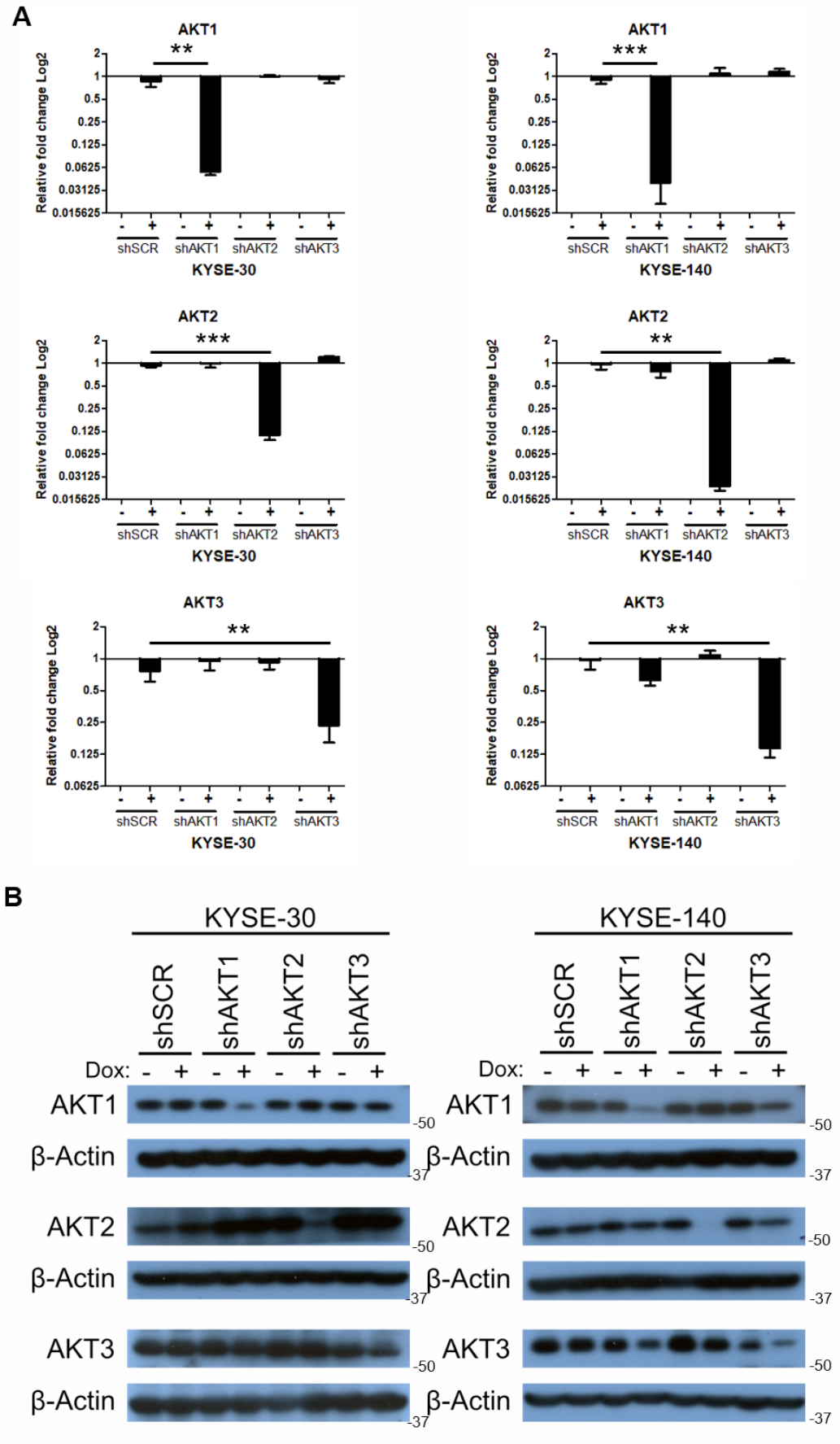
A
AKT1
**
Relative fold change Log2
2
1
0.5
0.25
0.125
0.0625
0.03125
0.015625
- + - + - + - +
shSCR shAKT1 shAKT2 shAKT3
KYSE-30
AKT1
***
KYSE-140
AKT2
***
KYSE-30
AKT2
**
KYSE-140
AKT3
**
KYSE-30
AKT3
**
KYSE-140
B
KYSE-30
KYSE-140
shSCR
shAKT1
shAKT2
shAKT3
Dox: - + - + - + - +
AKT1
β-Actin
AKT2
β-Actin
AKT3
β-Actin
-50
-37

Figure 4.12: Inducible shRNAs targetted to AKT isoforms show specific knockdown of corresponding RNA and protein in KYSE-30 and KYSE-140 cell lines.
A.RT-qPCR analysis of AKT isoform mRNA expression in KYSE-30 and KYSE-140 cell lines transduced with shRNAs specific to the 3 AKT isoforms. Cell lines were maintained $\pm$ 0.5 μg/mL doxycycline for 7 days. RT-qPCR was performed using SYBR green chemistry, and expression levels of the AKT isoforms was calculated using the $\Delta\Delta$Ct method relative to the comparable no dox control, normalising to the *TBP* housekeeping gene. Significant differences compared to shSCR + dox controls were determined using an unpaired t-test, two tailed P values: * $p \leq 0.05$, ** $p \leq 0.01$, *** $p \leq 0.001$. **B.** Western blot using samples generated as in A. RT-qPCR results represent the mean $\pm$SD from 3 experimental repeats and western blot data is representative of 3 experimental repeats.

4.10 AKT3 knockdown in SOX2-amplified squamous cell line impacts proliferation and increases death

Following generation and validation of squamous cell lines with inducible shRNAs to AKT isoforms discussed in the previous section, cell growth assays were used to study the effect of AKT isoform knockdown on proliferation in non *SOX2*-amplified and *SOX2*-amplified squamous cell lines (Figure 4.13). Scramble shRNA controls showed no significant impact on proliferation in both cell lines. Knockdown of AKT1, AKT2 or AKT3 in KYSE-30 cells showed no impact on proliferation when compared to scramble controls (Figure 4.13). AKT1 and AKT3 knockdown in KYSE-140 cells showed significant reduction in proliferation, whereas AKT2 knockdown did not show any impact (Figure 4.13).

AKT1 and AKT3 knockdown in KYSE-140 cells showed the same impact on proliferation. To investigate phenotypic differences between AKT1 and AKT3 knockdown and to further recapitulate the *in vivo* epithelial lining, KYSE-140 inducible shRNA cells were maintained at 100% confluence before addition of doxycycline. Confluent KYSE-140 cells with AKT3 knockdown showed increased cell death, observed via phase-contrast microscopy as floating cells in the culture media and patches emerging in the monolayer, when compared to AKT1 and AKT2 knockdown (Figure 4.14).

4.10.1 Towards studying AKT3 inhibition in squamous cell carcinomas *in vivo*

In order to study AKT3 inhibition *in vivo*, a mouse tail vein injection experiment was performed. KYSE-140 shSCR control cells and KYSE-140 shAKT3 cells were injected into the tail veins of immunodeficient NSG^{TM} mice and then placed on doxycycline drinking water 24 h after injection. One of the first capillary beds that cells reach after injection is in the lungs and typically forms the most common site of cell engraftment and tumour growth. This model serves as a useful tool for studying tumour cells in the lung without a genetically engineered mouse model (GEMM) (Mohanty and Xu, 2010). 7 weeks after injection, the mice were culled, with no tumours observed in the lungs in either control or experimental cells. It was concluded that these cells were not adapted to survive the stress of intravenous injection and plans for setting up subcutaneous xenografts in NSG^{TM} mice have been made, although this comes with the disadvantage of cells not being within the lung when forming tumours.

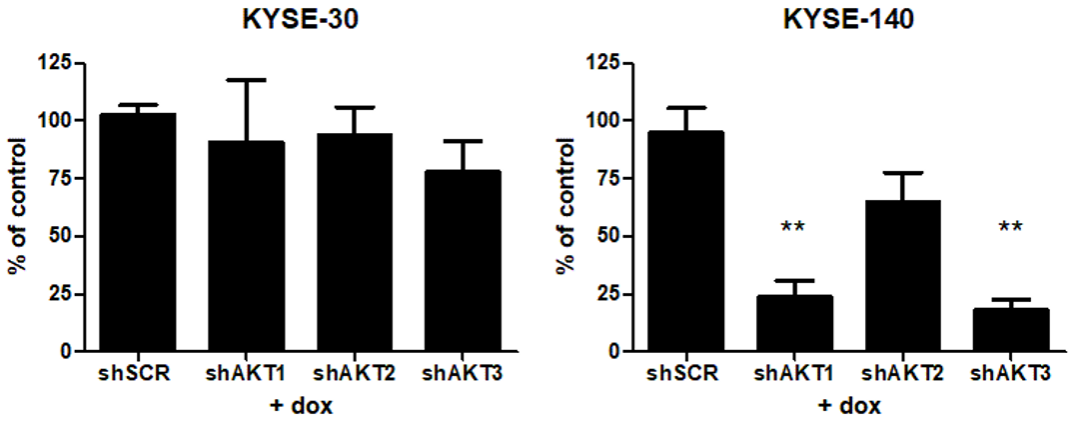

Figure 4.13: Knockdown of AKT1 or AKT3 in SOX2-amplified squamous cells, KYSE-140, significantly reduces proliferation.
Proliferation assays using cell lines with inducible shRNAs generated previously (Figure 4.12). Cells maintained in growth phase were treated $\pm$0.5 μg/mL doxycycline for 7 days before viable cells were quantified using the resazurin assay. Proliferation assay results represent the mean $\pm$SD from 3 experimental repeats. Significant differences compared to shSCR controls were determined using an unpaired t-test, two tailed P values: * p$\leq$0.05, ** p$\leq$0.01, *** p$\leq$0.001.

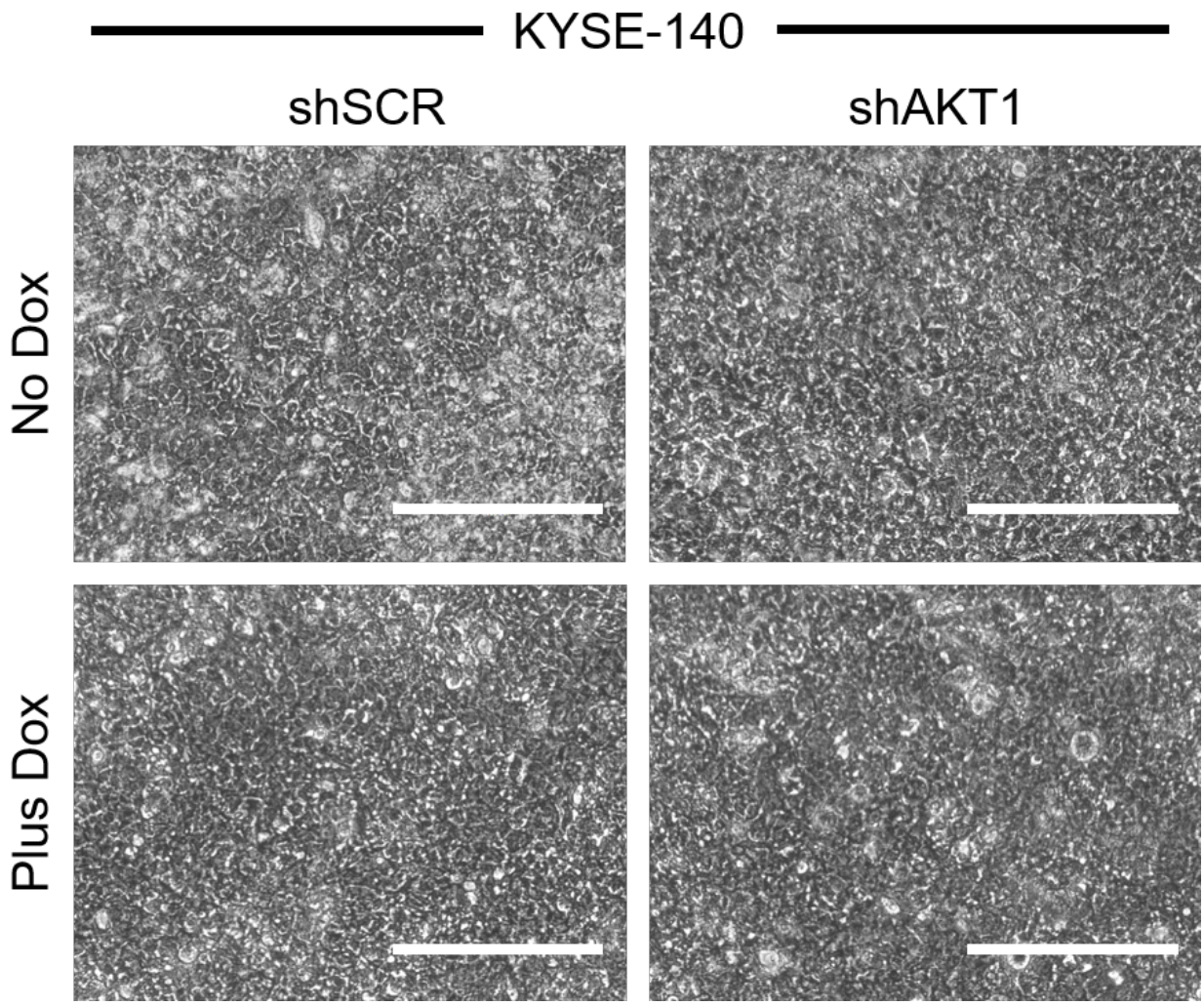
KYSE-140
shSCR
shAKT1
No Dox
Plus Dox

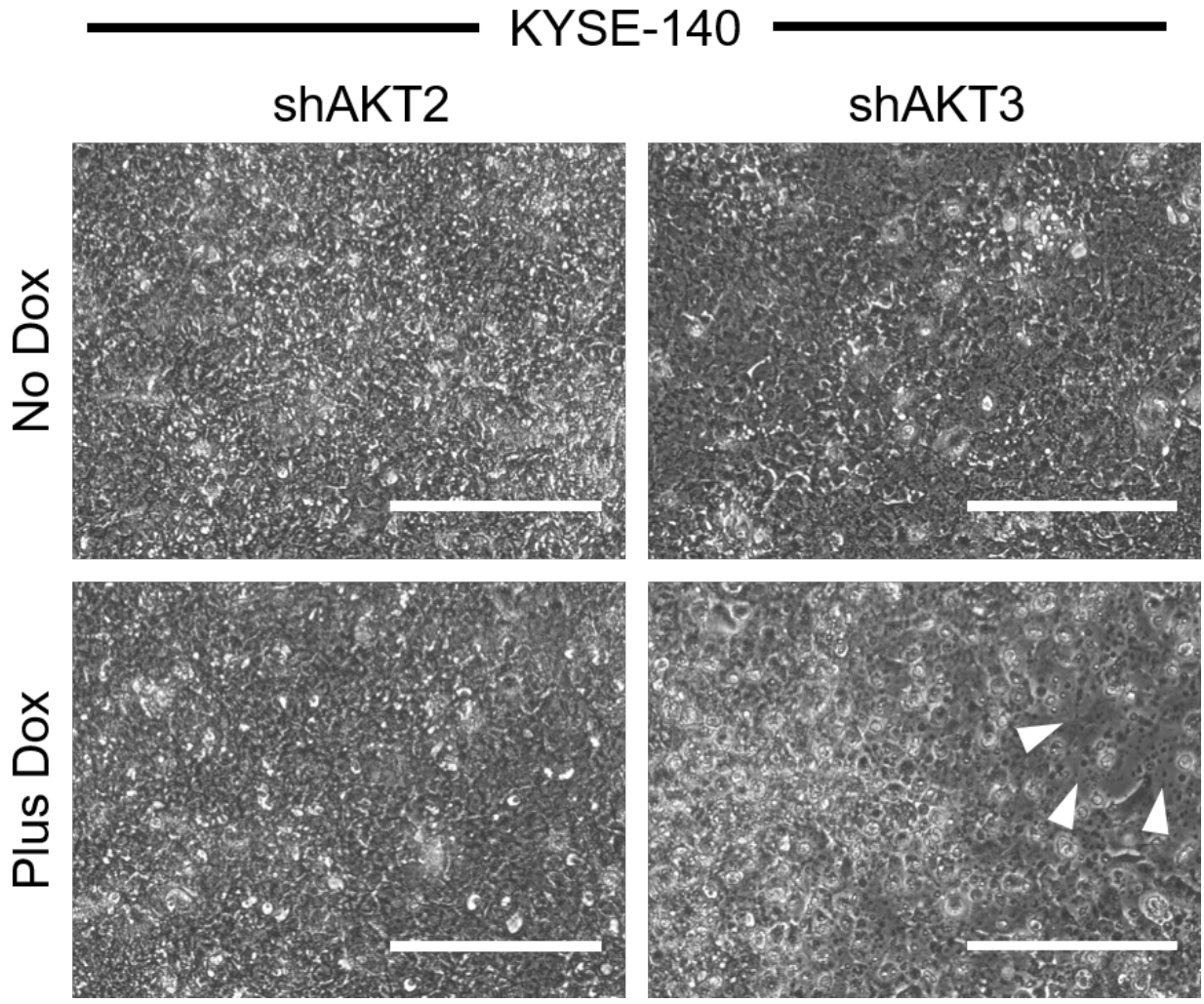

Figure 4.14: Knockdown of AKT3 in confluent KYSE-140 cells shows increased death compared to AKT1 and AKT2 knockdown.
KYSE-140 cells with inducible shRNAs from figure 4.12 were grown until 100% confluent. When confluent, cells were maintained for 5 days $\pm$0.5 μg/mL doxycycline. At confluence media was changed on day 1, 2 and 3, images were taken on day 5. Patches in the confluent epithelium are indicated by white triangles. Scale bars = 200 μm. Images are representative of 3 experimental repeats.

4.11 Discussion

4.11.1 Summary

In this study AKT3 vulnerability in SOX2-driven SQC was identified. RNA-sequencing data showed that, of the AKT isoforms, AKT3 was upregulated to the greatest extent as a result of SOX2 deregulation in the OTC model, validated using RT-qPCR. Although AKT1, AKT2 and AKT3 protein levels all increased upon SOX2 induction a clear redundancy for AKT2 in the formation of SOX2-driven dysplasia and a vulnerability to AKT3 knockdown was shown, using genetic knockout and RNAi-mediated knockdown of the AKT isoforms. AKT isoform expression was verified using clinical samples, showing that AKT3 mRNA upregulation was not an artefact of the OTC model and was positively correlated with SOX2 expression in SOX2-amplified SQC tumours. SOX2-amplified squamous carcinoma cell lines showed a vulnerability to AKT1 or AKT3 knockdown for significant inhibition of proliferation, when compared to non SOX2-amplified cells that showed no impact in proliferation with any AKT isoform inhibition. Furthermore, a qualitative increase in cell death was observed in confluent cultures only with AKT3 knockdown in a SOX2-amplified squamous cell line, rather than AKT1 or AKT2 knockdown.

4.11.2 SOX2 deregulation correlates with AKT3 transcriptional upregulation in SQC clinical samples and the OTC model

Following on from results in Chaper 3 that showed pan-AKT inhibition rather than AKT1/2 inhibition had efficacy in chemoprevention of SOX2-driven SQC, I investigated the role of the three AKT isoforms in the OTC model and in clinical specimens. The clinical data available in this study supported the hypothesis that AKT3 is involved in SOX2-driven SQC, and that *in vitro* chemoprevention compound screens and RNA-sequencing data using the OTC model were not a consequence of artefacts of an artificially created *in vitro* model. The TCGA data showed a positive relationship between SOX2 and AKT3 mRNA expression in a large sample size of SOX2-amplified SQC tumours (n=242) (Figure

4.2). There was no significant correlation between SOX2 and AKT1 expressions, and a negative correlation was shown between SOX2 and AKT2 expressions. The AKT2 data from the TCGA conflicted with a recent study that tracked preinvasive SQC lesions, showing that increases in copy number at the AKT2 locus was associated with a small proportion of preinvasive lesions. However, it should be noted that this was in a much smaller sample size (n=39) than the TCGA data (Teixeira et al., 2019).

The protein expression data from the human TMA of high-grade bronchial dysplasia biopsies demonstrate that all AKT isoforms are expressed in preinvasive lesions, albeit to varying degrees. The TMA samples are archived from many years ago, this, combined with the limited number of samples available, meant that one cannot draw firm conclusions. However, the results from the TMA provide rational for forthcoming experiments investigating the roles of the AKT isoforms in SQC.

The increased transcription or expression of AKT isoforms is interesting and, together with downstream effector activation and the genetic/therapeutic screening data, is consistent with these proteins having a key role. However, it is important to stress that AKT isoform activation cannot be measured without evidence of isoform specific phosphorylation. In this context it would have been very informative to perform a comprehensive phosphoproteomic analysis or have access to phosphorylated AKT3 specific antibodies.

The OTC model would need to be scaled up significantly in order to generate enough sample for phosphoproteomics studies, and this was beyond the scope of this PhD project. pAKT3 specific antibodies were not available at the time of writing and pAKT1 and pAKT2 specific antibodies were only recently generated and characterised (Wang et al., 2018).

A curious observation from the OTC data is an upregulation of AKT1 at the protein level upon SOX2 deregulation, but with no significant change in AKT1 transcription levels. This suggests that AKT1 mRNA or protein may be stabilised as a result of SOX2 induction. Preliminary ChIP-sequencing results from the OTC showed SOX2 enriched binding sites at the transcriptional start sites (TSS) of *AKT1* and *AKT2*. This data at first appeared contradictory to the mRNA data, as SOX2 binding to the TSS would be assumed to promote transcription of AKT (Appendices, Figure 7.1). However, this could be SOX2 acting

as a pioneer factor and require further cofactor binding to upregulate transcription of AKT directly (Iwafuchi-Doi, 2019).

An enriched SOX2 binding site, 6kb upstream of the *AKT3* TSS, is shown in the OTC ChIP-Sequencing data and is hypothesised to be an enhancer region for *AKT3* (Appendices, Figure 7.1). Using ChIP-Sequencing data from 7 cell lines available on the UCSC database, peaks corresponding to H3K27Ac enriched sites were present at the same site that SOX2 bound upstream of the TSS of *AKT3* (Appendices, Figure 7.2). H3K27Ac are histone modifications that mark active transcription enhancer regions, and are consistent with SOX2 directly inducing *AKT3* transcription (Calo and Wysocka, 2013). Further time course data on SOX2 binding and the transcriptional status of AKT isoforms is required to analyse any transcriptional regulation by SOX2, as well as further investigation into the potential enhancer region for AKT3. Experiments to delete the enhancer region using CRISPR-Cas9 to determine whether AKT3 transcription levels are effected upon SOX2 deregulation could elucidate the functionality of this proposed SOX2 induced *AKT3* enhancer region. Pilot data for SOX2 pulldown experiments in SOX2-positive cell lines, H520 and KYSE-140, showed SOX2 binding to the 5 'terminus of *AKT3*, suggesting that this may be a common binding site for SOX2 (Appendices, Figure 7.3). Future experiments to analyse SOX2 binding sites around *AKT1* and *AKT2* using ChIP-PCR in these cell lines are required to give further evidence for common SOX2 binding sites in a range of cell lines.

4.11.3 Gene knockout using CRISPR-Cas9 show that AKT2 is not required for the formation of lesions in the OTC

The results presented in Chapter 3, the plausibility of AKT as a therapeutic target, and the variable correlation between AKT isoform expression and SOX2 expression in clinical samples provided the rationale for pursuing functional studies to investigate the necessity of the AKT isoforms in SOX2-driven SQC. This was further reinforced by data from breast, melanoma and ovarian cancers showing AKT3 was critical for proliferation and tumour development (Stahl et al., 2004; Chin et al., 2014; Liu et al., 2017).

An approach to use CRISPR-Cas9 to knockout the AKT isoforms in bronchial epithelial cells, KTshP53iSOX2 cells, used in the OTC model was started with. To ensure that complete knockouts were achieved, single cell cloning was used to generate monoclonal populations that would have constitutive p53 knock down, inducible SOX2 and knockouts of individual AKT isoforms. Prior to the beginning the CRISPR experiments, a concern was that cell sorting based on GFP positivity from the transiently transfected px458 CRISPR-Cas9 constructs would not be possible as parental cells already had constitutive GFP-shP53 constructs. However, clear GFP++ populations, consistent with KTshP53iSOX2 transiently transfected with px458 CRISPR-Cas9 constructs, were present (Figure 4.5A).

Monoclonal populations were screened for genetic disruptions caused by Cas9-mediated double-strand breaks in DNA. The error prone non-homologous end joining DNA repair pathway can cause insertions or deletions (InDels) in the DNA, which may result in frameshifts leading to dysfunctional protein or premature stop codons. Initial screening of CRISPR monoclonal populations suggested that some clones had insertions or deletions that would cause frameshifts in the coding sequence (Figure 4.5C,D,E). All AKT2 CRISPR clones and 1 AKT3 clone showed absence of protein when analysed by western blotting. However, all AKT1 CRISPR clones screened showed smaller, truncated bands compared to parental cells. Protein lysates from the AKT1 CRISPR clones showed band shifts in western blotting analysis, following treatment with phosphatase, showing that the truncated proteins were functional and able to signal via phosphorylation (Figure 4.7). As it was not possible to expand any AKT1 CRISPR clones without functional AKT1 protein, it was concluded that AKT1 was necessary in immortalised bronchial epithelial cells for cell population expansion.

AKT2$^{-/-}$ clones formed clear dysplastic lesions when used in the OTC model, and showed that AKT2 was not necessary for the formation of SOX2-driven lesions in SQC (Figure 4.8). The single AKT3$^{-/-}$ clone was slow to expand when compared to parental cells in both conventional culture conditions and in the OTC model. As with AKT1, it was concluded from these experiments that AKT3 was necessary in immortalised bronchial epithelial cells for cell population expansion (Figure 4.9).

Producing gene knockouts for monoclonal cell line derivation has a number of limitations.

In this study, AKT1 was shown to be essential for the survival of cells with knockout proving to be lethal. AKT1 has been shown to be essential *in vivo* too, AKT1$^{-/-}$ mice exhibit partial lethality between mid-embryonic development and weaning, with pups that survive post weaning remaining significantly smaller than WT mice (Cho et al., 2001b). An inducible method of knockout or knockdown of gene products would be an alternative method and is discussed in the next section. Another limitation of complete knockout cell lines is the need for single cell cloning. This necessitates an extreme selection pressure that has uncertain bias.

The use of monoclonal populations also changes the dynamics of the OTC model. The KTshP53iSOX2 cells used are polyclonal for inducible SOX2, but single cell cloning produces inducible SOX2 monoclonal populations. This is important as the levels of SOX2 in the OTC can impact the phenotypic outcome; data from my lab has shown that when very high levels of SOX2 in the OTC model are induced, a significant amount of cell death is observed. There is also heterogeneity in the human disease that monoclonal cell populations do not model *in vitro*.

4.11.4 Inducible knockdown of the AKT3 isoform impacts the formation of lesions in the OTC

Inducible RNAi methods were used to address some of the caveats associated with gene knockout experiments and further investigate the isoform specific roles of AKTs in SQC. A key advantage of using this system is that proteins required for the expansion of cells in normal tissue culture conditions, such as AKT1 and AKT3, can be repressed in a temporal manner. Another is that a polyclonal population of inducible SOX2 cells is maintained that is more representative of the original polyclonal OTC model, and indeed, the human disease.

Using shRNAs specific to the AKT isoforms, targeted knockdown of the AKT isoforms was observed (Figure 4.10B). A clear reduction in dysplastic lesion area was shown with AKT3 knockdown in the OTC, compared to no impact with AKT1 or AKT2 knockdown

(Figure 4.11). These experiments showed an AKT3 isoform vulnerability in polyclonal KTshP53iSOX2 cells in the OTC model.

There were a number of drawbacks to using doxycycline-inducible shRNAs in the OTC system. The first was that the inducible SOX2 in the system was also doxycycline controlled, so that SOX2 and shRNAs could not be controlled independently. The kinetics of the two doxycycline controlled tet-on constructs differed; SOX2 has been shown to be induced and detectable by western blotting within 24 hrs of doxycycline treatment in the OTC model (unpublished, Dr L. Corria, University of Cambridge), however, I show that 5 days of doxycycline is required for significant knockdown of target mRNAs (Figure 4.10B). This is likely to be because SOX2 induction causes upregulation of all three AKT isoforms thereby increasing the amount of time for shRNA-mediated knockdown to take effect; upregulation of all 3 AKT isoforms in parental KTshP53iSOX2 cells with 48 h SOX2 deregulation is observed (Figure 4.6). Although mRNA knockdown was significant with shRNAs to the AKT isoforms, it may not be sufficient in conferring a biological or phenotypic impact. One method that could be used to study the sufficiency of knockdowns would be to analyse AKT isoform-specific downstream signalling. However, there are no plausible options, very few downstream targets have been identified that show isoform specificity in a limited context in breast cancer: p21 CIP, SKP2 and paladin are AKT1 targets, and MDM2 and AS160 are AKT2 targets (Sangai et al., 2012). SOX2 deregulations alters the expression of p21, a cyclin-dependent kinase, and p53 repression may well impact MDM2 expression, a negative regulator of p53. There are no known AKT3 specific targets.

Due to the latency of sufficient knockdown, the involvement of AKT1 and AKT3 in the initiation (rather than the maintenance) of SOX2-driven lesions cannot be confirmed. It may be inferred that AKT3 is involved in the maintenance of SOX2-driven lesions, but without a more detailed time course for AKT3 levels in parental and inducible shRNA cells this hypothesis is not certain. Together with the AKT2$^{-/-}$ data, the AKT2 knockdown data shows that AKT2 is not required for the formation of SOX2-driven lesions in the OTC model. The knockdown data for AKT3 supports other studies that have shown AKT3 to be significant in proliferation and tumour development in ovarian cancer cell lines, melanoma

cell/*in vivo* models, and triple negative breast cancer (TNBC) spheroid/*in vivo* models (Stahl et al., 2004; Chin et al., 2014; Liu et al., 2017).

4.11.5 Inducible knockdown of AKT1 or AKT3 inhibits the proliferation of the SOX2-amplified cell line, KYSE-140

Inducible RNAi-mediated knockdown of AKT isoforms in squamous carcinoma cell lines were used to validate findings from the OTC model. These did not have the added complication of dual tet-on controlled systems, previously discussed as a drawback in the OTC-inducible shRNA model. It is important to note here that attempts were made to transduce another SOX2-amplified squamous carcinoma line, TE-6, in order to increase the number of cell lines tested in this study. However, TE-6 cells did not survive puromycin selection following multiple attempts at lentiviral transduction.

AKT isoform knockdown showed specific mRNA knockdown in KYSE-30 and KYSE-140 cell lines. However, in the SOX2-amplified KYSE-140 cells, shAKT1 led to a reduction in AKT3 protein as well as AKT1 protein, but no significant impact on the level of AKT3 mRNA. shAKT3 led to a reduction in AKT1 protein as well as AKT3 protein, but no significant impact on the level of AKT1 mRNA. The reason for this is unclear. One suggestion could be that AKT1 and AKT3 proteins stabilise each other through heterodimeric protein-protein interactions, and that depletion of one isoform could increase the rate of degradation of the other isoform.

In KYSE-30 cells AKT1-3 single isoform knockdown had no impact on cell population expansion. AKT1 and AKT3 knockdown in KYSE-140, SOX2-amplified cells, significantly impacted cell population expansion (Figure 4.13). This provided further evidence for vulnerability in SOX2-amplified SQCs to AKT3 inhibition. Although AKT1 knockdown inhibited proliferation to the same extent as AKT3 knockdown in KYSE-140 cells, this was not the case in the OTC model. It was surprising that proliferation was not inhibited by any AKT knockdown in KYSE-30 cells, despite detectable levels and relatively high abundancy of mRNA, compared to KYSE-140. Cell lines with high levels of AKT have been shown to not necessarily be sensitive to AKT inhibition, suggesting that other pathways

may support growth in addition to AKT (Koseoglu et al., 2007; Sangai et al., 2012). Further research is required to identify biomarkers that may indicate sensitivity to AKT inhibitors. From this study, it may be that high SOX2 expression, amplification or dependence may be a biomarker for susceptibility to AKT inhibition.

In contrast to the cell population expansion assays, there was a qualitative phenotypic difference between AKT1 and AKT3 knockdown when induced in confluent KYSE-140 cells (Figure 4.14). This experimental model potentially allows for differences between proliferation and maintenance to be probed. These experiments indicate isoform specific function for AKT3 over AKT1 in maintaining confluent cultures of cells, rather than proliferation of log-phase or sub-confluent cells. Qualitative phenotypic differences were observed via phase-contrast microscopy showing patches of cell death in the epithelial layer and increased floating dead cells, compared to controls and AKT1 or AKT2 knockdown. A study in embryonic stem cells (ESCs) shows inhibiting AKT3 rather than AKT1 or AKT2 leads to an increase in apoptosis (Wang et al., 2017). Future experiments could employ biochemical analysis to quantify and identify the mode of death in the confluent KYSE-140 cell cultures. Cells may also be grown in transwells at the ALI in order to further recapitulate *in vivo* conditions for these experiments.

To date, the only AKT inhibitors to proceed through clinical trials have been pan-AKT inhibitors that have shown toxicity, resistance or no improvements in standard of care. The AKT isoforms are involved in a wide range of tissue homeostasis and the idea of AKT isoform-specific inhibition, rather than pan-AKT inhibition, has been proposed as having an increased therapeutic window due to lowering general toxicity and reducing potential paradoxical effects of pan-AKT inhibition (Chin et al., 2014). There have been studies that show upregulation AKT1 drives proliferation and tumorigenesis, but hyperactivation of AKT1 can also protect against migration and metastasis (Liu et al., 2006; Hutchinson et al., 2004). This supports the notion of developing and investigating isoform-specific AKT inhibition in the clinic.

4.11.6 Conclusions

In this study a novel candidate, AKT3, has been identified that could be targeted in the chemoprevention of SOX2-driven SQC, as well as potential application in more advanced disease. Using the OTC model and squamous cell line studies rationale is provided for further *in vitro* and *in vivo* experiments to examine the role of AKT3 in the progression and maintenance of SOX2-driven lesions, particularly in the lung. For clinical studies there is a need for the development of AKT3 specific inhibitors, as isoform specific inhibition has been proposed in a number of cancers and may reduce general toxicity and drug resistance associated with pan-AKT inhibition.

Chapter 5

Novel target evaluation in SOX2-amplified squamous cell lung cancer

5.1 Introduction

The main aims and focus of this PhD project work were presented in chapter 3 and chapter 4. However, further potential targets for chemoprevention implied in RNA-sequencing data and unpublished ChIP-sequencing data flagged a number of other targets that are potentially tractable for SOX2-driven squamous disease.

A series of pilot experiments were performed to evaluate two of these targets, SIK2 and bromodomain inhibition, the latter as part of a collaboration with AstraZeneca that was presented at the AstraZeneca & Cambridge Biomedical Campus Symposium in Respiratory, Inflammation & Autoimmunity Meeting, April 2018.

In addition to the work above, a third project involved a collaboration with Nicola Pellicciotta and Dr Pietro Cicuta at the Cavendish Laboratory, Department of Physics, University of Cambridge. In this collaboration we used the cells utilised in the OTC model in a microfluidic and airflow device that has the potential to combine bronchial dysplasia modelling with dynamic air and blood channels. This model, with further development, could provide opportunities for new predictive biomarkers for lung cancer, as well as providing a screening tool for inhaled drug delivery for the chemoprevention of SQC.

5.2 Salt Inducible Kinase 2 (SIK2), a novel target in SOX2-driven squamous cell carcinomas?

5.2.1 Introduction

SIK2 in normal physiology

The OTC model is a powerful tool to investigate downstream events as a consequence of SOX2 deregulation in human bronchial dysplasia, the precursor lesion to SQC. RNA-sequencing data was used to identify novel targets that were significantly altered when SOX2 was induced and could play a critical role in the progression of SOX2-driven squamous carcinomas.

SIK2 was among the most significantly deregulated genes in the OTC model (Appendices, Table 7.1). SIK2 is a member of the AMPK (AMP-activated protein kinase) family, members of this family sense changes in cellular energy and regulate AMP/ATP levels (Kahn et al., 2005). SIK2 is activated in response to metabolic stresses by regulating CREB1-mediated gene transcription. CREB1 is a transcription factor that binds to cAMP response elements (CRE), driving transcription.

SIK2 implication in cancers

SIK2 has been implicated in a number of cancers including ovarian, prostate and breast. Ahmed et al. (2010) describe a previously unknown involvement for SIK2 in centrosome splitting and mitotic progression in ovarian cancers, together with a correlation between high SIK2 expression and poor survival rates in high grade serous ovarian cancers. Building on the work by Ahmed et al. (2010), overexpression of SIK2 was found to be common in adipocyte-rich metastatic sites in ovarian cancers (Miranda et al., 2016). *In vivo* experiments showed SIK2 overexpression promoted metastasis. SIK2 is required for prostate cancer cell growth, depletion of SIK2 inhibited proliferation and induced cell death (Bon et al., 2015).

Although there have been many reports on the oncogenic role of SIK2, a recent study highlighted SIK2 having a tumour suppressor role in breast cancer (Zohrap et al., 2018). It was found that SIK2 was frequently downregulated in invasive breast cancers and negatively correlated with mitotic activity of cells. This study highlights a potential dichotomous role for SIK2 in tumorigenicity, and that differences in pathways involved and mutational signatures in specific cellular contexts may give rise to disparate phenotypes.

5.2.2 SOX2 directly upregulates SIK2 in the OTC model

RNA-sequencing data, generated by Dr L. Correia (University of Cambridge, UK), showed that SIK2 was in the top 30 deregulated genes when SOX2 was induced for 4 days at ALI in the OTC model, and of statistical significance (p-value: **** $p \leq 0.0001$, false discovery rate: **** $p \leq 0.0001$). This transcriptomic data was validated by RT-qPCR for SIK2 in RNA samples from the OTC model at 4 and 8 days ALI, showing significant and maintained upregulation of SIK2 when SOX2 was induced in the OTC model (Figure 5.1A). Transcriptional upregulation of SIK2 was accompanied by an upregulation of SIK2 protein at 4 and 6 days ALI (Figure 5.1B).

ChIP-sequencing data (unpublished) generated 4 days post SOX2 induction, that is at the same timepoint as the RNA-sequencing data, showed that SOX2 binds the transcriptional start site (TSS) of *SIK2*, suggesting that *SIK2* is a direct transcriptional target of SOX2 (Figure 5.2A). To ensure that SOX2 binding in the OTC was not an artefact of the model, SOX2 ChIP pulldown experiments were performed in two SOX2 positive cell lines, H520 and KYSE-140. ChIP-PCR validation was performed using primers targeting the 5'TSS of *SIK2*, confirming that SOX2 binds the 5'TSS of *SIK2* in both SOX2 positive cell lines (Figure 5.2B).

A

Gene	LogFC	P- Value	FDR
SIK2	1.8076	$3.55x10^{-34}$	$1.79x10^{-31}$

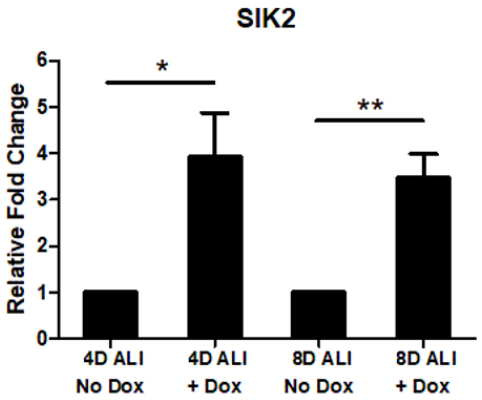

B

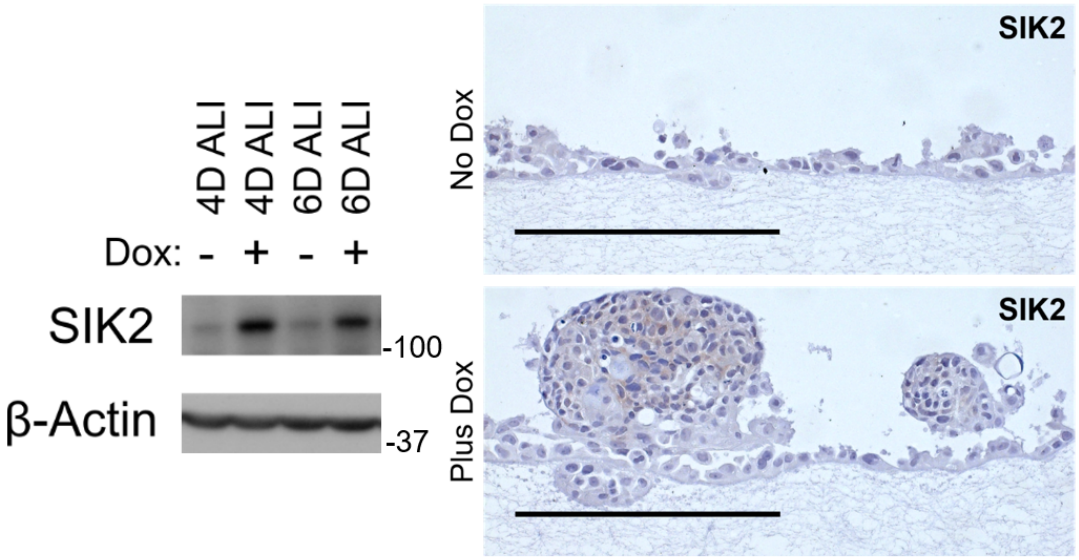

Figure 5.1: SIK2 is upregulated in the OTC model upon SOX2 induction at both the transcriptional and protein level.
A. RNA-sequencing results for SIK2 (left), comparing plus doxycycline to no doxycycline at 4 days ALI in the OTC model. LogFC = Log Fold Change. FDR = False Discovery Rate. RNA-sequencing results confirmed using RT-qPCR analysis at 2 time points post SOX2 induction (right). RT-qPCR was performed using SYBR green chemistry, and expression of SIK2 was calculated using the $\Delta\Delta$Ct method relative to the comparable no doxycycline control, normalising to *TBP* housekeeping gene. **B.** SIK2 protein levels in the OTC model were analysed using western blot (left) and IHC (right). IHC sections are from 6 day ALI OTC model. RNA-sequencing experiments carried out by Dr L. Correia (University of Cambridge, UK). Samples used for IHC generated by Dr L. Correia. RNA-sequencing and RT-qPCR results represent the mean $\pm$SD from 3 experimental repeats. Western blot and IHC data representative of 2 experimental repeats. Significant differences were determined using an unpaired t-test, two tailed P values: * $p \leq 0.05$, ** $p \leq 0.01$, *** $p \leq 0.001$. Scale bar = 200 μm.

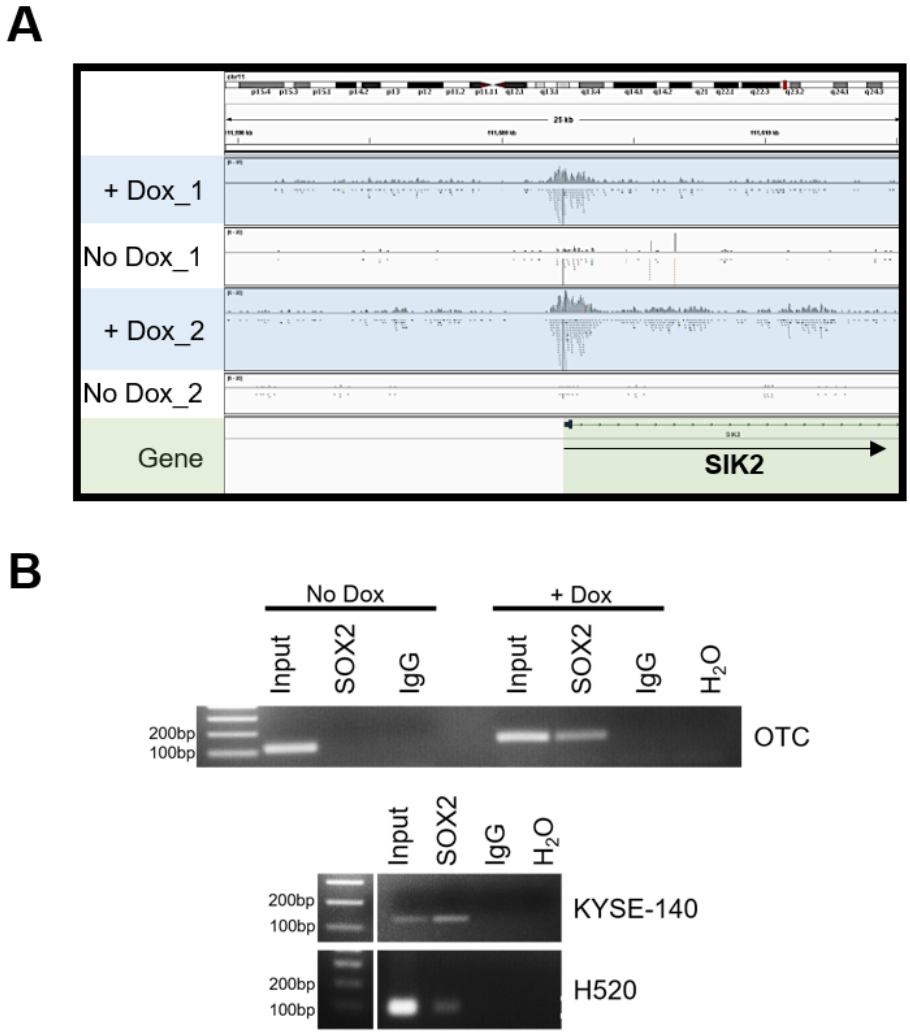

Figure 5.2: SOX2 binds the 5'terminus of *SIK2* in the OTC model and in two SOX2 positive cell lines.
A.ChIP-Sequencing results for SOX2 pull down in the OTC model at 4 days ALI ±doxycycline. The genomic region shown correspond to the 5'terminal of the gene. Peaks of enriched reads are seen where SOX2 is bound to the chromatin at the TSS. **B.**ChIP-PCR using primers targeting the 5'TSS of *SIK2*. Samples generated from SOX2 pulldowns in OTC (A.) and two SOX2 positive cell lines. Amplicons show that SOX2 binds the 5'TSS of *SIK2*. ChIP-sequencing experiments in the OTC (A.) performed by Dr L. Correia (University of Cambridge, UK). ChIP-Sequencing viewed and screenshots taken using Integrated Genomics Viewer. ChIP-sequence data represents 3 experimental repeats.

5.2.3 Pan-SIK inhibition causes epithelial denudation in the OTC model

I have shown that *SIK2* is a direct target of SOX2 in both the OTC model and SOX2 positive cell lines, and that SIK2 is significantly upregulated in the OTC model upon SOX2 induction. A SIK2 inhibitor was pursued to test the necessity for SIK2 expression in the progression and maintenance of SOX2 deregulated SQC using the OTC model. To date, there is only one SIK2-specific small molecule inhibitor, ARN-3236. Attempts were made to collaborate with the drugs company responsible for producing this compound, however this failed and access to the compound was not possible. Therefore I tested a pan-SIK inhibitor (HG-9-91-01) in the OTC model and in cell line proliferation assays. SOX2 amplified KYSE-140 cells were sensitive to pan-SIK inhibition, proliferation was significantly impacted when compared to vehicle controls (Figure 5.3A). In the primary chemoprevention model (experimental schematic shown in Figure 3.2A), pan-SIK inhibition showed denudation of the epithelial layer at concentrations used in other *in vitro* assays using this compound (Patel et al., 2014) (Figure 5.3B). Patches in the epithelial layer are visible from phase-contrast images, fibroblasts embedded within the collagen layer were visible.

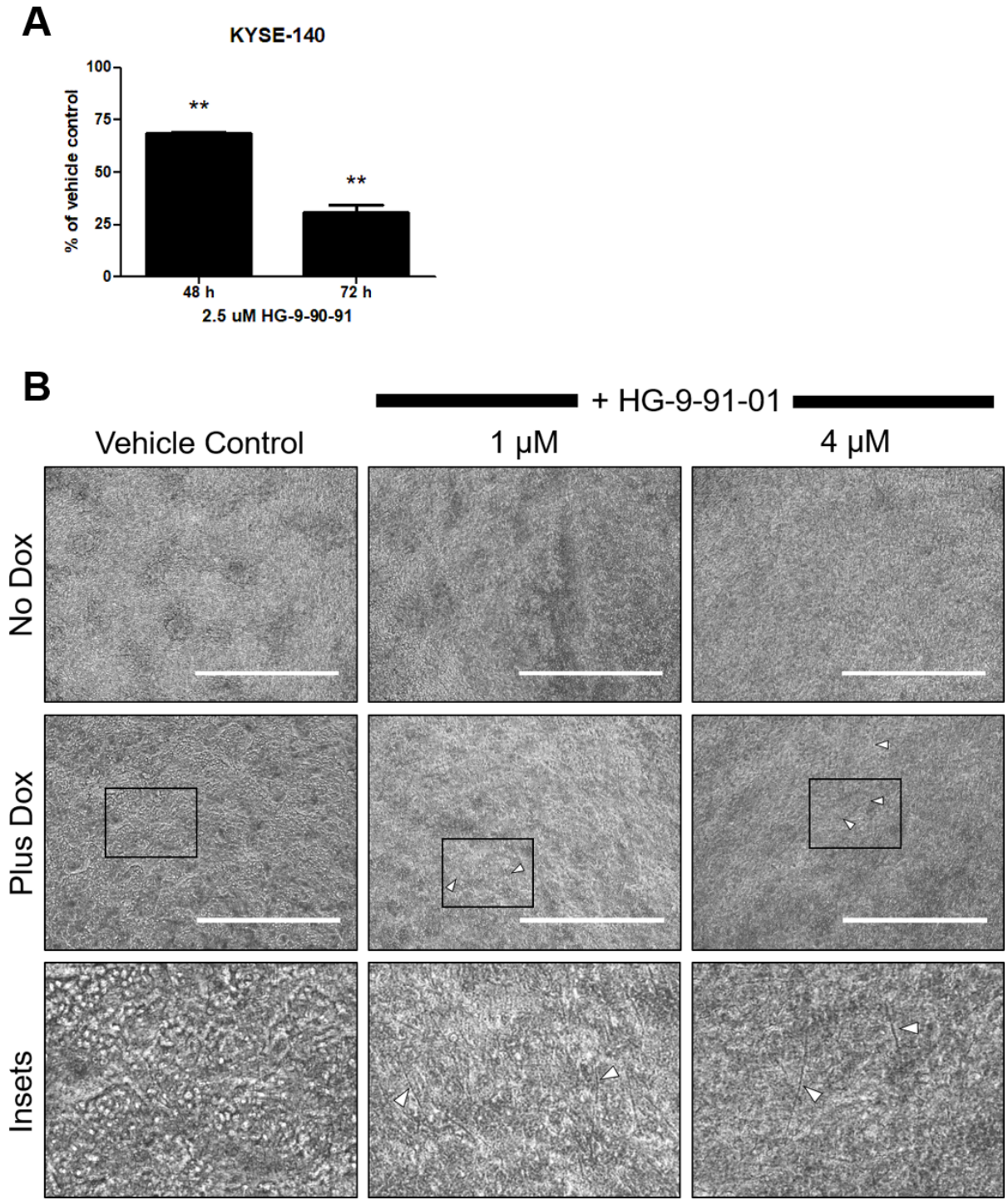
A
KYSE-140
% of vehicle control
100
75
50
25
0
**
**
48 h
72 h
2.5 uM HG-9-90-91
B
+ HG-9-91-01
Vehicle Control
1 μM
4 μM
No Dox
Plus Dox
Insets

Figure 5.3: Pan-SIK inhibition significantly impacts proliferation of KYSE-140 cell lines and causes epithelial denudation in the OTC model.
A. Proliferation assay $\pm$ 2.5 μM Pan-SIK inhibitor, HG-9-91-01 on KYSE-140 cell line. The resazurin assay was used to measure viable cells after treatment compared to vehicle controls. **B.** Pan-SIK inhibitor, HG-9-91-01, was used in primary chemoprevention assay, schematic shown in figure 3.2. Briefly, cells were treated once brought to ALI every 48 h with HG-9-91-01 $\pm$doxycycline for a total of 5 days at ALI. Phenotypic responses were monitored via phase-contrast microscopy. White arrows show fibroblasts visible in the collagen matrix as a result of gaps in the epithelium. Proliferation data represents the mean $\pm$SD from 3 experimental repeats. Images are representative of 3 experimental repeats. Significant differences were determined using an unpaired t-test, two tailed P values: * $p \leq 0.05$, ** $p \leq 0.01$, *** $p \leq 0.001$. Scale bars = 1000 μm.

5.2.4 SIK2 knockdown has no impact on proliferation of squamous carcinoma cell lines

With specific inhibition of SIK2 not possible via small molecule inhibitors, the next strategy was to inhibit SIK2 via siRNA-mediated knockdown. Transient methods of genetic knockdown are not possible in the OTC model. Cells must be maintained at confluence and at ALI deeming transient transfection methods impossible without compromising the confluent epithelial layer or cells exposure to air. Added complications for the OTC model include the collagen-fibroblast matrix disc absorbing transfection reagents and increasing toxicity, and also comparatively long culture times (with regard to transient transfections) required to observe phenotypic changes. Instead I used KYSE-30 and KYSE-140 cell lines, a non SOX2-amplified and a SOX2-amplified squamous cell carcinoma line, to investigate the necessity of SIK2 for proliferation in squamous carcinoma lines. Using transiently transfected siRNA specific to SIK2, SIK2 was knocked down in both cell lines at RNA and protein level (Figure 5.4A). SIK2 knockdown showed no significant impact on proliferation in KYSE-30 or KYSE-140 cell lines at 48 h and 72 h post siRNA transfection (Figure 5.4B).

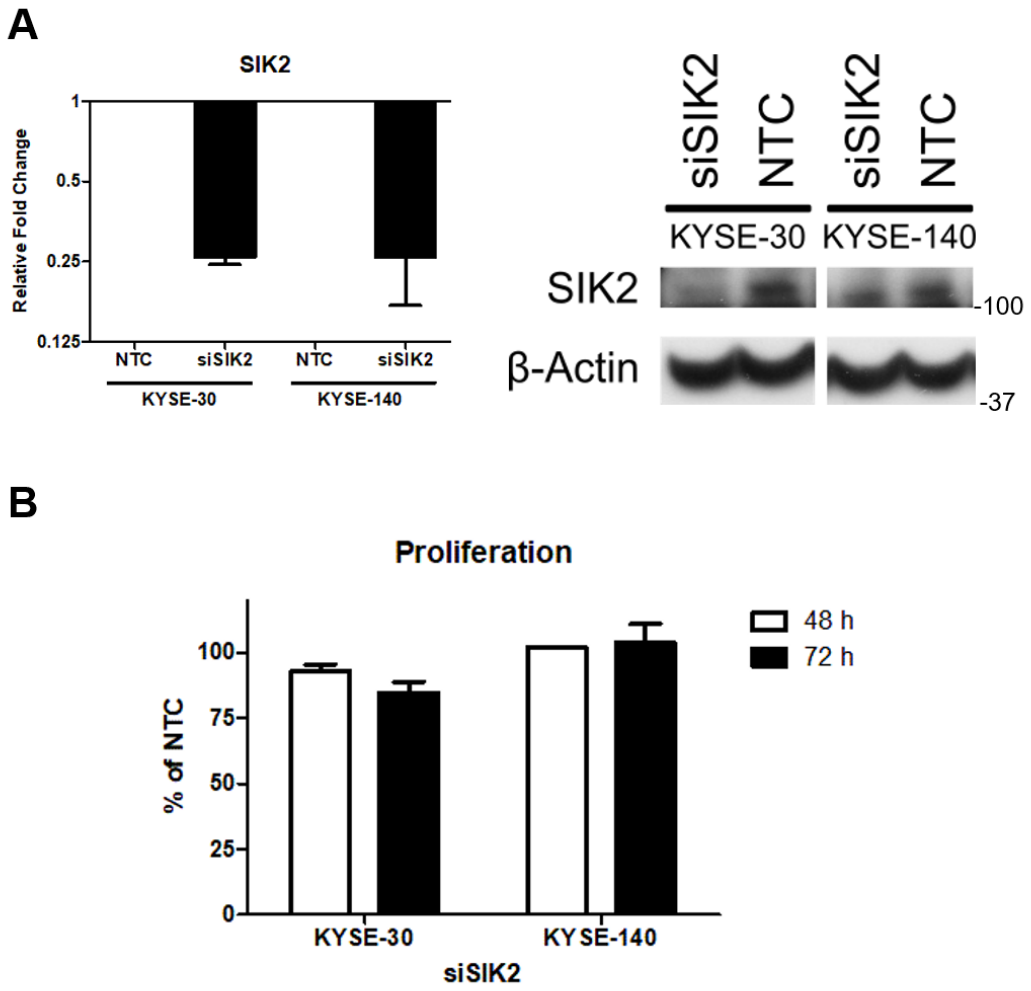

Figure 5.4: Knockdown of SIK2 in SOX2 amplified and non-SOX2 amplified squamous cell carcinoma cell lines does not impact proliferation.
A. SIK2 knockdown in two cell lines using transiently transfected siRNA. RNA expression was analysed 48 h post transfection via RT-qPCR (left). 200 ng of RNA was used for cDNA synthesis. RT-qPCR was then performed using SYBR green chemistry, and expression of SIK2 was calculated using the $\Delta\Delta$Ct method relative to the comparative NTC, normalising to *TBP* housekeeping gene. Protein was analysed 96 h post transfection via western blot (right). Non-targeting siRNA (NTC) was used as comparative controls in each cell line. **B.** Proliferation was measured using the resazurin assay. Viable cells were assayed and fluorescence was measured. Percentage of NTC is shown at 48 h and 72 h post transfection. RT-qPCR and proliferation data represents the mean $\pm$SD from 3 experimental repeats. Western blot data is representative of 2 experimental repeats.

5.2.5 Discussion

It has been shown in multiple model systems that *SIK2* is a direct target of SOX2, and SIK2 is significantly upregulated upon SOX2 induction in the OTC model (Figure 5.2 and 5.1). When pan-SIK inhibition is used in the OTC model, cytotoxicity is observed in the epithelial layer (Figure 5.3B). This suggests pan-SIK inhibition may not be an appropriate therapeutic strategy. Using two squamous cell carcinoma lines to investigate SIK2 specific inhibition, it was shown that SIK2 knockdown had no impact on proliferation, albeit with a modest reduction in protein in KYSE-140 cells (Figure 5.4). Due to the lack of clear response to targeted inhibition and lack of availability of a specific inhibitor, despite best efforts, it was decided to not pursue SIK2 knockdown or knockout strategies in cells in the OTC model. This project was under way at the same time as the AKT inhibition project presented in Chapters 3 and 4, and due to limitations on time and resources it was decided to focus on that project.

For the siRNA studies Dharmacon SMART Pool: ON-TARGET Plus technology was used that is validated and guaranteed for specific knockdown and vastly reduced off-target effects. Analysis of SIK1 or SIK3 transcript/protein levels was not performed during siRNA validation. However, if the siRNA had not been isoform specific and one of the other isoforms had been impacted, the proliferation data still shows no impact with knockdown, implying that any SIK isoform knockdown would not impact proliferation.

This project highlights the use of the OTC model to identify targets for rationalised drug screening, although this relies on compounds to be available for use that are specific for one's target of interest. A limitation of the OTC model for target validation is that it is not suitable for transient transfection studies for siRNA mediated knockdown experiments. Longer term experiments involving gene knockouts or stable shRNA mediated knockdown can be performed using the OTC model, demonstrated and discussed in Chapter 4.

Although SIK2 has been suggested as a potential therapeutic target in a number of cancers, such as ovarian and prostate cancer (Ahmed et al., 2010; Bon et al., 2015), to date it has not been implicated in SQC. Indeed, it is noted, the SQC TCGA data shows high SOX2 expression correlates with low SIK2 expression (Spearman rank correlation r = -

0.25, p = 6.9e-5). Taken together with Zohrap et al. (2018) who show that invasive breast cancers have downregulated SIK2, it is proposed that at present SIK2 is not a suitable target to pursue in SOX2-driven disease.

5.3 Bromodomain and extraterminal domain (BET) inhibition for chemoprevention of SQC

5.3.1 Introduction

BET Proteins

BET proteins are epigenetic readers comprising of ubiquitously expressed BRD2, BRD3 and BRD4 and the testis specific BRDT that recognises acetylated lysine residues of histone 4 (Stathis and Bertoni, 2018). BET proteins act as scaffolds for other proteins to bind enhancers of active genes and promoters to drive transcription. BRD4 is shown to associate with mediator complex, a multi-protein complex involved in transcription initiation (Dawson et al., 2012).

BET proteins in cancer

BET proteins were initially shown to be important in many hematologic cancers, as well as a number of solid malignancies. *Myc* is a downstream target of BRD4 and is central to many oncogenic processes such as proliferation, apoptosis and metabolism, and is deregulated in over 50% of human cancers (Chen et al., 2018a). BRD4 inhibition using a small molecule inhibitor led to reduction in MYC and cell cycle arrest in acute myeloid leukemia (AML) cells (Zuber et al., 2011). Ectopic MYC expression conferred resistance to the phenotypic effects of BRD4 inhibition, suggesting a role for BRD4 in maintaining oncogenic MYC expression. Wyce et al. (2013) report BET inhibition in neuroblastoma models resulted in potent anti-proliferative activity, not only by *MYC* suppression but by suppression of the key anti-apoptotic gene, *BCL2*. BRD4 is critical in the pathogenesis of nuclear protein in testis (NUT) midline carcinomas. The *NUT* gene is commonly involved in chromosomal rearrangements involving fusion to *BRD4*, resulting in an oncogenic *BRD4-NUT*, driven by the BRD4 promoter (French et al., 2003). BET inhibition has been reported as a target in castration-resistant prostate cancers too (Asangani et al., 2014).

Enhancers are regions of non-coding DNA that regulate the transcription of common housekeeping genes, and can be situated many kilobases away from the target gene promoter. Enhancers recruit protein complexes that facilitate transcription machinery binding to gene promoters, a process that is further regulated by specific histone modifications. Super-enhancers are clusters of enhancers that, together, regulate gene expression of cell type-specific gene signatures, and are commonly densely populated with BRD4 (Sengupta and George, 2017). Super-enhancers associated with oncogenic signaling have been shown to be acquired during tumorigenesis, implying a key role for super-enhancers in controlling cancer (Hnisz et al., 2013).

Tumour cells treated with BET inhibitors result in reduction of BET proteins across many enhancer and promoter regions accompanied by downregulation of transcript levels. This effect is accentuated in super-enhancer-driven genes, such as *MYC*, where BET inhibition in multiple myeloma and diffuse large B cell lymphoma cells showed preferential loss of BRD4 at super enhancer sites, leading to marked reduction in transcript levels (Lovén et al., 2013; Chapuy et al., 2013).

BET inhibition in respiratory diseases

BET inhibition has been suggested as a therapeutic strategy in a broad range of diseases, including diabetes, chronic kidney disease and rheumatoid arthritis. However, the focus of this collaboration with the Respiratory & Inflammation iMED Department, AstraZeneca, was BET inhibition in respiratory diseases such as asthma, COPD and lung cancer. Asthma is characterized by inflammation and increased secretion of mucus, and BET inhibition has been shown to lower pulmonary inflammation in a mouse model of asthma, as well as improve overall lung function (Manni et al., 2017). Similarly in COPD, a respiratory disease associated with chronic inflammatory responses, BET inhibition has been shown to reduce pro-inflammatory cytokine signalling *in vivo* (Malhotra et al., 2017).

A number of studies have been carried out in NSCLCs, and show that BET inhibition is effective in reducing the growth of these cancers *in vitro* and *in vivo*. Gao et al. (2018) show BET inhibition in a small panel of NSCLC cell lines suppressed growth, however the

cell lines used were predominantly ADC and large cell derived cell lines, and only one SQC cell line. Further BET inhibition experiments were carried out *in vivo*, however only a xenograft model using large cell lung cancer cell line, H460, was used, demonstrating limited relevance for SQC. Similarly, Jauset et al. (2018) present data showing significant therapeutic potential with BET inhibition in NSCLC *in vitro* and *in vivo* models. However, all of these models were KRAS-driven, a genetic aberration very rarely seen in SQC.

Here data is presented as part of a collaboration that utilised a model of differentiated normal bronchial epithelium (not yet presented in this thesis), and the OTC model of bronchial dysplasia/early SQC, to explore BET inhibition using the tool compound JQ1, in a normal physiological context and in a disease context with respect to the chemoprevention of SQC.

5.3.2 BET inhibition reverts dysplastic lesions to a monolayer

Experiments were carried out to test BET inhibition in the chemoprevention of SQC. BET inhibitor, JQ1, was added to the OTC model once a distinct phenotype was present 4 days after bringing cells to ALI and doxycycline addition (experimental schematic shown in Figure 3.3A). Doses used in previous cell line studies enabled a dose range of 0.1 - 5 μM JQ1 to be set (Stratikopoulos et al., 2015; Gao et al., 2018). The impact of BET inhibition on established lesions was monitored and compared to vehicle controls. There was a dose responsive impact on lesions with BET inhibition (Figure 5.5). 0.1 μM JQ1 showed moderate impact on dysplastic lesions, whereas 0.5 μM JQ1 reverted lesions back to a monolayer. A higher dose of 5 μM JQ1 showed cytotoxicity, epithelial cell denudation occurred - gaps in the epithelium were visible in H&E sections and fibroblasts were visible in the collagen matrix from phase-contrast images (indicated by white triangles in Figure 5.5).

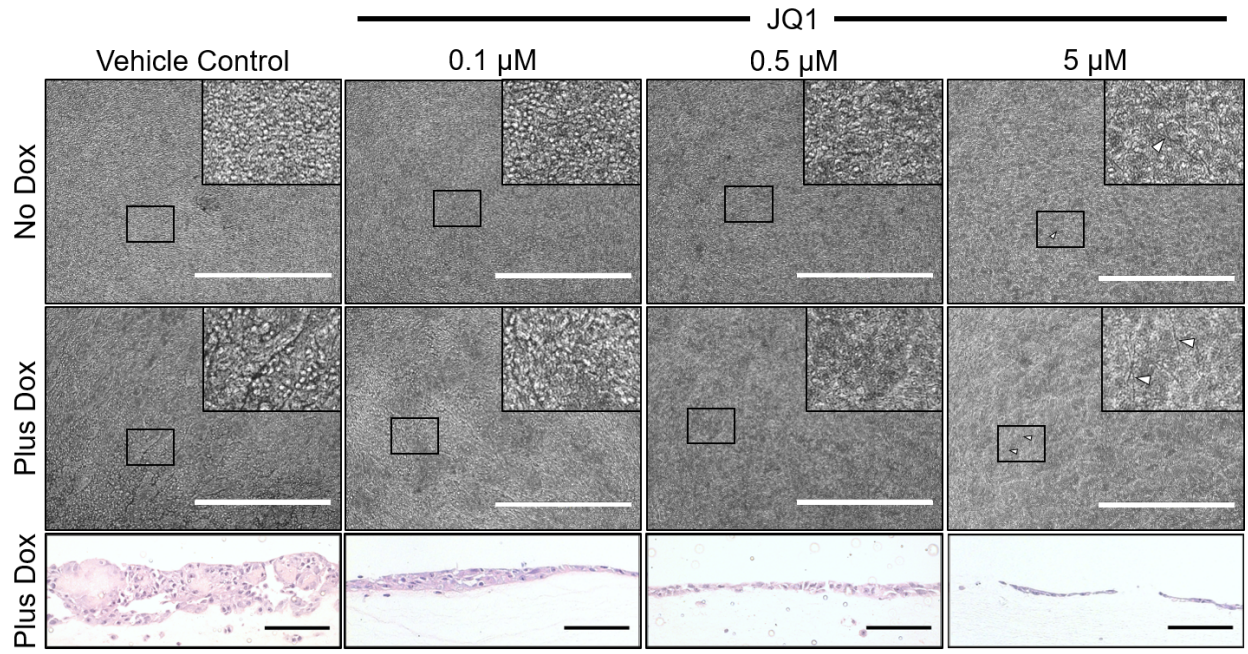

Figure 5.5: BET inhibition, in secondary chemoprevention assays reverts dysplastic phenotype to a monolayer in the OTC model.
JQ1 was used in a secondary chemoprevention assay as per the schematic in figure 3.3. Briefly, JQ1 was added once a clear dysplastic phenotype was present. Cells were treated every 24 h with JQ1 and ±doxycycline for a total of 96 h treatment. Phenotypic responses were monitored via phase-contrast microscopy, and fixed & processed for histology. At high dosage, 5 μM, epithelial denudation was apparent, white arrows show fibroblasts visible in the collagen matrix as a result of gaps in the epithelium. Images are representative of 3 experimental repeats. Phase-contrast scale bars = 1000 μm. H&E scale bars = 100 μm.

5.3.3 Bronchial epithelial cells expressing markers of differentiation remain following BET inhibition

The experiments above (Figure 5.5) suggested there may be a rationale for BET inhibition in the chemoprevention of SQC. BET inhibition has been shown to affect differentiation programmes in various cell types such as chondrocytes and erythrocytes, suggesting it may be toxic to differentiated adult tissues (Niu et al., 2016; Lamonica et al., 2011). Therefore the affects of BET inhibition on normal differentiated human bronchial epithelial cells (hBECs) was investigated. Primary hBECs were differentiated at the ALI using proprietary differentiation medium (protocol described in section 2.1.4). Once differentiated, the cells

were exposed to the dose of JQ1 that was effective but non-toxic in the chemoprevention experiments (Figure 5.5), the differentiation experimental schematic is shown in Figure 5.6A. Basal cells, expressing cytokeratin 5 and p63 markers, can self-renew and differentiate into secretory goblet cells and ciliated columnar cells of the adult airway, with a population of basal cells remaining (Rock et al., 2009).

Goblet cells, ciliated cells and basal cells were assessed following treatment with JQ1 by staining for markers of differentiation: MUC5AC (Goblet), acetylated tubulin (Ciliated) and cytokeratin 5 (Basal) (Figure 5.6B). The first observation was that JQ1 was well tolerated by differentiated hBECs at the 0.5 μM dose. Phase-contrast images of JQ1 treated differentiated hBECs did suggest a qualitative decrease in mucus production, however MUC5AC positive goblet cells were readily detected (Figure 5.6B). Basal cells and differentiated ciliated cells were also detected after JQ1 treatment, shown by keratin 5 and acetylated tubulin staining (Figure 5.6B). Altogether no qualitative differences in MUC5AC, acetylated tubulin or cytokeratin 5-positive cells were seen between vehicle control and JQ1 treated cultures.

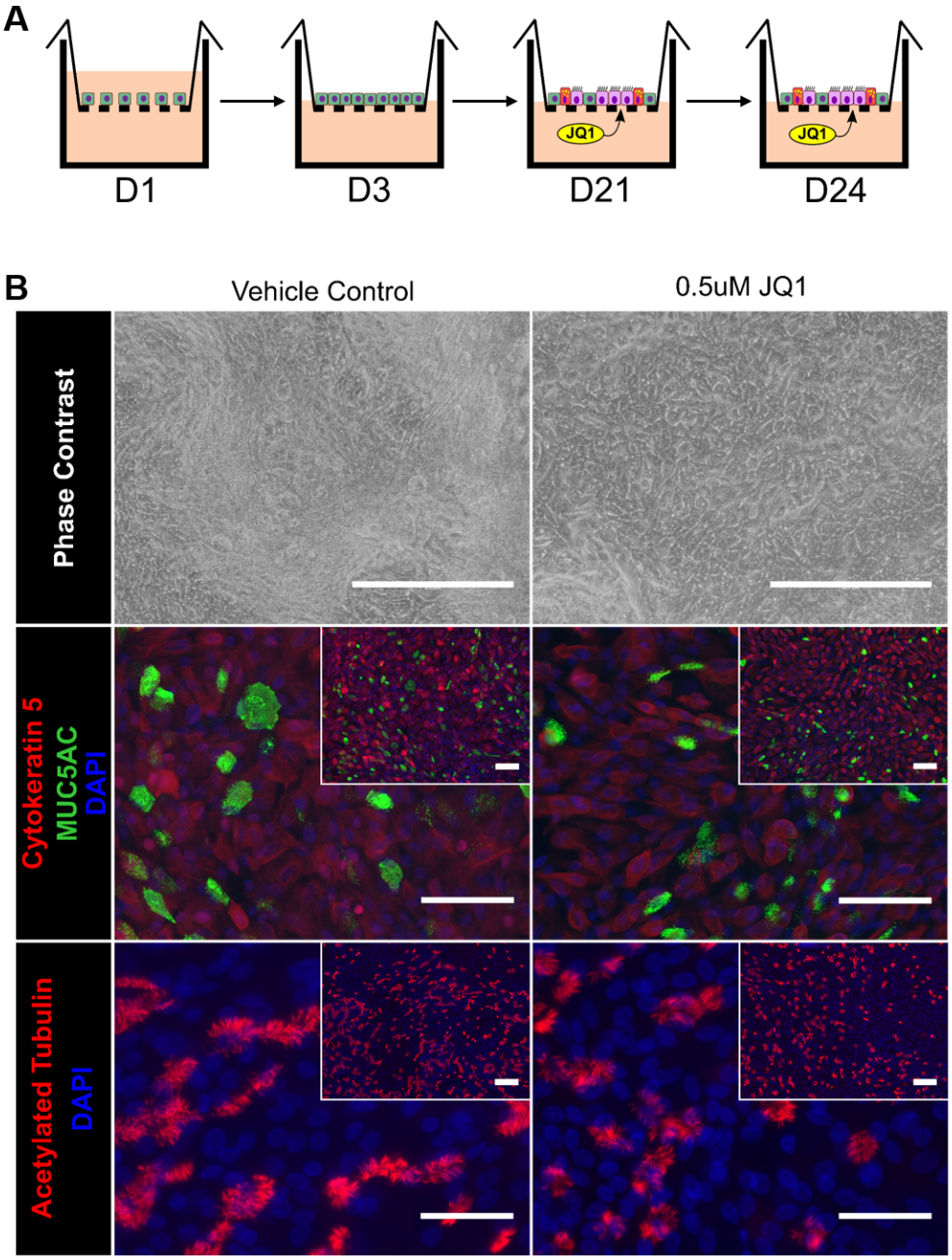

Figure 5.6: Differentiated primary hBECs retain markers of differentiation following BET inhibition.
A. Schematic showing assay to test compounds on differentiated primary hBECs. Primary hBECs are brought to ALI once confluent, and maintained in proprietary ALI medium (Pneumacult) for 18 days. Cells differentiated into goblet and ciliated cells of the human bronchial epithelium and were then treated for 72 h with 0.5 μM JQ1, retreated every 24 h. **B.** Phenotypic responses to 72 h treatment with JQ1 were monitored via phase-contrast microscopy, cells were fixed & processed for IF staining. Images and IF staining data are representative of 2 experimental repeats. Phase-contrast scale bars = 1000 μm. IF scale bars = 100 μm.

5.3.4 Discussion

It was demonstrated that BET inhibition using the tool compound, JQ1, reverts established dysplastic lesions to a monolayer in an OTC secondary chemoprevention model of early SQC. There have been a number of previous studies exploring BET inhibition in NSCLCs previously mentioned, but these have been primarily KRAS-driven ADC, rather than SQC (Jauset et al., 2018; Gao et al., 2018). This data provides early rationale for BET inhibition in the chemoprevention of SOX2 amplified SQC. Further experiments using ChIP to investigate SOX2 and MYC binding sites could elucidate whether BET inhibition reduced binding of these pleiotropic transcription factors to enhancer sites crucial for driving oncogenic signalling in SQC.

The potential for using BET inhibition in a wide variety of respiratory diseases such as asthma, COPD and lung cancer raises the issue of toxicity and phenotypic impact to surrounding normal tissue of the airways. BET inhibition, at a dose demonstrated to be efficacious in the disease model, does not show toxicity or have an overt qualitative impact on the presence of differentiated cells in a model of normal differentiated human bronchial epithelium. This is preliminary data and more work would be required to justify a conclusion that JQ1, at the dose capable of reversing premalignancy in the OTC model, is tolerated by normal bronchial epithelium. This would include extended duration of exposure, assaying cells from multiple donors and employing some more complex analyses of airway epithelial cell function such as ciliogenesis/ciliary movement Kukic et al. (2016); transepithelial resistance (TEER) (Srinivasan et al., 2015) and measurements of oxidative and other cellular stress (Deavall et al., 2012).

Although JQ1 has demonstrated potent inhibition at low nanomolar concentrations in preclinical studies, it has proved unsuitable for *in vivo* use. Pharmacokinetic data show that it has a half-life of less than 1 hour in blood plasma (Wadhwa and Nicolaides, 2016; Mio et al., 2019). However, it was used here as a tool compound in collaboration with AstraZeneca to pursue BET inhibition in respiratory diseases and to develop more appropriate BET inhibitors for clinical use. AstraZeneca have a particular interest in novel therapeutic approaches for the treatment of COPD. Given the established link between

COPD and lung cancer there is some rationale to the hope that improving treatment of this chronic inflammatory condition could contribute to lowering lung cancer incidence (Durham and Adcock, 2015).

A number of BET inhibitors have been developed, but to date only one is in Phase III clinical trials for cardiovascular disease (RVX208, Clinical Trials Identifier NCT02586155). Around a dozen other clinical Phase I/II trials are under way with a range of BET inhibitors for treatment of cancers. Overall preliminary results from these trials show favourable safety profiles and, with many of the reported adverse events, particularly thrombocytopenia, being reversible with treatment breaks (Stathis and Bertoni, 2018). That said, there is a concern with long-term effectiveness for these compounds, and require further investigation, potentially in combination therapies.

A significant concern with BET inhibitors is their current lack of specificity between the 4 isoforms. Andrieu et al. (2016) highlight that each BET protein controls distinct transcriptional pathways that are important for other functions beyond cancer cell proliferation, and that further development of isoform specific BET inhibitors could target disease more effectively, as well as reduce expected side effects.

Encouraging pilot data is presented here suggesting a potential role for BET inhibition in the chemoprevention of SQC at doses with no overt impact on normal differentiated bronchial epithelium. This merits further evaluation and could also be regarded as encouraging if there was a rationale to use BET inhibitors in other respiratory diseases. Further work to elucidate whether BRD isoform specificity in disease could increase therapeutic index and lower toxicity when taken into *in vivo* studies.

5.4 Towards a microfluidic and airflow model of bronchial dysplasia

5.4.1 Introduction

Organs-on-a-chip

Drug development is challenged and slowed by the lack of models that are predictive of physiological responses *in vivo* (Sontheimer-Phelps et al., 2019). Progressing *in vitro* studies to preclinical *in vivo* studies involves huge amounts of resources and costs. Many studies fail as responses observed *in vitro* do not reflect the *in vivo* outcome. Therefore efforts to more faithfully replicate structural and functional complexity of organs to enhance predictive powers of *in vitro* models are being pursued to address this issue (Huh, 2015). One way to recapitulate physiological complexity is to use organ-on-a-chip devices (OoC). These devices facilitate culture of cells, often of different cell types native to the organ, within controlled microphysiological environments, with vascular like perfusion (Probst et al., 2018). Perfusion of medium is facilitated by microfluidics, and in the case of modelling the lung, airflow can be applied to cells too.

One of the pioneer OoC models of the lung was the “human breathing lung on a chip” (Huh et al., 2010). This modelled the alveolar-capillary interface together with mechanical stretching of the cell layers to mimic breathing. It recapitulated inflammatory responses induced by TNF-alpha and bacterial infections similar to those seen in whole lung studies *in vivo*. OoC models have been applied to a lung cancer setting, specifically, Hassell et al. (2017) adapted the breathing lung on a chip model to study NSCLC. They discovered that the mechanical stretch motions associated with breathing impacted cancer cell growth and responses to drugs when compared to the static OoC model. Microfluidic models have been used to study metastasis of circulating tumour cells and screen compounds that may combat metastasis (Kong et al., 2016; Skardal et al., 2016).

Inhalation therapies

Inhalation therapies deliver drugs directly to the respiratory system via inhalers or nebulisers. These are currently used in a number of lung diseases such as asthma, COPD and cystic fibrosis. Smaller doses and reduced systemic side effects can be achieved due to localised drug delivery directly to the lungs (Ibrahim et al., 2015). Hiemstra et al. (2018) highlight the advantages that microfluidic models using epithelial cells at the ALI have over current *in vitro* models for inhalation toxicology. The toxicology models currently used often use inappropriate cell types and media-submerged cell cultures (Hiemstra et al., 2018). For example, two common cell lines used in inhalation toxicology screens are BEAS-2B and Calu-3 cell lines. The BEAS-2B are a virally immortilised bronchial epithelial cell line that do not have the capacity to differentiate, nor do they form tight junctions, a key characteristic for epithelial barrier integrity (Section 1.2.1). Calu-3 cells are derived from a lung ADC, and are therefore inappropriate as a toxicology screening tool as many cellular processes may be deregulated.

The concept of inhaled therapeutics for treating lung cancer has been explored in a number of studies summarised by Mangal et al. (2017). One clear advantage is the greater local dosage in the lungs than with parenteral administration. Lower systemic distribution and associated toxicity was also observed in studies delivering gemcitabine and doxorubicin via inhalation (Otterson et al., 2007; Lemarie et al., 2011). Although these compounds were tolerated in phase I studies, later studies were not reported. There is the potential to optimise this approach via sustained release preparations, for example, using nanoparticles loaded with a compound; and specific targeting of malignant cells to reduce the impact on healthy lung tissue (Gill et al., 2011).

Non-invasive biomarker discovery for lung cancer

It was first noted in the 1980s that there were several volatile organic compounds (VOCs) within the exhaled breath of lung cancer patients that were associated with the disease. Thus sparking interest in lung cancer specific biomarkers in exhaled breath (Gordon et al.,

1985). To date, no universal lung cancer biomarker has been implicated and then validated appropriately in a second population. However, it may be that a combination of various VOCs and changes in concentrations compared to healthy breath could provide a more accurate detection of lung cancer (Saalberg and Wolff, 2016). Owlstone Medical are running the LuCID study, an ongoing phase II study. The study, the largest of its kind, aims to analyze the breath of 4000 people suspected of having lung cancer to look for a "breath signature" that indicates the presence of the disease (ClinicalTrials.gov identifier NCT02612532).

The microfluidic and airflow devices presented here for modelling bronchial dysplasia could be further developed to enable screening approaches for inhalation chemoprevention therapies for SQC. The airflow aspect of the device provides scope for future studies to search for biomarker "breath" signatures specific to SOX2 deregulation in early SQC.

5.4.2 Construction and setup of microfluidic and airflow device suitable for the culture of bronchial epithelial cells

The microfluidic devices were built by Nicola Pellicciotta (Cavendish Laboratory, University of Cambridge, UK) based on previous microfluidic devices designs (Dennis Trieu, 2014). Briefly, polydimethylsiloxane (PDMS), a silicone based organic polymer was cast into a block with a channel 1 mm x 1 mm rectangular area and 12 mm long, with 2 x 2 mm holes punched through the PDMS block at either end of the channel. Using PDMS prepolymer as a glue, the PDMS block with moulded channel was fixed to the top of a transwell insert's porous membrane and allowed to cure. Tubing was inserted into the holes at each end of the channel to facilitate airflow across the top of the membrane, as well as media containing cells when seeding. Complete devices were sterilised under UV for 30 minutes. Device setup for airflow applications is shown in Figure 5.7, this setup can be modified to a microfluidic device with the addition of tubing and pump to the bottom chamber of the transwell. Here medium is constantly pumped in to the bottom chamber of the transwell and waste medium collected in a separate chamber. PDMS has been used for a number of years for microfluidic and airflow devices due to its properties in gas

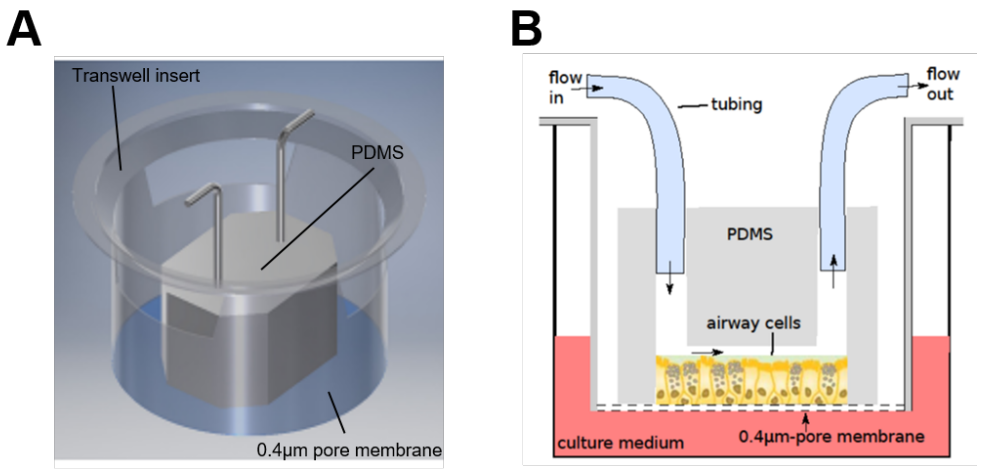

Figure 5.7: Illustrations outlining construction and setup of the airflow device. **A.** Illustration showing the PDMS block (containing the culture channel) fixed to the top of the porous membrane within a transwell insert. Tubing emerging from the PDMS block allows cells to be seeded into the channel and airflow to be applied. **B.** Cross section of (A) showing the channel within the PDMS block where cells are seeded on top of the porous membrane. *Illustrations provided by Nicola Pellicciotta*.

permeability, optical transparency, flexibility, and it has been shown to be able to support long term cultures of many cell types (Tourovskaia et al., 2005; Benam et al., 2015).

5.4.3 Deregulation of SOX2 in the microfluidic/airflow device drives a dysplastic phenotype

The microfluidic/airflow devices seen in Figure 5.7 had been demonstrated for use in differentiation studies using primary mouse bronchial epithelial cells at the Cavendish Laboratory. Cell number seeding densities, washes while establishing the ALI, doxycycline dosage and microscopy techniques for human KT-derived cells were all optimised (data not shown).

These pilot experiments were performed to establish whether KTshP53iSOX2 cells could recreate the dysplastic phenotype in the microfluidic/airflow device. This protocol could then be utilised in further experiments to investigate novel biomarkers or test nebulised drugs discussed in the project introduction (Section 5.4.1). First it was required to establish the culture conditions and replicate SOX2-driven phenotype, therefore the following pilot experiments did not have microfluidics or airflow applied.

Using phase-contrast microscopy to view cells maintained at the ALI was not possible, cells could not be seen clearly and shadows were cast across much of the channel (Figure 5.8A). This was only an issue when cells were at the ALI, submerged cells in the channel could be imaged via phase-contrast microscopy. The ALI was is a vital aspect of modelling the bronchial epithelium and could not be compromised for the sake of imaging. Therefore high quality phase-contrast images were not achievable when cells were at the ALI in PDMS channels.

However, using fluorescent imaging to visualise the cells at ALI within the channel avoided the issues associated with phase-contrast imaging. Qualitative changes in phenotype were monitored via fluorescent GFP imaging in KTshP53iSOX2 cells (due to constitutively expressed shP53-GFP construct) when SOX2 was induced with doxycycline (Figure 5.8B, C). Clear phenotypic differences were observed within 6 days of SOX2 induction. Disorganisation and expansive outgrowths across the epithelium were seen via GFP fluorescence similar to phenotypes seen in the OTC model.

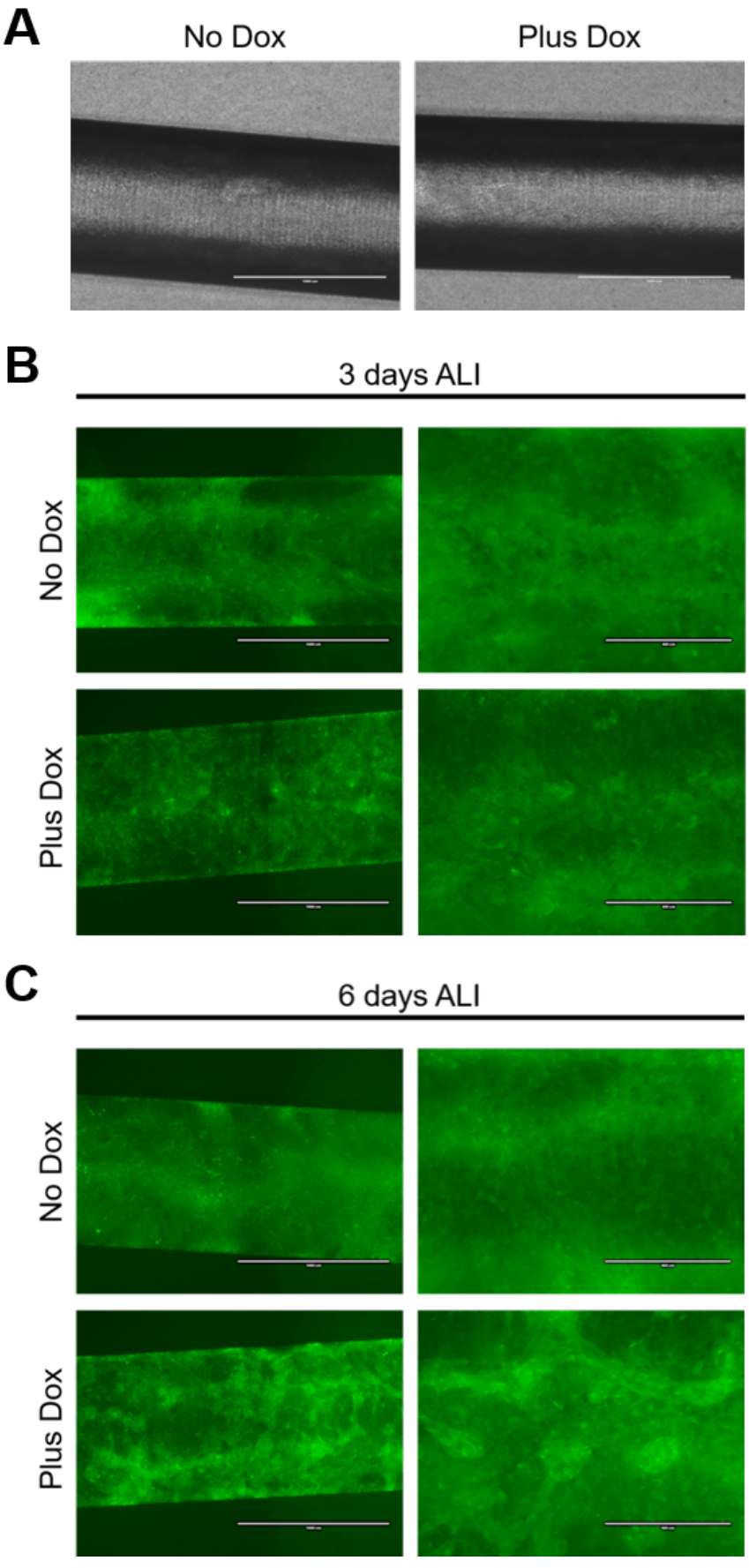
A
No Dox
Plus Dox
B
3 days ALI
No Dox
Plus Dox
C
6 days ALI
No Dox
Plus Dox

Figure 5.8: Towards a microfluidic and airflow model of bronchial dysplasia
Membranes in the microfluidic/airflow devices were coated with rat tail collagen I at 300 μg/mL overnight at 37°C. KTshP53iSOX2 cells were seeded at 8 x 10^5 cells/100 μL in cKSFM, with cKSFM in the bottom of the transwell. Cells were allowed to attach overnight then washed gently with PBS to remove detached and dead cells from the channel. Cells at confluence were brought to ALI by removing all medium from the channel and replacing cKSFM in the bottom chamber only with Pneumacult complete ALI medium $\pm$0.5 μg/mL doxycycline. **A.** PDMS channels seeded with cells at the ALI. Visualisation using phase-contrast microscopy show poor optical qualities when cells maintained at ALI in the microfluidic devices. **B.** GFP fluorescent imaging of KTshP53iSOX2 cells maintained at ALI for 3 days. **C.** GFP fluorescent imaging of KTshP53iSOX2 cells maintained at ALI for 6 days. Disorganisation and expansive outgrowths across the epithelium with SOX2 induction. Scale bars in (A.) and (left GFP images) = 1000 μm. Scale bars (right GFP images) = 400 μm. Images are representative of 3 experimental repeats.

5.4.4 Discussion

In this collaboration it was demonstrated that SOX2 deregulation in KTshP53iSOX2 cells seeded onto collagen coated membranes within devices constructed for application of microfluidics/airflow drives a phenotype similar to the OTC model of bronchial dysplasia. It was possible to monitor phenotype using fluorescent imaging of GFP positive cells, but phase-contrast microscopy was rendered unsuitable due to poor optical qualities of the device. With the model producing a consistent phenotype future plans are to apply flow to both the basal channel (mimicking blood flow) and the air channel on the apical side of the transwells above the epithelial layer. A number of different kinds of experiments could be contemplated with the novel aspects added to the existing model, examples follow.

Since completion of this work in the lab, a collaboration with Owlstone Medical has been established to analyse VOCs from the air flow. Pilot experiments are commencing to establish the scale of the model required to produce sufficient VOCs for detection in Owlstone's current detector platforms. There are a number of processes to optimise, including an assessment of the number of cells required to produce signals high enough for detection above background VOC signals from the medium in the system. The sample volume, airflow rate and sample collection times will also need to be optimised for greatest detection sensitivity. Once this process is optimised, experiments are planned to investigate

whether a specific VOC signature is present as a result of SOX2 deregulation, which could then be applied to a diagnostic tool for early SQC.

With regard to the chemoprevention of lung cancer, therapies that could be administered via inhalation are attractive. A successful chemoprevention strategy would ideally target a large number of people at high risk for lung cancer with an effective compound delivered locally to the lung, without any local or systemic side effects. This treatment would need to be affordable too, as a large number of patients would be targeted. Although the microfluidic/airflow system presented here would not be suitable for high-throughput screening of nebulised compounds for inhalation chemoprevention therapies, it could be used as a preclinical model for lead candidate compounds before validation in animal models. That is assuming that the airflow aspect previously demonstrated could be successfully adapted for the administration of nebulised test compounds.

Further plans for utilising the microfluidic aspect of this model involve sampling the medium flowing from the system for biomarkers. Liquid biopsy biomarker research has increased in the last decade with improvements to sequencing technologies. Bracht et al. (2018) review 4 liquid biosources, tumour-educated platelets (TEPs), cell-free DNA (cfDNA), circulating tumour cells (CTCs) and extracellular vesicles (EVs). Currently liquid biopsies are not sufficient to detect early stage disease, but do offer alternatives for monitoring disease progression and acquired resistance following treatment that is more sensitive than current radiography monitoring techniques. Early detection of lung cancer has been proven in a number of CT screening trials, however, as discussed in previous sections the successful implementation of these require a huge amount of investment and patient participation (section 1.6.3). Using liquid biomarkers for early detection has the same limitations, as well as currently lacking the same efficiency and specificity for detecting early disease as CT screening. Clearly, further research is required for more effective early stage disease biomarkers.

In the microfluidic model presented, the medium could be sampled in timecourse experiments following SOX2 deregulation to investigate whether a specific biomarker signature is present as a result of SOX2 deregulation. However, with the degree of efficacy of CT screening as an early detection tool for lung cancer, the bar for the ability of liquid biopsies

to improve on this has been raised.

The microfluidic/airflow model has the potential to be developed further with the addition of multiple cell types to increase complexity of the model, to recapitulate the local tissue microenvironment more faithfully, and to answer a range of biological questions. Cells types could be marked with different fluorescent proteins for imaging the devices and interactions between multiple cell types in a 3D environment. Cell migration along the device channels could be investigated using epithelial cells with particular reporter colours and genotypes. Fibroblasts and cancer-associated fibroblasts (CAFs) could be added to the model, CAFs have shown to play an important role in cancer progression in squamous carcinomas of the lung and esophagus (Ha et al., 2014; Yurugi et al., 2017). Further understanding of the biological processes behind enhanced disease progression and poor prognosis with CAF positive disease is required. The addition of endothelial cells on the underside of the channel exposed to the medium would further recapitulate the *in vivo* environment and could provide a model to investigate angiogenesis in SQC. Cavarga et al. (2009) report increased microvessel density as an early event in the pathogenesis of SQC. Further, SQC biopsies showed a 25% increase in angiogenic signaling, via hypoxia-inducible factor 1 alpha (HIF-1α) expression, than ADC samples and 40% more than SCLC samples (Karetsi et al., 2012).

This project has demonstrated further adaptation of the OTC model to microfluidic and airflow model that may have application in liquid/breath biomarker discovery, therapeutic screening and complex cellular modelling of the bronchial epithelium in early SQC.

Chapter 6

Final Remarks

Squamous cell lung cancer has a dismal outlook from diagnosis. As early stage disease is often asymptomatic, diagnosis is commonly made when tumours are advanced, leaving limited treatment options. The challenge of improving the outcome of these patients can be addressed using a combination of better targeted therapies, earlier detection and chemoprevention strategies. Advancements in disease modelling is required to further our understanding of the molecular pathogenesis of SQC and develop more appropriate intervention strategies.

I have used a novel SOX2-driven OTC model that recapitulates early, preinvasive human SQC, demonstrating the model's suitability for phenotypic screening of compounds for chemoprevention strategies. I identified a vulnerability to AKT inhibition in both primary and secondary chemoprevention assays. Further investigations using compounds with varying potencies to the 3 AKT isoforms suggested there may be an isoform vulnerability in SOX2-driven disease, sparking more detailed investigations for AKT isoform roles in SQC.

Genetic studies using CRISPR-mediated gene knockouts and RNAi-mediated gene knockdown showed a redundancy for AKT2 in the SOX2-driven OTC model and SOX2-amplified squamous cell lines. Dysplastic phenotype and proliferation were unaffected in both knockout and knockdown experiments.

AKT1 and AKT3 knockout in the immortalised hBECs severely impacted the growth of cells, but knockdown approaches in the OTC model gave contrasting results. AKT1 knockdown did not impact the SOX2-driven phenotype, but AKT3 knockdown significantly reduced the SOX2-driven phenotypic outcome in the OTC model. AKT1 and AKT3 knockdown in SOX2-amplified squamous cell lines significantly reduced cell population expansion, along with pilot data suggesting that AKT3, not AKT1, knockdown in confluent SOX2-amplified cell cultures induced death.

AKT3 emerged as a potential therapeutic target in SOX2 positive squamous disease. Clinical samples showed that AKT3 was a plausible target in SOX2 positive SQC. SOX2 and AKT3 transcript levels showed significant positive correlation in TCGA data and AKT3 protein expression was identified in SOX2 positive high grade bronchial dysplasia biopsies. I have demonstrated the use of the OTC model for screening small molecule compounds

for the chemoprevention of SOX2-driven SQC. I have successfully validated findings from the compound screens, demonstrating the OTC model can be used for CRISPR gene knockout experiments and inducible gene knockdown experiments using RNAi. Cell line studies complimented findings from the OTC model.

I have identified a plausible therapeutic target in SQC, that has previously not been demonstrated in this disease setting. There are currently no compounds specific to this target, but the advantages of isoform specific AKT inhibition are attractive. It would offer the opportunity of less toxicity, enabling the other 2 AKT isoforms to function in normal tissues. Hypothetically, less toxicity than pan-isoform inhibitors may lend itself suitability as a chemopreventative agent, as well as in more advanced disease.

In addition to the main body of work, I have established a collaboration that aims to further develop the OTC model with the hope of detecting VOCs and establishing whether a specific VOC signature may be present with SOX2 deregulation. This may offer hope for one day establishing a breath test that could detect lung cancer earlier and be treated sooner. Together, I hope that this research has contributed, no matter how small, to our knowledge of lung cancer, and takes us a step closer to improved therapies, and ultimately, fewer deaths from lung cancers.

Chapter 7

Appendices

Table 7.1: RNA-Sequencing data showing the top 50 genes differentially expressed upon SOX2 activation for 4 days in the OTC model compared to no SOX2 activation. FC = Fold Change, FDR = False Discovery Rate. Unpublished data generated by Dr L. Correia (University of Cambridge, UK).

Gene Name	logFC	P Value	FDR
SOX2	12.43474998	3.91E-197	5.54E-193
MAP2	4.41745144	4.12E-88	2.91E-84
SLC2A12	4.74929237	6.28E-83	2.96E-79
HEPHL1	5.926387173	2.11E-81	7.48E-78
DHRS9	6.160227894	2.57E-74	7.28E-71
CEMIP	3.80411784	2.70E-61	6.38E-58
FLRT2	2.938604851	2.95E-58	5.97E-55
SERPINI1	3.929101404	5.42E-58	9.60E-55
ABCB1	8.048695476	2.53E-52	3.98E-49
TLR4	5.714141412	6.69E-47	9.47E-44
KCNV1	9.677498046	1.76E-45	2.26E-42
MOXD1	4.355867644	5.15E-43	6.07E-40
RGMB	2.13093827	4.46E-42	4.85E-39
KCTD4	7.308040958	1.13E-38	1.13E-35
GSDMA	4.807498227	1.19E-38	1.13E-35
DACH1	6.62675858	1.57E-38	1.39E-35
TNFRSF21	-1.991623293	2.62E-38	2.18E-35
FAT4	3.94981751	5.05E-38	3.97E-35
PADI4	7.732954589	4.06E-37	3.02E-34
NPNT	3.235647381	7.07E-37	5.01E-34
PLEKHH2	3.447301527	1.10E-36	7.39E-34
PECAM1	6.428616831	2.08E-36	1.34E-33
TP53INP2	2.129825077	3.47E-36	2.13E-33
NOL4	7.055285103	4.08E-36	2.40E-33
EPB41L1	2.147425492	4.23E-36	2.40E-33
AF131217.1	6.310468415	5.45E-36	2.97E-33

MMP10	5.550979799	7.53E-35	3.95E-32
SIK2	1.807589085	3.55E-34	1.79E-31
TNFSF10	-1.988869183	1.84E-33	8.99E-31
ATRNL1	6.045965381	2.69E-33	1.27E-30
TRIM2	2.387559039	3.85E-33	1.76E-30
ABCA13	3.762941353	7.10E-33	3.14E-30
OSBPL11	1.911264215	1.96E-32	8.40E-30
TTLL7	2.333126321	1.24E-31	5.15E-29
RASL11A	4.321370302	4.26E-31	1.72E-28
MFAP5	5.403411023	6.77E-31	2.66E-28
TREM1	-2.591758206	8.00E-31	3.06E-28
HSPB1	-2.004046761	8.93E-31	3.33E-28
CALCRL	2.817156511	9.82E-31	3.56E-28
SLIT2	4.222249719	1.31E-30	4.65E-28
DSEL	2.816017916	1.88E-30	6.49E-28
SEMA3D	5.38596897	2.48E-30	8.37E-28
CALB1	6.353615285	5.19E-30	1.71E-27
FA2H	5.454387428	9.37E-30	3.01E-27
PDGFD	6.784067556	1.33E-29	4.19E-27
MMP7	5.712024463	1.84E-29	5.68E-27
MMP28	-1.644607493	2.02E-29	6.09E-27
SLITRK5	2.899489644	2.64E-29	7.80E-27
REPS2	2.485140365	3.26E-29	9.42E-27
CYP2S1	2.816664198	4.51E-29	1.28E-26

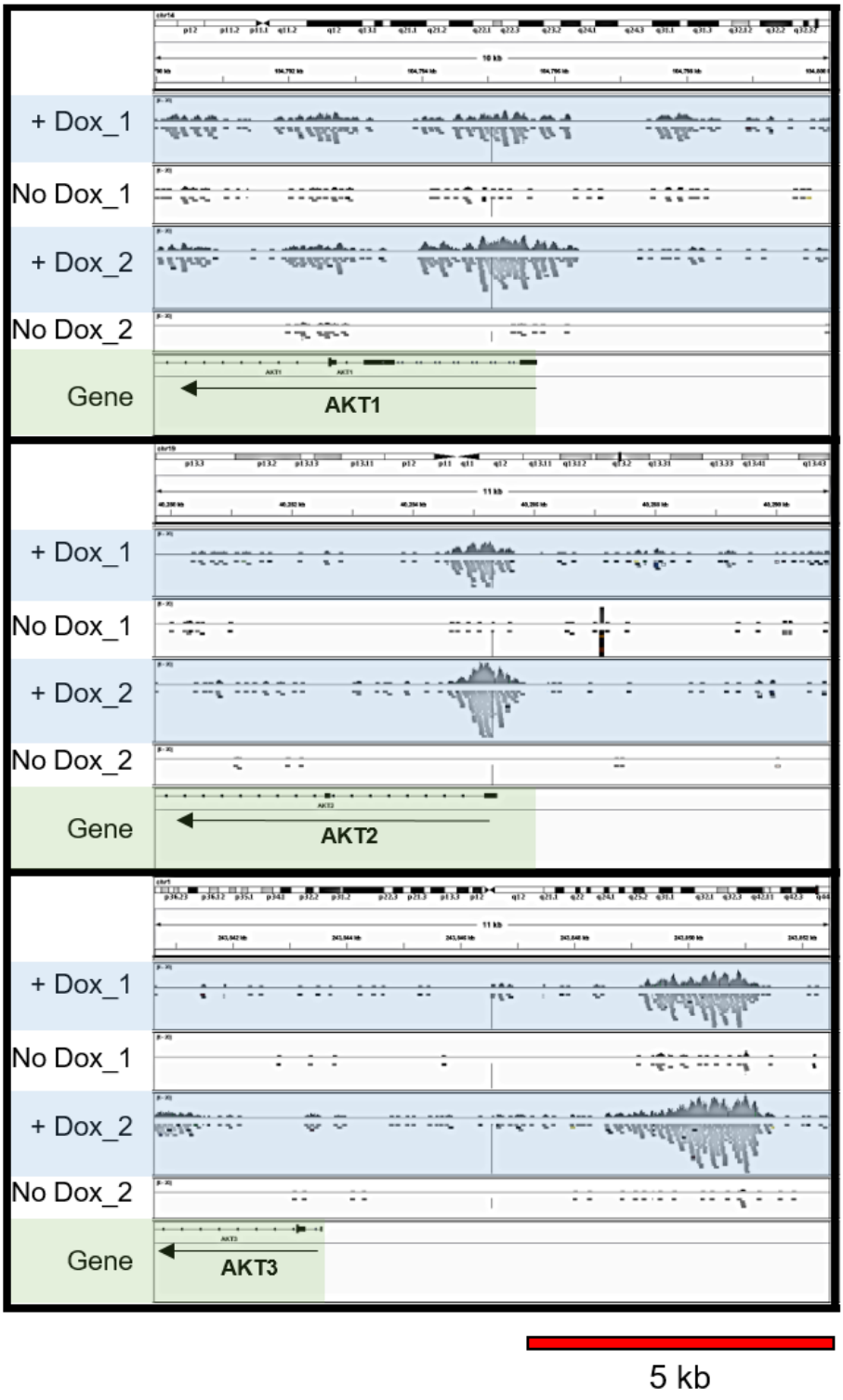
+ Dox_1
No Dox_1
+ Dox_2
No Dox_2
Gene
AKT1
+ Dox_1
No Dox_1
+ Dox_2
No Dox_2
Gene
AKT2
+ Dox_1
No Dox_1
+ Dox_2
No Dox_2
Gene
AKT3
5 kb

Figure 7.1: ChIP-Sequence analysis shows that SOX2 binds to AKT1 and AKT2 transcriptional start site, and upstream of the AKT3 transcriptional start site in the OTC.
ChIP-Sequence results for SOX2 pull down in the OTC model at 4 days ALI ±doxycycline. The genomic regions shown correspond to the transcriptional start sites of AKT1, AKT2 and AKT3 genes respectively. Peaks of enriched reads are seen in doxycycline treated OTCs where SOX2 is bound to the chromatin at the transcriptional start site of AKT1 and AKT2, and 6kb upstream of the AKT3 transcriptional start site. ChIP-sequence experiments performed by Dr L. Correia (University of Cambridge, UK) represent 3 biological experiments. ChIP-Sequence viewed and screenshots taken using Integrated Genomics Viewer, for each gene duplicate experimental chromatograms are shown per condition. Scale bar = 5 kb.

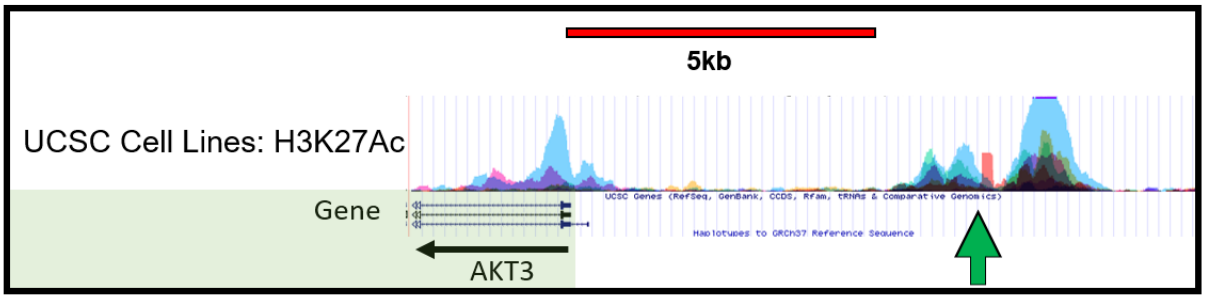

Figure 7.2: Active enhancer element H3K27Ac is present at the SOX2 bind site 6 kb upstream of *AKT3* transcriptional start site in 7 different cell lines reported on the UCSC genome browser.
ChIP-Seq results taken from the UCSC for H3K27Ac pull down in a panel of 7 cell lines. Peaks of enriched reads representing active enhancer element histone marker, H3K27Ac, from the 7 cell lines are overlayed on one chromatogram, each colour representing a different cell line. The green arrow shows where SOX2 bound upstream of the *AKT3* transcriptional start site (Figure 7.1). This shows that in a range of cell lines there is a H3K27Ac marker found in the same place, 6 kb upstream of the *AKT3* transcriptional start site, that SOX2 is found bound in the OTC model. ChIP-Seq viewed and screenshots taken using the UCSC genome browser (www.genome.ucsc.edu/).

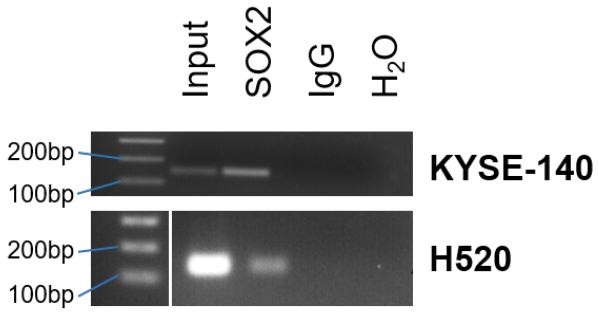

Figure 7.3: SOX2 binds 5'terminus of *AKT3* in SOX2 positive H520 and KYSE-140 cell lines.
ChIP-PCR using primers flanking the 5'TSS of *AKT3*. Samples generated from SOX2 pulldowns in SOX2 positive cell lines H520 and KYSE-140. Amplicons show that SOX2 binds 5'TSS of *AKT3*.

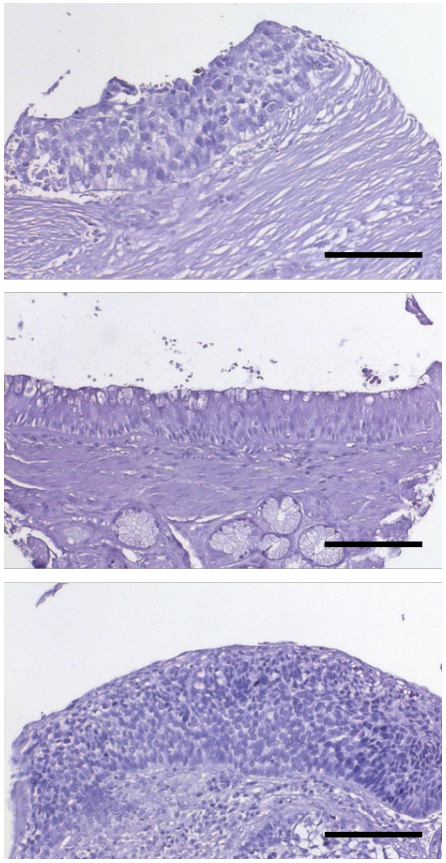

Figure 7.4: Human TMA IHC controls using secondary antibody only.
Secondary antibody only controls show that there was no non-specific binding of the secondary antibody when staining for AKT1, AKT2 and AKT3 on human TMA samples (Figure 4.3). The primary antibodies for AKT1, AKT2 and AKT3 staining were polyclonal so IgG controls could not be used. Scale bars = 200 μm.

References

F Vanden Abeele, Y Shuba, M Roudbaraki, L Lemonnier, K Vanoverberghe, P Mariot, R Skryma, and N Prevarskaya. Store-operated ca2+ channels in prostate cancer epithelial cells: function, regulation, and role in carcinogenesis. *Cell calcium*, 33(5-6): 357–373, 2003.

DR Aberle, AM Adams, CD Berg, WC Black, JD Clapp, RM Fagerstrom, et al. Reduced lung-cancer mortality with low-dose computed tomographic screening. *New England Journal of Medicine*, 365(5):395–409, 2011.

Charu Aggarwal, Mary Weber Redman, Primo Lara, Hossein Borghaei, Philip C. Hoffman, Jeffrey D. Bradley, et al. Phase II study of the FGFR inhibitor AZD4547 in previously treated patients with FGF pathway-activated stage IV squamous cell lung cancer (sqN-SCLC): LUNG-MAP sub-study SWOG S1400D. *Journal of Clinical Oncology*, 35(15): 9055–9055, 2017.

Ashour Ahmed, Zhen Lu, Nicholas B. Jennings, Dariush Etemadmoghadam, Luisa Capalbo, Rodrigo O. Jacamo, et al. SIK2 Is a Centrosome Kinase Required for Bipolar Mitotic Spindle Formation that Provides a Potential Target for Therapy in Ovarian Cancer. *Cancer Cell*, 18(2):109–121, 2010.

Michelle A Albert. Biomarkers and heart disease. *Journal of Clinical Sleep Medicine*, 7 (05):S9–S11, 2011.

Dario R Alessi, Mirjana Andjelkovic, Barry Caudwell, Peter Cron, Nick Morrice, P Cohen, and BA Hemmings. Mechanism of activation of protein kinase B by insulin and IGF-1. *The EMBO journal*, 15(23):6541–6551, 1996.

Dario R Alessi, Stephen R James, C Peter Downes, Andrew B Holmes, Piers RJ Gaffney, Colin B Reese, and Philip Cohen. Characterization of a 3-phosphoinositide-dependent protein kinase which phosphorylates and activates protein kinase bα. *Current biology*, 7(4):261–269, 1997.

Mirjana Andjelković, Teresa Jakubowicz, Peter Cron, Xiu-Fen Ming, Jeung-Whan Han, and Brian A Hemmings. Activation and phosphorylation of a pleckstrin homology domain containing protein kinase (rac-pk/pkb) promoted by serum and protein phosphatase inhibitors. *Proceedings of the National Academy of Sciences*, 93(12):5699–5704, 1996.

Guillaume Andrieu, Anna C Belkina, and Gerald V Denis. Clinical trials for BET inhibitors run ahead of the science. *Drug Discovery Today: Technologies*, 19:45–50, 2016.

Katrin Arnold, Abby Sarkar, Mary Anna Yram, Jose M Polo, Rod Bronson, Sumitra Sengupta, Marco Seandel, Niels Geijsen, and Konrad Hochedlinger. Sox2+ adult stem and progenitor cells are important for tissue regeneration and survival of mice. *Cell stem cell*, 9(4):317–329, 2011.

Irfan A Asangani, Vijaya L Dommeti, Xiaoju Wang, Rohit Malik, Marcin Cieslik, Rendong Yang, et al. Therapeutic targeting of BET bromodomain proteins in castration-resistant prostate cancer. *Nature*, 510(7504):278–282, 2014.

Ariel A Avilion, Silvia K Nicolis, Larysa H Pevny, Lidia Perez, Nigel Vivian, and Robin Lovell-Badge. Multipotent cell lineages in early mouse development depend on SOX2 function. *Genes & development*, 17(1):126–140, 2003.

Jordi Barretina, Giordano Caponigro, Nicolas Stransky, Kavitha Venkatesan, Adam A Margolin, Sungjoon Kim, Christopher J Wilson, Joseph Lehár, Gregory V Kryukov, Dmitriy Sonkin, et al. The cancer cell line encyclopedia enables predictive modelling of anticancer drug sensitivity. *Nature*, 483(7391):603, 2012.

Adam J Bass, Hideo Watanabe, Craig H Mermel, Soyoung Yu, Sven Perner, Roel G Verhaak, et al. SOX2 is an amplified lineage-survival oncogene in lung and esophageal squamous cell carcinomas. *Nature genetics*, 41(11):1238–42, 2009.

Panagiotis Baxevanos and Giannis Mountzios. Novel chemotherapy regimens for advanced lung cancer: have we reached a plateau? *Annals of translational medicine*, 6 (8), 2018.

Richard S Beard Jr, Brian A Hoettels, Jamie E Meegan, Travis S Wertz, Byeong J Cha, Xiaoyuan Yang, et al. AKT2 maintains brain endothelial claudin-5 expression and selective activation of IR/AKT2/FOXO1-signaling reverses barrier dysfunction. *Journal of Cerebral Blood Flow & Metabolism*, pages 1–18, 2018.

Kambez H Benam, Remi Villenave, Carolina Lucchesi, Antonio Varone, Cedric Hubeau, Hyun-Hee Lee, Stephen E Alves, Michael Salmon, Thomas C Ferrante, James C Weaver, et al. Small airway-on-a-chip enables analysis of human lung inflammation and drug responses in vitro. *Nature methods*, 13(2):151, 2015.

Vassiliki Benetou, Areti Lagiou, and Pagona Lagiou. Chemoprevention of cancer: current evidence and future prospects. *F1000Research*, 4(F1000 Faculty Rev), 2015.

Justin A Bishop, Julie Teruya-Feldstein, William H Westra, Giuseppe Pelosi, William D Travis, and Natasha Rekhtman. p40 (δnp63) is superior to p63 for the diagnosis of pulmonary squamous cell carcinoma. *Modern pathology*, 25(3):405, 2012.

Sean Blandin Knight, Phil A Crosbie, Haval Balata, Jakub Chudziak, Tracy Hussell, and Caroline Dive. Progress and prospects of early detection in lung cancer. *Open biology*, 7(9), 2017.

James E Boers, Anton W Ambergen, and Frederik BJM Thunnissen. Number and proliferation of basal and parabasal cells in normal human airway epithelium. *American journal of respiratory and critical care medicine*, 157(6):2000–2006, 1998.

Hélène Bon, Karan Wadhwa, Alexander Schreiner, Michelle Osborne, Thomas Carroll, Antonio Ramos-Montoya, et al. Salt-inducible kinase 2 regulates mitotic progression and transcription in prostate cancer. *Molecular cancer research : MCR*, 13(4):620–35, apr 2015.

Josephine Bowles, Goslik Schepers, and Peter Koopman. Phylogeny of the SOX family of developmental transcription factors based on sequence and structural indicators. *Developmental biology*, 227(2):239–255, 2000.

Laurie A Boyer, Tong Ihn Lee, Megan F Cole, Sarah E Johnstone, Stuart S Levine, Jacob P Zucker, et al. Core transcriptional regulatory circuitry in human embryonic stem cells. *Cell*, 122(6):947–956, 2005.

Lana Bozulic, Banu Surucu, Debby Hynx, and Brian A Hemmings. PKBα/akt1 acts downstream of DNA-PK in the DNA double-strand break response and promotes survival. *Molecular cell*, 30(2):203–213, 2008.

Jillian Wilhelmina Paulina Bracht, Clara Mayo-de-las Casas, Jordi Berenguer, Niki Karachaliou, and Rafael Rosell. The present and future of liquid biopsies in non-small cell lung cancer: combining four biosources for diagnosis, prognosis, prediction, and disease monitoring. *Current oncology reports*, 20(9):70, 2018.

Luka Brcic, Carol K Sherer, Yongli Shuai, Jason L Hornick, Lucian R Chirieac, and Sanja Dacic. Morphologic and clinicopathologic features of lung squamous cell carcinomas expressing SOX2. *American journal of clinical pathology*, 138(5):712–718, 2012.

Eva K. Brinkman, Tao Chen, Mario Amendola, and Bas Van Steensel. Easy quantitative assessment of genome editing by sequence trace decomposition. *Nucleic Acids Research*, 42(22), 2014.

Eliezer Calo and Joanna Wysocka. Modification of enhancer chromatin: what, how, and why? *Molecular cell*, 49(5):825–837, 2013.

John D Carpten, Andrew L Faber, Candice Horn, Gregory P Donoho, Stephen L Briggs, Christiane M Robbins, Galen Hostetter, Sophie Boguslawski, Tracy Y Moses, Stephanie Savage, et al. A transforming mutation in the pleckstrin homology domain of AKT1 in cancer. *Nature*, 448(7152):439, 2007.

I Cavarga, P Kocan, A Boor, J Belak, Z Kluchova, L Slavik, and R Tkacova. Immunohistochemical markers of proliferation and vascularisation in preneoplastic bronchial lesions and invasive non-small cell lung cancer. *Neoplasma*, 56(5):414–421, 2009.

Yuli C Chang, Kun-Tu Yeh, Ta-Chih Liu, and Jan-Gowth Chang. Molecular cytogenetic characterization of esophageal cancer detected by comparative genomic hybridization. *Journal of clinical laboratory analysis*, 24(3):167–174, 2010.

Bjoern Chapuy, Michael R McKeown, Charles Y Lin, Stefano Monti, Margaretha GM Roemer, Jun Qi, Peter B Rahl, Heather H Sun, Kelly T Yeda, John G Doench, et al. Discovery and characterization of super-enhancer-associated dependencies in diffuse large B cell lymphoma. *Cancer cell*, 24(6):777–790, 2013.

Bojiang Chen, Zhi Tan, Jun Gao, Wei Wu, Lida Liu, Wei Jin, et al. Hyperphosphorylation of ribosomal protein S6 predicts unfavorable clinical survival in non-small cell lung cancer. *Journal of experimental & clinical cancer research*, 34:126, 2015.

Hui Chen, Hudan Liu, and Guoliang Qing. Targeting oncogenic myc as a strategy for cancer treatment. *Signal transduction and targeted therapy*, 3(1):5, 2018a.

Shuang Chen, Andreas Giannakou, Sarah Wyman, Janet Gruzas, Jonathon Golas, Wenyan Zhong, et al. Cancer-associated fibroblasts suppress SOX2-induced dysplasia in a lung squamous cancer coculture. *Proceedings of the National Academy of Sciences*, 115(50):E11671–E11680, 2018b.

Si Chen, Xuefei Li, Dan Lu, Yingxi Xu, Wenjun Mou, Lina Wang, Yanan Chen, Yanhua Liu, Xiru Li, Lu-Yuan Li, et al. SOX2 regulates apoptosis through MAP4K4-survivin signaling pathway in human lung cancer cells. *Carcinogenesis*, 35(3):613–623, 2013.

Yupeng Chen, Lei Shi, Lirong Zhang, Ruifang Li, Jing Liang, Wenhua Yu, Luyang Sun, Xiaohan Yang, Yan Wang, Yu Zhang, et al. The molecular mechanism governing the oncogenic potential of SOX2 in breast cancer. *Journal of Biological Chemistry*, 283(26): 17969–17978, 2008.

Ting-Yuan David Cheng, Susanna M Cramb, Peter D Baade, Danny R Youlden, Chukwumere Nwogu, and Mary E Reid. The international epidemiology of lung cancer: latest trends, disparities, and tumor characteristics. *Journal of Thoracic Oncology*, 11 (10):1653–1671, 2016.

Rebecca Chin, Taku Toshida, Andriy Marusyk, and Alex Toker. Targeting AKT3 Signaling In Triple Negative Breast Cancer. *Cancer Research*, 74(3):964–973, 2014.

Rebecca Chin, Steven Balk, and Alex Toker. PTEN deficient tumours depend on AKT2 for maintenance and survival. *Cancer Discovery*, 4(8):942–955, 2015.

Han Cho, James Mu, Jason K Kim, Joanne L Thorvaldsen, E Bryan Chu, Marisa S Kaestner, Gerald I Shulman, and Morris J Birnbaum. Insulin resistance and a diabetes mellitus-like syndrome in mice lacking the protein kinase akt2 (PKBβ). *Science*, 292 (5522):1728–1731, 2001a.

Han Cho, Joanne L Thorvaldsen, Qingwei Chu, Fei Feng, and Morris J Birnbaum. AKT1/PKBα is required for normal growth but dispensable for maintenance of glucose homeostasis in mice. *Journal of Biological Chemistry*, 276(42):38349–38352, 2001b.

Melanie M Choe, Alice a Tomei, and Melody a Swartz. Physiological 3D tissue model of the airway wall and mucosa. *Nature protocols*, 1(1):357–362, 2006.

Yu-Ting Chou, Chih-Chan Lee, Shih-Hsin Hsiao, Sey-En Lin, Sheng-Chieh Lin, Chih-Hung Chung, et al. The emerging role of SOX2 in cell proliferation and survival and its crosstalk with oncogenic signaling in lung cancer. *Stem cells*, 31(12):2607–2619, 2013.

Lucia Correia, Jo-anne Johnson, Peter Mcerlean, Doris M Rassl, Emma L Rawlins, Trevor D Littlewood, Gerard I Evan, Frank M Mccaughan, et al. SOX2 Drives Bronchial

Dysplasia in a Novel Organotypic Model of Early Human Squamous Lung Cancer. *American Journal of Respiratory and Critical Care Medicine*, 195(11):1494–1508, 2017.

Darren AE Cross, Dario R Alessi, Philip Cohen, Mirjana Andjelkovich, and Brian A Hemmings. Inhibition of glycogen synthase kinase-3 by insulin mediated by protein kinase B. *Nature*, 378(6559):785, 1995.

CRUK. Lung cancer. `https://www.cancerresearchuk.org/`, 2018.

Charles S Dela Cruz, Lynn T Tanoue, and Richard A Matthay. Lung cancer: epidemiology, etiology, and prevention. *Clinics in chest medicine*, 32(4):605–644, 2011.

Ewa M Czekanska. Assessment of cell proliferation with resazurin-based fluorescent dye. In *Mammalian Cell Viability*, pages 27–32. Springer, 2011.

Avais M Daulat, François Bertucci, Stéphane Audebert, Arnauld Sergé, Pascal Finetti, Emmanuelle Josselin, Rémy Castellano, Daniel Birnbaum, Stéphane Angers, and Jean-Paul Borg. PRICKLE1 contributes to cancer cell dissemination through its interaction with mTORC2. *Developmental cell*, 37(4):311–325, 2016.

Morgan R. Davidson, Adi F. Gazdar, and Belinda E. Clarke. The pivotal role of pathology in the management of lung cancer. *Journal of Thoracic Disease*, 5(5), 2013.

Barry R Davies, Hannah Greenwood, Phillippa Dudley, Claire Crafter, De-hua Yu, Jingchuan Zhang, et al. Preclinical Pharmacology of AZD5363, an Inhibitor of AKT: Pharmacodynamics, Antitumor Activity and Correlation of Monotherapy Activity with Genetic Background. *Molecular Cancer Therapeutics*, 11:873–888, 2012.

Mark A Dawson, Tony Kouzarides, and Brian JP Huntly. Targeting epigenetic readers in cancer. *New England Journal of Medicine*, 367(7):647–657, 2012.

H De Koning, C Van Der Aalst, K Ten Haaf, and M Oudkerk. Effects of volume CT lung cancer screening: Mortality results of the NELSON randomised-controlled population based trial. *Journal of Thoracic Oncology*, 13(10):S185, 2018.

Damian G Deavall, Elizabeth A Martin, Judith M Horner, and Ruth Roberts. Drug-induced oxidative stress and toxicity. *Journal of toxicology*, 2012, 2012.

Alison P McGuigan Dennis Trieu, Thomas K Waddell. A microfluidic device to apply shear stresses to polarizing ciliated airway epithelium using air flow. *Biomicrofluidics*, 8 (6):064104, 2014.

Benjamin A Derman, Kathryn F Mileham, Philip D Bonomi, Marta Batus, and Mary J Fidler. Treatment of advanced squamous cell carcinoma of the lung: a review. *Translational lung cancer research*, 4(5):524–32, 2015.

G Di Maira, M Salvi, G Arrigoni, O Marin, S Sarno, F Brustolon, LA Pinna, and M Ruzzene. Protein kinase CK2 phosphorylates and upregulates AKT/PKB. *Cell death and differentiation*, 12(6):668, 2005.

David A Drew, Yin Cao, and Andrew T Chan. Aspirin and colorectal cancer: the promise of precision chemoprevention. *Nature Reviews Cancer*, 16(3):173, 2016.

Marc Dufour, Anne Dormond-Meuwly, Catherine Pythoud, Nicolas Demartines, and Olivier Dormond. Reactivation of AKT signaling following treatment of cancer cells with PI3K inhibitors attenuates their antitumor effects. *Biochemical and biophysical research communications*, 438(1):32–37, 2013.

A L Durham and I M Adcock. Lung Cancer The relationship between COPD and lung cancer. *Lung Cancer*, 90:121–127, 2015.

Rachael M Easton, Han Cho, Kristin Roovers, Diana W Shineman, Moshe Mizrahi, Matthias Szabolcs, et al. Role for AKT3/protein kinase Bγ in attainment of normal brain size. *Molecular and cellular biology*, 25(5):1869–1878, 2005.

Michael Elashoff, Kate Porta Smith, J Scott Ferguson, Ed Parsons, Nandita Mitra, Jerome Brody, Marc E Lenburg, and Avrum Spira. A Bronchial Genomic Classifier for the Diagnostic Evaluation of Lung Cancer. *N Engl J Med*, 373(3):243–251, 2015.

Majid Ezzati and Alan D Lopez. Estimates of global mortality attributable to smoking in 2000. *The lancet*, 362(9387):847–852, 2003.

Wen-Tsen Fang, Chi-Chen Fan, Shih-Miao Li, Te-Hsuan Jang, Hsiu-Ping Lin, Neng-Yao Shih, Chung-Hsing Chen, et al. Downregulation of a putative tumor suppressor BMP4 by SOX2 promotes growth of lung squamous cell carcinoma. *International journal of cancer*, 135(4):809–819, 2014.

Giustina Ferone, Ji-Ying Song, Kate Sutherland, Rajith Bhaskaran, Kim Monkhorst, Jan-Paul Lambooij, et al. SOX2 Is the Determining Oncogenic Switch in Promoting Lung Squamous Cell Carcinoma from Different Cells of Origin. *Cancer Cell*, 30(4):519–532, 2016.

Bernard Fisher, Joseph P Costantino, D Lawrence Wickerham, Carol K Redmond, Victor Vogel, André Robidoux, Nikolay Dimitrov, James Atkins, et al. Tamoxifen for prevention of breast cancer: report of the national surgical adjuvant breast and bowel project p-1 study. *JNCI: Journal of the National Cancer Institute*, 90(18):1371–1388, 1998.

Helen Fong, Kristi A Hohenstein, and Peter J Donovan. Regulation of self-renewal and pluripotency by SOX2 in human embryonic stem cells. *Stem cells*, 26(8):1931–1938, 2008.

Anne-Marie Fortier, Eric Asselin, and Monique Cadrin. Functional specificity of akt isoforms in cancer progression. *Biomolecular concepts*, 2(1-2):1–11, 2011.

Thomas F Franke, David R Kaplan, Lewis C Cantley, and Alex Toker. Direct regulation of the AKT proto-oncogene product by phosphatidylinositol-3, 4-bisphosphate. *Science*, 275(5300):665–668, 1997.

W a Franklin, a F Gazdar, J Haney, I I Wistuba, F G La rosa, T Kennedy, D M Ritchy, and Y E Miller. Widely dispersed p53 mutation in respiratory epithelium. *J. Clin. Invest.*, 100 (8):2133–2137, 1997.

Christopher A French, Isao Miyoshi, Ichiro Kubonishi, Holcombe E Grier, Antonio R Perez-Atayde, and Jonathan A Fletcher. BRD4-NUT fusion oncogene: a novel mechanism in aggressive carcinoma. *Cancer research*, 63(2):304–307, 2003.

Takuya Fukazawa, Minzhe Guo, Naomasa Ishida, Tomoki Yamatsuji, Munenori Takaoka, Etsuko Yokota, Minoru Haisa, Noriko Miyake, Tomoko Ikeda, Tatsuo Okui, et al. SOX2 suppresses CDKN1A to sustain growth of lung squamous cell carcinoma. *Scientific reports*, 6:20113, 2016.

David R Gandara, Peter S Hammerman, Martin L Sos, Primo N Lara Jr, and Fred R Hirsch. Squamous Cell Lung Cancer From Tumor Genomics to Cancer Therapeutics. *Clin Cancer Res*, 21(10):2236–2244, 2015.

Tianyan Gao, Frank Furnari, and Alexandra C Newton. PHLPP: a phosphatase that directly dephosphorylates akt, promotes apoptosis, and suppresses tumor growth. *Molecular cell*, 18(1):13–24, 2005.

Zhongyuan Gao, Ting Yuan, Xiao Zhou, Ping Ni, Geng Sun, Ping Li, Zhixiang Cheng, and Xuerong Wang. Targeting BRD4 proteins suppresses the growth of NSCLC through downregulation of eIF4E expression. *Cancer biology & therapy*, 19(5):407–415, 2018.

L A Garraway and W R Sellers. Lineage dependency and lineage-survival oncogenes in human cancer. *Nat Rev Cancer*, 6(8):593–602, 2006.

Yasuyuki Gen, Kohichiroh Yasui, Yoh Zen, Keika Zen, Osamu Dohi, Mio Endo, et al. SOX2 identified as a target gene for the amplification at 3q26 that is frequently detected in esophageal squamous cell carcinoma. *Cancer Genetics and Cytogenetics*, 202(2): 82–93, 2010a.

Yasuyuki Gen, Kohichiroh Yasui, Yoh Zen, Keika Zen, Osamu Dohi, Mio Endo, et al. SOX2 identified as a target gene for the amplification at 3q26 that is frequently detected in esophageal squamous cell carcinoma. *Cancer genetics and cytogenetics*, 202(2): 82–93, 2010b.

Yasuyuki Gen, Kohichiroh Yasui, Taichiro Nishikawa, and Toshikazu Yoshikawa. SOX2 promotes tumor growth of esophageal squamous cell carcinoma through the AKT/mammalian target of rapamycin complex 1 signaling pathway. *Cancer science*, 104(7):810–816, 2013.

Philip Jeremy George, Anindo K Banerjee, Catherine A Read, Caoihme O' sullivan, Mary Falzon, Francesco Pezzella, et al. Surveillance for the detection of early lung cancer in patients with bronchial dysplasia. *Thorax*, 62(1):43–50, 2007.

Kanwaldeep K Gill, Sami Nazzal, and Amal Kaddoumi. Paclitaxel loaded PEG5000–DSPE micelles as pulmonary delivery platform: Formulation characterization, tissue distribution, plasma pharmacokinetics, and toxicological evaluation. *European Journal of Pharmaceutics and Biopharmaceutics*, 79(2):276–284, 2011.

Sasha D Girouard, Alvaro C Laga, Martin C Mihm, Richard A Scolyer, John F Thompson, Qian Zhan, Hans R Widlund, Chung-Wei Lee, and George F Murphy. SOX2 contributes to melanoma cell invasion. *Laboratory investigation*, 92(3):362, 2012.

Briana D Ormsbee Golden, Erin L Wuebben, and Angie Rizzino. SOX2 expression is regulated by a negative feedback loop in embryonic stem cells that involves AKT signaling and FoxO1. *PloS one*, 8(10):e76345, 2013.

Cristina Gontan, Anne de Munck, Marcel Vermeij, Frank Grosveld, Dick Tibboel, and Robbert Rottier. Sox2 is important for two crucial processes in lung development: Branching morphogenesis and epithelial cell differentiation. *Developmental Biology*, 317(1):296–309, 2008.

Eva Gonzalez and Timothy E McGraw. The akt kinases: isoform specificity in metabolism and cancer. *Cell cycle*, 8(16):2502–2508, 2009.

SM Gordon, JP Szidon, BK Krotoszynski, RD Gibbons, and HJ O'Neill. Volatile organic compounds in exhaled air from patients with lung cancer. *Clinical chemistry*, 31(8): 1278–1282, 1985.

John Gubbay, Jérôme Collignon, Peter Koopman, Blanche Capel, Androulla Economou, Andrea Münsterberg, et al. A gene mapping to the sex-determining region of the mouse Y chromosome is a member of a novel family of embryonically expressed genes. *Nature*, 346(6281):245, 1990.

Muhammet F Gulen, Katarzyna Bulek, Hui Xiao, Ji Yu, Lillian Sun, Eleonore Beurel, et al. Inactivation of the enzyme GSK3α by the kinase IKKi promotes AKT-mTOR signaling pathway that mediates interleukin-1-induced th17 cell maintenance. *Immunity*, 37(5): 800–812, 2012.

Huifang Guo, Meng Gao, Yiling Lu, Jiyong Liang, Philip L Lorenzi, Shanshan Bai, et al. Coordinate phosphorylation of multiple residues on single AKT1 and AKT2 molecules. *Oncogene*, 33(26):3463, 2014.

A M Gustafson, R Soldi, C Anderlind, M B Scholand, J Qian, X Zhang, et al. Airway PI3K pathway activation is an early and reversible event in lung cancer development. *Sci Transl Med*, 2(26):26ra25, 2010.

Sang Yun Ha, So-Young Yeo, Yan-hiua Xuan, and Seok-Hyung Kim. The prognostic significance of cancer-associated fibroblasts in esophageal squamous cell carcinoma. *PloS one*, 9(6):e99955, 2014.

Koichi Hagiwara, Mary G McMenamin, Ko Miura, and Curtis C Harris. Mutational analysis of the p63/p73l/p51/p40/CUSP/KET gene in human cancer cell lines using intronic primers. *Cancer research*, 59(17):4165–4169, 1999.

Peter Hammerman, Michael Lawrence, Douglas Voet, Rui Jing, Kristian Cibulskis, Andrey Sivachenko, et al. Comprehensive genomic characterization of squamous cell lung cancers. *Nature*, 489(7417):519–525, 2012.

Wei Han, Joell J. Gills, Regan M. Memmott, Stephen Lam, and Phillip A. Dennis. The chemopreventive agent myoinositol inhibits Akt and extracellular signal-regulated kinase in bronchial lesions from heavy smokers. *Cancer Prevention Research*, 2(4): 370–376, 2009.

Masahito Hanada, Jianhua Feng, and Brian A Hemmings. Structure, regulation and function of PKB/AKT-a major therapeutic target. *Biochimica et Biophysica Acta (BBA)-Proteins and Proteomics*, 1697(1-2):3–16, 2004.

Douglas Hanahan and Robert A Weinberg. Hallmarks of cancer: the next generation. *Cell*, 144(5):646–74, 2011.

Neda Hashemi-Sadraei and Nasser Hanna. Targeting FGFR in squamous cell carcinoma of the lung. *Targeted oncology*, 12(6):741–755, 2017.

Bryan A Hassell, Girija Goyal, Esak Lee, Alexandra Sontheimer-Phelps, Oren Levy, Christopher S Chen, and Donald E Ingber. Human organ chip models recapitulate orthotopic lung cancer growth, therapeutic responses, and tumor dormancy in vitro. *Cell reports*, 21(2):508–516, 2017.

Hideko Hayashi, Yoshiki Tsuchiya, Kei Nakayama, Takayuki Satoh, and Eisuke Nishida. Down-regulation of the PI3-kinase/Akt pathway by ERK MAP kinase in growth factor signaling. *Genes to Cells*, 13(9):941–947, 2008.

Takuo Hayashi, Patrice Desmeules, Roger S Smith, and Alexander Drilon. RASA1 and NF1 are Preferentially Co-Mutated and Define A Distinct Genetic Subset of Smoking-Associated NonâĂŞSmall Cell Lung Carcinomas Sensitive to MEK Inhibition. *Clinical Cancer Research*, 24(6), 2018.

Roy S. Herbst, Mary W. Redman, Edward S. Kim, Thomas J. Semrad, Lyudmila Bazhenova, Gregory Masters, Oettel, et al. Cetuximab plus carboplatin and paclitaxel with or without bevacizumab versus carboplatin and paclitaxel with or without bevacizumab in advanced NSCLC (SWOG S0819): a randomised, phase 3 study. *The Lancet Oncology*, 19(1):101–114, 2018. ISSN 14745488.

Manuel Hidalgo, Elizabeth Bruckheimer, NV Rajeshkumar, Ignacio Garrido-Laguna, Elizabeth De Oliveira, Belen Rubio-Viqueira, et al. A pilot clinical study of treatment guided by personalized tumorgrafts in patients with advanced cancer. *Molecular cancer therapeutics*, 10(8):1311–1316, 2011.

Pieter S Hiemstra, Gwendolynn Grootaers, Anne M van der Does, Cyrille AM Krul, and Ingeborg M Kooter. Human lung epithelial cell cultures for analysis of inhaled toxicants: Lessons learned and future directions. *Toxicology in Vitro*, 47:137–146, 2018.

Denes Hnisz, Brian J Abraham, Tong Ihn Lee, Ashley Lau, Violaine Saint-André, Alla A Sigova, et al. Super-enhancers in the control of cell identity and disease. *Cell*, 155(4): 934–947, 2013.

Dongeun Huh. A human breathing lung-on-a-chip. *Annals of the American Thoracic Society*, 12(Supplement 1):S42–S44, 2015.

Dongeun Huh, Benjamin D Matthews, Akiko Mammoto, Martín Montoya-Zavala, Hong Yuan Hsin, and Donald E Ingber. Reconstituting organ-level lung functions on a chip. *Science*, 328(5986):1662–1668, 2010.

Thomas Hussenet, Soraya Dali, Julien Exinger, Ben Monga, Bernard Jost, Doulaye Dembel, et al. SOX2 is an oncogene activated by recurrent 3q26.3 amplifications in human lung squamous cell carcinomas. *PLoS ONE*, 5(1), 2010.

John N Hutchinson, Jing Jin, Robert D Cardiff, Jim R Woodgett, and William J Muller. Activation of akt1 (PKB-α) can accelerate erbB-2-mediated mammary tumorigenesis but suppresses tumor invasion. *Cancer research*, 64(9):3171–3178, 2004.

Hung Huynh, Khee Chee Soo, Pierce KH Chow, and Evelyn Tran. Targeted inhibition of the extracellular signal-regulated kinase kinase pathway with AZD6244 (ARRY142886) in the treatment of hepatocellular carcinoma. *Molecular cancer therapeutics*, 6(1):138–146, 2007.

Mariam Ibrahim, Rahul Verma, and Lucila Garcia-Contreras. Inhalation drug delivery devices: technology update. *Medical Devices (Auckland, NZ)*, 8:131, 2015.

Hanna Y Irie, Rachel V Pearline, Dorre Grueneberg, Maximilian Hsia, Preethi Ravichandran, Nayantara Kothari, et al. Distinct roles of akt1 and akt2 in regulating cell migration and epithelial–mesenchymal transition. *The Journal of cell biology*, 171(6):1023–1034, 2005.

Makiko Iwafuchi-Doi. The mechanistic basis for chromatin regulation by pioneer transcription factors. *Wiley Interdisciplinary Reviews: Systems Biology and Medicine*, 11 (1):e1427, 2019.

Stephen R James, C Peter Downes, Gigg Roy, Simon JA Grove, Andrew B Holmes, and Dario R Alessi. Specific binding of the akt-1 protein kinase to phosphatidylinositol 3, 4, 5-trisphosphate without subsequent activation. *Biochemical Journal*, 315(3):709–713, 1996.

Toni Jauset, Daniel Massó-Vallés, Sandra Martínez-Martín, Marie-Eve Beaulieu, Laia Foradada, Francesco Paolo Fiorentino, Jun Yokota, Bernard Haendler, Stephan Siegel, Jonathan R Whitfield, et al. BET inhibition is an effective approach against KRAS-driven PDAC and NSCLC. *Oncotarget*, 9(27):18734, 2018.

Prabhat Jha, Chinthanie Ramasundarahettige, Victoria Landsman, Brian Rostron, Michael Thun, Robert N Anderson, Tim McAfee, and Richard Peto. 21st-century hazards of smoking and benefits of cessation in the united states. *New England Journal of Medicine*, 368(4):341–350, 2013.

Xianpei Jia, Xuefei Li, Yingxi Xu, Shu Zhang, Wenjun Mou, Yanhua Liu, et al. SOX2 promotes tumorigenesis and increases the anti-apoptotic property of human prostate cancer cell. *Journal of molecular cell biology*, 3(4):230–238, 2011.

Verline Justilien, Michael Walsh, Syed Ali, and Alan Dields. The PRKCI and SOX2 Oncogenes are Co amplified and Cooperate to Activate Hedgehog Signaling in Lung Squamous Cell Carcinoma. *Cancer Cell*, 25(2):139–151, 2014.

Humam Kadara, Junya Fujimoto, Suk-Young Yoo, Yuho Maki, Adam C Gower, Mohamed Kabbout, et al. Transcriptomic architecture of the adjacent airway field cancerization

in non–small cell lung cancer. *JNCI: Journal of the National Cancer Institute*, 106(3), 2014.

Barbara B Kahn, Thierry Alquier, David Carling, and D Grahame Hardie. AMP-activated protein kinase: ancient energy gauge provides clues to modern understanding of metabolism. *Cell metabolism*, 1(1):15–25, 2005.

Yusuke Kamachi and Hisato Kondoh. Sox proteins: regulators of cell fate specification and differentiation. *Development*, 140(20):4129–4144, 2013.

Yusuke Kamachi, Masanori Uchikawa, and Hisato Kondoh. Pairing SOX off: with partners in the regulation of embryonic development. *Trends in Genetics*, 16(4):182–187, 2000.

Eleni Karetsi, Maria G Ioannou, Theodora Kerenidi, Markos Minas, Paschalis A Molyvdas, Konstantinos I Gourgoulianis, and Efrosyni Paraskeva. Differential expression of hypoxia-inducible factor 1α in non-small cell lung cancer and small cell lung cancer. *Clinics*, 67(12):1373–1378, 2012.

Pierre Edouard Kastner, Stéphane Le Calvé, Wuyin Zheng, Anne Casset, and Françoise Pons. A dynamic system for single and repeated exposure of airway epithelial cells to gaseous pollutants. *Toxicology in Vitro*, 27(2):632–640, 2013.

Robert L Keith and York E Miller. Lung cancer chemoprevention: current status and future prospects. *Nature reviews. Clinical oncology*, 10(6):334–43, 2013.

Bo Ram Kim, Emily Van de Laar, Michael Cabanero, Shintaro Tarumi, Stefan Hasenoeder, Dennis Wang, et al. SOX2 and PI3K Cooperate to Induce and Stabilize a Squamous-Committed Stem Cell Injury State during Lung Squamous Cell Carcinoma Pathogenesis. *PLoS Biology*, 14(11), 2016.

Seung-Wook Kim, Kyounga Cheon, Chang-Hoon Kim, and Ja Seok Koo. Proteomics-Based Identification of Proteins Secreted in Apical Surface Fluid of Squamous Metaplastic Human Tracheobronchial Epithelial Cells Cultured by Three-Dimensional Organotypic Air- Liquid Interface Method. *Cancer Research*, 67(14):6565–6573, 2007.

Jing Kong, Yong Luo, Dong Jin, Fan An, Wenyuan Zhang, Lilu Liu, Jiao Li, Shimeng Fang, Xiaojie Li, Xuesong Yang, et al. A novel microfluidic model can mimic organ-specific metastasis of circulating tumor cells. *Oncotarget*, 7(48):78421, 2016.

Janel L Kopp, Briana D Ormsbee, Michelle Desler, and Angie Rizzino. Small increases in the level of SOX2 trigger the differentiation of mouse embryonic stem cells. *Stem cells*, 26(4):903–911, 2008.

Sandra Koseoglu, Zhuomei Lu, Chandra Kumar, Paul Kirschmeier, and Jun Zou. AKT1, AKT2 and AKT3-dependent cell survival is cell line-specific and knockdown of all three isoforms selectively induces apoptosis in 20 human tumor cell lines. *Cancer biology & therapy*, 6(5):755–762, 2007.

Ira Kukic, Felix Rivera-Molina, and Derek Toomre. The IN/OUT assay: a new tool to study ciliogenesis. *Cilia*, 5(1):23, 2016.

Vinay Kumar, Abul K Abbas, Jon C Aster, Stanley Leonard Robbins, et al. *Robbins basic pathology*. Philadelphia, PA: Elsevier/Saunders„ 2013.

H Yi Kyung and Josh Lauring. Recurrent AKT mutations in human cancers: functional consequences and effects on drug sensitivity. *Oncotarget*, 7(4):4241, 2016.

Adam Lackey and Jessica S Donington. Surgical management of lung cancer. In *Seminars in interventional radiology*, volume 30, page 133. Thieme Medical Publishers, 2013.

Stephen Lam, Sumithra J Mandrekar, Yaron Gesthalter, Katie L Allen Ziegler, Drew K Seisler, David E Midthun, et al. A randomized phase IIb trial of myo-inositol in smokers with bronchial dysplasia. *Cancer Prevention Research*, 9:906–914, 2016.

Rebecca Lamb, Bela Ozsvari, Anthony Lisanti, Ubaldo E Martinez-Outschoorn, Federica Sotgia, Michael P Lisanti, et al. Antibiotics that target mitochondria effectively eradicate cancer stem cells, across multiple tumor types: treating cancer like an infectious disease. *Oncotarget*, 6(7):4569, 2015.

Janine M Lamonica, Wulan Deng, Stephan Kadauke, Amy E Campbell, Roland Gamsjaeger, Hongxin Wang, Yong Cheng, Andrew N Billin, Ross C Hardison, Joel P Mackay, et al. Bromodomain protein BRD3 associates with acetylated GATA1 to promote its chromatin occupancy at erythroid target genes. *Proceedings of the National Academy of Sciences*, 108(22):E159–E168, 2011.

Corey J Langer, Mary W Redman, James L Wade, Charu Aggarwal, Jeffrey D Bradley, Jeffrey Crawford, et al. SWOG S1400B (NCT02785913), a phase II study of GDC-0032 (Taselisib) for previously treated PI3K-positive patients with stage IV squamous cell lung cancer (lung-MAPsub-study). epub ahead of print. *Journal of Thoracic Oncology*, 2019.

J Jack Lee, Diane Liu, Jin Soo Lee, Jonathan M Kurie, Fadlo R Khuri, Heladio Ibarguen, Rodolfo C Morice, Garrett Walsh, Jae Y Ro, Anita Broxson, et al. Long-term impact of smoking on lung epithelial proliferation in current and former smokers. *Journal of the National Cancer Institute*, 93(14):1081–1088, 2001.

Jangson Lee, Seung Hee Ryu, Waun Ki Hong, and Ja Seok Koo. Prevention of Bronchial Hyperplasia by EGFR Pathway Inhibitors in an Organotypic Culture Model. *Cancer Prev Res (Phila)*, 4(8):1306–1315, 2011.

SH Lee, SY Oh, SI Do, HJ Lee, HJ Kang, YS Rho, WJ Bae, and YC Lim. SOX2 regulates self-renewal and tumorigenicity of stem-like cells of head and neck squamous cell carcinoma. *British journal of cancer*, 111(11):2122, 2014.

Etienne Lemarie, Laurent Vecellio, Jose Hureaux, Caroline Prunier, Chantal Valat, Daniel Grimbert, Michele Boidron-Celle, Bruno Giraudeau, Alain le Pape, Eric Pichon, et al. Aerosolized gemcitabine in patients with carcinoma of the lung: feasibility and safety study. *Journal of aerosol medicine and pulmonary drug delivery*, 24(6):261–270, 2011.

Hassan Lemjabbar-Alaoui, Omer UI Hassan, Yi-Wei Yang, and Petra Buchanan. Lung cancer: Biology and treatment options. *Biochimica et Biophysica Acta (BBA)-Reviews on Cancer*, 1856(2):189–210, 2015.

Josien Levenga, Helen Wong, Ryan A Milstead, Bailey N Keller, Lauren E LaPlante, and Charles A Hoeffer. AKT isoforms have distinct hippocampal expression and roles in synaptic plasticity. *Elife*, 6:e30640, 2017.

F Lin, P Lin, D Zhao, Y Chen, L Xiao, W Qin, et al. SOX2 targets cyclin E, p27 and survivin to regulate androgen-independent human prostate cancer cell proliferation and apoptosis. *Cell Proliferation*, 45(3):207–216, 2012.

Nicolle M. Linnerth-Petrik, Lisa A. Santry, James J. Petrik, and Sarah K. Wootton. Opposing functions of Akt isoforms in lung tumor initiation and progression. *PLoS ONE*, 9 (4), 2014.

Geng Liu, Timothy J McDonnell, Roberto Montes de Oca Luna, Mini Kapoor, Betsy Mims, Adel K El-Naggar, and Guillermina Lozano. High metastatic potential in mice inheriting a targeted p53 missense mutation. *Proceedings of the National Academy of Sciences*, 97(8):4174–4179, 2000.

Hong Liu, Derek C Radisky, Celeste M Nelson, Hui Zhang, Jimmie E Fata, Richard A Roth, and Mina J Bissell. Mechanism of AKT1 inhibition of breast cancer cell invasion reveals a protumorigenic role for TSC2. *Proceedings of the National Academy of Sciences*, 103 (11):4134–4139, 2006.

Jing Liu, Xiu Jun Zhao, Xiao Lin Zhang, Xiao Hua Wu, and Tai Ping Zhao. Knock-down Akt3 inhibits ovarian cancer cell growth and migration. *International journal of clinical experimental medicine*, 10(5):8566–8573, 2017.

Miao Lou, Li-na Zhang, Pei-gang Ji, Fu-qiang Feng, Jing-hui Liu, Chen Yang, Bao-fu Li, and Liang Wang. Quercetin nanoparticles induced autophagy and apoptosis through AKT / ERK / Caspase-3 signaling pathway in human neuroglioma cells : In vitro and in vivo. *Biomedicine et Pharmacotherapy*, 84:1–9, 2016.

Jakob Lovén, Heather A Hoke, Charles Y Lin, Ashley Lau, David A Orlando, Christopher R Vakoc, James E Bradner, Tong Ihn Lee, and Richard A Young. Selective inhibition of tumor oncogenes by disruption of super-enhancers. *Cell*, 153(2):320–334, 2013.

Yiling Lu, Melissa Muller, Debra Smith, Bhaskar Dutta, Kakajan Komurov, Sergio Iadevaia, et al. Kinome siRNA-phosphoproteomic screen identifies networks regulating AKT signaling. *Oncogene*, 30(45):4567, 2011.

Tomohiko Maehama and Jack E Dixon. The tumor suppressor, PTEN/MMAC1, dephosphorylates the lipid second messenger, phosphatidylinositol 3, 4, 5-trisphosphate. *Journal of Biological Chemistry*, 273(22):13375–13378, 1998.

Kiran Mahajan and Nupam Mahajan. PI3K-Independent AKT Activation in Cancers: A Treasure Trove for Novel Therapeutics. *Journal of cell physiology*, 227(9):3178–3184, 2012.

Rajneesh Malhotra, Nisha Kurian, Xiao-Hong Zhou, Fanyi Jiang, Susan Monkley, Amy DeMicco, Ib G Clausen, Göran Delgren, Goran Edenro, Miika J Ahdesmäki, et al. Altered regulation and expression of genes by BET family of proteins in COPD patients. *PloS one*, 12(3):e0173115, 2017.

Eusebio Manchado, Susann Weissmueller, John P. Morris, Chi Chao Chen, Ramona Wullenkord, Amaia Lujambio, et al. A combinatorial strategy for treating KRAS-mutant lung cancer. *Nature*, 534(7609):647–651, 2016.

Sharad Mangal, Wei Gao, Tonglei Li, and Qi Tony Zhou. Pulmonary delivery of nanoparticle chemotherapy for the treatment of lung cancers: challenges and opportunities. *Acta Pharmacologica Sinica*, 38(6):782, 2017.

Michelle L Manni, Sivanarayana Mandalapu, Andres Salmeron, Jose M Lora, Jay K Kolls, and John F Alcorn. Bromodomain and extra-terminal protein inhibition attenuates neutrophil-dominant allergic airway disease. *Scientific reports*, 7:43139, 2017.

Brendan D Manning and Lewis C Cantley. AKT/PKB signaling: navigating downstream. *Cell*, 129(7):1261–74, 2007.

Brendan D. Manning and Alex Toker. AKT/PKB signaling: Navigating the network. *Cell*, 169(3):381–405, 2017.

Li Mao, Jin Soo Lee, Jonathan M Kurie, You Hong Fan, Scott M Lippman, Anita Broxson, et al. Clonal genetic alterations in the lungs of current and former smokers. *Journal of the National Cancer Institute*, 89(12):857–862, 1997.

Melissa Marko, Alan R Dahl, Kory S Engelke, Michael E Placke, Anthony R Imondi, James L Mulshine, et al. Topical delivery of 13-cis-retinoic acid by inhalation upregulates expression of rodent lung but not liver retinoic acid receptors. *Clinical cancer research*, 6(9):3636–3645, 2000.

AM Martelli, PL Tazzari, G Tabellini, R Bortul, AM Billi, L Manzoli, A Ruggeri, R Conte, and L Cocco. A new selective akt pharmacological inhibitor reduces resistance to chemotherapeutic drugs, trail, all-trans-retinoic acid, and ionizing radiation of human leukemia cells. *Leukemia*, 17:1794–1805, 2003.

Iñigo Martincorena and Peter J Campbell. Somatic mutation in cancer and normal cells. *Science*, 349(6255):1483–1489, 2015.

Nadine Martinet, François Alla, Guillaume Farré, Taonfika Labib, Hèlène Drouot, Reynald Vidili, et al. Retinoic acid receptor and retinoid X receptor alterations in lung cancer precursor lesions. *Cancer Research*, 60(11):2869–2875, 2000.

Pierre P Massion, Peter M Taflan, SM Jamshedur Rahman, Pinar Yildiz, Yu Shyr, Mary E Edgerton, Matthew D Westfall, John R Roberts, Jennifer A Pietenpol, David P Carbone, et al. Significance of p63 amplification and overexpression in lung cancer development and prognosis. *Cancer research*, 63(21):7113–7121, 2003a.

Pierre P Massion, Peter M Taflan, SM Jamshedur Rahman, Pinar Yildiz, Yu Shyr, Mary E Edgerton, et al. Significance of p63 amplification and overexpression in lung cancer development and prognosis. *Cancer Research*, 63(21):7113–7121, 2003b.

Shinji Masui, Yuhki Nakatake, Yayoi Toyooka, Daisuke Shimosato, Rika Yagi, Kazue Takahashi, et al. Pluripotency governed by sox2 via regulation of oct3/4 expression in mouse embryonic stem cells. *Nature cell biology*, 9(6):625, 2007.

Frank McCaughan, Jessica C.M. Pole, Alan T. Bankier, Bernard A. Konfortov, Bernadette Carroll, Mary Falzon, Terence H. Rabbitts, et al. Progressive 3q amplification consistently targets SOX2 in preinvasive squamous lung cancer. *American Journal of Respiratory and Critical Care Medicine*, 182(1):83–91, 2010.

Frank McCaughan, Christodoulos P Pipinikas, Sam M Janes, P Jeremy George, Pamela H Rabbitts, and Paul H Dear. Genomic evidence of pre-invasive clonal expansion, dispersal and progression in bronchial dysplasia. *The Journal of Pathology*, 224(2):153–9, 2011.

Katherine B Mccauley, Finn Hawkins, Maria Serra, Dylan C Thomas, Anjali Jacob, and Darrell N Kotton. Efficient Derivation of Functional Human Airway Epithelium from Pluripotent Stem Cells via Temporal Regulation of Wnt Signaling. *Cell Stem Cell*, 20: 844–857, 2017.

Regan Memmott and Dennis Philip. The role of the Akt/mTOR pathway in tobacco-carcinogen induced lung tumorigenesis. *Clin Cancer Res*, 16(1):4–10, 2010. ISSN 15378276.

Michelle Mendoza, Emrah Er, and John Blenis. The Ras-ERK and PI3K-mTOR Pathways: Cross-talk and Compensation. *Trends Biochem Sci*, 36(6):320–328, 2011.

Catia Mio, Stefania Bulotta, Diego Russo, and Giuseppe Damante. Reading cancer: Chromatin readers as druggable targets for cancer treatment. *Cancers*, 11(1):61, 2019.

Fabrizio Miranda, David Mannion, Shujuan Liu, Yiyan Zheng, LingegowdaÂăS. Mangala, Clara Redondo, et al. Salt-Inducible Kinase 2 Couples Ovarian Cancer Cell Metabolism with Survival at the Adipocyte-Rich Metastatic Niche. *Cancer Cell*, pages 273–289, 2016.

Sonali Mohanty and Lei Xu. Experimental metastasis assay. *Journal of visualized experiments: JoVE*, (42), 2010.

Gurkan Mollaoglu, Alex Jones, Sarah J Wait, Anandaroop Mukhopadhyay, Sangmin Jeong, Rahul Arya, et al. The lineage-defining transcription factors SOX2 and NKX2-1 determine lung cancer cell fate and shape the tumor immune microenvironment. *Immunity*, 49(4):764–779, 2018.

Massimo Moro, Giulia Bertolini, Monica Tortoreto, Ugo Pastorino, Gabriella Sozzi, and Luca Roz. Patient-derived xenografts of non small cell lung cancer: resurgence of an old model for investigation of modern concepts of tailored therapy and cancer stem cells. *BioMed Research International*, 2012, 2012.

Hongmei Mou, Vladimir Vinarsky, Purushothama Rao Tata, Soon H Choi, Adrianne K Crooke, Bing Zhang, et al. Dual SMAD signaling inhibition enables long-term expansion of diverse epithelial basal cells. *Cell Stem Cell*, 19(2):217–231, 2016.

Anandaroop Mukhopadhyay, Kristofer C. Berrett, Ushma Kc, Phillip M. Clair, Benjamin L. Pop, and Trudy G. Oliver. Sox2 cooperates with lkb1 loss in a mouse model of squamous cell lung cancer. *Cell Reports*, 8(1):40–49, 2014.

James T Neal, Xingnan Li, Junjie Zhu, Valeria Giangarra, Caitlin L Grzeskowiak, Jihang Ju, et al. Organoid modeling of the tumor immune microenvironment. *Cell*, 175(7): 1972–1988, 2018.

Timothy Neuberger, Bill Burton, Heather Clark, and Fredrick Van Goor. Use of primary cultures of human bronchial epithelial cells isolated from cystic fibrosis patients for the pre-clinical testing of CFTR modulators. In *Cystic Fibrosis*, pages 39–54. Springer, 2011.

Guidance NICE. NICE guidance. `https://www.nice.org.uk/guidance/`, 2019.

Ningning Niu, Rui Shao, Guang Yan, and Weiguo Zou. Bromodomain and extra-terminal (BET) protein inhibitors suppress chondrocyte differentiation and restrain bone growth. *Journal of Biological Chemistry*, 291(52):26647–26657, 2016.

Daniel Novak, Laura Hüser, Jonathan J Elton, Viktor Umansky, Peter Altevogt, and Jochen Utikal. SOX2 in development and cancer biology. In *Seminars in cancer biology*. Elsevier, 2019.

Kenneth P Olive, David A Tuveson, Zachary C Ruhe, Bob Yin, Roderick T Bronson, Denise Crowley, and Tyler Jacks. Mutant p53 gain of function in two mouse models of li-fraumeni syndrome. *Cell*, 119(6):847–860, 2004.

Gregory A Otterson, Miguel A Villalona-Calero, Sunil Sharma, Mark G Kris, Anthony Imondi, Mirjam Gerber, et al. Phase I study of inhaled doxorubicin for patients with metastatic tumors to the lungs. *Clinical Cancer Research*, 13(4):1246–1252, 2007.

Kashyap Patel, Marc Foretz, Allison Marion, David G Campbell, Robert Gourlay, Nadia Boudaba, Emilie Tournier, Paul Titchenell, Mark Peggie, Maria Deak, et al. The lkb1-salt-inducible kinase pathway functions as a key gluconeogenic suppressor in the liver. *Nature communications*, 5:4535, 2014.

Giuseppe Pelosi, Giulio Rossi, Fabrizio Bianchi, Patrick Maisonneuve, Domenico Galetta, Angelica Sonzogni, et al. Immunhistochemistry by means of widely agreed-upon markers (cytokeratins 5/6 and 7, p63, thyroid transcription factor-1, and vimentin) on small biopsies of non-small cell lung cancer effectively parallels the corresponding profiling and eventual diagnoses on surgical specimens. *Journal of Thoracic Oncology*, 6(6): 1039–1049, 2011.

Beate Pesch, Benjamin Kendzia, Per Gustavsson, Karl-Heinz Jöckel, Georg Johnen, Hermann Pohlabeln, et al. Cigarette smoking and lung cancer relative risk estimates for the major histological types from a pooled analysis of case control studies. *International journal of cancer*, 131(5):1210–1219, 2012.

Solange Peters, Rolf A Stahel, Urania Dafni, Santiago Ponce Aix, Bartomeu Massutí, Oliver Gautschi, et al. Randomized phase III trial of erlotinib versus docetaxel in patients with advanced squamous cell non–small cell lung cancer failing first-line platinum-based doublet chemotherapy stratified by veristrat good versus veristrat poor. the european thoracic oncology platform (ETOP) EMPHASIS-lung trial. *Journal of Thoracic Oncology*, 12(4):752–762, 2017.

Solange Peters, Keith M Kerr, and Rolf Stahel. PD1 blockade in advanced NSCLC a focus on pembrolizumab. *Cancer treatment reviews*, 62:39–49, 2018.

Richard Peto, Sarah Darby, Harz Deo, Paul Silcocks, Elise Whitley, and Richard Doll. Smoking, smoking cessation, and lung cancer in the uk since 1950: combination of national statistics with two case-control studies. *BMJ*, 321:323–329, 2000.

Thuy L Phung, Wa Du, Qi Xue, Sriram Ayyaswamy, Damien Gerald, Zeus Antonello, et al. AKT1 and AKT3 exert opposing roles in the regulation of vascular tumor growth. *Cancer research*, 75(1):40–50, 2015.

Kurt G Pike, Karine Malagu, Marc G Hummersone, Keith A Menear, Heather ME Duggan, Sylvie Gomez, et al. Optimization of potent and selective dual mTORC1 and mTORC2 inhibitors: the discovery of AZD8055 and AZD2014. *Bioorganic & medicinal chemistry letters*, 23(5):1212–1216, 2013.

Charles N Prabhakar. Epidermal growth factor receptor in NSCLC. *Translational lung cancer research*, 4(2):110, 2015.

Christopher Probst, Stefan Schneider, and Peter Loskill. High-throughput organ-on-a-chip systems: Current status and remaining challenges. *Current Opinion in Biomedical Engineering*, 2018.

Jianwen Que, Xiaoyan Luo, Robert J Schwartz, and Brigid LM Hogan. Multiple roles for sox2 in the developing and adult mouse trachea. *Development*, 136(11):1899–1907, 2009.

Raju VS Rajala and Ammaji Rajala. Redundant and nonredundant functions of akt isoforms in the retina. In *Retinal Degenerative Diseases*, pages 585–591. Springer, 2018.

Minerva Ramos-Gomez, Mi-Kyoung Kwak, Patrick M Dolan, Ken Itoh, Masayuki Yamamoto, Paul Talalay, and Thomas W Kensler. Sensitivity to carcinogenesis is increased and chemoprotective efficacy of enzyme inducers is lost in nrf2 transcription factor-deficient mice. *Proceedings of the National Academy of Sciences*, 98(6):3410–3415, 2001.

Zhen-Hu Ren, Chen-Ping Zhang, and Tong Ji. Expression of SOX2 in oral squamous cell carcinoma and the association with lymph node metastasis. *Oncology letters*, 11(3): 1973–1979, 2016.

Markus J Riemenschneider, Rebecca A Betensky, Saskia M Pasedag, and David N Louis. AKT activation in human glioblastomas enhances proliferation via TSC2 and S6 kinase signaling. *Cancer research*, 66(11):5618–5623, 2006.

James W Rocco, Chee-Onn Leong, Nicolas Kuperwasser, Maurice Phillip DeYoung, and Leif W Ellisen. p63 mediates survival in squamous cell carcinoma by suppression of p73-dependent apoptosis. *Cancer cell*, 9(1):45–56, 2006.

Jason R Rock, Mark W Onaitis, Emma L Rawlins, Yun Lu, Cheryl P Clark, Yan Xue, Scott H Randell, and Brigid L M Hogan. Basal cells as stem cells of the mouse trachea and human airway epithelium. *Proc Natl Acad Sci U S A*, 106(31):12771–12775, 2009.

Jason R Rock, Scott H Randell, and Brigid LM Hogan. Airway basal stem cells: a perspective on their roles in epithelial homeostasis and remodeling. *Disease models & mechanisms*, 3(9-10):545–556, 2010.

Yannick Saalberg and Marcus Wolff. VOC breath biomarkers in lung cancer. *Clinica Chimica Acta*, 459:5–9, 2016.

Yasemin Sancak, Carson C Thoreen, Timothy R Peterson, Robert A Lindquist, Seong A Kang, Eric Spooner, et al. PRAS40 is an insulin-regulated inhibitor of the mTORC1 protein kinase. *Molecular cell*, 25(6):903–915, 2007.

Takafumi Sangai, Argun Akcakanat, Huiqin Chen, Emily Tarco, Yun Wu, Kim Anh Do, Todd W. Miller, et al. Biomarkers of rsponse to Akt inhibitor MK-2206 in breast cancer. *Clinical Cancer Research*, 18(20):5816–5828, 2012.

Dos D Sarbassov, David A Guertin, Siraj M Ali, and David M Sabatini. Phosphorylation and regulation of akt/PKB by the rictor-mTOR complex. *Science*, 307(5712):1098–1101, 2005.

Inderpal Sarkaria, O Pornchai, Simon G Talbot, Pabbathi G Reddy, Ivan Ngai, Ellie Maghami, et al. Squamous cell carcinoma related oncogene/DCUN1D1 is highly conserved and activated by amplification in squamous cell carcinomas. *Cancer Research*, 66(19):9437–9444, 2006.

Mitsuo Sato, Melville B. Vaughan, Luc Girard, Michael Peyton, Woochang Lee, David S. Shames, et al. Multiple oncogenic changes (K-RASV12, p53 knockdown, mutant EGFRs, p16 bypass, telomerase) are not sufficient to confer a full malignant phenotype on human bronchial epithelial cells. *Cancer Research*, 66(4):2116–2128, 2006.

Thorsten Schaefer and Claudia Lengerke. SOX2 protein biochemistry in stemness, reprogramming, and cancer: the PI3K/AKT/SOX2 axis and beyond. *Oncogene*, pages 1–15, 2019.

Nagashree Seetharamu, Isabel R Preeshagul, and Kevin M Sullivan. New PD-L1 inhibitors in non-small cell lung cancer - impact of Atezolizumab. *Lung Cancer (Auckland, N.Z.)*, 8:67–78, 2017.

Satyaki Sengupta and Rani E George. Super-enhancer-driven transcriptional dependencies in cancer. *Trends in cancer*, 3(4):269–281, 2017.

Jasmin M Siegle, Alice Basin, Ana Sastre-Perona, Yoshiya Yonekubo, Jessie Brown, Rachel Sennett, et al. SOX2 is a cancer-specific regulator of tumour initiating potential in cutaneous squamous cell carcinoma. *Nature communications*, 5:4511, 2014.

Anju Singh, Vikas Misra, Rajesh K Thimmulappa, Hannah Lee, Stephen Ames, Mohammad O Hoque, et al. Dysfunctional KEAP1–NRF2 interaction in non-small-cell lung cancer. *PLoS medicine*, 3(10):e420, 2006.

Aleksander Skardal, Mahesh Devarasetty, Steven Forsythe, Anthony Atala, and Shay Soker. A reductionist metastasis-on-a-chip platform for in vitro tumor progression modeling and drug screening. *Biotechnology and bioengineering*, 113(9):2020–2032, 2016.

Alexandra Sontheimer-Phelps, Bryan A Hassell, and Donald E Ingber. Modelling cancer in microfluidic human organs-on-chips. *Nature Reviews Cancer*, page 1, 2019.

Gabriella Sozzi, Mattia Boeri, Marta Rossi, Carla Verri, Paola Suatoni, Francesca Bravi, et al. Clinical utility of a plasma-based miRNA signature classifier within computed tomography lung cancer screening: A correlative MILD trial study. *Journal of Clinical Oncology*, 32(8):768–773, 2014.

Michael B Sporn and Karen T Liby. Cancer chemoprevention: scientific promise, clinical uncertainty. *Nature Reviews Clinical Oncology*, 2(10):518, 2005.

Balaji Srinivasan, Aditya Reddy Kolli, Mandy Brigitte Esch, Hasan Erbil Abaci, Michael L Shuler, and James J Hickman. TEER measurement techniques for in vitro barrier model systems. *Journal of laboratory automation*, 20(2):107–126, 2015.

Jill M Stahl, Arati Sharma, Mitchell Cheung, Melissa Zimmerman, Jin Q Cheng, Marcus W Bosenberg, Mark Kester, Lakshman Sandirasegarane, and Gavin P Robertson. Deregulated Akt3 Activity Promotes Development of Malignant Melanoma. *Cancer Research*, 64(12):7002–7010, 2004.

Anastasios Stathis and Francesco Bertoni. BET proteins as targets for anticancer treatment. *Cancer discovery*, 8(1):24–36, 2018.

Casey Stottrup, Tiffany Tsang, and Y Rebecca Chin. Upregulation of AKT3 confers resistance to AKT inhibitor MK2206 in breast cancer. *Molecular Cancer Therapeutics*, 15 (8):1964–1974, 2016.

Elias E Stratikopoulos, Meaghan Dendy, Matthias Szabolcs, Alan J Khaykin, Celine Lefebvre, Ming-ming Zhou, and Ramon Parsons. Kinase and BET Inhibitors Together Clamp Inhibition of PI3K Signaling and Overcome Resistance to Therapy. *Cancer Cell*, 27(6):837–851, 2015.

V Sundaresan, P Ganly, P Hasleton, R Rudd, G Sinha, NM Bleehen, and P Rabbitts. p53 and chromosome 3 abnormalities, characteristic of malignant lung tumours, are detectable in preinvasive lesions of the bronchus. *Oncogene*, 7(10):1989–1997, 1992.

Takafumi Suzuki, Tatsuhiro Shibata, Kai Takaya, Kouya Shiraishi, Takashi Kohno, Hideo Kunitoh, et al. Regulatory nexus of synthesis and degradation deciphers cellular nrf2 expression levels. *Molecular and cellular biology*, 33(12):2402–2412, 2013.

K Takahashi and S Yamanaka. Induction of pluripotent stem cells from mouse embryonic and adult fibroblast cultures by defined factors. *Cell*, 126(4):663–676, 2006.

Shinya Tanaka, Yusuke Kamachi, Aki Tanouchi, Hiroshi Hamada, Naihe Jing, and Hisato Kondoh. Interplay of SOX and POU factors in regulation of the nestin gene in neural primordial cells. *Molecular and cellular biology*, 24(20):8834–8846, 2004.

Toshimichi Tanaka, Masahiko Watanabe, and Keishi Yamashita. Potential therapeutic targets of TP53 gene in the context of its classically canonical functions and its latest non-canonical functions in human cancer. *Oncotarget*, 9(22):16234–16247, 2018.

Zefang Tang, Chenwei Li, Boxi Kang, Ge Gao, Cheng Li, and Zemin Zhang. GEPIA: a web server for cancer and normal gene expression profiling and interactive analyses. *Nucleic acids research*, 45(W1):W98–W102, 2017.

Vitor Teixeira, Stephan Beck, Andy G. Lynch, Charles Swanton, Peter J. Campbell, et al. Deciphering the genomic, epigenomic, and transcriptomic landscapes of pre-invasive lung cancer lesions. *Nature Medicine*, 25(March):517–525, 2019.

Nick Thatcher, Fred R Hirsch, Alexander V Luft, Aleksandra Szczesna, Tudor E Ciuleanu, Mircea Dediu, et al. Necitumumab plus gemcitabine and cisplatin versus gemcitabine and cisplatin alone as first-line therapy in patients with stage IV squamous non-small-cell lung cancer (SQUIRE): an open-label, randomised, controlled phase 3 trial. *The lancet oncology*, 16(7):763–774, 2015.

Anna Tourovskaia, Xavier Figueroa-Masot, and Albert Folch. Differentiation-on-a-chip: a microfluidic platform for long-term cell culture studies. *Lab on a Chip*, 5(1):14–19, 2005.

Mathias Uhlén, Linn Fagerberg, Björn M Hallström, Cecilia Lindskog, Per Oksvold, Adil Mardinoglu, et al. Tissue-based map of the human proteome. *Science*, 347(6220): 1260419, 2015.

Robert AA Van Boerdonk, Johannes MA Daniels, Peter JF Snijders, Katrien Grünberg, Erik Thunnissen, Mark A Van De Wiel, et al. DNA copy number aberrations in endobronchial lesions: a validated predictor for cancer. *Thorax*, 69(5):451–457, 2014.

Kristan E van der Vos and Paul J Coffer. The extending network of FoxO transcriptional target genes. *Antioxidants & Redox Signaling*, 14(4):579–592, 2011.

Johan F Vansteenkiste, Jean-Luc Canon, Filippo De Braud, Francesco Grossi, Tommaso De Pas, Jhanelle E Gray, et al. Safety and efficacy of buparlisib (BKM120) in patients with PI3K pathway-activated non-small cell lung cancer: results from the phase II BASALT-1 study. *Journal of Thoracic Oncology*, 10(9):1319–1327, 2015.

Bert Vogelstein and Kenneth W Kinzler. The multistep nature of cancer. *Trends in genetics*, 9(4):138–141, 1993.

Siniša Volarević, Mary J Stewart, Birgit Ledermann, Frederic Zilberman, Luigi Terracciano, Eugenio Montini, et al. Proliferation, but not growth, blocked by conditional deletion of 40s ribosomal protein s6. *Science*, 288(5473):2045–2047, 2000.

Elizabeth Wadhwa and Theodore Nicolaides. Bromodomain inhibitor review: bromodomain and extra-terminal family protein inhibitors as a potential new therapy in central nervous system tumors. *Cureus*, 8(5), 2016.

Jue Wang, Wei Zhao, Huifang Guo, Yong Fang, Sarah Elizabeth Stockman, Shanshan Bai, Patrick Kwok-Shing Ng, Yang Li, Qinghua Yu, Yiling Lu, et al. AKT isoform-specific expression and activation across cancer lineages. *BMC cancer*, 18(1):742, 2018.

Ling Wang, Delun Huang, Zongliang Jiang, Yan Luo, Carol Norris, Ming Zhang, and Xiuchun Cindy Tian. Akt3 is responsible for the survival and proliferation of embryonic stem cells. *Biology Open*, 6:850–861, 2017.

Xiaojie Wang, Xiaoning Ji, Jiazhou Chen, Dong Yan, Zhenbo Zhang, Qifeng Wang, et al. SOX2 enhances the migration and invasion of ovarian cancer cells via src kinase. *PloS one*, 9(6), 2014a.

Zhiqiang Wang, Qiao Qiao, Min Chen, Xianhua Li, Zhenjun Wang, Chuanxin Liu, and Zongtao Xie. mir-625 down-regulation promotes proliferation and invasion in esophageal cancer by targeting sox2. *FEBS letters*, 588(6):915–921, 2014b.

Hideo Watanabe, Qiuping Ma, Shouyong Peng, Guillaume Adelmant, Danielle Swain, Wenyu Song, et al. SOX2 and p63 colocalize at genetic loci in squamous cell carcinomas. *Journal of Clinical Investigation*, 124(4):1636–1645, 2014.

Marjan M Weiss, Ernst J Kuipers, Mario AJA Hermsen, Nicole CT van Grieken, Johan Offerhaus, Jan PA Baak, et al. Barrett's adenocarcinomas resemble adenocarcinomas of the gastric cardia in terms of chromosomal copy number changes, but relate to squamous cell carcinomas of the distal oesophagus with respect to the presence of high-level amplifications. *The Journal of Pathology: A Journal of the Pathological Society of Great Britain and Ireland*, 199(2):157–165, 2003.

Michael J Whitcutt, Kenneth B Adler, and Reen Wu. A biphasic chamber system for maintaining polarity of differentiation of culture respiratory tract epithelial cells. *In vitro cellular & developmental biology*, 24(5):420–428, 1988.

Ignacio Wistuba. Molecular Pathogenesis of Non-Small Cell Lung Carcinomas. *Journal of Lung Cancer*, 11(1):12–20, 2012.

Ignacio I Wistuba, Carmen Behrens, Sara Milchgrub, David Bryant, Jaclyn Hung, John D Minna, and Adi F Gazdar. Sequential molecular abnormalities are involved in the multistage development of squamous cell lung carcinoma. *Oncogene*, 18(3):643, 1999.

Anastasia Wyce, Gopinath Ganji, Kimberly N Smitheman, Chun-wa Chung, Susan Korenchuk, Peter Craggs, et al. BET inhibition silences expression of MYCN and BCL2 and induces cytotoxicity in neuroblastoma tumor models. *PloS one*, 8(8):e72967, 2013.

R Xiang, D Liao, T Cheng, H Zhou, Q Shi, TS Chuang, D Markowitz, RA Reisfeld, and Y Luo. Downregulation of transcription factor SOX2 in cancer stem cells suppresses growth and metastasis of lung cancer. *British journal of cancer*, 104(9):1410, 2011.

Chunxiao Xu, Christine M Fillmore, Shohei Koyama, Hongbo Wu, Zhao Chen, Grit S Herter-sprie, et al. Loss of Lkb1 and Pten Leads to Lung Squamous Cell Carcinoma with Elevated PD-L1 Expression. *Cancer Cell*, 25(5):590–604, 2014.

Hiromasa Yamamoto, Hisayuki Shigematsu, Masaharu Nomura, William W Lockwood, Mitsuo Sato, Naoki Okumura, Junichi Soh, et al. PIK3CA mutations and copy number gains in human lung cancers. *Cancer research*, 68(17):6913–6921, 2008.

M Yamaya, WE Finkbeiner, SY Chun, and JH Widdicombe. Differentiated structure and function of cultures from human tracheal epithelium. *American Journal of Physiology: Lung Cellular and Molecular Physiology*, 262(6):L713–L724, 1992.

Li Yan. Abstract #ddt01-1: Mk-2206: A potent oral allosteric akt inhibitor. *Cancer Research*, 69(9 Supplement):DDT01–1–DDT01–1, 2009.

Bin Yang, Ting Yan, Heyang Cui, Enwei Xu, Yanchun Ma, Caixia Cheng, et al. The macro-evolutionary events in esophageal squamous cell carcinoma. *Oncotarget*, 8(68): 112770, 2017a.

Ning Yang, Lian Hui, Yan Wang, Huijun Yang, and Xuejun Jiang. Overexpression of SOX2 promotes migration, invasion, and epithelial-mesenchymal transition through the wnt/β-catenin pathway in laryngeal cancer hep-2 cells. *Tumor Biology*, 35(8):7965–7973, 2014.

Zuyao Yang, Allan Hackshaw, Qi Feng, Xiaohong Fu, Yuelun Zhang, Chen Mao, and Jinling Tang. Comparison of gefitinib, erlotinib and afatinib in non-small cell lung cancer: A meta-analysis. *International journal of cancer*, 140(12):2805–2819, 2017b.

Shuai Ye, Kwang Bok Lee, Man Hee Park, Ju-Seog Lee, and Soo Mi Kim. p63 regulates growth of esophageal squamous carcinoma cells via the AKT signaling pathway. *International Journal of Oncology*, 44(6):2153–2159, 2014.

Hong In Yoon, Kyu Hyun Park, Eun-Jung Lee, Ki Chang Keum, Chang Geol Lee, Chul Hoon Kim, and Yong Bae Kim. Overexpression of SOX2 is associated with better overall survival in squamous cell lung cancer patients treated with adjuvant radiotherapy. *Cancer research and treatment: official journal of Korean Cancer Association*, 48 (2):473, 2016.

Ping Yuan, Humam Kadara, Carmen Behrens, Ximing Tang, Denise Woods, Luisa M Solis, et al. Sex determining region Y-box 2 (SOX2) is a potential cell-lineage gene highly expressed in the pathogenesis of squamous cell carcinomas of the lung. *PloS one*, 5(2):e9112, 2010.

Yohei Yurugi, Makoto Wakahara, Yuki Matsuoka, Tomohiko Sakabe, Yasuaki Kubouchi, Tomohiro Haruki, et al. Podoplanin expression in cancer-associated fibroblasts predicts poor prognosis in patients with squamous cell carcinoma of the lung. *Anticancer research*, 37(1):207–213, 2017.

Ran Zhao, Bu Young Choi, Mee Hyun Lee, Ann M. Bode, and Zigang Dong. Implications of Genetic and Epigenetic Alterations of CDKN2A (p16INK4a) in Cancer. *EBioMedicine*, 8:30–39, 2016.

Jian Zheng, Qiuping Shu, Zhi-Hua Li, Jen-Ian Tsao, Lawrence M Weiss, and Darryl Shibata. Patterns of p53 mutations in squamous cell carcinoma of the lung. Acquisition at a relatively early age. *The American journal of pathology*, 145(6):1444, 1994.

Wei Zheng, Natasha Thorne, and John C McKew. Phenotypic screens as a renewed approach for drug discovery. *Drug discovery today*, 18(21-22):1067–1073, 2013.

S Zhou, L Liu, H Li, G Eilers, Y Kuang, S Shi, Z Yan, X Li, JM Corson, F Meng, et al. Multipoint targeting of the PI3K/mTOR pathway in mesothelioma. *British journal of cancer*, 110(10):2479, 2014.

Neslihan Zohrap, Özge Saatci, Burcak Ozes, Ipek Coban, Hasan Murat Atay, Esra Battaloglu, Özgür Şahin, and Kuyas Bugra. SIK2 attenuates proliferation and survival of breast cancer cells with simultaneous perturbation of MAPK and PI3K/akt pathways. *Oncotarget*, 9(31):21876, 2018.

Johannes Zuber, Junwei Shi, Eric Wang, Amy R Rappaport, Harald Herrmann, Edward A Sison, Daniel Magoon, Jun Qi, Katharina Blatt, Mark Wunderlich, et al. Rnai screen identifies brd4 as a therapeutic target in acute myeloid leukaemia. *Nature*, 478(7370): 524, 2011.